The role of CD18 and regulatory T cells in skin inflammation

Dissertation

Zur Erlangung des Grades

Doktor der Naturwissenschaften

Am Fachbereich Biologie

Der Johannes Gutenberg-Universität Mainz

Tanja Klaus

geb. am 16.12.1990 in Nürnberg

Mainz, September 2023

Dekan: Prof. Dr. Eckhard Thines

Dekanatsleitung: Dr. Mark Bajohrs

1. Gutachter: [redacted]

2. Gutachter: [redacted]

Tag der mündlichen Prüfung: 18.12.2023

Declaration

The scientific studies presented herein were conducted from February 19th, 2020 until Mai 1th, 2023 at the Department of Dermatology (Paul-Klein-Zentrum für Immunintervention) of the University Medical Center of the Johannes Gutenberg-University in Mainz under supervision of Prof. Dr. Stephan Grabbe.

I, Tanja Klaus, hereby declare that I wrote the dissertation submitted without any unauthorized external assistance and used only sources acknowledged in this work. All textual passages which are appropriate verbatim or paraphrased from published and unpublished texts, as well as all information obtained from oral sources, are duly indicated and listed in accordance with bibliographical rules. In carrying out this research, I complied with the rules of standard scientific practice as formulated in the statutes of Johannes Gutenberg-University Mainz to insure standard scientific practice.

……

Tanja Klaus

Mainz, 25th September 2023

Abstract

β_2-integrins are essential for cell-cell communication and the extravasation of leukocytes from blood into inflamed tissues. These surface receptors are composed of a variable α chain and a constant β chain known as CD18 and are specifically expressed by leukocytes. Four different α chains pair intracellularly with the common β chain: αL (CD11a), αM (CD11b), αX (CD11c) and αD (CD11d). The leukocyte function-associated antigen 1 (LFA-1, also known as CD11a/CD18) is the only β_2-integrin family member expressed on T cells. As part of the immunological synapse (IS), LFA-1 binds to intercellular adhesion molecules (ICAM) expressed by other leukocytes, especially by dendritic cells (DC) and other antigen-presenting cells (APC) and thereby enhances T cell receptor (TCR) mediated T cell activation. LFA-1 engaging ICAM-1 on endothelial cells also facilitates T cell entry into peripheral tissues, enabling migration to sites of inflammation and infection. Moreover, LFA-1/ICAM-1 signaling, in combination with TCR stimulation, influences human T cell polarization by modulating T-helper cell 1 (T_H1), T_H2, and T_H17 responses.

Humans with reduced or defective β_2-integrin expression develop Leukocyte Adhesion Deficiency Syndrome Type-1 (LAD-1). This rare disease results from mutations in the gene encoding for the common β-chain of the β_2-integrin family (*Itgb2*, also known as CD18). The most prominent clinical symptoms are profound leukocytosis and high susceptibility to infections. At the same time, LAD-1 patients are prone to develop autoimmune diseases like inflammatory bowel diseases (IBD). However, the molecular and cellular mechanisms that result in coexisting immunodeficiency and autoimmunity are still unresolved.

Regulatory T cells (Treg) are crucial for the maintenance of peripheral tolerance and the regulation of immune responses. The immunosuppressive function of Treg depends on different mechanisms, cytokine production, and suppressive receptor interactions with T cells, APC, and other types of leukocytes. Mutational inactivation of the transcription factor forkhead box p3 (Foxp3*)*, a crucial key regulator of Treg, causes the loss of functional Treg, and leads to severe systemic multi-organ autoimmunity.

So far, different mouse strains with deleted CD11a or CD18 expression, respectively, have been established to study the role of LFA-1 for T cell functions under homeostatic conditions and in disease models. Those strains, in which the β subunit of β_2-integrins was constitutively deleted, recapitulate the leukocytosis, immune deficiency, and seemingly contradictory autoimmune aspects of LAD-1. In common with the CD18-deficient mouse strains, CD11a-deficient mice show a defect in Treg function but have no obvious skin phenotype. However, as all leukocytes are affected, it is difficult to delineate the direct contribution of specific leukocyte populations to the various phenotypic alterations.

This work aimed to understand the role of LFA-1 for Treg functions and the manifestation of autoimmunity and inflammation. We hypothesized that LFA-1-deficient Treg are functionally distorted and thereby may substantially contribute to the manifestation of (auto)inflammatory skin diseases. To overcome the limitations of the existing mouse models, we generated mice specifically lacking CD18 on Treg ($CD18^{Foxp3}$), resulting in defective LFA-1. These mice spontaneously developed systemic immune activation, severe skin inflammation, including ears and tails, and lung tissue damage resembling an atopy-like phenotype. Furthermore, a profound

activation of the T_H2 pathway in $CD18^{Foxp3}$ mice was observed, which also exhibited massively elevated IgE, eosinophilia, and enhanced allergic contact hypersensitivity responses.
Furthermore, gene expression profiles of LFA-1-deficient Treg revealed increased expression of several genes associated with atopic dermatitis and asthma. Besides the atopy-like phenotype, $CD18^{Foxp3}$ mice develop a coexisting autoimmune phenotype characterized by the presence of autoantibodies in the serum against basement membrane components and/or basal keratinocytes. In this respect, the spontaneous phenotype of $CD18^{Foxp3}$ mice shares many aspects with that of scurfy mice. In addition, LFA-1-deficient Treg developed less contacts with DC, which in turn increased DC activation, which may result in T cell hyperactivation and exacerbated type II immune responses due to T_H2-promoting DC. Deficiency of LFA-1 on Treg thereby has a similar negative effect on self-tolerance as the loss of *Foxp3*. These observations suggest an indispensable role of LFA-1 on Treg to maintain immune homeostasis and implicate LFA-1-deficient Treg in the pathogenesis of the autoimmunity seen in LAD-1 patients.

Graphical abstract

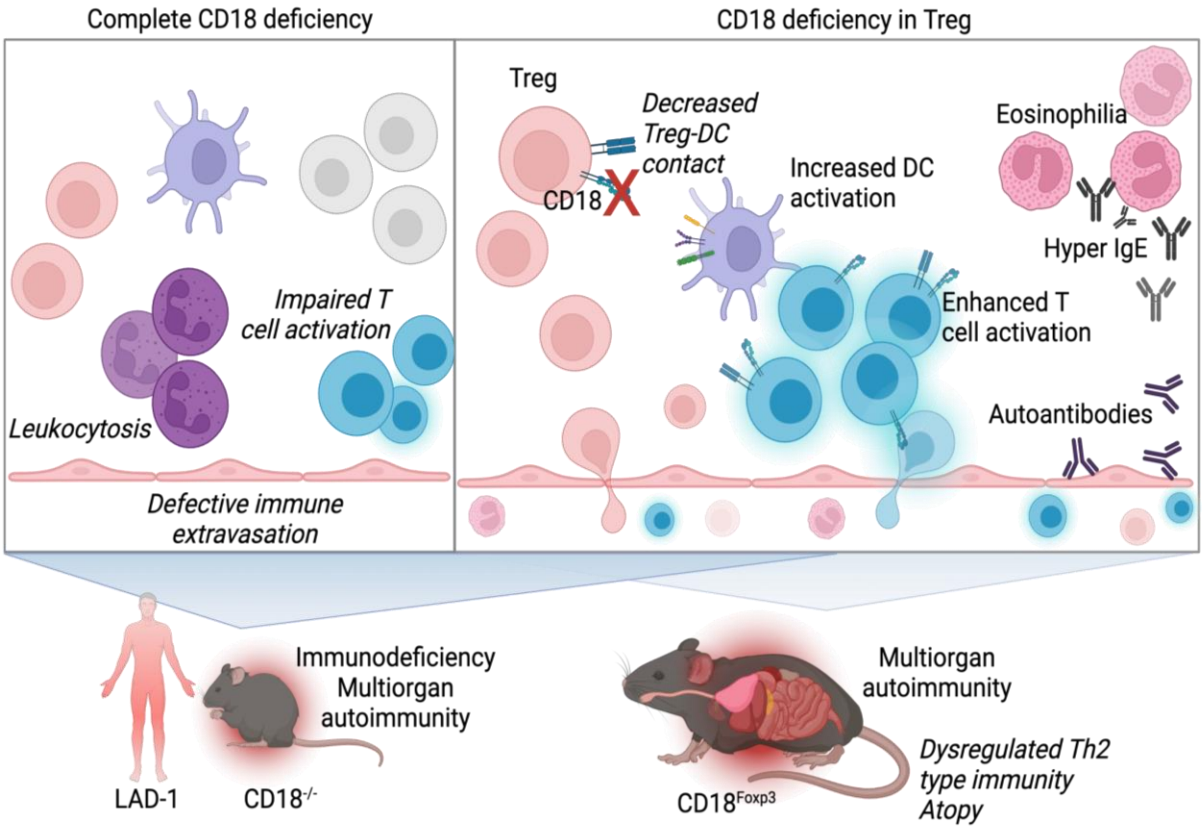

Adapted from [1]

Zusammenfassung

β_2-Integrine sind Oberflächenmoleküle, welche eine wichtige Rolle für die Leukozyten-Kommunikation sowie die Migration von Leukozyten aus dem Blut in entzündetes Gewebe spielen. Sie bestehen aus einer variablen α und einer konstanten β Kette (CD18) und werden spezifisch von allen Leukozyten exprimiert. Es existieren vier unterschiedliche α-Ketten, welche intrazellulär mit der gemeinsamen β-Kette hetero-dimerisieren: αL (CD11a), αM (CD11b), αX (CD11c) und αD (CD11d). Leukocyte function-associated antigen 1 (LFA-1) ist dabei das einzige β_2-Integrin, das von T Zellen exprimiert wird. LFA-1 ist ein Teil der immunologischen Synapse (IS) und bindet an intrazelluläre Adhesionsmoleküle (ICAM) die von vaskulären Endothelzellen und anderen Leukozyten, wie beispielsweise Antigen-präsentierenden Zellen (APC), wie dendritische Zellen (DC) exprimiert werden. LFA-1 auf T Zellen ermöglicht diesen Zellen den Eintritt in lymphatisches Gewebe und die Migration zu Entzündungs- und Infektionsherden. Des Weiteren beeinflusst die LFA-1/ICAM-1 Interaktion im Kontext mit einer T-Zell-Rezeptor (TCR) Aktivierung die Polarisierung von humanen T Zellen zu entweder T-Helferzellen 1, (T_H1) -2 (T_H2) oder -17 (T_H17) Immunantworten.

Eine reduzierte Expression funktionsfähiger β_2-Integrine verursachen eine seltene Erbkrankheit, die als Leukozyten Adhesionsdefizienz 1 (LAD-1) bezeichnet wird. LAD-1 Patienten weisen eine Leukozytose und eine hohe Anfälligkeit für Infektionen auf, können aber auch gleichzeitig Autoimmunerkrankungen, wie beispielsweise chronisch entzündliche Darmerkrankungen, entwickeln. Die Ursache für die Koexistenz von Inflammation und Autoimmunität bei LAD-1 Patienten ist derzeit noch ungeklärt.

Regulatorische T Zellen (Treg) sind wichtige Immunzellen bei der Aufrechterhaltung der peripheren Toleranz und Regulation von Immunantworten. Die immunsuppressive Wirkung von Treg hängt von verschiedenen Mechanismen und löslichen Komponenten ab, wie der Produktion anti-inflammatorischer Zytokine und der Suppression von APC, T Zellen oder anderen Immunzellen. Mutationen in dem wichtigen Transkriptionsfaktor forkhead box p3 (*Foxp3*) in Treg führt zu einem Funktionsverlust und somit Autoimmunität.

Im Zusammenhang mit LAD-1 wurden verschiedene transgene Mausmodelle entwickelt, bei denen die Leukozyten kein CD11a oder CD18 exprimieren, um die Bedeutung von β_2-Integrinen auf T Zellen unter homöostatischen Bedingungen und in Krankheitsmodellen zu untersuchen. Da allerdings in diesen Mausmodellen keine β_2-Integrine exprimiert werden oder ein bestimmtes β_2-Integrin auf Immunzellen funktionsunfähig ist, ist es schwierig die zelltypische Relevanz von β_2-Integrinen im Krankheitskontext aufzuklären.

Der Schwerpunkt dieser Arbeit liegt darin, die Funktion von LFA-1 auf Treg für die Manifestation von Autoimmunität und Inflammation besser zu verstehen. Laut unserer Hypothese sind LFA-1-defiziente Treg in ihrer immunsuppressiven Funktion gestört und tragen somit zu Autoimmunität bei. Um diese Hypothese zu überprüfen, haben wir ein Mausmodell entwickelt, in dem Treg-spezifisch kein CD18 und somit LFA-1 exprimiert ($CD18^{Foxp3}$) wird. Diese Mäuse entwickeln spontan systemische Entzündungen, einschließlich einer atopischen Dermatitis, sowie eine spezifische Immunaktivierung anderer Organe wie beispielsweise in der Lunge. Des Weiteren haben wir eine Verschiebung hin zu einer T_H2 Immunantwort verbunden

mit einer massiven Ausschüttung von IgE, Eosinophilie, und höheren Anfälligkeit für Kontaktallergien feststellen können.
Außerdem zeigten LFA-1-defiziente Treg eine im Vergleich zu Wildtyp-Treg eine starke Aufregulation von Genen, welche mit atopischer Dermatitis und Asthma assoziiert sind. Neben dem Atopie-ähnlichen Phänotyp entwickeln $CD18^{Foxp3}$ Mäuse ebenfalls Autoimmunität, welche durch das Vorhandensein von Autoantikörpern im Serum gegen Komponenten der Basalmembran beziehungsweise basale Keratinozyten gekennzeichnet ist. Die unkontrollierte Immunaktivierung durch β_2-Integrin-defiziente Treg wird möglicherweise, zumindest partiell, durch reduzierte Kontakte zwischen Treg und DC ausgelöst, was zur verminderten Suppression führt und der Expansion aktivierter, T_H2-induzierenden DC führt. Fehlendes LFA-1 auf der Oberfläche von Treg hat dementsprechend einen ähnlichen Effekt auf die Immuntoleranz wie der Verlust von Foxp3. Die im Rahmen der vorliegenden Arbeit charakterisierten $CD18^{Foxp3}$ Mäuse stellen dabei das erste murine Mausmodel dar, um die Rolle von LFA-1 spezifisch auf Treg zu untersuchen. Die hier vorgestellten Ergebnisse zeigen, dass LFA-1 auf Treg für die Aufrechterhaltung der Immunhomöostase unverzichtbar ist und dessen Mangel auf Treg bei LAD-1 Patienten zu deren Prädisposition beitragen dürfte, Autoimmunerkrankungen zu entwickeln.

Publication list

This work resulted in a total of two first author publications. Further publications are in progress.

(1) **Klaus T**, Wilson AS. et al., The Role of LFA-1 for the Differentiation and Function of Regulatory T Cells-Lessons Learned from Different Transgenic Mouse Models. *Int J Mol Sci*. 2023;24(7):6331. Published 2023 Mar 28. doi:10.3390/ijms24076331

(2) **Klaus T**, Wilson AS, et al. Impaired Treg-DC interactions contribute to autoimmunity in leukocyte adhesion deficiency type 1. *JCI Insight*. 2022;7(24):e162580. Published 2022 Dec 22. doi:10.1172/jci.insight.162580

(3) Bednarczyk M, Bolduan V. Haist M. Stege H; Hieber C, Johann L, Schelmbauer, C, Blanfeld M, Karram K, Schunke J, **Klaus T**, Tubbe I, Montermann E, Röhrig N, Hartmann M, Schlosser J, Bopp T, Clausen B.E, Waisman A, Bros M, Grabbe S. β2 Integrins on Dendritic Cells Modulate Cytokine Signaling and Inflammation-Associated Gene Expression, and Are Required for Induction of Autoimmune Encephalomyelitis. *Cells* 2022, *11*, 2188. https://doi.org/10.3390/cells11142188

(4) Simon J, Fichter M, Kuhn G, Brückner M, Kappel C, Schunke S, **Klaus T**, Grabbe S, Landfester K, Mailänder V,Achieving dendritic cell subset-specific targeting in vivo by site-directed conjugation of targeting antibodies to nanocarriers, *Nano Today* 2022 Volume 43,101375, ISSN 1748-0132,https://doi.org/10.1016/j.nantod.2022.101375.

Table of content

1. Introduction

A healthy immune system requires a precise balance between tolerance and immunity. In this context, Treg are known to be master regulators of immune homeostasis and self-tolerance. Their relevance for mice and humans is underlined by the observation that autoimmunity develops when Treg are dysfunctional or missing [2, 3].
The αβ-integrin receptor family is a large group of heterodimeric surface receptors. The β_2-integrin subfamily consists of four different, surface-expressed receptors, resulting in multiple regulatory functions for the innate and adaptive immune system [4, 5].
This work focuses on the role of β_2-integrins, especially on Treg. In the following chapter, the αβ-integrin family and the specific role of LFA-1, the only member of the β_2-integrin subfamily expressed by T cells, as well as the general function of Treg, is introduced.

(1) Klaus Tanja, et al. The Role of LFA-1 for the Differentiation and Function of Regulatory T Cells - Lessons Learned from Different Transgenic Mouse Models. *Int J Mol Sci*. 2023;24(7):6331. Published 2023 Mar 28. doi:10.3390/ijms24076331

1.1. The αβ-integrin receptor family

The first part of the introduction gives a short overview of the αβ-integrin family regarding their classification, function, and therapeutical relevance. The main focus is on the β_2-integrin LFA-1 and its role on Treg, to be described in more detail in the following chapters.

1.1.1. Classification and expression patterns

Integrins are a large family of evolutionarily conserved, heterodimeric surface receptors composed of an α and a β chain and are specifically expressed by leukocytes [6]. The integrin family has a very long evolutionary history, and both subunits were found in all invertebrates, including early metazoans [7].
Integrin αβ heterodimers are divided into four classes (leukocyte, collagen-binding, Arg-Gly-Asp (RGD)-binding, and laminin-binding integrins) based on ligand specificity and evolutionary origin [8]. In vertebrates, 18 different integrin α subunits and 8 β subunits can be expressed [7, 9, 10], whereas β_1, β_2, and αV-containing integrins built the largest three groups of this family according to their classification (Figure 1) [6, 9]. To date, in total 24 β-integrin combinations are known to be expressed by humans [8].

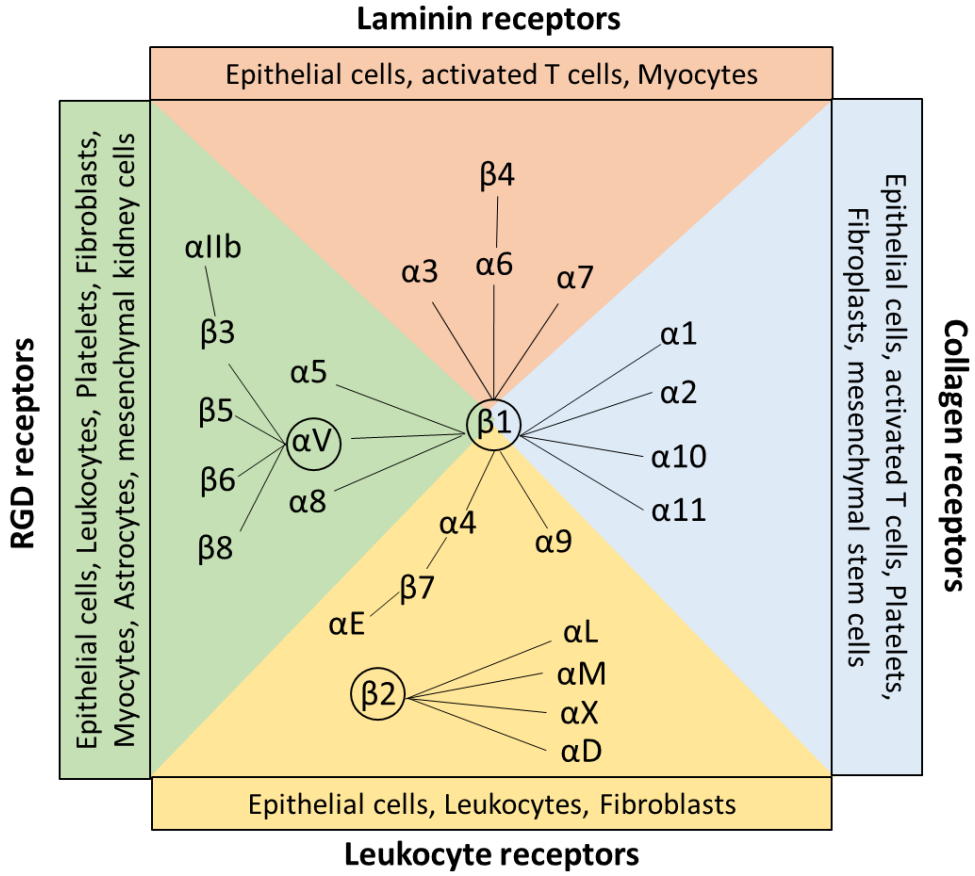

Figure 1 ***Classification and expression pattern of the αβ-integrin receptor family.*** *Integrin heterodimers consist of different combinations of the α and β subunits. In general integrins are classified to their ligand specificity in RGD-recognizing integrins ($\alpha_5\beta_1$, $\alpha_V\beta_1$, $\alpha_V\beta_3$, $\alpha_V\beta_5$, $\alpha_V\beta_6$, $\alpha_V\beta_8$, $\alpha_{IIb}\beta_3$) shown in green, laminin-binding integrins ($\alpha_3\beta_1$, $\alpha_6\beta_1$, $\alpha_7\beta_1$, and $\alpha_6\beta_4$) shown in red, collagen-binding integrins ($\alpha_1\beta_1$, $\alpha_2\beta_1$, $\alpha_{10}\beta_1$, and $\alpha_{11}\beta_1$) shown in blue, and leukocyte integrins ($\alpha_9\beta_1$, $\alpha_4\beta_1$, $\alpha_E\beta_7$, $\alpha_L\beta_2$, $\alpha_M\beta_2$, $\alpha_X\beta_2$, and $\alpha_D\beta_2$) shown in yellow [8, 11]. The β_1, β_2, and αV containing integrins built the largest groups of the family. All integrins are expressed by a wide range of cells, including, for example, leukocytes, epithelial cells, and fibroblasts (adapted from [6, 9, 11, 12]).*

Usually, their ligand binding ability is conferred by recognizing small peptide sequences of extracellular matrix molecules (ECM) and non-ECM molecules [12]. Target sequences are arginylglycylaspartic acid Arg–Gly–Asp (RGD), triple-helical GFOGER peptides, and two homologous sequences Leu-Asp-Val (LDV) and Ile-Asp-Ala-Pro (IDAP) [10, 13].
The tripeptide motif RGD binds to $\alpha_v\beta_1$, $\alpha_v\beta_3$, $\alpha_v\beta_5$, $\alpha_v\beta_6$, $\alpha_v\beta_8$, $\alpha_5\beta_1$, $\alpha_8\beta_1$, and $\alpha II_b\beta_3$. RGD receptors are expressed by a wide range of cell types, including for example, astrocytes, leukocytes, and fibroblasts [11].
GFOGER binding integrins are collagen receptors, including $\alpha_1\beta_1$, $\alpha_2\beta_1$, $\alpha_{10}\beta_1$, and $\alpha_{11}\beta_1$ which are expressed by fibroblast, stem cells, and epithelial cells. The tripeptide LDV is recognized by the leukocyte receptors $\alpha_4\beta_1$, $\alpha_4\beta_7$, and β_2 subunits, which are expressed mainly on leukocytes and epithelial cells [11] (Figure 1). The target sequence IDAP is, besides LDV and RGD, a peptide sequence of fibronectin and is an active binding side of $\alpha_4\beta_1$ [13].

All integrins are grouped by the target sequences they specifically recognize [12]. Once they have bound to their peptide, integrins provide adhesion and initial signaling, allowing cells to respond to mechanical or chemical factors [12].

1.1.2. αβ-integrin immune functions and targeted therapies

Their general functions, namely mediation of cell adhesion to ECM, the migration along the endothelium, and the intracellular communication have been established early in invertebrates such as *C. elegans* and *drosophila* [7]. The adhesion and communication of cells are fundamental processes and identify the integrin family as an indispensable key player in the link between the extracellular environment and the cytoskeleton [14]. Beyond these well-known roles, integrin engagement has also been described for ligands not located in the ECM, including eukaryotes, prokaryotes, and fungal cells. Within eukaryotes, integrins are known to coordinate processes like stem cell homing, tumor cell migration, and erythrocyte development [12].

RGD-binding integrins

The RGD subfamily is a large group of integrins that interacts with many different ligands, such as the glycoprotein vitronectin, E-cadherin, and transforming growth factor β (TGF-β). RGD receptors are essential for vascular smooth muscle cell migration, phagocytosis, and the activation of TGF-β, which regulates innate immunity and anti-inflammatory surveillance, respectively [11]. Most of the eight RGD-binding integrins are expressed in various cancers, regulating pathophysiological processes like promoting tumor invasion and metastasis formation [14]. However, they are also known to be involved in other diseases like sepsis [15], fibrosis [16] and viral infections [17]. In this regard, integrin targeting is highly interesting to deliver effective platforms against specific diseases, such as exosome-loaded RGD-peptides. Exosomes are important mediators of intracellular crosstalk by distributing their cargo. RGD-loaded exosomes were shown to yield therapeutic effects in breast cancer models after intravenous injections [14, 18]. Furthermore, preclinical studies showed that using RGD integrin antagonists, such as RGD-based cyclic peptides, efficiently suppressed tumor angiogenesis [19]. The most prominent example is Cilengitide, an $\alpha_v\beta_3/\alpha_v\beta_5$ antagonist against glioblastoma, which however, failed its clinical endpoint [14]. Interestingly, the administration of low-dose Cilengitide *in vitr*o and in animal models revealed that it promoted tumor angiogenesis instead of inhibiting it [20]. Subsequently, so far, no successful RGD-targeted peptide therapy is available [14].

Laminin-binding integrins

Laminin receptors play critical roles in regulating cell adhesion, proliferation, migration, and survival and are important for the development of the brain, lung, skin, and muscles [11]. Like RGD-binding integrins, laminin receptor expression has also been identified to correlate with tumor progression. In some cases, positive and negative correlations have been reported for breast and oral squamous cell carcinomas [21]. Moreover, mutations in

the receptor $\alpha_6\beta_4$ resulted in junctional epidermolysis bullosa, a blistering skin disease [22]. So far, no specific therapy targeting laminin-binding integrins is available.

Collagen-binding integrins

The collagen receptor $\alpha_1\beta_1$, also known as very late antigen 1 (VLA-1), was first identified on activated T cells [23]. In T cells, it functions as a promoter of inflammatory responses and facilitates monocyte transmigration by binding collagen XIII [11]. SAN-300 is a monoclonal antibody directed against $\alpha_1\beta_1$-integrin and was used in a clinical phase II study for the treatment of patients with rheumatoid arthritis [11]. Furthermore, the inhibition of the interaction of $\alpha_1\beta_1$ and collagen lead to reduced T cell accumulation in the epidermis and consequently inhibited the development of psoriasis *in vivo* [24].

The integrin $\alpha_2\beta_1$, also known as VLA-2, is expressed on platelets and mediates collagen binding at sides of inflammation. In this regard, Vatelizumab, a monoclonal antibody targeting the α_2 subunit (CD49b) of VLA-2, was investigated in a clinical phase II study in multiple sclerosis (MS) patients [25]. After treatment with Vatelizumab, higher Treg frequencies were observed in MS patients, which might have resulted from the inhibition of p38 mitogen-activated protein kinase (MAPK) signaling, which is critically involved in the polarization of T helper 17 (T_H17) cells and is activated by the α_2-integrin cytoplasmic domain. Even though the clinical trial did not reach the endpoint, blockade of VLA-2 might be a way to shift the T_H17/Treg balance towards Treg differentiation [25].

Leukocyte receptors

Leukocyte receptors play critical roles in leukocyte recruitment and (auto)inflammatory diseases. This family consists of the β_2-integrins (described in more detail in the following chapters) as well as the $\alpha_4\beta_1$ (VLA-4; CD49d/CD29) and integrin $\alpha_4\beta_7$ (LPAM-1) [26]. $\alpha_4\beta_1$ integrin was shown to be important for leukocyte recruitment to the inflamed central nervous system (CNS) in experimental autoimmune encephalomyelitis (EAE), a mouse model to investigate MS [27]. Studies showed that $\alpha_4\beta_1$-integrin/VCAM-1 interaction mediated leukocyte adherence in the CNS. This knowledge resulted in the development of Natalizumab, a monoclonal IgG4 antibody against α_4, which blocks $\alpha_4\beta_1$ integrin and has been approved for treating MS [28]. The inhibition of $\alpha_4\beta_1$ rather than $\alpha_4\beta_7$-integrin was less effective [29]. Natalizumab enabled the first targeted therapy for the treatment of relapsing-remitting MS [26].

In addition, $\alpha_4\beta_1$ was shown to play a critical role in hematopoietic stem cell (HSC) homing. $\alpha_4\beta_1$ interaction with its ligand vascular cell adhesion molecule-1 (VCAM-1) mediates HSC retention in the bone marrow (BM) [12]. The importance of $\alpha_4\beta_1$ is underlined by the use of α_4-integrin knockout mice that presented with elevated numbers of HSC in the bloodstream compared to wildtype littermates [30]. Treating mice with the VCAM-1 antagonist Bortezomib also increased HSC migration [31]. Therefore, Bortezomib is of great interest for harvesting HSC from the blood of healthy patients for use in transplantations [12].

In contrast, the overexpression of the $\alpha_4\beta_7$-integrin counter-receptor mucosal address cell adhesion molecule 1 (MAdCAM-1) with a tetracycline (TET)-inducible transgenic mouse model did not affect EAE severity [32]. Furthermore, Vedolizumab and Etrolizumab have

been developed to target $\alpha_4\beta_7$-integrin [26, 33]. Vedolizumab is a humanized IgG1 monoclonal antibody that proved to be effective of moderate in severe Crohn's disease [26]. Etrolizumab is a humanized monoclonal antibody that selectively binds the β_7-subunit of both the $\alpha_4\beta_7$ and $\alpha_E\beta_7$-integrin heterodimers, thereby antagonizing $\alpha_4\beta_7$-MAdCAM-1-mediated lymphocyte recruitment and the interaction with $\alpha_E\beta_7$-E-cadherin [34]. Etrolizumab was shown to have a beneficial influence on treating patients with severe IBD [35]. Moreover, Kunkel *et al.*, by using $\beta_7^{-/-}$ mice, demonstrated that $\alpha_4\beta_7$-integrin is involved in the adhesion of leukocytes to Peyer's patch endothelial venules [36]. Treatment with anti-β_7 and anti-MAdCAM-1 antibodies relieved experimental murine chronic colitis [37].

1.2. The β_2-integrin subfamily and their ligands

β_2-integrins belong to the leukocyte receptor subfamily of the αβ-integrins. The common β_2 (CD18) chain has received attention because of its involvement in different inflammatory receptors such as CD11a/CD18 ($\alpha_L\beta_2$, LFA-1), CD11b/CD18 ($\alpha_M\beta_2$, MAC-1, complement receptor 3 (CR3)) CD11c/CD18 ($\alpha_X\beta_2$, p150.95, CR4), and CD11d/CD18 ($\alpha_D\beta_2$) (Figure 2) [4, 6]. β_2-integrins are commonly known to bind ligands via the αI-domain [5], whereas the α subunit of each β_2-integrin determines the extracellular ligand specificity to different ligands such as intracellular adhesion molecules (ICAM), VCAM, and endothelial cell-specific molecule (ESM) as well as other cell surface and serum molecules [4, 8, 38].

LFA-1 is predominantly expressed by all types of leukocytes, especially T cells. Activated LFA-1 engages ICAM 1-5, junctional adhesion molecule (JAM)-1, JAM-A, and ESM-1 [6, 39, 40].

Myeloid cells can express all four members of the β_2-integrin family. Macrophage-1 antigen (MAC-1) is predominantly expressed on polymorphonuclear neutrophils (PMN), macrophages, monocytes, and DC [6, 41]. In circulating leukocytes, MAC-1 is normally expressed in an inactive form, but it mediates firm adhesion to endothelial cells during inflammation. MAC-1 binds to many ligands, including surface receptors like ICAM 1-4, VCAM-1, JAM-3, advanced glycation end products (RAGE), thymus cell antigen 1 (Thy-1), platelet glycoprotein Ibα (GPIbα), DC-specific ICAM-3-grabbing non-integrin (DC-SIGN) [6, 42], E-selectin and many others [43-48] (Figure 2). In addition, MAC-1 binds several matrix proteins like fibronectin and collagen [49, 50], plasma proteins including fibrinogen, elastase, matrix metalloproteinase-2 (MMP-2) and MMP-9 and microbial ligands like lipopolysaccharide (LPS) [43]. Furthermore, MAC-1 is also known as complement receptor 3 (CR3) and binds iC3b of the complement system, promoting the phagocytosis of complement-opsonized pathogens [51, 52].

CD11c is a classical marker for murine DC but in humans it is also expressed on other myeloid cells like macrophages, PMN, and monocytes [53]. CD11c also engages diverse ligands such as ICAM-1, -2, and -4, [54-57] bacterial components like LPS [58], complement proteins like iC3b as well as fibrinogen and collagen-1 [59, 60]. In addition, CD11c strongly binds VCAM-1, and as shown for monocytes, this interaction stops the

rolling of the cells on endothelia and allows the transmigration through inflamed endothelial cells of the aorta [57].
The integrin CD11d/CD18 is the most recently discovered β_2-integrin and is expressed under basal conditions by a few types of leukocytes, but is most abundant on macrophages and upregulated upon inflammation like MAC-1 [6]. In humans, CD11d/CD18 is highly expressed on natural killer cells (NK), B cells, and γδ T cells [6, 61]. It binds to cellular receptors like VCAM-1 and ICAM-3 [62] and, like MAC-1 to matrix proteins including fibronectin, vitronectin, and fibrinogen [5].

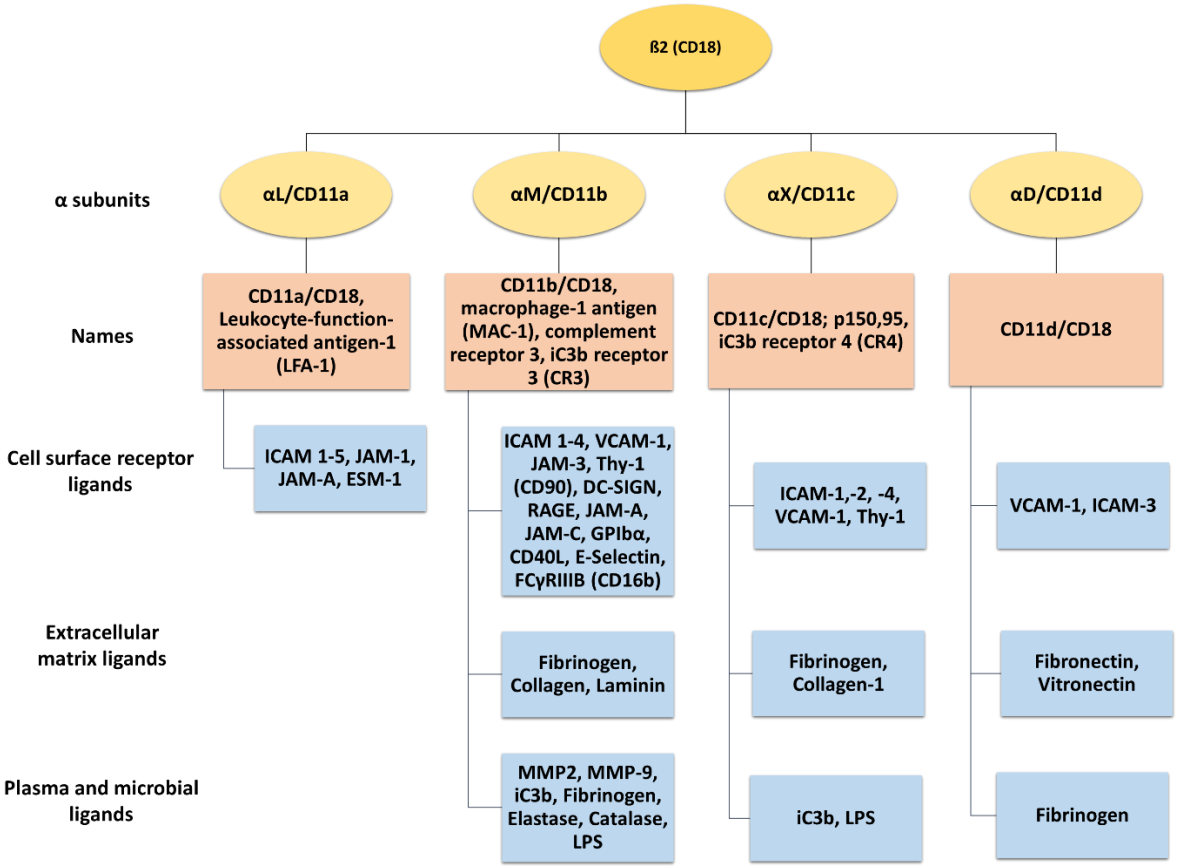

Figure 2 ***The β_2-integrin receptor subfamily and their ligands.*** *The common β_2-integrin subunit (CD18) can pair with one of the four α subunits (α_L-CD11a, α_M-CD11b, α_X-CD11c, and α_D-CD11d), forming LFA-1, MAC-1, complement receptor 4 (150.95/CR4), and CD11d/CD18, respectively [63]. LFA-1 is the only β_2-integrin expressed on T cells [64], while CD11b/CD18, CD11c/CD18, and CD11d/CD18 are also expressed on myeloid cells [6, 8, 63, 65]. β_2-integrins can pair with a wide range of ligands including cell surface receptor, extracellular matrix ligands, plasma and microbial ligands [11, 12].*

1.2.1. Multidimensional functions of β_2-integrins

Immune trafficking

Activated β_2-integrins exert numerous immune functions (Figure 3) [8]. They are crucial for the adhesion and trafficking of leukocytes from the bloodstream to sites of tissue inflammation by binding proteins of the ECM. Leukocyte adhesion comprises multiple steps, including rolling along endothelia, adhesion, arrest, crawling, and finally,

extravasation along a chemokine gradient to navigate to inflammatory sites [66]. Ligand binding to selectins and ICAM induces β_2-integrin clustering and the formation of multi-protein complexes that consist of intracellular signaling and adaptor proteins connecting β_2-integrins with the actin cytoskeleton [67]. Ligand binding and activating integrins allow the cells' adhesion process along the endothelium. Leukocyte rolling is mediated by glycoproteins on the leukocyte cell surface, such as P-selectin glycoprotein ligand-1 (PSGL-1), which binds to endothelial selectins [12]. Chemokine stimulation enables β_2-integrins to undergo a change in their conformation, acquiring a high-affinity state (see Chapter 1.2.2). This leads to the binding of cell adhesion molecules like ICAM and JAM on endothelial cells, resulting in a migration arrest [12, 66, 68]. Subsequently, integrin-ligand bonds are broken, reformed, and stabilized by cytoskeletal proteins such as talin and kindlin, which results in actin reorganization and spreading of the cells and finally, leukocyte transmigration through the endothelium [4].

In this respect, LFA-1 and MAC-1 are essential for the migration of myeloid cells as well as T cells. In PMN migration, LFA-1 is known to regulate the adhesion to the endothelium and MAC-1 to facilitate intravascular crawling [69]. In contrast, in case of monocytes and lymphocytes, the crawling process is mediated by LFA-1 [70]. Chemotactic migration mediated by integrins activates the p38 MAPK and phosphoinositide 3-kinase (PI3K) pathways. Heit *et al.* demonstrated chemotactic migration towards fLMP (N-Formyl-Met-Leu-Phe*)* which requires MAC-1, whereas LFA-1 is important for PMN migration towards IL-8, allowing PMN to navigate to sites of infections [71]. Furthermore, MAC-1 was found crucial for the migration of activated macrophages from the peritoneum to the lymphatics, suggesting that MAC-1 may play a central role in the resolution of acute inflammation [72].

CD11d/CD18 and $\alpha_4\beta_1$ were shown to be essential for leukocyte arrest during extravasation by binding to VCAM-1 [5]. Under steady-state conditions, CD11d/CD18 is not highly expressed and consequently might play a minimal role in VCAM-1 mediated extravasation compared to $\alpha4\beta1$. In contrast, under inflammatory conditions, CD11d/CD18 is highly expressed on peripheral leukocytes, which may enhance their importance to regulate extravasation [5]. Moreover, differential expression of CD11d/CD18 results in diverse migration patterns between M1 and M2 macrophages [61, 73]. High expression of CD11d confines M1 macrophages to sites of inflammation, while moderate CD11d expression on M2 macrophages is important for migration to mesenchymal tissues [73]. Thus, the relative expression of both integrins thereby might dictate their role in leukocyte extravasation [5, 74].

CD11c/CD18 and MAC-1 are known to play critical roles in cell adhesion via binding to their common ligand fibrinogen. Human monocytes, monocyte-derived macrophages, and monocyte-derived DC express both β_2-integrins. Under physiological conditions, CD11c/CD18 was reported to be dominant, conferring the adhesion to fibrinogen [53]. Moreover, CD11c/CD18 was shown to facilitate the adhesion and migration of activated memory B cells. This allowed activated B cells to establish close contact with fibrinogen-covered follicular DC (FDC). These contacts facilitate the binding of antigens stored by FDC, allowing B cells' survival and proliferation [75].

Immunological synapse and cell signaling

Besides their role in leukocyte trafficking, β_2-integrins also facilitate cell-cell contacts. LFA-1 is part of the IS and is positioned in the peripheral supramolecular activation cluster (p-SMAC). LFA-1 is linked to the intracellular proteins talin, kindlin-3, and Rap1, which stabilize the interaction between the TCR and major histocompatibility complex II (MHCII) loaded peptide at the center of the contact area (c-SMAC) [4, 76, 77]. Besides TCR and MHC, the cSMAC contains TCR-associated co-receptors like CD3, CD4, and CD8 [6, 78-80]. In addition, receptor pairs are required to transmit stimulatory signals from the APC (e.g., CD80, CD86) to antigen-specific T cells (CD28) [6]. The IS can be formed, for example, between T cells and APC as well as T cells and NK cells [4, 76, 81, 82]. Upon activation and binding to ICAM-1, LFA-1 initiates T cell signaling, thereby contributing to T cell activation and polarization of the T cell response [83] (summarized in more detail in chapter 1.2.3.). In addition to T cell activation, LFA-1 on activated $CD8^+$ T cells is involved in the killing of infected target cells by stabilizing the contact between the T cell and the target cell within the IS and sealing the contact zone to direct cytolytic granules [4, 83]. Furthermore, LFA-1 can function as so-called mechanical gate to attract granules containing perforin and granzyme and trigger their fusion with the synaptic membrane [84]. These degranulation mainly occur in regions of active force exertion within a cytotoxic synapse and suggest that mechanosensing releases cytolytic granules [84, 85].

Since many leukocyte populations express both β_2-integrins and their according ligands, and as integrins require activation to acquire a high-affinity binding state, analysis of integrin-mediated cell-cell interactions and interaction pathways can be complex. For example, activation of β_2-integrins is actively suppressed in DC by a mechanism that involves cytohesin-1 and cytohesin-1-interacting protein (CYTIP) that engages CD18 [6, 86]. Cytohesin-1 upregulates RhoA activity in DC, which is important for chemokine-induced conformational changes of β_2-integrins and consequently their activation [87]. CYTIP thereby traps Cytohesin-1 in the cytoplasm, which limits its interaction with β_2-integrins [88, 89]. Studies have shown that viral pathogens inhibit CYTIP in DC, resulting in higher LFA-1 activity, thereby increasing the cell adhesion of DC [6, 90, 91].

Moreover, CD11b is a component of the receptor complex that regulates toll-like receptor (TLR) 4 internalization into bone marrow-derived DC (BMDC) [6]. It can serve on one hand, as a positive regulator of TLR4-induced signaling in myeloid-derived DC [92]. In line, CD11b deficiency reduces DC activation via TLR4 upon LPS stimulation, which diminishes its T cell stimulatory capacity [6]. On the other hand, Querrey and coworkers [93] identified CD11b as a negative regulator of TLR4/MyD88 signaling in non-classical monocytes after lung transplantation in a murine model of primary graft dysfunction. When CD11b-deficient lungs were transplanted to recipient mice, lung injury in these mice was aggravated due to the increased production of the PMN-attractive chemokine CXCL2 and, consequently PMN infiltration into the lungs [93].

Correspondingly, Yee and Hamerman [94] reported that $CD18^{-/-}$ murine BM-derived macrophages and DC were hypersensitive towards various TLR ligands through exacerbated production of pro-inflammatory cytokines like IL-12 and IL-6. These findings

suggest an individual cell-specific role of β_2-integrins regarding their effect on TLR-mediated stimulation, depending on homeostatic versus inflammatory conditions [94]. In contrast, DC gene enrichment analysis of mice with a CD11c-specific deletion of β_2-integrins were characterized by the reduced expression of genes involved in inflammatory pathways, including tumor necrosis factor (TNF)-α signaling and interferon (IFN)-γ response [95]. Positive regulatory genes of TLR-induced signaling like *Wdfy1* (WD Repeat and FYVE Domain Containing 1) were upregulated, whereas *Comm2* (COMM Domain Containing 2) an inhibitor of NF-κB-dependent gene expression was significantly downregulated. In an EAE model, these CD18-deficient DC limited the T_H1/T_H17 auto-inflammatory response by the impaired induction of T-bet expressing T cells and a delayed and milder course of disease, suggesting the β_2-integrins on DC are responsible for the induction of inflammatory responses [95].
Further, MAC-1 clustering and activation was shown to initiate a gene program that promotes vascular inflammation. Shi *et al*. [96] demonstrated that MAC-1 deficiency resulted in reduced vessel wall inflammation after experimental angioplasty. In this study, MAC-1 was shown to trigger a Toll/IL-1 receptor superfamily–like signaling cascade 1, which induced nuclear factor k-light-chain-enhancer of activated B cells (NF-κB) activity. NF-κB is known to regulate genes encoding for cytokines like TNF-α, chemokines, and ICAM-1 [96]. Moreover, MAC-1-ICAM-1 interaction on human macrophages indirectly inhibited TLR signaling by promoting the expression of IL-10, SOCS (suppressor of cytokine signaling) 3, and ABIN-3 (A20-binding inhibitor of NF-κB activation 3). Additionally, Bednarczyk *et al.* demonstrated a dysregulation of the signal transducer and activator of transcription/suppressor of cytokine signaling proteins (STAT/SOCS) signaling axis in CD18-deficient DC. Mice with a CD11c-specific deletion of CD18 showed exacerbated production of the cytokines TNF-α and IL-6, as a result of enhanced activity of STAT-1, -3, and -5 and the reduction of SOCS proteins [95]. It is known that the activation of STAT through Janus kinase-mediated phosphorylation enhances the expression of cytokines. SOCS proteins thereby limit the cytokine production in leukocytes by the inhibition of STAT activation [95, 97]. Furthermore, MAC-1 impaired B cell receptor signaling to maintain autoreactive B cell tolerance and to reduce TLR-3-dependent NK stimulation [6, 98].

Immune suppression

β_2-integrins are also associated with different immune suppressive functions. In macrophages, β_2-integrins can inhibit TLR signaling via a negative feedback loop involving anti-inflammatory cytokines like IL-10 [4, 99, 100]. TLR stimulation activates phosphoinositide-3-kinase (PI(3)K)- and RapL-mediated inside-out signaling and activates β_2-integrins (see chapter 1.2.2.) [99, 101]. In turn, integrin outside-in signaling activates Src/Syk, which leads to the degradation of the TLR signaling transducers MyD88 and TIR-domain-containing adapter-inducing interferon-β (TRIF) and thereby downregulation of TLR signaling [99]. MAC-1-dependent suppression of TLR responses has been shown to be involved in the inhibition of the NF-κB pathway and MAPK pathway [94]. Furthermore, activated β_2-integrins have been found to suppress DC-mediated T cell

activation [89, 102, 103], and MAC-1 on APC can suppress antigen presentation and T_H17 differentiation, leading to immune tolerance [4, 104]. In addition, MAC-1 and CD11c/CD18 recognize iC3b-opsonized apoptotic cells, which prevented the inhibition of pro-inflammatory cytokine production through NF-κB inhibition [105]. LFA-1-mediated contact between T cells and DC enables actin-related cytoskeletal rearrangement. This conformational change causes DC lethargy, preventing their activation of T cell proliferation, which results in their suppression [106].

Phagocytosis

Phagocytes, which include PMN, monocytes/macrophages, and conventional DC, remove foreign particles, bacteria, and dead or dying cells from the circulation. Phagocytosis is a unique form of cell endocytosis whereby cells internalize solid particles through vesicles, including microbial pathogens [107-109]. MAC-1 and CD11c/CD18 are essential for the phagocytosis of opsonized pathogens by PMN and other phagocytic cells via β_2-integrin-induced Rho activity [4, 110, 111]. MAC-1 and CD11c/CD18 play important roles in the clearance of pathogens, cellular debris, and apoptotic cells opsonized with complement factor C3 and C4, respectively [6, 112]. Moreover, MAC-1 physically interacts with FcγRIIA in human PMN by rearranging the cytoskeleton and enables calcium-mediated signaling of FcγRIIA/B, resulting in phagocytosis and the release of pro-inflammatory cytokines [113]. The engulfment of apoptotic material via interaction of CD36 on apoptotic bodies with MAC-1 on DC suppressed their APC activity. Moreover, apoptotic bodies derived from tumor cells can be taken up by MAC-1 on myeloid cells, conventional DC (cDC) and NK cells, and CD36 on DC, which in either case induces tolerance [114]. MAC-1 and CD11c/CD18 are the most critical opsonophagocytic receptors of DC [6, 115].

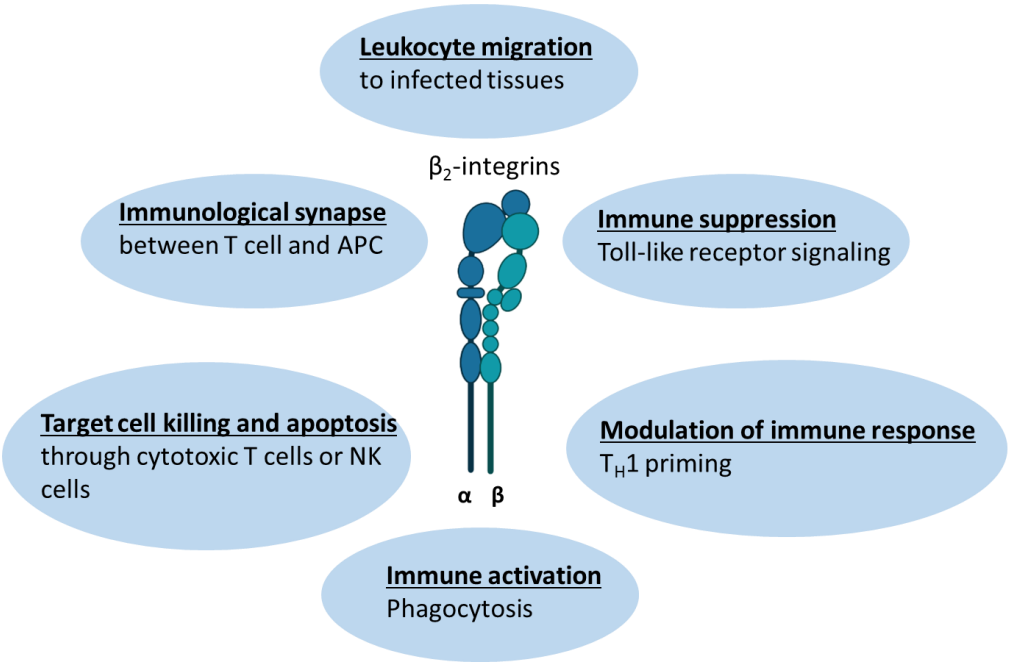

Figure 3 ***Main roles of β2-integrins in the immune system*** *(adapted from [4]). (Icon created with BioRender.com, accessed on 31 August 2023)*

1.2.2. Structure and activation of the β2-integrin LFA-1

The α and β subunit

LFA-1 is the only β2-integrin family member expressed on T cells [64]. The various α (CD11a-d) and the common β subunit (CD18) are each composed of three different domains: a long extracellular domain, a transmembrane domain, and a cytoplasmic tail [83] (Figure 4 A)

The extracellular domain of the α subunit is comprised of a globular headpiece and tailpiece. The former is composed of the αI-unit, β-propeller, and thigh domains. The lower tailpiece domains consist of the calf-1 and calf-2 regions [116, 117]. By expanding the cleft between the β propeller and the αI domain, LFA-1 is able to interact with larger ligands [6]. The top of the αI domain contains a metal ion-dependent adhesion site (MIDAS) that binds magnesium (Mg^{2+}) to coordinate glutamic acid residues of ICAM-1 [118], which is required for conformational changes and further integrin activation [116, 117].

The β subunit is connected to the cytoskeleton and transmits outside and inside signals [6]. The headpiece and tailpiece of the β subunit consist of the βI-domain, a so-called hybrid domain, a plexin-semaphorin-integrin (PSI) component, four epidermal growth factor (EGF)-like domains, and a β-tail. The βI-domain contains a MIDAS (like as the αI unit), which binds Mg^{2+} and forms a bridge with a ligand or the glutamate residues of the αI domain [6, 116, 117].

Activation of LFA-1

Inactive integrins are in the bent-close form with low affinity to their ligands. Upon ligand binding, LFA-1 undergoes sequential conformational changes via extended-closed with an intermediate affinity state towards extended-open with high ligand affinity (Figure 4 B) [117, 119, 120]. Inside the cell, integrin-binding adapter proteins like talin-1 and kindlin-3 attach to the cytoplasmatic domain of CD18 and trigger the high-affinity state of β_2-integrins [11]. The leg piece extends and opens the headpiece with the hybrid domain swinging out. The extension movements of the ectodomains occur between the thigh and calf-1 of the α subunit and between I-EGF1 and I-EGF2 of the β subunit. The αI-domain engages ICAM-1, which makes a glutamic acid residue in the linker region available to bind the βI MIDAS. The hybrid domain swings out, resulting in integrin activation [116, 117]. At the high-affinity state, integrins can cluster into many types of adhesion complexes. Integrin engagement and activation lead to bidirectional mechanotransduction and signaling across the plasma membrane of the cells [11].

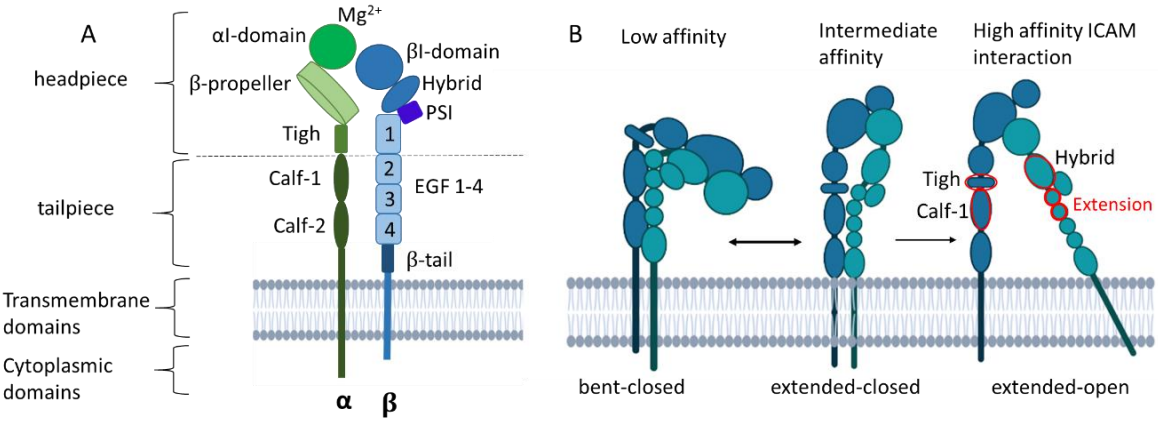

Figure 4 ***Structure of LFA-1 and conformational changes during integrin activation*** *(adapted from [116, 121]).* ***(A)*** *LFA-1 can be divided into three domains: an extracellular domain with a headpiece and tailpiece, a transmembrane, and cytoplasmic domain.* ***(B)*** *LFA-1 undergoes three conformational changes from bent-closed towards extended-closed with intermediated affinity state and extended-open with high affinity to ligands. Upon ligand binding, the headpiece swings out of the hybrid domain with intermediate affinity. The extension and high-affinity state occur between the tigh and calf-1 domain of the α subunit, the hybrid, and EGF1-2 of the β-domain (shown in red). (Icons created with BioRender.com, accessed on 31 August 2023)*

Inside-out signaling

The multistep activation process from bent-close to extended-open, including the process through which intracellular signals induce integrin activation that favors its extension, is called 'inside-out' signaling [11, 122]. Inside-out signaling is mediated by cytokine/chemokine stimulation, TCR activation, or through phorbol esters, leading to downstream signaling and cytoskeletal rearrangements [123] (Figure 5A).

Inside-out triggering leads to the recruitment of Rap1-GTP. Rap-1 activation is mediated by the regulator of adhesion and polarization enriched in lymphocytes (RAPL) molecule that engages CD11a [6, 122]. RIAM (Rap-1-GTP interacting adaptor molecule) engages both active Rap-1 and the β subunit [124] and binds the actin cytoskeletal adaptors talin-1

and kindlin-3 [6, 121], which stabilizes the intermediate and high-affinity state by binding to different membrane-motifs of the β subunit [11, 121, 125] (Figure 5 B). Talin is the main intracellular binding protein that disrupts the interaction between the α and the β subunits, thereby extending the leg piece of the β subunit [126]. Talins' interaction with F-actin is important to anchor LFA-1 to the actin cytoskeleton [125]. Additional binding of paxillin and vinculin forms a frame for interaction with cytoskeletal elements [121]. Both are adaptor proteins with multiple binding sites for other adhesion components like talin and focal adhesion kinase (FAK). FAK is a cytoplasmic tyrosine kinase that is activated by intramolecular interactions and in turn, phosphorylates paxillin, promoting exposure of additional protein docking sites that can regulate downstream processes such as migration and chemotaxis [11].

Outside-in signaling

Additionally, rearrangement of the cytoskeleton and intracellular responses due to integrin binding to ligands induce 'outside-in' signaling [127] (Figure 5A). This leads to the acquisition of a high-affinity state of LFA-1 [123, 128, 129]. ICAM binding, actin-derived adhesive forces as well as extracellular interferon-stimulated gene 15 (ISG1), an ubiquitin-like secreted protein, and Mg^{2+} can induce IFN-γ expression by binding the αI-domain, thereby promoting outside-in signaling [121, 130]. Outside-in signaling modulates gene expression, cell proliferation, survival, and apoptosis [11, 131].
In response to activation, cytoskeletal proteins and kinases, as well as key adapters, assemble at the cell membrane, forming adhesion complexes that transfer signals from the ECM to the cell surface [11]. Adapter proteins in LFA-1-mediated signal transduction pathways can be divided into structural adaptors, scaffolding adaptors, and catalytic adaptors. Structural adapters such as talin-1 recruit the protein complex Arp2/3 via association with vinculin, together facilitating cytoskeletal reorganization. This so-called `molecular clutch` is crucial for the mechanotransduction and activation of the cell [11, 127]. Scaffolding adaptors like adhesion and degranulation-promoting adapter protein (ADAP) couple LFA-1 and regulate its IL-2 secretion, F-actin clustering, cell polarization, and T cell motility. Catalytic adaptors facilitate the catalysis of specific reactions like targeting protein kinases A (PKA) and protein kinases C (PKC) to the membrane, cytoskeleton, and filopodia of migrating T cells [127].

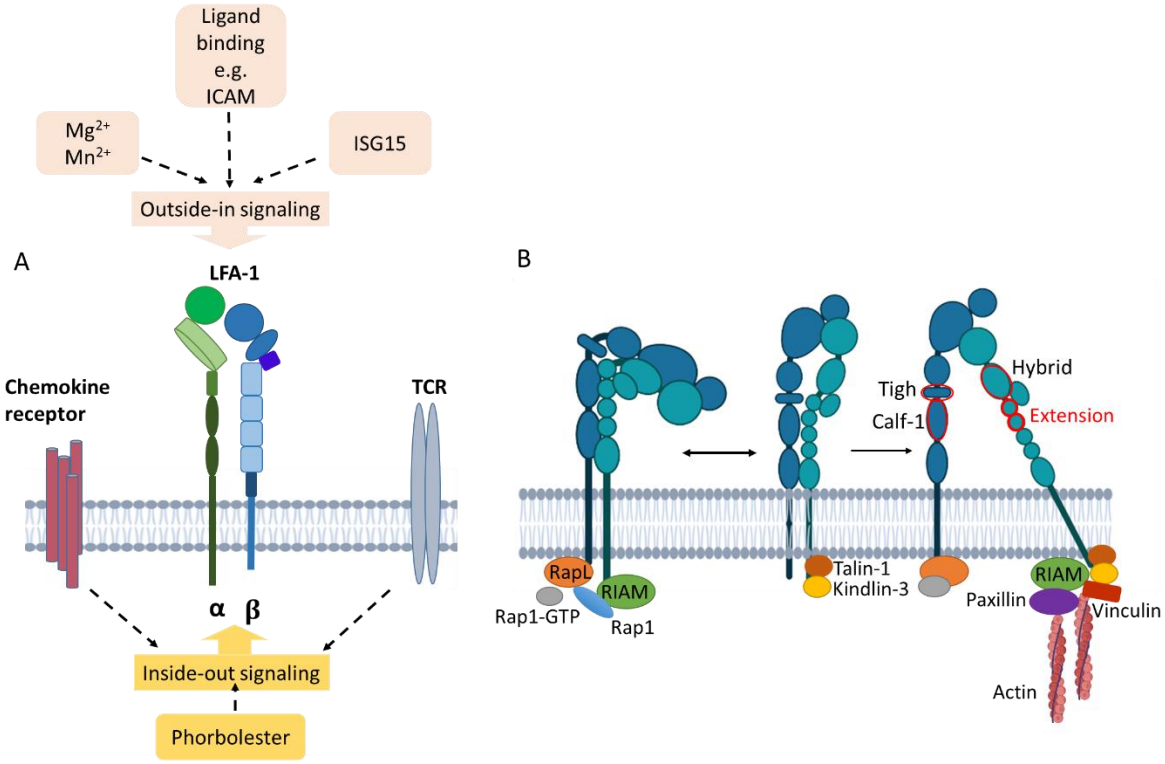

Figure 5 ***Triggering bidirectional inside-out and outside-in signals of LFA-1. (A)*** *Inside-out signaling is triggered by chemokine/cytokine receptors, TCR stimulation, or phorbol ester from within the cell, resulting in activation of LFA-1. Outside-in signaling is induced by ligand-binding such as ICAM-1 as well as ISG15 and Mg^{2+}/Mn^{2+} [121, 127].* ***(B)*** *Inside-out signaling through chemokine or TCR stimulation recruits Rap1-GTP. RAPL engages CD11a and activates Rap-1 [6]. RIAM engages Rap-1 and the β subunit. The β subunit binds talin-1 and kindlin-3, stabilizing the intermediate and high affinity state. Additional binding of paxillin and vinculin forms a frame for interaction with cytoskeletal elements. Outside-in signaling activates adapter proteins such as talin-1, which mediate downstream signal- and mechanotransduction [121, 127]. (Icons created with BioRender.com, accessed on 31 August 2023)*

1.2.3. Specific roles of LFA-1 on T cells

T effector cells (T_{eff}) play an indispensable role in the defense against infections, whereas Treg serve to maintain immune homeostasis. Therefore, targeted migration (`homing´) of T cells into peripheral tissue is important for immune surveillance. LFA-1 binds ICAM expressed by vascular endothelial cells and other leukocytes, like APC, within the IS [121]. LFA-1 also facilitates T cell entry into lymphatic tissues to enable migration to sites of inflammation and infection [132, 133]. The entry of naïve lymphocytes into the lymph node (LN) requires their arrest on specialized post-capillary venules, the so-called high endothelial venules (HEV), via LFA-1 interactions with ICAM-1 and ICAM-2 [121, 134]. Activation-dependent conformational changes determine the binding affinity of LFA-1 [6, 128]. At its low-affinity state (bent-closed formation), LFA-1 does not bind ICAM, thereby enabling T cell circulation through the bloodstream. Chemokines like chemokine ligand (CCL) 19 and CCL21 secreted by activated endothelial cells or DC activate LFA-1 via inside-out signaling and allow its high-affinity (extended-open) binding to ICAM-1. This is essential for binding peptide-MHC complexes presented on the DC within the IS [121, 135, 136]. Normally, T cells engage with MHC via multiple short-term contacts called

kinapses [137] before long-lasting contacts are formed for their full activation. The integrin conformation change can lead to a 10,000-fold affinity increase of LFA-1 to ICAM-1 on APC [83, 138]. Bleijs and co-workers observed that low-affinity binding of ICAM-3, together with high-affinity binding to ICAM-1, induced large cluster formations of LFA-1 [139]. Moreover, low-affinity LFA-1/ICAM-3 interactions contributed to stabilize the LFA-1/ICAM-1 cell-cell contact. The high-affinity adhesiveness of LFA-1 is essential for the full activation of T cells [121]. Chen *et al*. demonstrated strong LFA-1-dependent adhesion between human Treg ($CD4^+CD127^{low}CD49D^-CD25^+$) and murine Treg ($CD4^+CD25^+$) with APC leading to cytoskeletal rearrangements in the latter and a lethargic state of DC, which resulted in impaired T cell priming [106] (Figure 6 A). These findings support a LFA-1 contact-dependent suppressive mechanism of Treg [106]. However, in this study the cocultured murine $CD4^+CD25^+$ T cells were considered as Treg but may actually comprise also T_{eff}.

Moreover, LFA-1/ICAM interaction influenced human T cell polarization by modulating T_H1 and T_H2 responses [123, 140]. An imbalance between T_H1 and T_H2 has been associated with several autoimmune diseases, including, for example, MS, rheumatoid arthritis, and type-1 diabetes [141]. In this regard, LFA-1 signaling together with TCR stimulation triggered glycogen synthase kinase (GSK)3β-dependent Notch1 activation by γ-secretase proteolytic cleavage and upregulated T-bet expression favoring a shift to T_H1 cytokine production, specifically of IL-2 and IFN-γ [141] as depicted in Figure 6B. Notch is known to be a critical differentiation factor for T cell effector function and supports the so-called `second touch hypothesis´ [142]. This theory suggested that signaling induced by LFA-1/ICAM interaction fine-tunes the immune response via Notch1 to enhance T cell effector priming and migration to sites of inflammation [123].

Furthermore, it was shown that LFA-1 cross-linking phosphorylated STAT3, which is associated with a tubulin depolymerizing protein (stathmin), controlling the cytoskeleton reorganization process in migrating human T cells [143]. The STAT family comprises transcription factors that are activated by many cytokines and growth factors. STAT3 is activated by tyrosine phosphorylation and translocation out of the nucleus [127, 144]. In another study, LFA-1 stimulation and subsequent STAT3 activation induced transcriptional genes like *SMAD7* (SMAD Family Member 7), *SMURF2* (E3 ubiquitin-protein ligase), *SKI (*SKI Proto-Oncogene), and *SKIL* (SKI Like Proto-Oncogene) that are associated with TGF-β pathway inhibition. Blockade of TGF-β signaling resulted in the reduction of Treg in the periphery [145] and the polarization of human and murine T cells into functional phenotypes of T_H17 ($Foxp3^+ROR\gamma t^+$) or induced $Foxp3^+$ (iTreg) and the secretion of IL-2 [140] (Figure 6 C). In contrast, TGF-β is necessary for the conversion of iTreg from naïve T cells in an *in vitro* culture [146]. Altogether, these findings outline the complexity of LFA-1 signaling to modulate immune responses.

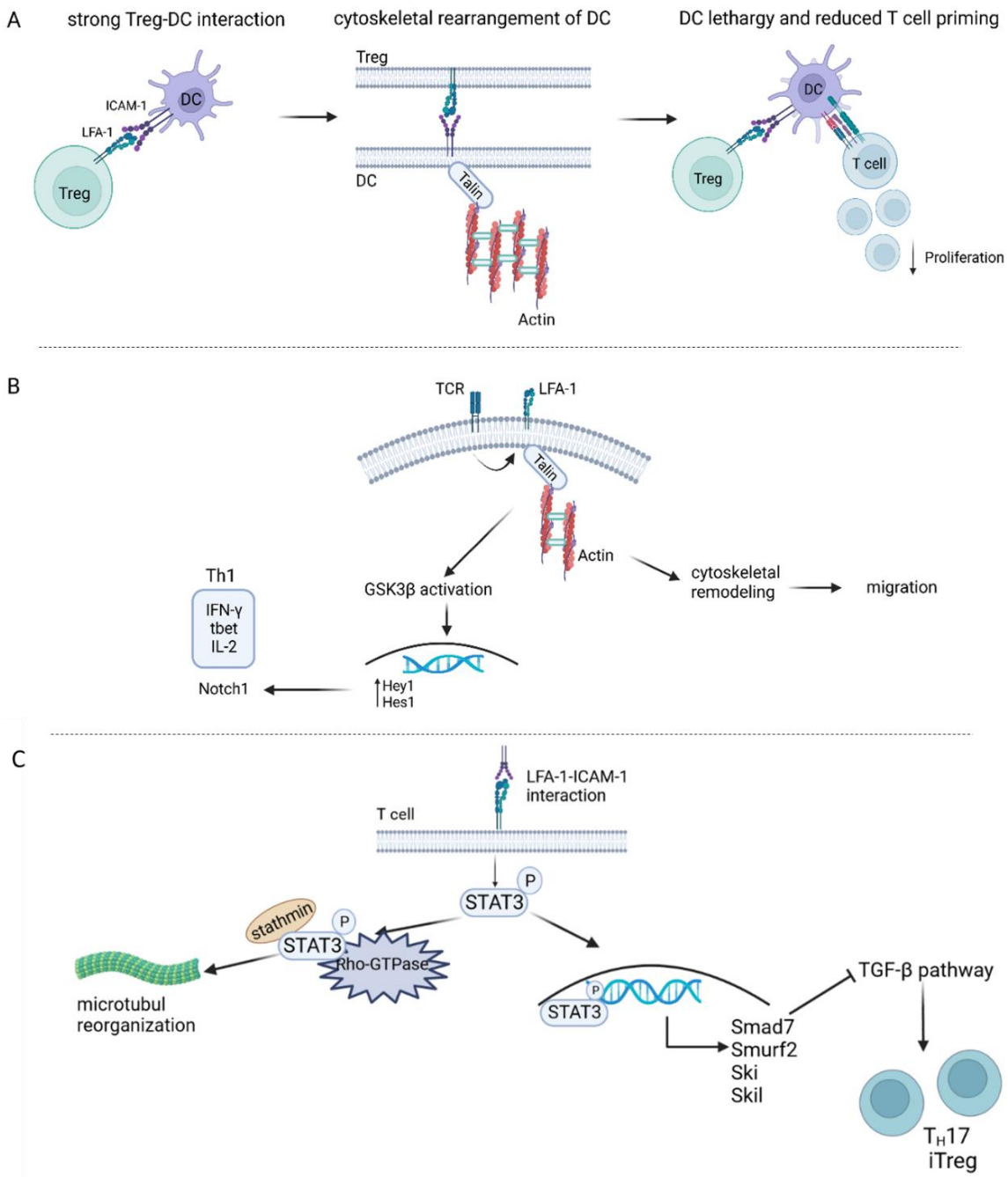

Figure 6 ***Role of LFA-1-mediated contact for suppression and T cell response. (A) LFA-1-mediated suppression of T cells****. Long-lasting high-affinity contact of Treg and DC via LFA-1-ICAM-1 interaction activates cytoskeletal rearrangement of Fascin-1 dependent actin polarization in DC. This conformational change causes DC lethargy, preventing their activation of T cell proliferation. This mechanistic control of T cell activation underlines a Treg-mediated DC suppression in a LFA-1 contact-dependent manner [106].* ***(B) LFA-1 signaling drives T_H1 response in T cells****. TCR inside-out-signaling leads to the binding of Talin-1 to the β_2-tail of LFA-1, enabling its high-affinity activation. Following this, LFA-1 triggers downstream signaling pathways that control cytoskeletal rearrangement and migration of activated T cells. LFA-1 also induces glycogen synthase kinase (GSK)3β-dependent Notch1 activation and produces T_H-1-related cytokines and transcription factors [121, 140, 141].* ***(C) LFA-1 triggers STAT3 activation and interrupts TGF-β signaling****. LFA-1 triggers STAT3 activation by phosphorylation (P), translocating STAT3 to the nucleus, and its interaction with stathmin and Rho GTPase controls microtubule dynamics. In the nucleus, STAT3 upregulates the expression of the TGF-β-inhibiting transcription factors Smad7, Smurf2, Ski, and Skil. These proteins hinder TGF-β-mediated inhibition of IL-2 secretion and Tcell differentiation into T_H17*

or iTreg cells [127, 143] (adapted from [129]; created with BioRender.com, accessed on 7 March 2023 and 31 August 2023).

1.2.4. Targeted therapies of LFA-1

An elevated expression of LFA-1 on T cells has been shown to correlate with systemic sclerosis and lupus, as well as rheumatoid arthritis and autoimmune thrombocytopenia [147]. Monoclonal antibodies (mAb) interfering with LFA-1/ICAM-1 interactions have been extensively analyzed in numerous pre-clinical studies [148]. LFA-1 signaling interruption is often combined with additional therapies like simultaneous blockade of either ICAM-1 or CD40L. For example, treatment with anti-LFA-1 in combination with anti-CD40L mAb after islet transplantation *in vivo* resulted in a tolerance that was defined as ‘dominant`, which was not observed in case of monotherapy with either murine mAb [149].

Furthermore, in a clinical phase II study, anti-LFA-1 and anti-CD2 mAb therapy in combination with T cell depletion of the BM prevented rejection of transplanted BM for acute lymphoblastic leukemia. [150]. CD2 is known to upregulate LFA-1 avidity and, therefore the adhesion to the cells [151]. Anti-LFA-1 and anti-CD2 mAb therapy might interrupt optimal cell-to-cell interaction and thereby intracellular signaling. However, this effect was not observed in adults, as published in an earlier study [152].

Efalizumab, a humanized IgG1 anti-LFA-1 antibody, has been used in several clinical studies investigating moderate plaque psoriasis [148, 153, 154]. It is directed against CD11a and blocks LFA-1/ICAM-1 interaction in order to suppress T cell priming and effector functions of immune cells, resulting in diminished inflammatory cell recruitment and reversal of keratinocyte hyperplasia at psoriatic lesions [154-156]. Despite this beneficial effect, Efalizumab was not effective against psoriatic arthritis [157]. It was less effective in psoriasis than established therapies including, for example cyclosporine and ultraviolet radiation-based therapies [158]. In 2009, Efalizumab was withdrawn from the market because of high risk of John Cunningham polyomavirus reactivation and development of progressive multifocal leukoencephalopathy in patients under long-term administration [159-161].

By now, LFA-1 targeted therapies aimed to modulate the activation state of T cells. However, as mentioned above β_2-integrins exert their function in a cell-specific manner, for example, limit T cell activation when expressed on DC [162], but activate T cell function when expressed on T cells [4].

1.3. Treg subsets and functions within the immune system

Treg are a specialized subgroup of $CD4^+$ T cells and can be divided into two main subsets based on their origin. Naturally occurring thymus-derived Treg (tTreg), as well as peripherally induced Treg (pTreg) [163, 164]. tTreg have a TCR repertoire with a high affinity to autoantigens and maintain peripheral tolerance by suppressing autoreactive $CD4^+$ T cells [163]. In general, Treg are characterized by constitutive expression of the cell surface α chain of the high affinity IL-2 receptor (CD25) and the transcription factor Foxp3. tTreg development requires activation of the TCR and upregulation of markers like

glucocorticoid-induced TNF receptor-related (GITR), the TNF family member OX40, TNFR2, and CD25. Next, IL-2 and STAT5 are responsible for differentiation into mature Foxp3-expressing tTreg [165].

In contrast to tTreg, pTreg originate extrathymically from naive $CD4^+$ $Foxp3^-$ T cells upon TCR stimulation in the presence of TGF-ß and IL-10. They are mostly generated in response to DC which present self and harmless environmental antigens in the absence of costimulation [164, 166, 167]. Unlike tTreg, pTreg are negative for the ikaros family member HELIOS and Neuropilin-1 (NRP1) [168]. In addition, *ex vivo* Treg can be induced (iTreg) in an *in vitro* culture from naive $CD4^+$ $Foxp3^-$ T cells by the addition of exogenous TGF-ß [169, 170]. All aforementioned Treg subsets exert their suppressive function in a Foxp3-dependent manner.

Foxp3-independent Treg subsets develop in the periphery. These Treg subsets comprise type 1 pTreg (Tr1) and iTr35 [169, 171]. Tr1 Treg produce high levels of the anti-inflammatory cytokine IL-10 and co-express the surface markers lymphocyte-activation gene 3 (LAG 3) and CD49b [172, 173]. iTr35 Treg are induced by IL-35, and in contrast to Tr1 Treg mediate suppression via IL-35. These unique Treg subsets are known to regulate infectious [174], as well as transplantation tolerance, and play an important role in suppressing autoimmunity [175-177].

In non-lymphoid tissue, Treg are defined as tissue-resident Treg. These Treg are identified by the expression of the interleukin 33 (IL-33) receptor (ST2) and killer cell lectin-like receptor subfamily G1 (Klrg1), named "tisTregST2". These ST2-positive tissue Treg express tissue-regenerative factors such as Amphiregulin (Areg), alongside T_H2-associated factors, including high levels of the transcription factor Gata3 [178]. Tissue homeostasis and specific functions of ST2-positive Treg cells have been characterized in different non-lymphoid tissues like visceral adipose tissue (VAT), muscle, colon, and skin [179-182]. All these Treg subtypes are thought to be essential for maintaining tissue homeostasis and immune tolerance [169, 180]. Figure 7 presents an overview of the mentioned Treg subsets and their key markers in different tissues.

Autoimmune reactions are often characterized by a reduced number of functionally active Treg [183]. For example, reduced levels of Treg have been described in psoriatic arthritis [184], systemic lupus [185, 186], and Kawasaki disease [183, 187]. Treg can suppress $CD4^+$ T cell activation and proliferation both in a contact-dependent and -independent way. Co-culturing Treg with APC and antigen-specific responder $CD4^+$ and $CD8^+$ T cells in the presence of specific antigen suppresses responder cell proliferation and reduces IL-2 production. Treg consume IL-2 produced by the responding T cells via CD25 thereby inhibiting their proliferation [188].

In vitro studies have shown that Treg confer suppression of T_{eff} cells y a variety of different mechanisms like anti-inflammatory cytokines (e.g. IL-10, TGF-β) [189, 190], induction of apoptosis [191, 192], metabolic pathways [193, 194] and modulation of the maturation and function of APC [189, 195-198]. However, Treg can also support T_H responses by reflecting the functions of different T_H cell subsets. For example, T_H1-like Treg produce IFN-γ, T_H17-like Treg generate IL-17, whereas T_H2-like Treg produce IL-4 [199]. The β_2-integrin receptor LFA-1 has been demonstrated to be critical for Treg differentiation [200].

In many cases, Foxp3 is a crucial control gene in the development and function of Treg and T_{eff} as well. [121, 183, 201-203]. Indeed, humans with a mutation in the *Foxp3* gene lack functionally active Treg and consequently develop immune dysregulation, polyendocrinopathy, and enteropathy X-linked (IPEX) syndrome that is linked to several autoimmune diseases like atopic dermatitis, IBD, and type 1 diabetes mellitus [201]. In IPEX patients, Treg can be present, but their phenotype is unstable and these Treg are impaired in their function. Consequently, such Treg are unable to inhibit the activation of T cells, their proliferation, and cytokine production.
Moreover, human Foxp3-deficient T_{eff} cells had a higher proliferative potential, showed altered TCR signaling response, and a reduced naïve T cell compartment that skews toward T_H2 immune response [204]. Additionally, the frequency of autoreactive B cells is increased, and IgA and IgE production, as well as the production of organ-specific autoantibodies is elevated. In scurfy mice, a loss-of-function mutation of *foxp3* results in an IPEX-like autoimmune phenotype [204].

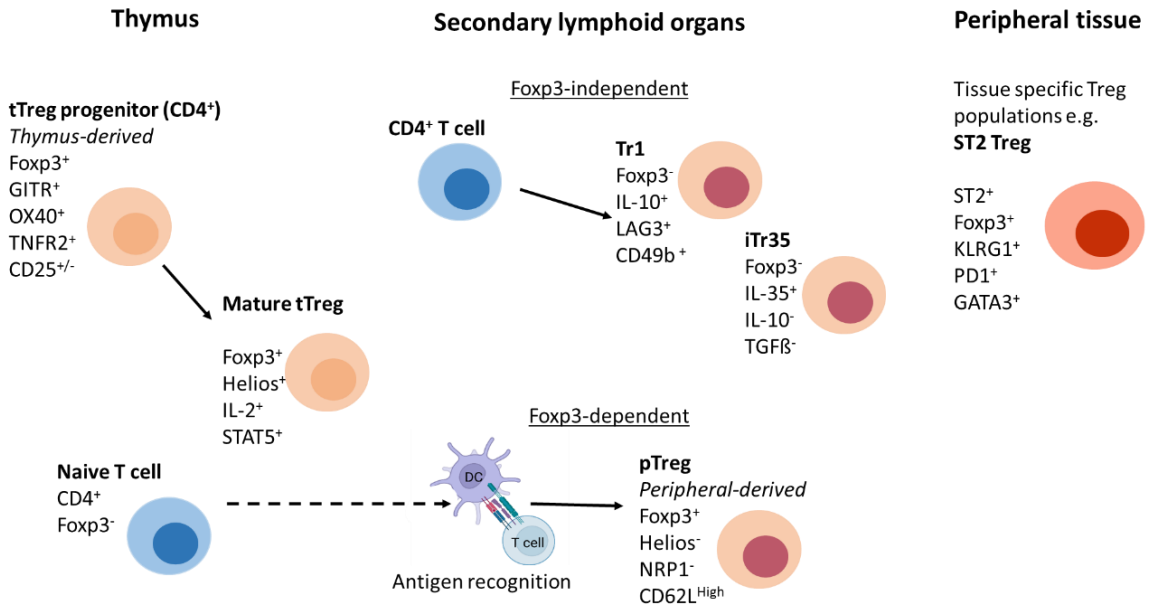

Figure 7 ***Overview of relevant Treg subsets and their key markers in thymus and periphery.*** *(Icon created with BioRender.com, accessed on 31 August 2023)*

1.4. Leukocyte Adhesion Deficiency Type-1 (LAD-1)

The crucial role of β_2-integrins for the immune system is emphasized by the phenotype of patients suffering from LAD-1. LAD-1 is a rare hereditary disorder that affects only one per million people worldwide [205]. In LAD-1 patients, a mutation in the CD18 gene leads to attenuated expression of functional heterodimeric β_2-integrins, resulting in impairment of leukocyte migration into tissue [206]. In some patients, CD18 expression differs between cell types and accordingly the severity of LAD-1 can be subdivided into a mild (>30%), moderate (2%-30%), and severe form (<2%) [207]. About 75% of patients with severe LAD-1 die by the age of 2 years. Patients with moderate LAD-1 survive childhood,

but their mortality amounts to 50% by the age of 40 years [208]. Cell type-dependent differential CD18 expression results in a very heterogeneous manifestation of the clinical phenotype predominantly related to defects in the PMN migration and pathogen-killing functions of PMN [209].

The most prevalent symptoms are recurrent bacterial infections of the skin, periodontitis, and poor wound healing [210-212]. In addition to these immunodeficiency symptoms, LAD-1 patients may suffer from autoimmune phenomena like IBD, type-1 diabetes or nephritis [213, 214]. Thus, the clinical symptoms of LAD-1 reflect immunodeficiency as well as autoimmunity. Until now, the only curative therapy is allogeneic hematopoietic stem cell transplantation [215, 216].

Patients with wildtype β_2-integrin suffering from autoimmune diseases like IBD presented with diminished Treg frequencies as described above [183]. It has been demonstrated that LAD-1 patients with IBD presented with a higher number of $Foxp3^+$ Treg, but these displayed reduced suppressive activity [217]. This finding suggested that β_2-integrins critically regulated Treg biology.

1.5. β_2-integrin deficient mouse models

The export of functional integrins from the endoplasmic reticulum is dependent on the formation of the β_2-integrin heterodimer. In the absence of the β subunit expression, the α subunit remains unstable in the cytoplasm and is degraded [218].

Different transgenic mouse models have been established by deleting either one of the various α subunits or the common β subunit to understand the role of the given β_2-integrins for leukocyte functions. In the following chapter the characteristics of the available β_2-integrin-deficient mouse models are compared, focusing on the clinical phenotype and the consequences of LFA-1 deletion on Treg (Figure 8).

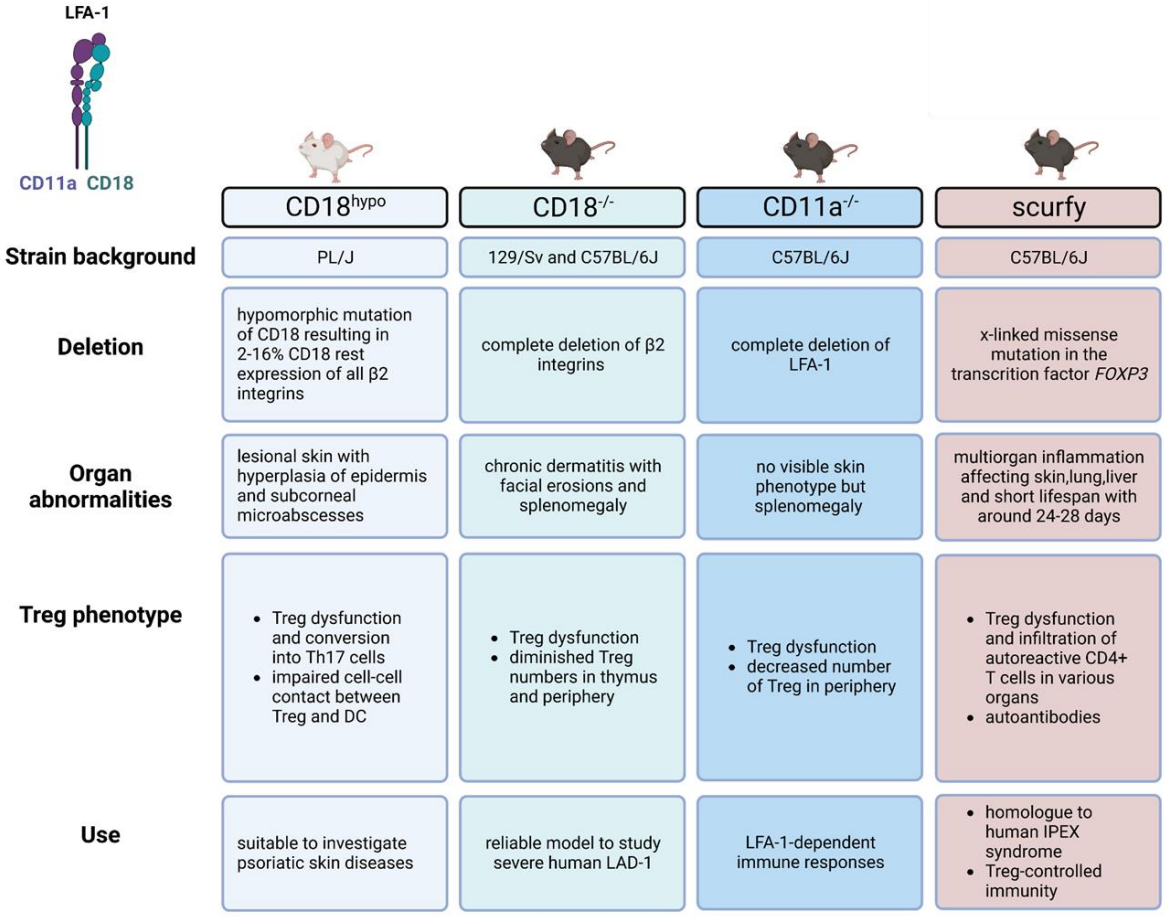

Figure 8 ***β2-integrin deficient mouse models in comparison to Foxp3-deficient scurfy mice.*** *(Adapted from [129]; created with BioRender.com, accessed on 7 March 2023)*

1.5.1. CD18^{hypo} mouse

CD18 hypomorphic (CD18^{hypo}) mice were originally established in 1993 [219]. An insertion mutation attenuated CD18 expression by 84-98%. This low-level CD18 expression is comparable to those levels observed in patients with a moderate form of LAD-1 [219, 220]. CD18^{hypo} mice display increased PMN counts and a reduced resistance to chemically induced peritonitis [220]. When backcrossing CD18^{hypo} mice (129Sv/C57BL/6J background) with PL/J mice, the offspring developed a chronic skin disorder characterized by hyperplasia of the epidermis, subcorneal microabscesses, as well as T cell infiltrates in the dermis, very reminiscent of human psoriatic dermatitis [221]. As no infectious agents were found on lesional skin, and the phenotype could be suppressed by corticosteroids, this skin disorder might be autoinflammation- or autoimmune-driven [222]. Only mice with a homozygous CD18^{hypo} PL/J mutation developed this phenotype, suggesting that the disorder is recessively inherited. However, backcrossing between the susceptible PL/J CD18^{hypo} strain and the resistant C57BL/6 CD18^{hypo} strain resulted in a F1 generation with no phenotype. When crossing back mice of this F1 generation with CD18^{hypo} PL/J mice, the F2 mice developed skin lesions suggesting that other yet unknown modifier genes were responsible for the development of the skin phenotype [221].

The skin disorder in these mice is mainly T cell-driven as the abundance of activated $CD4^+$ T cells secreting high levels of the T_H1-type cytokine IFNγ in the skin was increased and their depletion resulted in a complete resolution of psoriatic dermatitis [221]. Furthermore, the increased activation state of $CD4^+$ $CD25^+$ T cells suggested an altered T cell biology. Regarding Treg, $CD18^{hypo}$ PL/J mice had a reduced output of tTreg and under iTreg promoting conditions (naïve) T cells rather converted into T_H17 cells *in vitro* and *in vivo* [223]. Interestingly, cocultures of Treg derived from Balb/c mice and allogenic DC from $CD18^{hypo}$ PL/J mice showed no increase of T_H17-like Treg during coculture, indicating that reduced LFA-1 expression on Treg itself drives the pro-inflammatory milieu [223].

Moreover, reduced CD18 expression impaired cell-cell contacts between Treg and DC, and $CD18^{hypo}$ Treg failed to suppress DC-mediated activation of naïve T cells [224]. Reduced tTreg and iTreg numbers in $CD18^{hypo}$ mice, as well as the impaired suppressive activity of Treg converting into T_H17-like cells, may contribute to the activation of autoreactive $CD4^+$ T cells, which also displayed a higher activation state in lesional compared to healthy skin, thereby driving psoriasis-form dermatitis [223].

In line with these observations in $CD18^{hypo}$ mice, LAD-1 patients have been reported to suffer from psoriatic skin lesions. These skin infections progress mainly through polymicrobial infections including anaerobic organisms. Rarely, LAD-1 patients can develop pyoderma gangrenous, a chronic progressive necrosis of the skin [225]. As reduced CD18 expression levels have also been identified on leukocytes in psoriasis patients [223, 226-228], $CD18^{hypo}$ mice constitute an appropriate tool to investigate psoriatic skin disease in the context of attenuated CD18 expression, as well as the role of CD18 in chronic inflammatory processes.

1.5.2. $CD18^{-/-}$ mouse

The targeting construct that introduced a hypomorphic allele in case of $CD18^{hypo}$ mice was also used to insert a replacement mutation to generate the $CD18^{-/-}$ mouse strain with an originally mixed 129/Sv and C57BL/6J background [229]. This construct contains a neomycin-resistance cassette disrupting the 5′ boundary of exon 3, therefore preventing the synthesis of CD18 protein. Thus, $CD18^{-/-}$ mice completely lack β_2-integrins [230] and share essential characteristics with severe LAD-1 patients, including spontaneous mucocutaneous infections [229]. $CD18^{-/-}$ mice were characterized by chronic dermatitis with facial and submandibular erosions, splenomegaly, and PMN lymphadenopathy [230]. The absence of CD18 in these mice was accompanied by decreased tTreg and pTreg numbers, and these Treg populations were devoid of *in vitro* suppression activity and consequently failed to protect from colitis induction *in vivo* [64]. Therefore, CD18 plays a crucial role in the suppressive function of Treg. Furthermore, as described above, LFA-1 on T cells is critical for the formation of an IS with APC [121] and is required for the strong adhesion of Treg to DC [106]. With regard to the latter, Chen *et al.* demonstrated an indispensable role of LFA-1 on Treg to facilitate adhesion to DC and to prevent conventional T cells (T_{conv}) binding to DC due to an accumulation of cytoskeletal components within the DC/Treg contact area as an indirect suppressive mechanism [106].

Lack of suppressive function in $CD18^{-/-}$ Treg was also observed in LAD-1 patients, correlating with IBD in these patients [217].
Interestingly, backcrossing $CD18^{-/-}$ mice to the PL/J background did not result in psoriasis-form dermatitis as described for $CD18^{hypo}$ mice [221]. As mentioned above, pathogenic $CD4^+$ T cells might be responsible for the phenotype of $CD18^{hypo}$ mice [221]. $CD18^{-/-}$ $CD4^+$ T cells were not able to extravasate to sites of inflammation and, therefore could not exert inflammatory effector function in the skin [221, 231]. This was confirmed by Grabbe *et al.* in a T cell-mediated allergic contact dermatitis model [232]. Injection of hapten-induced T_{eff} cells isolated from hapten-sensitized $CD18^{-/-}$ mice directly into the ears of $CD18^{-/-}$ mice restored the ear swelling phenotype of these mice [232, 233]. Therefore, LFA-1 was not required for the priming of naïve T cells, but was important for their extravasation as previously reported [232].
Hence, β_2-integrin deficiency manifests a dysregulation of the immune homeostasis and contributes to the inflammatory phenotype of $CD18^{-/-}$ mice. These aberrant T cell-mediated immune responses in $CD18^{-/-}$ mice suggest that the pathology in LAD-1 patients may not only be due to defects in PMN but that T cell defects may contribute to many clinical symptoms [232]. Thus, $CD18^{-/-}$ mice are an appropriate model to study the relevance of β_2-integrins for the differentiation and function of leukocytes and constitute a reliable model for severe human LAD-1 in the context of chronic inflammation [230].

1.5.3. $CD11a^{-/-}$ mouse

In LFA-1 null mice (C57BL/6J background) both alleles of β_2-integrin α chain encoding CD11a are disrupted [234]. The gene targeting construct replaces exons 2-6, which encode the signal peptide and the extracellular region of CD11a. Initial characterizations of LFA-1-deficient mice revealed no obvious skin phenotype but splenomegaly and decreased LN size. Lymphocyte frequencies and $CD8^+$ T cell cytotoxic responses were normal [234]. Further studies described lower Treg numbers in lymphatic organs like spleen and LN. In contrast to $CD18^{-/-}$ mice which displayed a lower output of tTreg [64], $LFA^{-/-}$ mice showed increased Treg frequencies/numbers in the thymus as compared to wildtype (WT) mice [200]. However, LFA-1 seems to be important for Treg induction in the periphery since LFA-1 deficient mice showed limited capacity for the conversion of $CD4^+CD25^-$ T cells into functional Treg in peripheral tolerance induction assays. Further, similar to $CD18^{-/-}$ Treg [64] also $CD11a^{-/-}$ Treg failed to suppress T cell activation *in vitro* and were not able to suppress inflammation in experimental colitis [200]. Therefore, both strains share essential characteristics which delineate LFA-1 as critical for Treg functions.
Furthermore, it has been proposed that Treg might suppress T_{conv} activation in two distinct steps: Treg form aggregates with DC in a LFA-1-dependent manner, resulting in active downregulation of CD80/CD86 expression on DC in both a LFA-1 and CTLA-1-dependent way [235]. This suppression of DC maturation prevented antigen-reactive T cells from being activated, as reported in *in vitro* studies [235]. In agreement, LFA-1 deficiency abrogated the aggregation of Treg with DC. Accordingly, the absence of LFA-1 on Treg prevented the downregulation of CD80/CD86 expression on DC. The Treg-dependent DC suppression in this context prevented T cells from getting activated [235].

Further, *in vivo* experiments with CD11a$^{-/-}$ mice have shown an aggravated course of myelin oligodendrocyte glycoprotein (MOG)-dependent EAE [236]. Both in human MS and murine EAE, the (auto)inflammatory phenotype is mediated mainly by CD4^{+} T_H17 cells. Reduced numbers of Treg in the inflamed CNS of CD11a$^{-/-}$ mice correlated with enhanced expansion of autoreactive T cells [236]. In contrast to earlier data [200], the reduced number of Treg was associated with a lowered thymic output of Treg [236], which emphasized a fundamental role of LFA-1 in the generation of Treg and their homeostasis. In line, on one hand, the transfer of encephalogeneic WT T cells to CD11a$^{-/-}$ mice with reduced numbers in the CNS caused a severe EAE course. On the other hand, transferring encephalogeneic CD11a$^{-/-}$ T cells into WT mice resulted in a reduced course of EAE. This fact confirms that T cells require LFA-1 to get primed and to facilitate an inflammatory response [237].

2. Thesis objectives

β_2-integrins play important roles in cell-cell communication between leukocytes and in the extravasation of leukocytes from blood into inflamed tissues [7, 132, 133]. Mice that lack all β_2-integrins due to mutations in the *Itgb2* gene that encodes the CD18 subunit of the β_2-integrins display a substantial T cell activation and extravasation defect but at the same time develop generalized lymphocyte activation and features of autoimmunity [229, 231]. This work aimed to understand the role of LFA-1, as the only β_2-integrin expressed by T cells, for Treg functions. We hypothesized that β_2-integrin-deficient Treg are functionally distorted and thereby may substantially contribute to the manifestation of (auto)inflammatory skin diseases. To overcome the limitations of the existing mouse models, displaying constitutive knockouts (KO), we generated mice specifically lacking CD18 on Treg ($CD18^{Foxp3}$), resulting in LFA-1 deficiency. These $CD18^{Foxp3}$ mice provide the first murine model to investigate the role of LFA-1-dependent immune regulation on Treg *in vivo*. $CD18^{Foxp3}$ mice develop an inflammatory skin phenotype with scaling of the ears and tails at about eight weeks of age. Thus, LFA-1 seems to have a great impact on the immune homeostasis in these mice.

In particular, the specific aims are:

Aim 1: Characterization of the general (auto)inflammatory organ phenotype in $CD18^{Foxp3}$ mice by histology and flow cytometry.

Aim 2: Characterization of the Treg phenotype in $CD18^{Foxp3}$ mice by flow cytometry and bulk sequencing of splenic Treg.

Aim 3: Investigation of cell-cell contacts and duration time between LFA-1-deficient Treg and WT DC with live cell imaging.

Aim 4: Investigation of LFA-1-deficient Treg in disease models of imiquimod-induced psoriasis and hapten-induced acute contact dermatitis *in vivo.*

3. Material

3.1. Laboratory equipment

Table 1 ***List of used equipment***

Equipment	Model	Manufacturer
Animal razor	Aesculap Isis	Aesculap, Suhl, Germany
Bioanalyzer	Bioanalyzer 2100	Agilent, Sanat Clara, USA
Bioanalyzer	Bioanalyzer HS DNA	Agilent, Sanat Clara, USA
Bioanalyzer	HiSeq 2500	Illumina, San Diego, USA
Biological safety cabinet	LaminarAir HB 2448	Heraeus Instruments, Hanau, Germany
Caliper	Kroeplin Quicktest Aussentaster 0-10mm mit Kugel Tasterform	Kroeplin, Schlüchtern, Germany
Cell counting chamber	Countess 3	Invitrogen, Waltham, USA
Centrifuge	Heraeus Megafuge 40R	ThermoFisher Scientific, Schwerte, Germany
CO_2 incubator	CB220	Binder, Tüttlingen, Germany
Cryofixator	xZell Cryofixator	xZell, Singapure
Cryostainer	xZell Cryostainer	xZell, Singapure
Cryostat	Leica CM 3050S	Leica, Wetzlar, Germany
Electrophoresis power supply	EPS 3500 XL	Pharmacia Biotech, Uppsala, Sweden
Electrophoresis unit	ECPS 3000/150	Pharmacia Biotech, Uppsala, Sweden
Flow cytometer	Attune NxT	ThermoFisher Scientific, Schwerte, Germany
Flow cytometer	FacsCanto II	BD Bioscience Inc., Franklin Lakes, USA
Gel chamber	VGel	Roth, Karlsruhe, Germany
Gel documentation system	BioVision 3023 WL/26MX	PeqLab Biotechnologie GmbH, Erlangen, Germany
Inkubator	OkoLabs environmental inkubator	OkoLbas, Pozzuoli NA Italy
Isoflurane vaporizer	XGI-8 Gas anesthesia system	Caliper LifeScience, Hopkinton, USA
Microscope	Leica TCS SP8	Leica, Wetzlar, Germany
Microscope	EVOS M7000	Invitrogen, Waltham, USA
Microscope	Leica Thunder 3D Tissue Imager	Leica, Wetzlar, Germany
Microscope	Axioskop 40	Zeiss, Göttingen, Germany
Microwave	Micromat	AEG, Berlin, Germany
Organ bath system	Octal Bridge Amplifier	Radnoti, Covina, USA
PCR Thermocycler	FatsGene FG-TC01	Nippon Genetics Europe, Düren, Germany
pH Meter	Seven Compact	Mettler Toledo, Columbus, USA
Pipettes	Finnpipette 4500	ThermoFisher Scientific, Schwerte, Germany
Plate reader	Tecan Infinite 200	Tecan, Männersdorf, Switzerland

Plate reader for ELISA	EMaxPlus	Molecular Devices, San José, USA
Plate washer ELISA	Ultrawash Plus	Dynex Magellan Biosciences, Chantilly, USA
Thermomixer	MHR 13	Hettich AG, Bäch, Switzerland
Transducer	8/30 Power-Lab	ADInstruments, Sydney, Australia
Vortexer	Vortex	VWR, Darmstadt, Germany

3.2. Reagents

Table 2 ***List of used reagents***

Reagent	Manufacturer
100 bp DNA ladder	New England BioLabs, Frankfurt, Germany
5x MyTaq Red reaction buffer	Meridian Bioscience, Cincinnati, USA
Acetic acid	Sigma Aldrich, Deisenhofen, Germany
Acetic acid	Sigma Aldrich, Deisenhofen, Germany
Acetone	AppliChem, Darmstadt, Germany
Agarose	Roth, Karlsruhe, Germany
Aldara	Meda Pharma, Solna, Sweden
Ammoniumchloride (NH_4CL)	Sigma Aldrich, Deisenhofen, Germany
Anti-CD28 for cell culture	Invitrogen, Waltham, USA
Anti-CD3 for cell culture	Invitrogen, Waltham, USA
Bovine serum (BSA)	PAN-Biotech GmbH, Aidenbach, Germany
Calcein blue AM	Invitrogen, Waltham, USA
CellMask orange	ThermoFisher Scientific, Schwerte, Germany
CellTrace CFSE (Carboxyfluorescein succinimidyl ester)	Invitrogen, Waltham, USA
CellTrace violet (CTV)	Invitrogen, Waltham, USA
Collagenase A	Roche, Basel, Switzerland
Collagenase D	Roche, Basel, Switzerland
Collagensas IV	Worthingston Biochemical, Lakewood, USA
CompBeads	BD Bioscience Inc., Franklin Lakes, USA
Dimethylsulfoxid (DMSO)	Sigma Aldrich, Deisenhofen, Germany
Direkt PCR Ear Buffer	Viagen, Berlin, Germany
Dispase II	Roche, Basel, Switzerland
DNAse I	Roche, Basel, Switzerland
Eosin Y	Sigma Aldrich, Deisenhofen, Germany
Ethanol 100%	Roth, Karlsruhe, Germany
Ethanol 70%	Roth, Karlsruhe, Germany
Ethanol 95 %	Roth, Karlsruhe, Germany
Ethylenediaminetetraacetate (EDTA)	Roth, Karlsruhe, Germany
Fixable viability dye	
Formaldehyde	Sigma Aldrich, Deisenhofen, Germany
GelRed	Biotium, Fremont, USA
Gill III hematoxylin	Sigma Aldrich, Deisenhofen, Germany
GM-CSF	Homemade from supernatant of cell line X63
Goat serum	ThermoFisher Scientific, Schwerte, Germany
Hyaluronidase	Roche, Basel, Switzerland

Hydroxyethyl-piperazineethane-sulfonic acid buffer (HEPES) 1M	Sigma Aldrich, Deisenhofen, Germany
IL-2 for cell culture	Invitrogen, Waltham, USA
Ionomycin	Sigma Aldrich, Deisenhofen, Germany
Isoflurane	Piramal Critical Care, Voorschoten, Netherlands
Kaliumchloride	Sigma Aldrich, Deisenhofen, Germany
Kaliumhydrogencarbonate ($KHCO_3$)	Sigma Aldrich, Deisenhofen, Germany
L0-12 (8-amino-5-chloro-7-phenyl-pyrido[3,4-d]pyridazine-1,4(2H,3H)dione)	R&D Systems, Minneapolis, USA
MilliQ	B. Braun AG, Melsungen, Germany
Monensin	Thermo Fisher Scientific, Schwerte, Germany
Mounting medium	ConsulMount, Thermo Fisher Scientific, Schwerte, Germany
MyTaq DNA Polymerase	Meridian Bioscience, Cincinnati, USA
NA-EDTA	Roche, Basel, Switzerland
Natrium pyrovate	ThermoFisher Scientific, Schwerte, Germany
Nitroglycerine	Sigma Aldrich, Deisenhofen, Germany
Oxazolone	Sigma Aldrich, Deisenhofen, Germany
Paraffin	Sigma Aldrich, Deisenhofen, Germany
PDBu (phorbol ester dibutyrate)	Sigma Aldrich, Deisenhofen, Germany
Penicillin/streptavidin	Sigma Aldrich, Deisenhofen, Germany
PMA	Sigma Aldrich, Deisenhofen, Germany
Polymerase K	ThermoFisher Scientific, Schwerte, Germany
Prostglandin F2α	Sigma Aldrich, Deisenhofen, Germany
ß-Mercaptoethanol	Sigma-Aldrich, Deisenhofen, Germany
ß-mercaptoethanol	Roth, Karlsruhe, Germany
Streptavidin-PE	Biolegend, San Diego, USA
Terralin	Schülke&Mayr, Norderstedt, Germany
TGF-ß for cell culture	R&D Systems, Minneapolis, USA
TissueTek OCT	Sakura Finetek Europe, Umkirch, Germany
Tris(hydroxymethyl)aminomethan (Tris)	Roth, Karlsruhe, Germany
Tris-buffered saline (TBS)	Sigma Aldrich, Deisenhofen, Germany
Tween 20	Roth, Karlsruhe, Germany
Vaseline	Vaseline, USA
Xylene I/II	Sigma Aldrich, Deisenhofen, Germany
Zymosan A	ThermoFisher Scientific, Schwerte, Germany

3.3. Solutions and media

Table 3 ***List of used solutions and media***

Solution	Manufacturer
DAKO mounting medium	Sigma Aldrich, Deisenhofen, Germany
Eagle's Minimum Essential Medium (EMEM)	Sigma Aldrich, Deisenhofen, Germany
Iscove's Modified Dulbecco`s Medium (IMDM)	Sigma Aldrich, Deisenhofen, Germany
Phosphate-buffered saline (PBS)	Sigma Aldrich, Deisenhofen, Germany
RMPI	Gibco ThermoFisher Scientific, Schwerte, Germany

3.4. Buffers

Table 4 ***List of used buffers***

Buffer	Composition
50x TAE buffer	242,3 g Tris 18,61 g EDTA →solve in 700 ml MilliQ 57,1 ml acetic acid →fill up to 1000 ml pH 8,5
BMDC medium	Iscove's Modified Dulbecco`s Medium (IMDM) 5 % FCS 1 % Pen/Strep 1 % β-Mercaptoethanol 1 % Glutamin 10 ng/mL GM-CSF
CBA buffer	D-PBS 1% FCS
Cell fixation buffer	PBS 0.7% PFA
Culture medium	RPMI 10% FCS, 1 % Pen/Strep 1 % β-Mercaptoethanol 1 % Natrium pyruvate 1% HEPES 1% L-Glutamine
Cytometric bead array (CBA)buffer	PBS 1% FCS
ELISA wash buffer	100 ml Tris buffer 1 ml Tween 20 Fill up to 1000 ml with MilliQ

FACS buffer	D-PBS 2% FCS 2 mM EDTA
Gey's lysis buffer	8,29 g NH_4CL 1 g $KHCO_3$ 0,037 g EDTA 1000 ml MiliQ pH 7,4
Krebs-Henseleit buffer	98.93 mmol/L of NaCl, 4.69 mmol/L of KCl, 2.49 mmol/L of $CaCl_2$, 1.2 mmol/L of $MgSO_4$, 0.613 mmol/L of K_2HPO_4, 25 mmol/L of $NaHCO_3$, 11.1 mmol/L of d-glucose, 37 °C, pH 7.35 (working group of Susanne Karbach)
MACS Buffer	PBS 1% FCS
PBS-EDTA	PBS 2mM EDTA
Test medium	Iscove's Modified Dulbecco`s Medium (IMDM) 5 % FCS 1 % Pen/Strep 1 % β-Mercaptoethanol 1 % Glutamin
Tris Buffer	121,14 g Tris →solve in 1000 ml MilliQ pH 7,2
Wash medium for cell culture	Eagle's Minimum Essential Medium (EMEM) 2 % FCS 1 % Pen/Strep

3.5. Consumables

Table 5 ***List of used consumables***

Consumables	**Manufacturer**
23G needle	BD Becton Dickinson, Heidelberg, Germany
6-well ,24-well, 96-well plates	Thermo Fisher Scientific, Schwerte, Germany
cell strainer	Sarstedt AG&Co KG, Nümbrecht, Germany
Falcons	Greiner Bio-One GmbH, Frickenhausen, Germany
Ibidi 8-well	Ibidi, Gräfeling, Germany
PCR reaction tube	Nippon Genetics Europe, Düren, Germany
PCR tubes	Biozym Scientific GmbH, Hessisch Oldendorf, Germany
Percoll	Millipore Sigma, Sigma Aldrich, Deisenhofen, Germany
Pipette tips	Starlab, Hamburg, Germany
Syringe Omnifix®-F	B. Braun AG, Melsungen, Germany
TissueTek cryomold form	Sakura Finetek Europe, Umkirch, Germany
Small scissors	Roth, Karlsruhe, Germany
Curved forceps	Roth, Karlsruhe, Germany

3.6. Antibodies and primers

Table 6 ***List of used antibodies***

Antibody	Dilution	Manufacturer	Catalog number
anti-mouse IgG Alexafluor488	1/400	BioLegend	405319
B220 BV786	1/300	BD Biosciences	563894
CD103 BV711	1/300	BioLegend	121435
CD103 PE	1/300	BioLegend	121405
CD11a PE-Cy7	1/100	BioLegend,	153108
CD11b BV421	1/100	BioLegend	101251
CD11c APC	1/100	BioLegend	117309
CD11c APC-R700	1/100	BD Biosciences	565872
CD138 BB700	1/100	BD Biosciences	742124
CD16/23 (Fc Block)	1/100	Cytec Biosciences	SKU70-0161-U100
CD18 APC	1/100	BD Biosciences	562828
CD19 APC	1/200	BioLegend	115511
CD19 SB702	1/300	Thermo Fisher Scientific	67-0193
CD21/35 BV510	1/100	BD Biosciences	747764
CD23 BV570	1/100	BioLegend	101637
CD29 APC	1/400	Thermo Fisher Scientific	17-0291-80
CD3 BUV615	1/400	BD Biosciences	751443
CD4 BUV737	1/400	BD Biosciences	612844
CD40 BUV395	1/400	BD Biosciences	565202
CD44 APC-R700	1/400	BD Biosciences	565480
CD44 BUV737	1/400	BD Biosciences	612799
CD45 PE	1/400	eBioscience	12-0451-82
CD45.2 BUV805	1/400	BD Biosciences	741957
CD69 BUV395	1/300	BD Biosciences	740220
CD8 BV650	1/400	BioLegend	100742
CD8 BV711	1/400	BioLegend	100748
CD86 BUV615	1/300	BD Biosciences	751557
CD86 FITC	1/300	eBioscience	11086285
CD95 BV650	1/100	BD Biosciences	740507
DAPI	1/500	Roth	6335.1
F4-80 APC	1/200	eBioscience	17-4801-82
fixable viability dye eFluor 450	1/1000	Thermo Fisher Scientific	65-0863-14
fixable viability dye eFluor 506	1/1000	Thermo Fisher Scientific	65-0866-14
fixable viability dye eFluor 780	1/1000	Thermo Fisher Scientific	65-0865-18
Foxp3 FITC	1/100	eBioscience	11-5773-82
Foxp3 PE	1/100	BD Pharmingen	560414
Foxp3 PerCP-eFluor 710	1/100	Thermo Fisher Scientific	46-5773-82
Gata3 APC	1/100	Thermo Fisher Scientific	50-9966-42
Gata3 PE	1/100	eBioscience	12-9966-42
GL-7 BV421	1/100	BD Biosciences	568852
Helios FITC	1/100	BD Biosciences	563590
ICAM FITC	1/300	BioLegend	116106
IFN-γ BV605	1/100	BioLegend	505840
IgD BUV615	1/100	BD Biosciences	751267

IgM BUV496	1/100	BD Biosciences	750192
IL-10 PE	1/100	BD Biosciences	554467
IL-12 APC	1/100	BD Biosciences	554480
IL-17 BV421	1/100	BioLegend	506926
IL-2 PE-Cy7	1/100	Thermo Fisher Scientific	25-7021-82
IL-4 APC	1/100	eBioscience	17-7041-82
IL-5 PE	1/100	eBioscience	12-7052-81
IRF4 AF488	1/300	BioLegend	646405
KLRG1 PE-Dazzle	1/100	BioLegend	138424
Ly6C FITC	1/300	BD Biosciences	553104
Ly6G eFluor610	1/300	Thermo Fisher Scientific	48-5932-82
MHCII BV786	1/300	BD Biosciences	742894
PDL1BV605	1/300	BD Biosciences	568560
PDL2 BV605	1/300	Thermo Fisher Scientific	BDB752600
RORγt PE (BD	1/100	BD Biosciences	562607
Sirp1a PE-Cy7	1/100	BioLegend	144008
TCRγδ APC	1/300	eBioscience	17-5711-81
XCR1 BV650	1/300	BioLegend	148220

Table 7 ***List of used primers for genotyping***

PCR Primer	Sequence	Manufacturer
CD18	forward_CD18ex3 5`-GTG ACA CTT TAC TTG CGA CCA-3` Reverse_CD18loxp 5`-TGC CAA TAA AGA ATT TCA GAG CC-3´	Eurofins Scientific, Luxemburg, Belgium
Foxp3-Cre WT	forward_WTfic3308 5`-TGT GTG ATA GTG CCC GTG GTT C-3` reverse_WTfic3835 5`-TTC GCA AGA AGA GGA GCC AAC G-3`	Eurofins Scientific, Luxemburg, Belgium
Foxp3-Cre Neo	forward_fic7315 5`-CTG CTT CCT TCA CGA CAT TCA AC-3` reverse_fic7682 5`-AAG TGC TTT GTG CGA GTG GAG AGC-3`	Eurofins Scientific, Luxemburg, Belgium

3.7. Kits

Table 8 ***List of used kits***

Kits	Manufacturer
Bioline MyTaq DNA Polymerase	Meridian Bioscience, Cincinnati, USA
CBA Flex Set	BD Bioscience, Heidelberg, Germany
$CD4^+CD25^+$ Treg isolation kit	Miltenyi Biotec, Bergisch Glasbach, Germany
Foxp3/Transcription Factor Staining Buffer Set	eBioscience, San Diego, USA
HiSeq Rapid SBS Cluster kit v2	Illumina, San Diego, USA
HiSeq Rapid SR Cluster kit v2	Illumina, San Diego, USA
Mouse IgE ELISA kit	Invitrogen, Waltham, USA
Mouse IgG1 ELISA kit	Invitrogen, Waltham, USA
Mouse IgG2a ELISA kit	Invitrogen, Waltham, USA
Naïve T cell isolation kit	Miltenyi Biotec, Bergisch Glasbach, Germany
Pan DC isolation kit	Miltenyi Biotec, Bergisch Glasbach, Germany
Qubit HS Assay kit	Thermo Fisher Scientific, Schwerte, Germany
RNeasy Plus Mini kit	Qiagen, Hilden, Germany
xZell cryoimmunstaining kit	Catus Biotech, Tutzing, Germany

3.8. Software and databases

Table 9 ***List of used software and databases***

Name	Manufacturer
Attune NxT software	ThermoFisher Scientific, Waltham, USA
BD FACSDIVA™ software	BD Bioscience Inc., Franklin Lakes, USA
BioRender website	BioRender, Toronto, Canada
CLC genomic workbench v200	Qiagen, Hilden, Germany
FCAP Array™	BD Bioscience, Heidelberg, Germany
FlowJo v.10.8.1	FlowJo, Ashland, USA
Gene ontology enrichment analysis	http://www.geneontology.org/
GraphPad Prism v9.2.0	GraphPad Software Inc., San Diego, USA
ImageJ 1.54d	NIH, Bethesda, USA
Ingenuity Pathway Analysis	Qiagen, Hilden, Germany
Microsoft Office 2010	Microsoft Inc., Redmond, USA
Morpheus	StreamCast Networks
Panther db	University of Southern California, Los Angeles, USA
PowerPoint 2016	Microsoft Cooperation, Redmond, USA
VolcaNoseR	https://goedhart.shinyapps.io/VolcaNoseR/
ZEN	Carl Zeiss, Oberkochen, Germany

4. Methods

4.1. Animal model

4.1.1. Mice

Mice were maintained and bred in the Central Animal Facility of the Johannes-Gutenberg-University Mainz under specific pathogen-free conditions (SPF) according to the guidelines of the regional care committee. The "Principles of Laboratory Animal Care" (NIH publication no. 85-23, revised 1985) were followed. All experiments were performed with age and sex-matched mice. $CD18^{wt/wt}$ $Foxp3^{Cre}$ littermates are defined as wildtype controls.

Mice with a Treg-specific CD18 deletion were generated as follows. $CD18^{fl/fl}$ mice were generated with a linearized vector based on plasmid BO44.2 with a targeting construct of LoxP-FRT-neo-FRT-loxP cassette (PolyGene Transgenetics, Rümlang, Switzerland) (Figure 9). This construct is flanked by a 5' short and a 3' long arm of homology containing the sequence of CD18 Exon 3. Embryonic JM8 stem cells derived from male agouti C57BL/6N blastocysts [238] were electroporated with double-digested (*NotI*+*SalI*) vector DNA. *Sca1*-digested genomic DNA (WT allele: 15 kb; targeted allele: 6.2 kb due to vector-mediated introduction of *Sca1*) of expanded clones was screened for homologous integration of the targeting sequence by Southern blot including CD18 exon 1 (probe length: 569 bp; primers: sense, 5'-CAGTCCCCATCTCCACTCAG-3' and anti-sense, 5'-GGCACTCTTTGAAGCACCAA'3) and exon 7 (647 bp; 5'ACACATGACAGCTGGGAAGA-3'and 5'-GTCACCAACAGCGAACAGTT '3). Recombinant ES clones were injected into blastocysts that were subsequently transferred into the uterus of a recipient B6 Albino female mouse.

Chimeric offspring was selected according to the agouti coat color. Male chimera were back-crossed for one generation to the B6 Albino background. Agouti offspring were screened by PCR (542 bp; 5'-CAAGCTCTTCAGCAATATCACGGG-3' and 5'-CCTGTCCGGTGCCCTGAATGAACT-3') for the presence of the Neomycin (Neo) resistance gene. $Neo^{+}CD18^{wt/fl}$ chimera were crossed with Flp deleter mice (B6 background) (Figure 10). Derived WT and $Neo^{-}CD18^{wt/fl}$ mice were differentiated by PCR (WT: 233 bp; $Neo^{-}CD18^{wt/fl}$: 487 bp; 5'-GTGACACTTTACTTGCGACCA-3', 5'-TGCCAATAAAGAATTTCAGAGCC-3'). Heterozygous $CD18^{wt/fl}$ mice were further bred to obtain homozygous $CD18^{fl/fl}$ mice. Sequencing of a PCR-amplified (5´-GACCCCTAGATCTTCCCTGC-3', 5´-ATAGAACCACCAACCTCGCA-3´) 1.37 kb fragment of genomic DNA encompassing the targeted region confirmed sequence integrity.

$CD18^{fl/fl}$ mice were originally bred with $Foxp3^{Cre}$ mice [239] crossed to C57BL/6-inbred RFP reporter mice [240] resulting in heterozygotes $CD18^{wt/fl}$ $Foxp3^{Cre}$ offspring, crossed back to $CD18^{fl/fl}$ background. Since all mice were homozygous for the floxed (fl) allele, the offspring were screened by PCR (350 bp, 5`-CTGCTTTCACGACATTCAAC-3'and 5'-AAGTGCTTTGTGCGAGTGGAGAGC-3') for the presence of Cre recombinase.

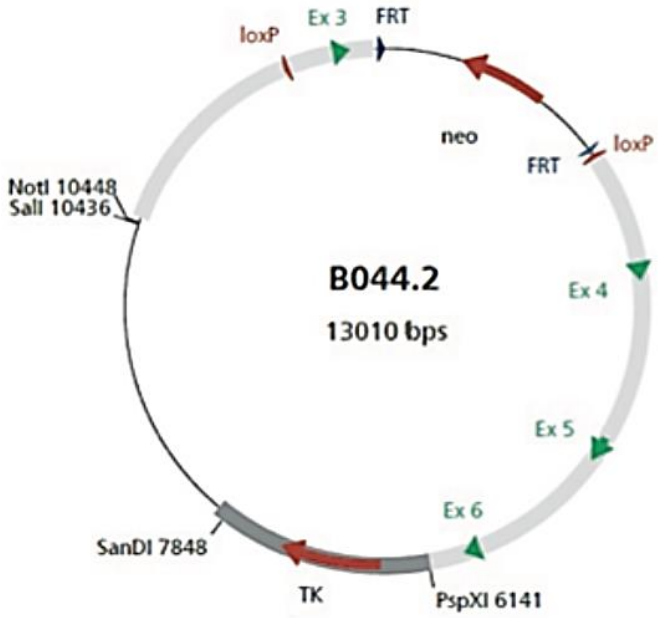

Figure 9 ***BO44.2 vector construct*** *[1]. The 13.010 bp long vector (Polygene) containing CD18 exon3-6 long arm of homology. Exon 3 containing Neo-cassette with FLP sites were flanked with loxP. Not1 and Sal1linearizing restriction sites were electroporated with the embryonic stem cells (clone JM8).*

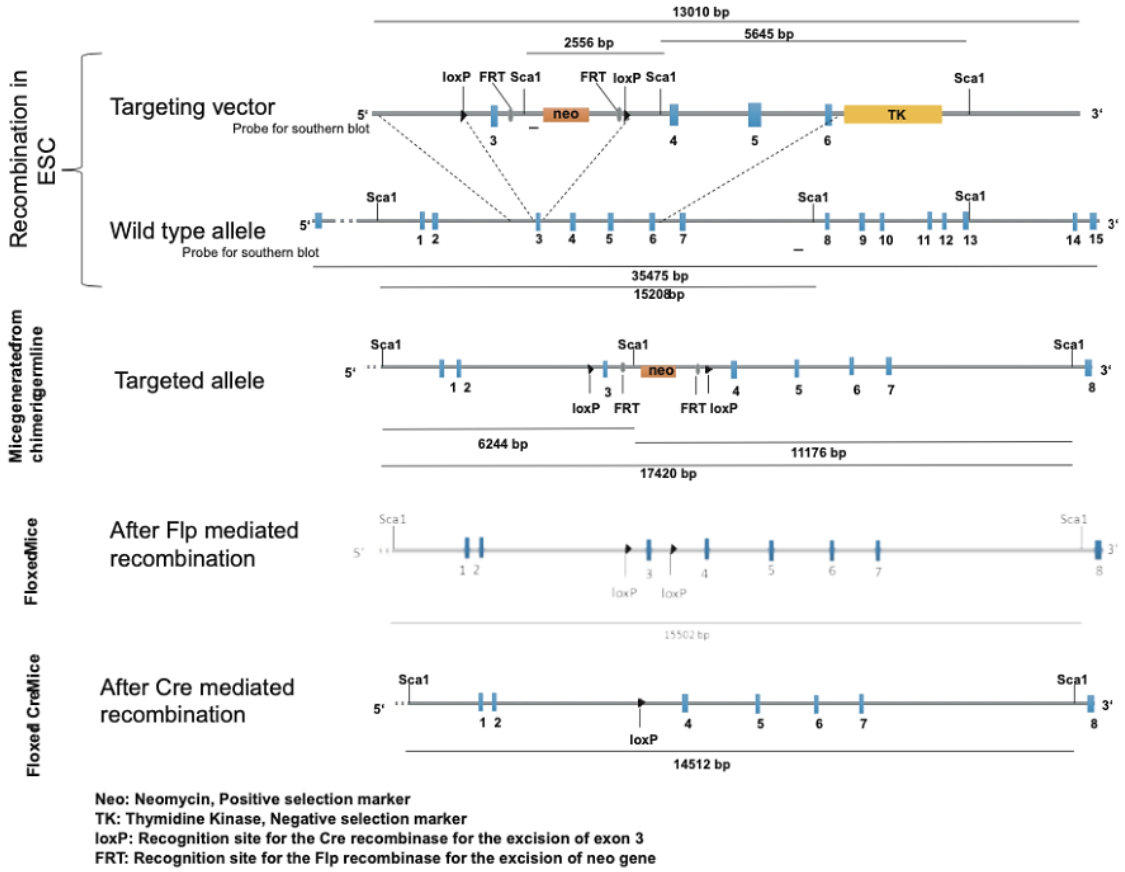

Figure 10 ***Recombination strategy for the generation of cell-specific Cre-mediated CD18 knockout*** *[95]. The targeting construct comprises the sequence of exon 3 of the CD18 gene containing a loxP-FRT-neo FRT-loxP cassette and long arm of homology, which is recombined with wild type embryonic stem cell DNA. Neomycin resistance gene facilitates the selection of recombined embryonic cells. After Flp recombination the Neomycin cassette was removed and Cre mediated recombination deleted exon 3 of the CD18 gene locus, leading to complete CD18 deletion in a specific cell type.*

4.1.2. Genotyping

DNA isolation

To identify the genotype of the mice, DNA was isolated from toes of $CD18^{Foxp3}$ mice. 100µl of direct polymerase chain reaction (PCR) direct Ear Buffer and 2 µl of proteinase K per sample were added to the samples and incubated for 60 minutes at 56 °C in a thermoshaker at 500 U/min in a 1,5 ml reaction tube. Afterwards, samples were incubated 5 minutes at 95°C to deactivate the proteinase K.

PCR primer and master mix

The genotyping was performed in three different polymerase chain reaction (PCR) reactions. One mix is prepared to amplify CD18 gene locus, and two reaction mix are prepared to identify the Cre-Foxp3 (WT and Neo KO) (Table 10). Stock primers are diluted 1:10 in MilliQ water and frozen at -20°C until use. 23,5 µl/sample of the master mix was given into a PCR reaction tube, and 1,5 µl/tube of each sample was added.

Table 10 ***Pipetting schema of the PCR master mix***

Reaction mix	Volume [µl] per sample
5x MyTaq Red reaction buffer	5
MilliQ	17,3
Primer (1:10)	1 or (0,5 each for WT and Neo)
Taq Polymerase	0,2
total	23,5

DNA Amplification

Following PCR programs were run in a PCR cycler:

Table 11 ***PCR programs for DNA amplification***

Program	Temperature [°C]	Time	Cycles
Foxp3 Cre WT/Neo	94	2 min 50 sec*	
	94	30 sec	
	58	30 sec	x35
	72	1 min	
	72	5 min	
	4	infinite	
CD18	95	3 min	
	95	30 sec	
	58	30 sec	x35
	72	45 sec	
	72	2 min	
	4	infinite	

*minutes (min), seconds (sec)

Gel electrophoresis

For gel electrophoresis, a 2% agarose gel was prepared. 2 g agarose was filled with 100 ml (1x) TAE buffer in an Erlenmeyerkolben. Agarose was heated in a microwave and afterwards, 20 µl of GelRed marker was added. Gel was filled in an appropriate gel chamber (filled with 1x TAE) with a gel comb. When the gel was hardened, 20 µl per comb bag of the PCR samples, as well as 5 µl of 100 bp marker in each row, were added and run at 90V for approximately 1 hour in the appropriate gel chamber system. DNA bands were visualized with BioVision 3023 document system, and pictures were taken.
For the CD18 PCR, three different results are possible (Figure 11). Bands of WT alleles (wt/wt) are 233 bp long, floxed KO bands (fl/fl) are 487 bp long, and heterozygotes mice (wt/fl) are a mixture of each. For Foxp3 wildtype PCR no band should be visible, whereas the Neo PCR band is 350 bp long for the cre recombinase.

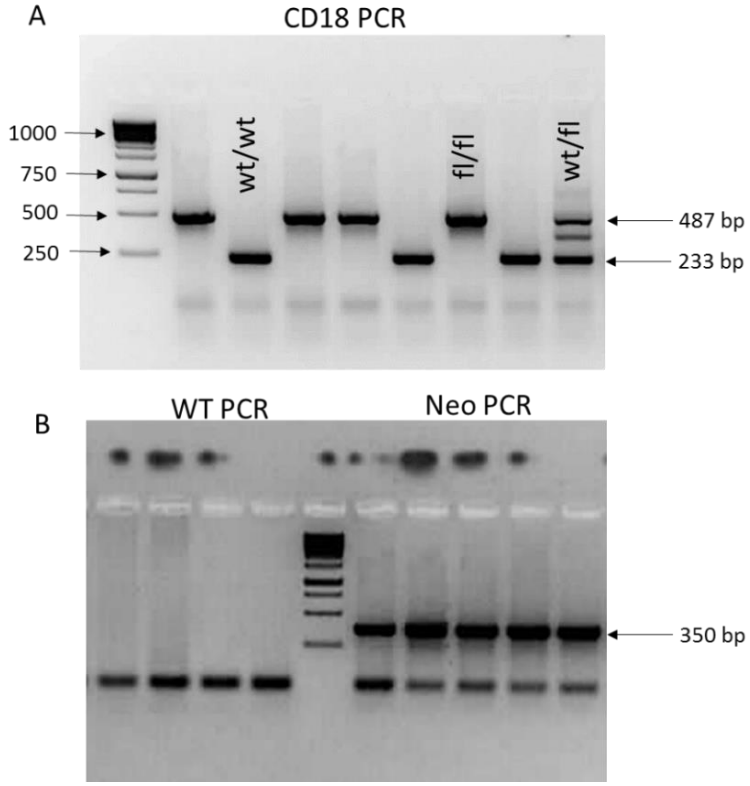

Figure 11 ***Gel electrophoresis of CD18^{Foxp3} mice. (A)*** *CD18 PCR with three possible genotypes. Bands of WT alleles (wt/wt) are 233 bp long KO bands (fl/fl) are 487 bp long and heterozygotes mice (wt/fl) are a mixture of each.* ***(B)*** *WT and Neo PCR. For Foxp3 wildtype PCR no band is visible whereas the Neo PCR band for the cre recombinase is 350 bp long.*

4.1.3. Breeding strategy

Heterozygotes CD18$^{wt/fl}$ Foxp3^{Cre} male and female mice were used for breeding. Three possible genotypes can occur through a combination of wt/fl x wt/fl CD18 (Figure 12), described further as CD18^{Foxp3} mice. CD18$^{fl/fl}$ Foxp3^{Cre} mice own the LFA-1 KO (red), CD18$^{wt/wt}$ Foxp3^{Cre} mice are the littermate controls, and CD18$^{wt/fl}$ Foxp3^{Cre} mice are used for further breeding. All mice are positive for Foxp3 cre recombinase, whereas cre is only active in the CD18 floxed mice.

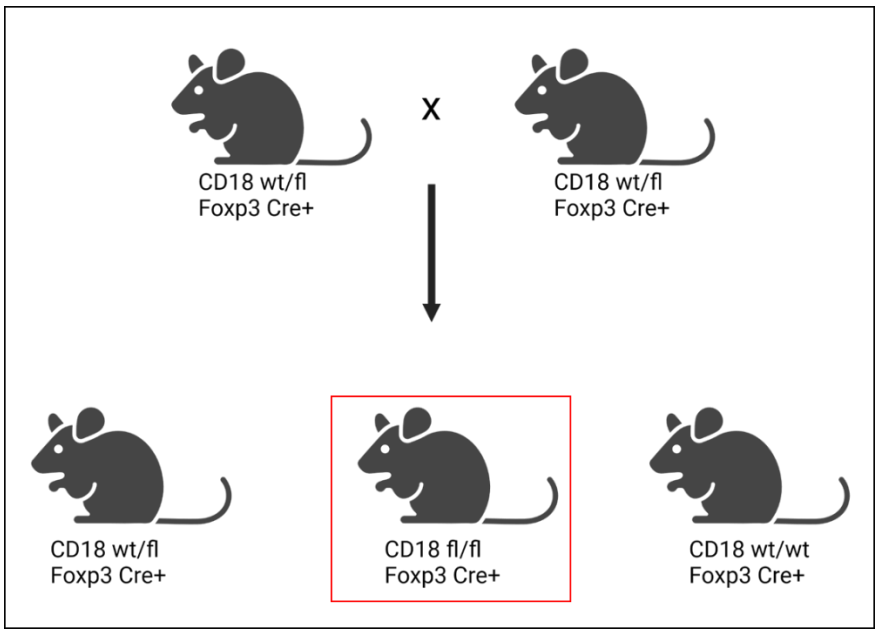

Figure 12 ***Breeding strategy of CD18^{Foxp3} mice***. *(Created with Biorender.com, accessed on 31 August 2023)*

4.2. Organ processing

All primary immune cells were obtained from CD18^{Foxp3} mice and corresponding WT littermates. Spleens, lungs, thymus, skin-draining LN (sdLN), and mesenteric LN (mLN) were mashed with a syringe plunger through a 40 µm cell strainer using 20 mL of FACS buffer. Single cell suspensions were centrifuged (300*g*, 8 minutes, 4°C) and resuspended in the appropriate buffer volume. Splenic and lung erythrocytes were lysed using Gey's lysis buffer.

Blood was collected by cardiac puncture into tubes containing 0.5 mM EDTA. Cells were centrifuged (300*g*, 8 minutes, 4°C) as above, and erythrocytes were lysed with Gey's lysis buffer.

Livers were mashed with a syringe plunger through a fine metal sieve. Cell suspensions were then centrifuged (400*g*, room temperature [RT]). Lymphocytes were then collected by centrifugation (870*g* at RT) through a Percoll bilayer (40% and 70% in DMEM) and washed twice with FACS buffer before resuspension in the appropriate buffer volume.

For isolation of leukocytes from ear skin, tissue was cut into small pieces and digested for 90 minutes at 37°C while shaking using 2 mg/mL Collagenase A, 20 µg/mL DNase I, and 1 mg/mL Dispase II in RPMI with 10% FCS. The tissue was incubated for a further 10 minutes with the addition of 10 mM Na-EDTA. Samples were filtered and washed using

70 µm cell strainers before single-cell suspensions were centrifuged (300*g*, 8 minutes, 4°C) and resuspended in appropriate buffer volume.
For DC isolation from spleen, splenic tissue was cut into small pieces and digested for 30 minutes at 37°C while shaking using 800 U/mL collagenase type IV and 50 U/mL DNAse I in RPMI 1640 (without FCS). Afterward, Na-EDTA was added to a concentration of 10 mM, and the tissue was incubated further for 10 minutes. Cell suspensions were filtered via a 70 µm cell strainer until staining for flow cytometry.

4.3. Bone marrow-derived dendritic cells (BMDC)

In vitro monocyte-derived BMDC were differentiated from BM progenitors (as described by Bros *et al*. [241] of $CD18^{Foxp3}$ mice and WT littermates. Mice were sacrificed by cervical dislocation and cleaned with ethanol. Femur and tibia bones of both legs were removed by peeling off the fur from the knee to the back dissecting the legs. Bones were cleaned with a dish and put into a 15 ml tube with wash medium. The bones were sterilized for 30 seconds with 70% ethanol in the falcon and poured into a petri dish under the clean bench. A 1ml syringe, with a 23G needle, was filled with PBS supplemented with 2% FCS, Pen/Strep, 2mM EDTA and positioned into the cavity of the bones filled with the BM. The BM was flushed out of the bones into the tube. This step was repeated until the whole BM was washed out of the bones. The cells were spun down (1400rpm for 5 minutes at 4°C), and the supernatant was discarded. The erythrocytes were lysed with 1ml Gey's lysis buffer for 1 minute and immediately diluted in 50 ml culture medium. The cells were counted with a cell counter, again spun down, and set to the concentration needed. The cell suspension were seeded into a 6-well plate with a final concentration of $5*10^5$ cells/well in IMDM culture medium (Supplemented with 5% FCS, 2 mM L-glutamine, 100 U/mL penicillin, 100 µg/mL streptomycin, 50 µM ß-mercaptoethanol, 10 ng/ml recombinant murine GM-CSF. The cells were incubated (37°C/5% CO_2) for 7 days. On day 2 and day 5 the medium was exchanged by adding 1 ml new medium. On day 7, BMDC were harvested in 50 ml tube, centrifuged as described, and resuspended in the appropriate medium and concertation needed for each assay.

4.4. Magnetic cell separation (MACS)

Magnetic cell separation (MACS) is based on antibodies coupled to magnetic beads and was used to separate certain cell types from single cell suspension. During incubation with a cell suspension, the antibody/bead mix binds to cells that express the corresponding epitope. When the cell suspension is placed into a magnetic field, magnetically labeled cells are retained, while unlabeled cells can be removed. To recover the labeled cells, the sample is removed from the magnetic field. Different kits from Miltenyi Biotec were used to isolate Treg, T cells, as well as DC with the MACS separators. Single cell suspension of the spleen was performed as described above (in 4.2.) and MACS separation was done as described in the manufacturer's protocols, respectively. After separation, the purity of the cells was determined by flow cytometry.

Treg isolation

For Treg isolation, the $CD4^+CD25^+$ kit from Miltenyi was used. The cell number of cell suspension was determined, and the cells were centrifuged (300*g*, 10 min, 4°C) and supernatant aspirated. The cell pellet was resuspended in 40 µl of MACS buffer per 10^7 total cells. 10 µl of the Biotin-Antibody Cocktail per 10^7 total cells were added, mixed, and incubated for 10 minutes in the refrigerator. 38 µl of MACS buffer, 20 µl of anti-biotin MicroBeads, and 2 µl of CD25-PE antibody per 107 cells were given to the cells. The mixture was incubated again for 15 minutes and proceeded to magnetic separation.
LD MACS column was placed in the magnetic field of the separator, and 2 ml of MACS buffer were added to the column. Cell suspension was applied onto the column, and unlabeled cells were collected as flow-through in a 15 ml falcon. The column was washed with 1 ml buffer, and flow-through was centrifuged again. The cell pellet was resuspened in 90 µl of buffer, 10 µl of Anti-PE Microbeads were added, and incubated for 15 minutes in the refrigerator. MACS MS Column was placed in the magnetic field of the separator. The column was washed with 500 µl of buffer and the cells were given onto the column. The column was then washed twice with 50 µl of buffer. Column was removed from the separator and placed into a 15 ml tube. 1 ml of buffer was pipetted onto the column and flushed out with the plunger into the tube. The columned contained the $CD4^+CD25^+$ Treg fraction, whereas the flow through contains all other cell populations.

Naïve T cell isolation

For T cell isolation the naïve T cell kit from Miltenyi was used. Cell preparation is performed as described above. After putting the biotin antibody onto the cells and incubation, 20 µl of buffer per 10^7 total cells were given onto the suspension. 20 µL of Anti-Biotin MicroBeads were added, as well as 10 µl of CD44 MicroBeads, and incubated for 10 minutes in the refrigerator. MACS LS column was placed in the magnetic field of the separator. 3 ml of MACS buffer and afterward cell suspension was given onto the column, and flow-through was collected in a 15 ml falcon, containing the enriched naive $CD4^+$ T cells.

DC isolation

DC isolation was performed with the Pan DC isolation kit from Miltenyi. Isolated spleens were placed in 6 cm petri-dish with 5 ml/spleen collagenase D solution (2 mg/mL in 10 mM Hepes-NaOH, pH 7.4,150 mM NaCl, 5 mM KCl, 1 mM $MgCl_2$, 1.8 mM $CaCl_2$). Spleens were injected with 500 µL of Collagenase D solution using a 1 mL syringe and a 25G needle. The tissue was cut into smaller pieces using sharp scissors and incubated for 30 minutes at 37 °C. The material was passed through a 70 µm strainer using a plunger and collected in a 15 mL tube. The cells were washed by adding MACS buffer to a final volume of 14 ml.
Cell number was determined and centrifuged as described. Cell pellet was resuspended in 350 µl of buffer per 10^8 total cells. 50 µL of Fc blocking reagent was added 100 µL of Pan DC antibody cocktail per 10^8 cells. Suspension was mixed and incubated for 10 minutes in the refrigerator. Cells were washed with 5 ml of buffer, centrifuged and the supernatant

was discarded. Pellet was resuspended in 800 µl of buffer, and 200 µL of anti-Biotin MicroBeads per 10^8 cells was added and incubated again for 10 minutes. MACS LS column was placed in the separator and washed with 3 ml of buffer. The cell suspension was given onto the column, and flow-through represents the enriched DC fraction.

4.5. Flow cytometry and antibody staining

4.5.1. Flow cytometry

Fluorescence-activated cell sorting (FACS® Beckton) is a specialized type of flow cytometry with a laser-based biophysical method to identify certain cell populations with distinct antibodies. This technology enables to access the quantification and immune phenotype of cells. The cell suspension stained with the antibody cocktail is taken through the fluidic system with a needle to transport single cells to past the laser. The components of the optical system include excitation light sources, lenses, and filters used to collect and move light around the instrument. When the laser light detects a single cell, some of the light will strike the physical structures of the cell, causing the light to scatter. The size scatters the beam of one laser, measured as area of the forwards scatter FSC-A, height FCS-H and width FSC-W. The side scatter (SSC) is based on the granularity (SSC-A, SSCH, SSC-W). Thereby, every single cell is detected and visualized as a single dot. Further, the light from the laser will excite all fluorophores on the cell, which produces a fluorescence emission spectrum. The light is collected by the detector and processed through the electronics of the flow cytometer.
The more fluorophores are used at once, the more spectral spillover occurs that has to be corrected. This process of so-called ‘compensation’ is necessary to remove partially overlapping (an overview of flow cytometry is given in [242-244]). In this work, flow cytometry was used as an essential tool to analyze the immune phenotype of cells by cell-specific marker expression.

4.5.2. Extra- and intracellular antibody staining

To detect immune cells and their subsets for flow cytometric analysis, cells have to be stained with specific antibodies labeled with certain fluorophores. For the direct, extracellular staining of specific surface markers, a minimum of 10^6 cells were resuspended in an appropriate volume of FACS buffer transferred in a 96 well plate. 5 µl of Fc block solution (1:10) was added and incubated for 5 minutes at 4°C. Cells were spun down (400*g*, 5 min, and 4°C), resuspended in 50µl antibody cocktail, and incubated for 30 minutes in the dark at 4°C. Cells were washed twice with FACS buffer and fixed with 200 µl fixation buffer. After incubation for 15 minutes in the dark, the cells were washed twice and finally resuspended in 100µl FACS buffer. Cells were kept in the fridge until cytometric measurement.
For intracellular cytokine staining, single cell suspensions were first restimulated for 4 hours at 37 °C using 50 ng/mL PMA, 1 µg/mL ionomycin in the presence of 1x monensin (1:1000) before proceeding with surface staining, fixation, and intracellular staining.
For intracellular staining, extracellular staining was performed as described and then washed twice with cold PBS. Cells were fixed with eBioscience™ Foxp3/Transcription

Factor Fixation kit as described in the manufacturer's instructions. 100µl/well of Fix concentrate/fix diluent mixture (1:3) was given to the cells, and fixation was performed for 20 minutes at room temperature in the dark. The extracellular staining was performed for 30 minutes in 1x Perm buffer. Finally, cells were washed with Perm buffer and resuspended in FACS buffer. Cells were kept in the fridge until cytometric measurement.
For machine setup and compensation, 5µl of BD™ CompBeads (anti-rat/hamster Ig and anti-mouse Ig) were mixed with 100µl FACS buffer and 1µl of the appropriate antibody for each fluorochrome. Negative Beads without the addition of antibodies served as control. Used antibodies are listed in Table 6. Before the measurement, the compensation was acquired. Flow cytometry data were collected using the BD FACS Symphony. Data were analyzed using FlowJo v10.8.1 as well as an Attune NxT, and data were analyzed using Attune^{TM} NxT software.

4.5.3. Gating strategies

The flow cytometry data were analyzed using FlowJo® and Invitrogen Attune^{TM} NxT software. Immune cells were identified through the application of the gating strategies shown below (Figures 13-20). Table 12 gives an overview of the identification markers used for different leukocyte populations.

Table 12 ***Identification markers of different cell populations analyzed by flow cytometry***

Cell population	Main identification markers
Treg (general)	$CD4^+$ $Foxp3^+$
Tissue Treg	$CD4^+$ $Foxp3^+$ $Klrg1^+$ $PD1^+$ $Gata3^+$
pTreg	$CD4^+$ $Foxp3^+$ $Helios^+$
tTreg	$CD4^+$ $Foxp3^+$ $Helios^-$
T_H1	$CD4^+$ $IFN\gamma^+$ $IL\text{-}17^-$
T_H2	$CD4^+$ $GATA3^+$
T_H17	$CD4^+$ $IL\text{-}17^+$ $IFN\gamma^-$
Cytotoxic T cells	$CD3^+$ $CD8^+$ $CD4^-$
Neutrophils	$CD11b^+$ $Ly6G^+$ $Ly6C^+$
Monocytes	$CD11b^+$ $Ly6G^-$ $Ly6C^{high}$
Macrophages	$CD64^+$ $F4/80^+$ $Ly6C^+$
Eosinophils	$CD11b^+$ $SiglecF^+$ $Ly6G^+$
DC (general)	$CD11c^+$ $MHCII^+$
Conventional cDC1	$XCR1^+$ $CD26^+$
Conventional cDC2	$XCR1^-$ $CD26^+$
T_H2-promoting cDC2	$CD11c^+$ $IRF4^+$ $PDL2^+$
pDC	$SiglecF^-PDCA1^+Ly6C^+$
B cells (general)	$CD19^+$ $B220^+$
Marginal zone B cells	$CD23^{low}$ $CD21/35^+$
Follicular B cells	$CD23^+$ $CD21/35^{low}$
Germinal center B cells	$GL\text{-}7^+$ $CD95^+$
Plasma B cells	$CD138^+$ $CD95^+$

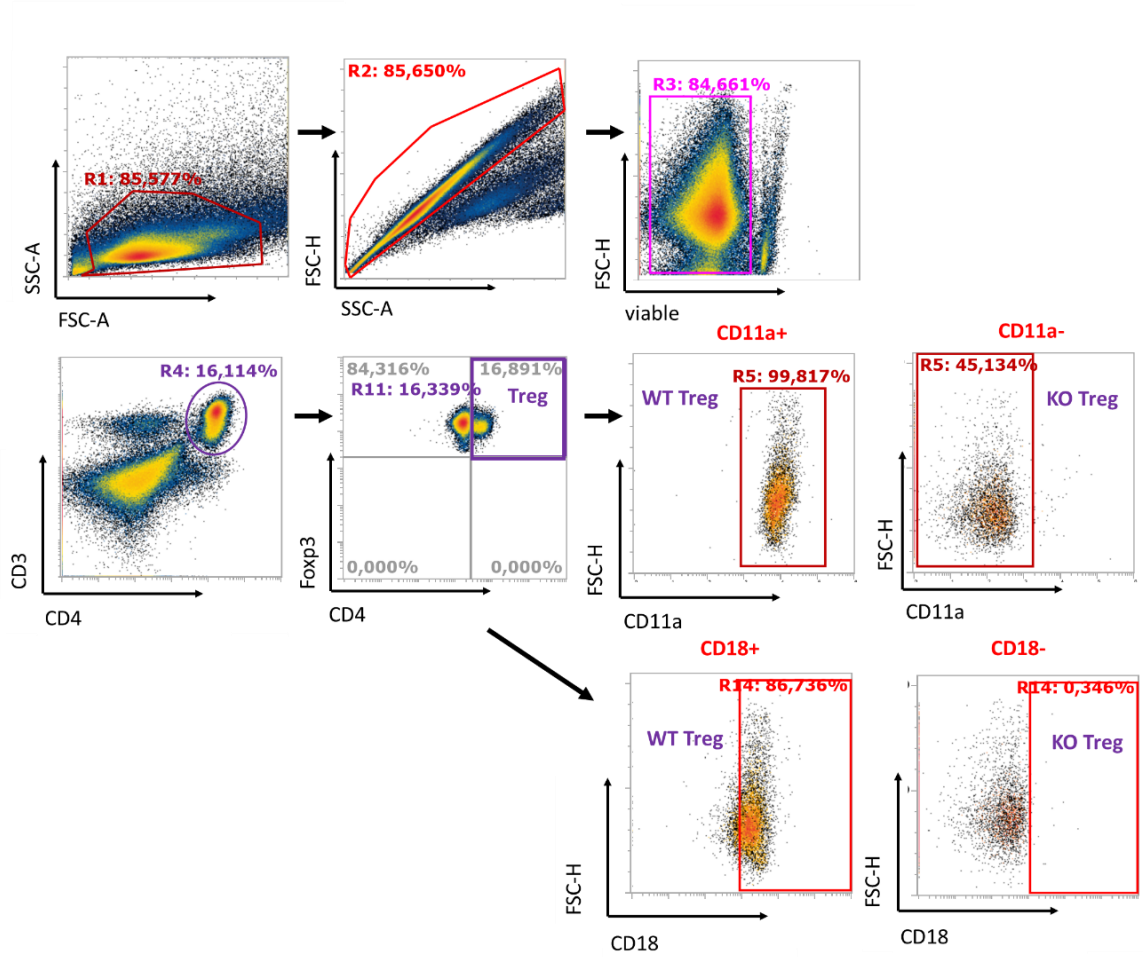

Figure 13 ***Flow cytometric gating strategy of LFA-1 WT and KO Treg.*** *Representative pictures of spleen cells are shown. All cells were gated by forward (FSC-A) versus sideward scatter area (SSC-A). Single cells were identified with FSC-A versus FSC-Height. Living leukocytes are negative for live/dead viability dye. Treg were identified as $CD4^{+}Foxp3^{+}$. LFA-1 WT Treg and LFA-1 KO Treg were identified with CD11a and CD18.*

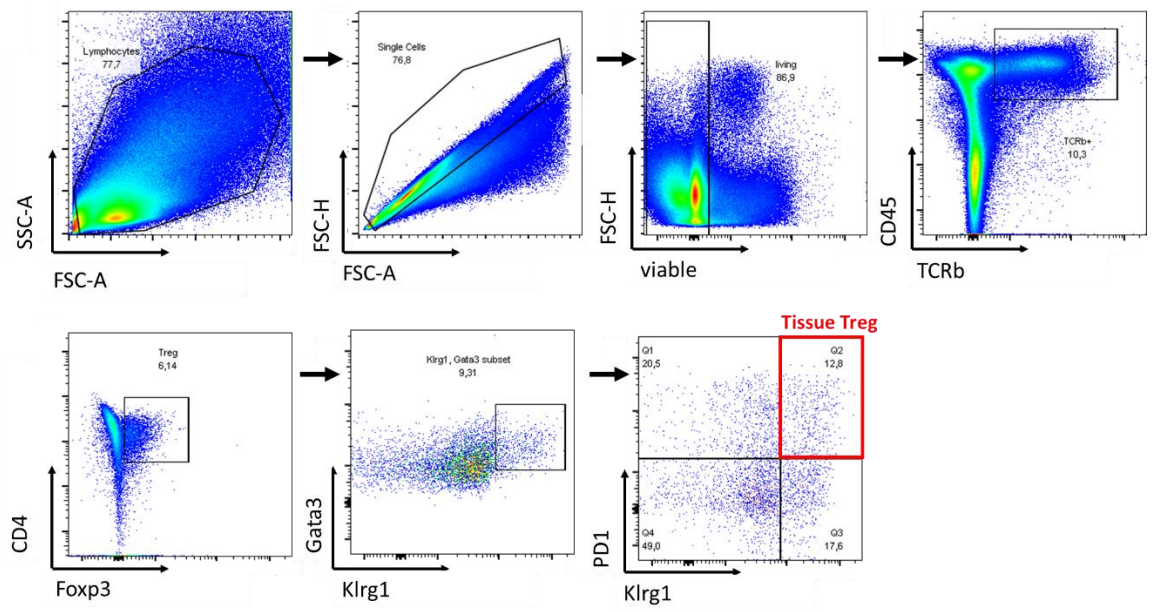

Figure 14 ***Flow cytometric gating strategy of tissue Treg.*** *Representative pictures of lung cells are shown. All cells were gated by FSC-A versus SSC-A. Single cells were identified with FSC-A versus FSC-Height. Living leukocytes are negative for live/dead viability dye. T cells were identified as TCRβ^{+}CD45^{+}. Treg were identified with Foxp3 and CD4 marker. Tissue Treg are positive for Klrg1^{+}Gata3^{+} and PD1^{+}.*

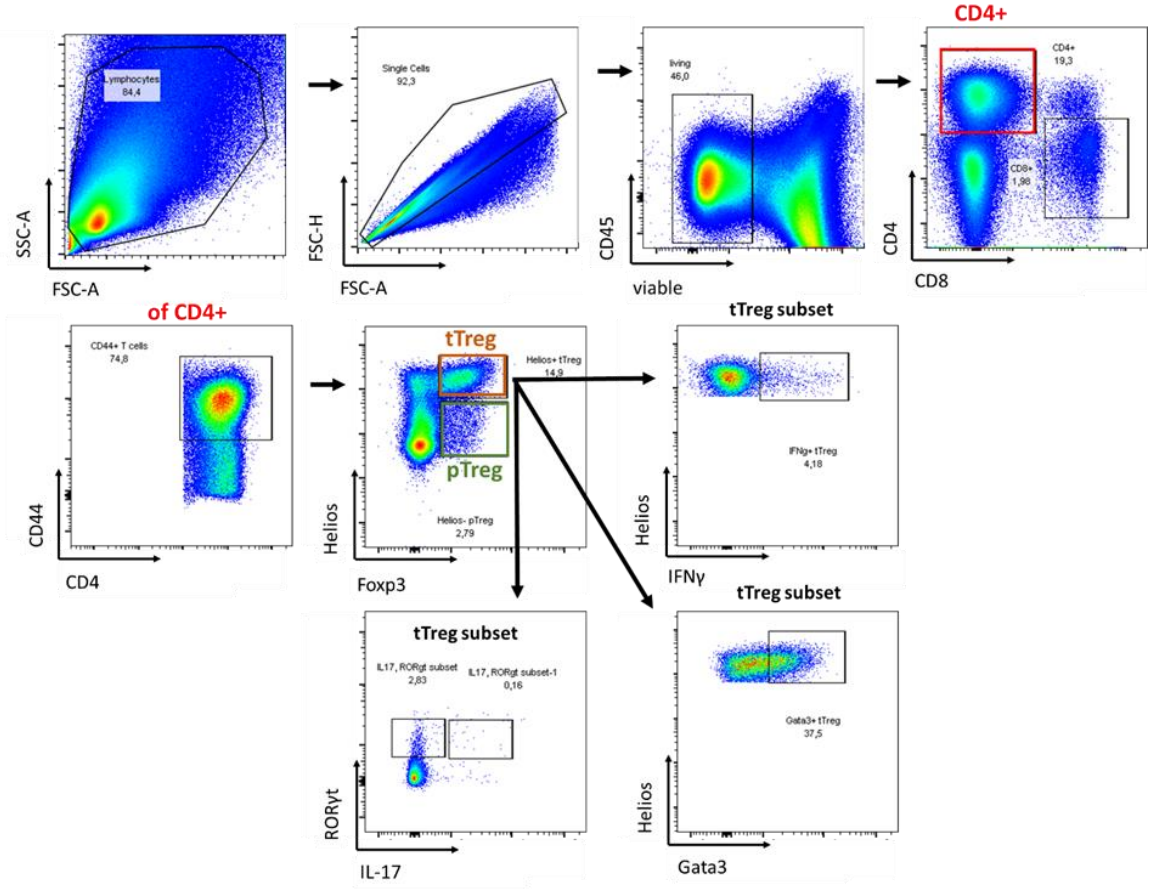

Figure 15 ***Flow cytometric gating strategy of tTreg and pTreg and their subsets.*** *Representative pictures of spleen cells are shown. All cells were gated by FSC-A versus SSC-A. Single cells were identified with FSC-A versus FSC-Height. Living leukocytes are negative for live/dead viability dye and positive for CD45.*

Activated T cells are positive for CD44. tTreg are identified as Foxp3^{+}Helios^{+} and pTreg as Foxp3^{+}Helios^{-}. Their subsets are identified with Gata3^{+} IFNγ^{+} and RORγt^{+}IL-17$^{-/+}$.

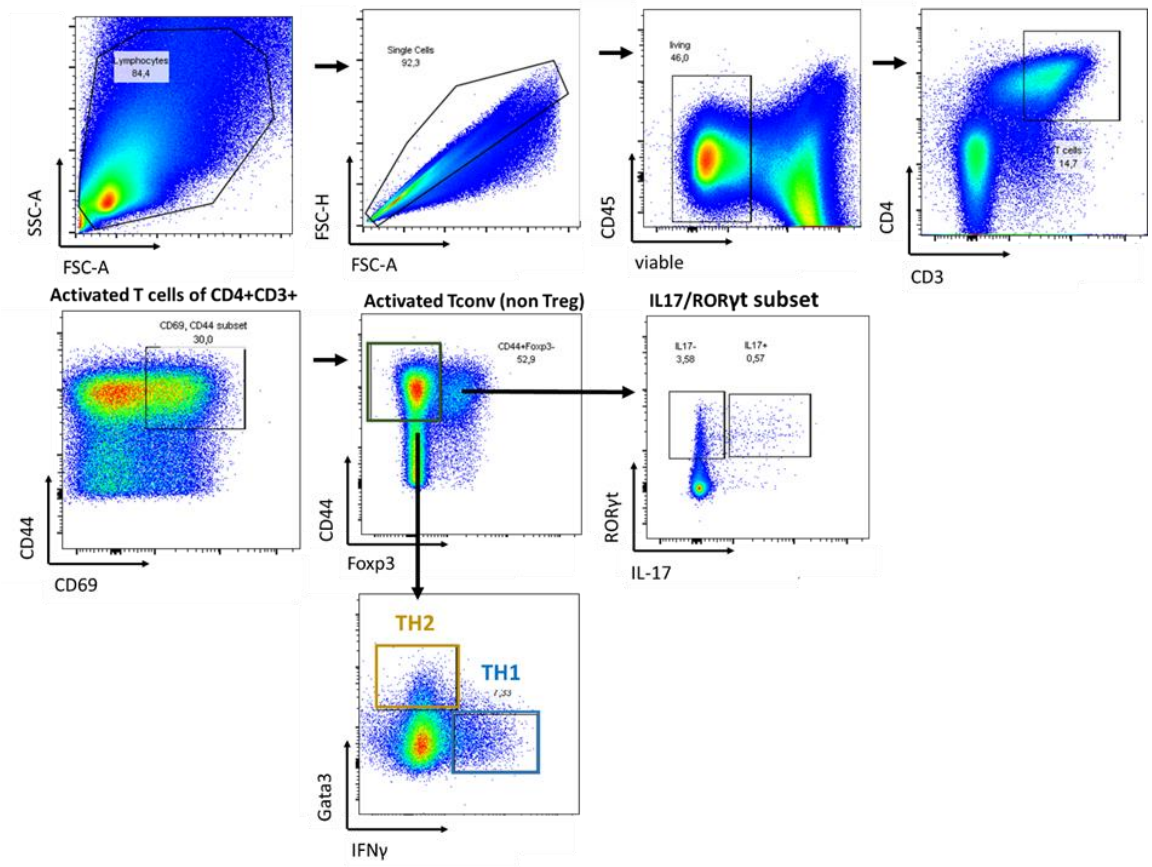

Figure 16 ***Flow cytometric gating strategy of T_{conv} cells and their subsets.*** *Representative pictures of spleen cells are shown**.** All cells were gated by FSC-A versus SSC-A. Single cells were identified with FSC-A versus FSC-Height. Living leukocytes are negative for live/dead viability dye and positive for CD45. T cells are identified as CD4^{+}CD3^{+}. Activated T cells are positive for CD44 and CD69. T_{conv} are identified as Foxp3^{-} (non Treg). T_{conv} subsets are T_H1 (IFNγ^{+}), T_H2 (Gata3^{+}), T_H17 (RORγt^{+}IL-17^{+}), and RORγt^{+}IL-17^{-}.*

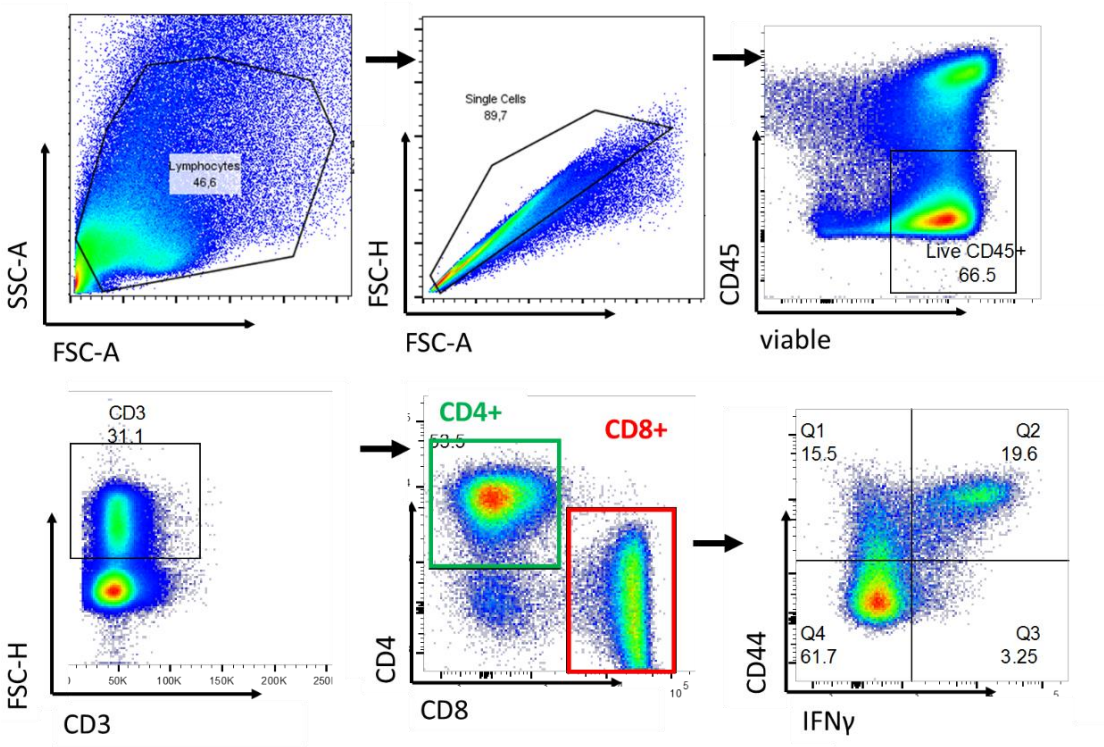

Figure 17 ***Flow cytometric gating strategy of CD8 T cells and their cytokines.*** *Representative pictures of spleen cells are shown. All cells were gated as described before. Leukocytes were gated with live/dead viability dye and CD45 marker. Cytotoxic T cells were identified as $CD3^+CD8^+$. $CD8^+CD44^+$ is representative for activated T cells. Outgoing the $CD8^+$ gate the cytokine expressions (here shown for IFN-γ) of these cells were identified.*

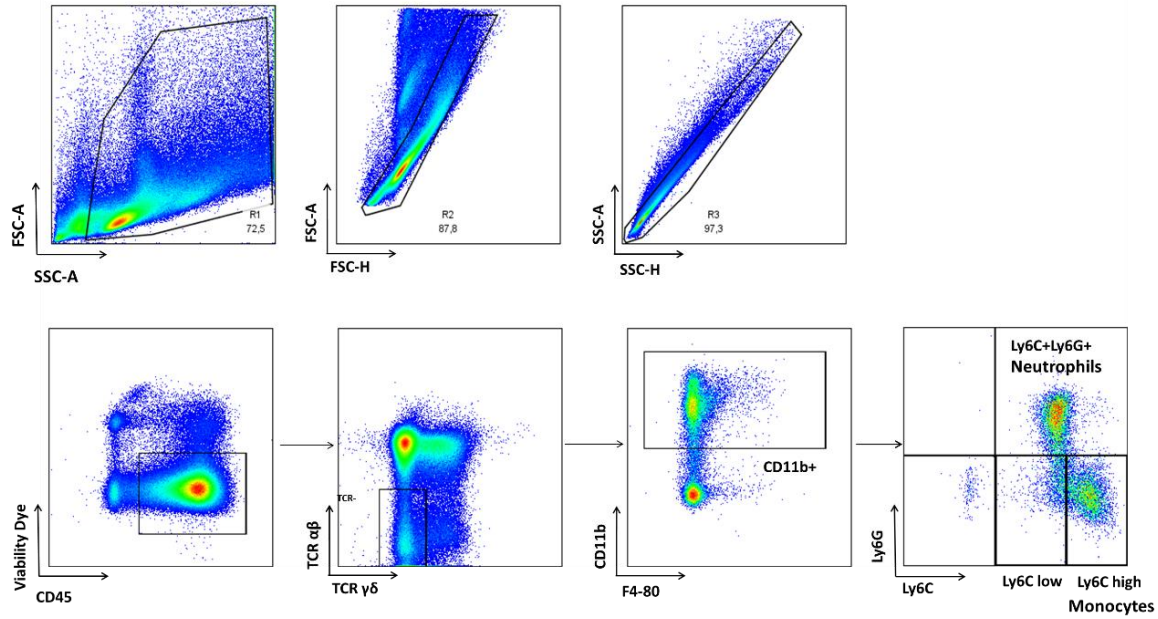

Figure 18 ***Flow cytometric gating strategy of neutrophils and monocytes.*** *Representative pictures of spleen cells are shown. All cells were gated as described before. Leukocytes were gated with live/dead viability dye and CD45 marker. Neutrophils and Monocytes are negative for TCR and positive for $CD11b^+$. Neutrophils are identified as $Ly6C^+Ly6G^+$ double positive cells whereas monocytes are negative for Ly6G but high positive for Ly6C.*

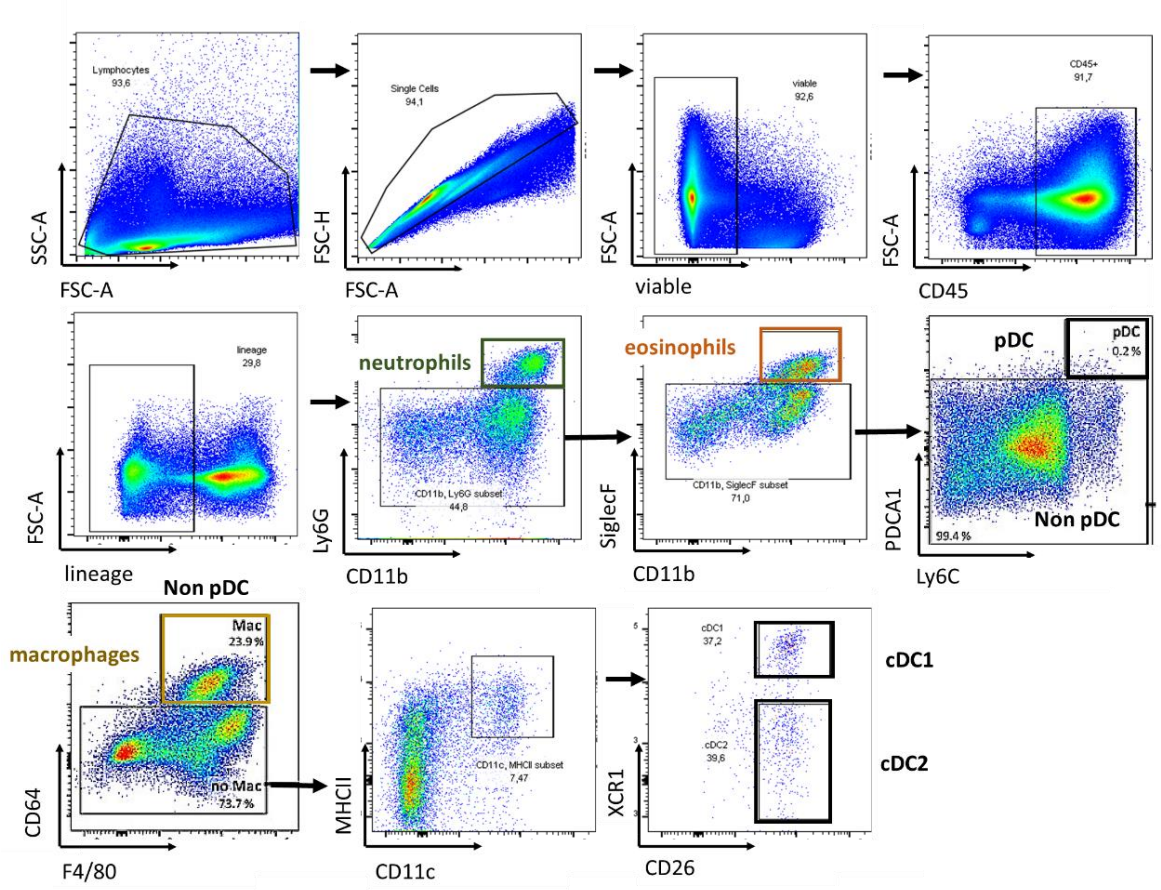

Figure 19 ***Flow cytometric gating strategy of myeloid cells.*** *Representative pictures of skin-draining LN cells are shown. All cells were gated as described before. In the first step dead and stromal cells (CD45$^-$) were excluded. Next the remaining hematopoietic-derived cell (CD45$^+$) lineage-negative cells, meaning T cells (CD90.2), NK cells (NK1.1) and B cells (CD19), were removed. Neutrophils (CD11b$^+$ Ly6G^{high}) and eosinophils (CD11b$^+$ SiglegF$^+$) as well as pDC (PDCA1$^+$Ly6C$^+$) were removed. The remaining population was named 'no pDC' and was further analyzed. Macrophages (CD64$^+$F4/80$^+$) were discriminated from non-macrophages (F4/80$^+$CD64$^-$). This population was further analyzed for DC (CD11c$^+$MHCII$^+$) and gated on cDC1 (XCR1$^+$CD26$^+$) and cDC2 (XCR1$^-$CD26$^+$). Gating strategy was adapted as described by Probst et al. [245].*

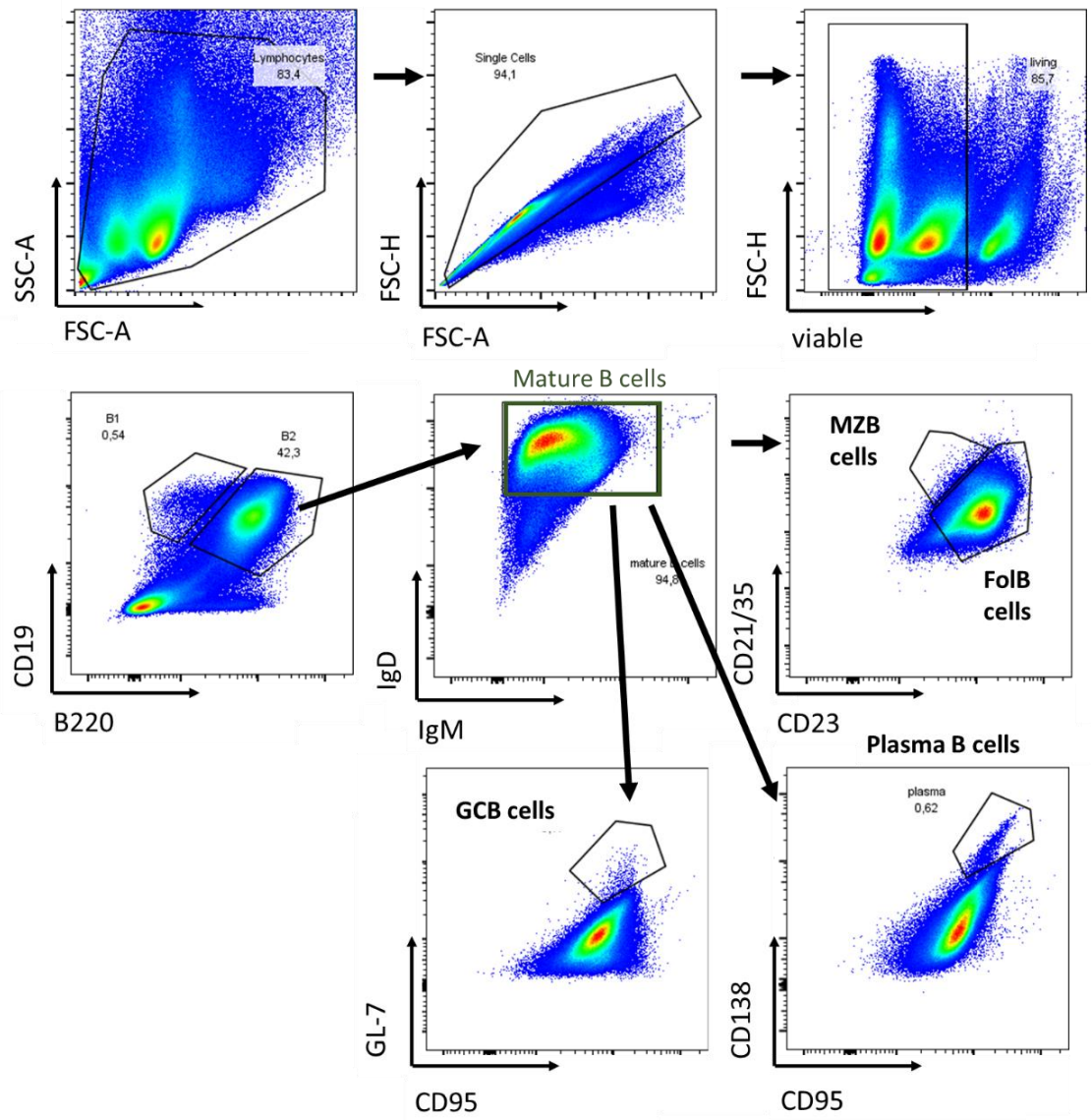

Figure 20 ***Flow cytometric gating strategy of B cells.*** *Representative pictures of spleen cells are shown. All single and living cells were gated as described before. B cells are identified as B220^{+} and CD19^{+}. Mature B cells are positive for IgM and IgD. Marginal zone B cells (MZB) are CD23^{low}CD21/35^{+}, Follicular B cells (FolB) are CD23^{+}CD21/35^{mid}, Germinal center B cells (GCB) are CD95^{+}GL-7^{+} and Plasma B cells are CD95^{+}CD138^{+}.*

4.6. *In vitro/ex vivo* experiments

4.6.1. Hematoxylin and eosin (H&E) staining

H&E staining is a principle method to visualize basic cell structures like pattern and shape in the histology [246]. The hematoxylin stains cell nuclei in blue, and eosin stains the extracellular matrix and cytoplasm pink. For the staining, mouse ears and tails were fixed in 4,5 % formaldehyde overnight and embedded in paraffin. Rewaxed and rehydrated tissue sections (2 µm) were stained with Gill III Hematoxylin for 2,5 minutes, washed, and stained with 0.5% eosin Y for 1 minute afterward. Slides were placed in 95% ethanol two times and transferred into 100% ethanol for 2 minutes. Slides were incubated with

xyleneI/II for 2 minutes, dried, and covered with mounting medium. Pictures were taken with an Invitrogen EVOS M7000 microscope (in cooperation with the working group of Dr. Eva Hadaschik, Heidelberg).

4.6.2. Immunfluorescence (IF) histology

The immunofluorescence (IF) histology, is a technique that permits visualization of virtually many components in any given tissue or cell type. This broad capability is achieved through combinations of specific antibodies labelled with fluorophores, similar to flow cytometry.

Ears of mice were cut off and embedded into *Tissue-Tek* O.C.T. compound in Tissue-Tek cryomold forms and frozen at -80 °C. Frozen blocks were then cut into cryosections (thickness 2-5 µm) with a Leica CM3050 S cryostat. Cyrosections were placed on a special xZell-provided coated slide and fixed and stained with CryoFixation and CryoStainer of xZell as recommended by the manufacturer (xZell, Singapore).

The xZell fixator has to be started at least 30 minutes prior to the samples being ready for fixation. The green light indicates that the fixator is ready. For fixation, methanol has to be added to the Cryofixation I, as indicated on the tube and fill up 1 cartridge for 2 slides (maximum 8) to stain and place cartridges in position I in the fixator. The cartridges were filled up with Cryofixation II and placed in position II in the fixator. After 5 minutes of waiting for the solutions to adjust to the temperature, the slides were given carefully into the cartridges in position I, the lid was closed, the green A button (left) was pressed, and the slides were incubated for 15 minutes. Afterwards, the slides were removed from position I, taped on a tissue, and transferred to position II. Green button B was pressed (right), and the slides were incubated again for 25 minutes.

Excess buffer was removed from the slides by tapping on a tissue and slides were put into the plastic cap holder (see manual, capillary gap should be void of any buffer) and positioned into the CryoStainer. 200 µl of cryostaining buffer I followed by 50 µl of prepared blocking solution (Table 13) were applied to the gap and incubated for 45 minutes by pushing the button. 50 µl of the prepared antibody solution (Table 14) was given to the cap gab and incubated again for 55 minutes. To detect Treg populations, sections were incubated with PE Foxp3 antibody. DAPI was used to stain nuclei. Slides were then washed with 200µl cryostaining buffer and 200 µl of premount buffer and incubated for 5 minutes. Slides were then again washed with 200 µl cryostaining buffer and cap gab was removed from the slides. 25 µl xZell mounting buffer, including DAPI (2 µl in 1 ml xZell mounting buffer) was given onto the slides and covered bubble-free with a slip on the sample. Slides were kept in the dark until analysis. Immunofluorescence imaging was performed with Leica Thunder 3D Tissue Imager. Thunder Imager is a fully automated tissue imaging system for recording multi-color 3D images (7 colors possible) (Table 15). Pictures were analyzed with ImageJ by counting $Foxp3^+$ cells.

Table 13 ***Preparation of blocking solution for one sample***

Blocking Buffer	
Number of slides	1
Blocking solution I	2,8
Blocking solution II	16,5
Fc-block (mouse (CD16/CD32)	2,0
Cryostaining buffer	25,0
DPBS	4,5
Total volume µl/sample	51

Table 14 ***Preparation of staining solution for one sample***

Staining panel	
Number of slides	1
Foxp3 (PE)	3
Cryostaining buffer	10
DPBS	37
Total volume µl/sample	50

Table 15 ***Thunder 3D microscope configurations***

Label Mikroskop	Channels	Filter	Filter	Filter
421	BV421/ DAPI/AF405	395/25	431/28	412lp
480	BV480	436/20	480/30	455lp
488	AF488 FITC	495/25	537/29	515lp
PE	PE, Propodium Iodid	546/10	537/29	556lp
594	AF594	599/13	632/28	612lp
DRQ	DRAQ5/AF647	642/20	697/60	660lp
PER	PerCP	445/30	697/60	510lp

4.6.3. Indirect immune fluorescence

Indirect immune fluorescence was used to detect autoantibodies in the serum of mice. This technique is normally used to diagnose autoimmune blistering diseases. Unlabeled primary antibodies from the serum bind to the target molecule in pre-prepared tissue samples. Secondary antibodies, which are conjugated with a fluorescent dye such as fluorescein isothiocyanate (FITC), bind to the primary antibody and can be detected by a microscope. Palate skin cryosections (see above) of C57BL/6N mice were fixed in acetone for 10 minutes, rehydrated in 1x TBS, and blocked with 5% goat-serum in TBS for 30 minutes at room temperature (RT). The primary Antibody (1:400) was incubated for 1 hour, and afterward serum of $CD18^{Foxp3}$ and WT littermates was given onto the skin slides for 1 hour. Slides were washed 3 times with TBS, and the secondary anti-mouse IgG antibody was given onto serum-treated slides for 1h (anti-mouse IgG Alexafluor488 diluted 1:400 in

1xTBS) to detect auto-antibodies. Slides were covered with DAKO-Fluorescence mounting medium. Fluorescence pictures were taken using an Axioskop 40 and the corresponding software. Fluorescing autoantibodies against specific structures of the skin were analyzed. Scoring of fluorescence intensity was determined as 0= negative, 1= weakly positive (+), 2= positive (++), and 3= strongly positive (+++) (in cooperation with the working group of Dr. Eva Hadaschik, Heidelberg).

4.6.4. Transcriptome analysis

Splenic RFP^+CD4^+ T cells (each about 1×10^5 per sample) were sorted by flow cytometry using a FACSAriaII (BD Biosciences) and lysed (RLT PlusLysis Buffer; Qiagen). Cells were incubated overnight with recombinant human IL-2 (5 U/mL). In parallel assays, agonistic anti-CD3 (1 µg/mL, BioLegend, catalog 100238) and anti-CD28 (2 µg/mL, BioLegend, catalog 102116) antibody were applied. Total RNA was purified using the RNeasy Plus Mini Kit as recommended. Isolated RNA was quantified employing a Qubit 2.0 fluorometer, and RNA quality was determined using a Bioanalyzer 2100 with a RNA 6000 Pico chip. Then, 10 ng of total RNA (integrity > 8) was used to generate barcoded mRNA-seq cDNA library using the NEBNext Poly(A) mRNA Magnetic Isolation Module and NEBNext Ultra II RNA Library Prep Kit for Illumina (both from NEB) with a final amplification of 15 PCR cycles. Afterward, RNA was quantified using the Qubit HS assay kit. The library size distribution was determined using the Bioanalyzer HS DNA assay. Then, barcoded RNA-Seq libraries were clustered using the HiSeq Rapid SR Cluster Kit v2 using 8 pM, and 59 base pairs were sequenced on the Illumina HiSeq2500 using HiSeq Rapid SBS Kit v2 (59 cycles). Primary sequencing results were processed according to the Illumina standard protocol. Afterward, sequence reads were trimmed (deleting adapter sequences) and processed using the CLC Genomics Workbench software (v20.0, default settings; Qiagen). Reads were aligned to GRCm38 genome. Differentially expressed genes with a fold change $\geq |1.5|$ and $-\log(\text{FDR}) \geq 2$ were calculated using CLC Genomics workbench. Analysis of the enrichment of gene ontology (GO) terms within the upregulated genes was performed using the GO Resource and PANTHER Overrepresentation Test [238, 239, 247] (annotation version and release date, GO Ontology database DOI: 10.5281/zenodo.6399963 Released 2022-03-22), using Fisher's exact test with FDR correction (in cooperation with the working group of Prof. Tobias Bopp, Mainz).

4.6.5. Gene enrichment analysis

Gene ontology (GO) describes the relationship between genes by annotating and categorizing a gene product's molecular function and the associated biological processes (series of molecular functions). The enrichment analysis of a gene set indicates which molecular functions and biological processes were overrepresented in the gene list [248]. To perform enrichment analysis, the GO Consortium's online tool (http://www.geneontology.org/) was used. Gene names from the list were copied into the GO tool, the species (*mus musculus*) and specific ontology (*molecular function* and *biological process*) for the enrichment analysis were selected. Fold enrichment compares the background frequency of total genes annotated to the designated species to the sample

frequency representing the number of genes inputted that are under the same term [248]. Over representation of genes is represented as a positive fold enrichment value with a p-value < 0.05, calculated by the Mann–Whitney U test.

4.6.6. Time-lapse microscopy

The confocal laser scanning microscopy was used to detect cell-cell contacts by time-lapse video recording. Therefore, cells were labeled with fluorescence dyes and interactions were screened in real time.

MACS-isolated $CD4^+CD25^+$ Treg of $CD18^{Foxp3}$ mice and wildtype littermates (CFSE), conventional wildtype $CD4^+CD25^-$ T cells (CellMask orange) and BMDC (CellTrace violet (CTV) were stained with fluorescence dye for 10 minutes at 37°C (each 5µM;). Cells were cocultured in (Treg: BMDC; Treg: T cell) in an Ibidi 8-well plate in culture medium. Cell cultures were kept under 5% CO_2, 37 °C, and 90% humidity in an OkoLabs environmental incubator (H-301K environmental chamber, Oko Touch, Oko Pump, T-Control and CO_2 control, OkoLabs, Italy) on the microscope table. Cell interaction was monitored by CLSM using a Leica TCS SP8 and was performed with a 20X 0.75 NA objective with 405 nm and 488 nm excitation and emission windows of 415 to 478 nm and 498 nm to 578 nm for respective CTV and CSFE detection and with scanning Differential Interference Contrast transmission imaging in a 580 µm x 580 µm frame format with 400 lines per second, 1.14 µm/pixel (512 x 512 pixel per frame) and with 2 times averaging per line with a frame acquisition of every 6 minutes per selected position within the chamber over 12 hours. Cell interactions were analyzed with ImageJ by counting every individual cell-cell contact in every picture section after 6 minutes (in cooperation with the microscopy core facility and Prof. Gregory Harms of the Paul-Klein-Zentrum, Mainz).

4.6.7. Cytometric bead array (CBA)

The cytometric bead array (CBA) is a flow cytometry application, which was performed to measure multiple cytokine secretion in the supernatant of cell cultures simultaneously. The secretion of pro- and anti-inflammatory cytokines is, besides the intracellular flow cytometry staining, also an important parameter to characterize immune cells. Specific cytokine patterns can give a conclusion on the type of immune response.

The basic principle of the CBA is to catch cytokines with beads labeled with cytokine-specific fluorescence antibodies by flow cytometry. Therefore, each cytokine has its fluorescence fingerprint to be detected. Cytokine levels in the cultures were measured, followed by the manufacturer's instructions. 300µl of the supernatant was collected from the cultures and frozen until analysis. For standard series dilution, 25 µl of CBA buffer was mixed with stock standard solution. 1:2 Serial dilution was followed (from 0 to 10,000 pg/ml). To capture the specific cytokines 10 µl of each sample was mixed with 10 µl of capture beads master mix (0.2 µl of each bead was mixed with CBA buffer to 10 µl in total). After 1 hour incubation in the dark at RT, 10 µl of detection antibody master mix (0.2 µl of each bead was mixed with CBA buffer to 10 µl in total) was added to the samples. Samples were incubated again for 1 hour and then washed with 1 ml CBA buffer and centrifuged (300g, 5 min, 4 °C). Afterwards, samples were resuspended in 100 µl CBA

buffer and measured within an hour by an Attune flow cytometer and analyzed with FCAP Array™ software.

4.6.8. Cocultures

Splenic MACS-isolated $CD4^+CD25^+$ Treg of $CD18^{Foxp3}$ mice and wildtype littermates as well as MACS-isolated DC from wildtype mice were cocultured (3:1; DC:Treg mixture, 48-well plate or 96-well plate) in culture medium for 48 hours, 5% CO_2, 37 °C. The cytokine analysis of the supernatant was performed with Cytometric bead array flex set system as described.

4.6.9. Enzyme-linked immunosorbent assay (ELISA)

The ELISA was used to detect Ig levels in the serum of $CD18^{Foxp3}$ mice. Mice were sacrificed with CO_2, and blood was collected from the heart and then centrifuged for 1 minute at 10000 rpm. Serum (upper layer of the tube) was collected and frozen at -20°C until use. For all ELISA the uncoated ELISA kits from Invitrogen were used. Assays were performed as described in the manufacturer's protocols respectively.

IgE ELISA

The coating buffer (10X) was diluted 1:10 with 10x PBS in deionized water. Corning™ Costar™ plate 9018 was coated with 100µl/well of capture antibody in coating buffer (1X). The plate was sealed and incubated overnight at 4°C.
The next day, the blocking buffer (2X) was diluted 1:10 with assay buffer A concentrate (20X) in deionized water. Wells were washed twice with 400 µl/well wash buffer in a plate washer. After each washing, the plate was plotted on an absorbent paper to remove residual buffer. Wells were blocked with 200 µl blocking buffer and incubated for 2 hours at RT. The plate was washed again as described before.
The IgE standards were reconstituted for 20 minutes by adding distilled water as stated on the label of the standard vial (500 ng/ml). 2-fold serial dilution of the standards was performed with 1X assay buffer A. Therefore, stock assay buffer A was diluted 1:20 in deionized water. 100 µl of 1X assay buffer A was added to the standard wells. 100 µl of the standard was added in duplicates to well A1 and A2 (250 ng/ml), mixed and 100 µl of these wells are transferred to B1 and B2, respectively. This was repeated for 5 times. 100 µl of assay buffer A was added to the blank wells and 50 µl to the sample wells. The plate was covered and incubated for 2 hours at RT on a thermoshaker at 400 rpm. Afterwards four washing steps were performed.
The detection antibody was diluted 1:250 in assay buffer A (1X) and 100 µl per well were added. Plate was again incubated for 1 hour at the thermoshaker and later washed four times.
Streptavidin-HRP was diluted 1:400 in assay buffer A (1X) and 100 µl per well were added to the plate. The plate was incubated for a further 30 minutes at RT and washed again.
100 µl/well of substrate solution was added and incubated for 10-15 minutes. Afterward 100 µl/well stop solution was added, and the plate was read at 450 nm in a plate reader. Data were analyzed with Prism.

IgG1 and IgG2a ELISA

The procedure of the IgG1 and IgG2a ELISA is performed as described above without the Streptavidin-HRP step.

4.6.10. Calcein transfer assay

To assess cell communication *in vitro*, certain substances such as calcein are transported via gap junction between the cells. Gap junctions are intercellular membrane channels, which constitute the protein connexin that facilitates the transport of small molecules (<1.5 kD) across cells. The passage is passive, and the continuous flux of materials between cells through the channels is known as gap junction intercellular communication (GJIC). Treg are stained with calcein acetoxymethyl ester (Calcein AM), which is hydrolyzed upon cellular uptake by cytoplasmic esterases. It yields calcein, which is membrane-impermeable and can be transported via gap junction [249].
$1*10^6$ splenic MACS-isolated $CD4^+CD25^+$ Treg of $CD18^{Foxp3}$ mice and wildtype littermates were stained with 2µg/ml calcein blue AM in RPMI with 5% FCS (1:1) for 30 min, 37°C, 5% CO_2. $1*10^6$ differentiated BMDC as well as MACS-isolated DC and naïve $CD4^+$ from wildtype mice were stained with CTV as described for 30 min, 37°C, 5% CO_2. $5*10^5$ Treg/DC, Treg/BMDC, and Treg/$CD4^+$ were cocultured (1:1) for 24h. Calcein from Treg was transferred to the CTV^+ cell types. DC, BMDC, and T cells were then identified as double positive for calein/CTV. Calcein transfer of double positive CTV/Calcein cells was analyzed with an Attune flow cytometer (Figure 21).

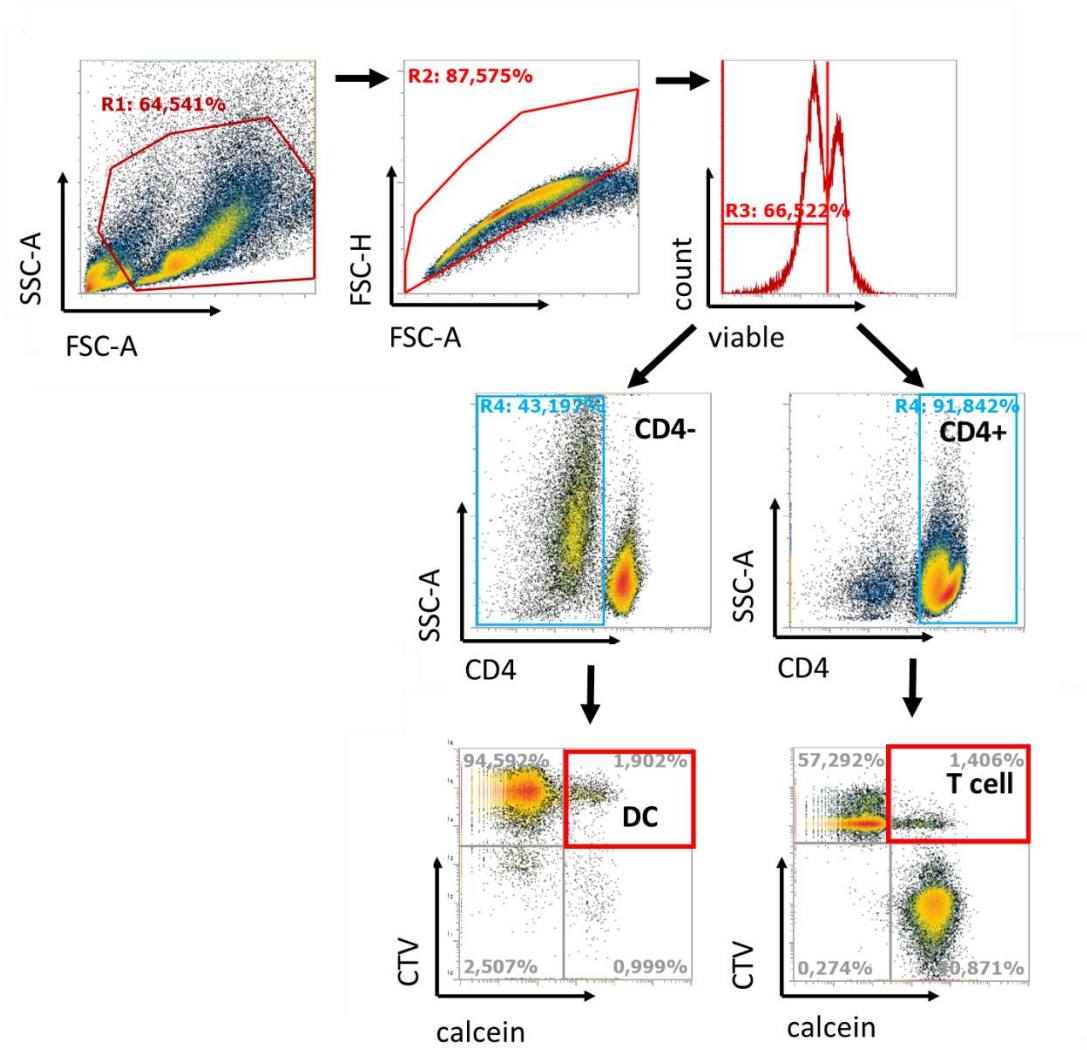

Figure 21 ***Gating strategy of calcein/CTV double positive cells.*** *Single, viable cells were gated as described before. Calcein/CTV positive DC and BMDC were pregated as CD4$^-$. Calcein/CTV positive T cells are pregated as CD4$^+$.*

4.6.11. Induced Treg (iTreg) culture

CD4$^+$ naïve T cells isolated from spleens can be induced to express Foxp3 *in vitro* by T cell activation in the presence of TGF-β1 and IL-2. A 24-well plate was coated with plate-bound anti-CD3 (10 µg/ml)/ anti-CD28 (4 µg/ml) for 1h in the incubator. 2*10^6/well splenic MACS-isolated naïve CD4$^+$ T cells of CD18^{Foxp3} mice and wildtype littermates were given in the plate and were cultured in 1 ml/well with 10 ng/ml TGF-ß and 250 ng/ml IL-2 in culture medium for 5 days (37°C, 5% CO_2). Foxp3 expression, as well as CD11a deletion of LFA-1deficient iTreg were assessed daily by flow cytometry with an attune NxT cytometer (Figure 22).

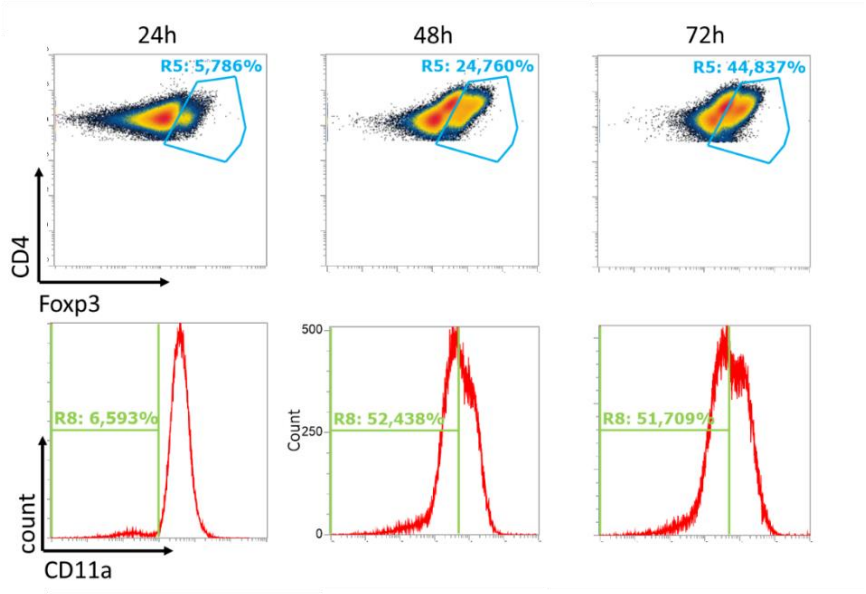

Figure 22 ***Flow cytometric monitoring of iTreg culture.*** *Cells were pregated as described before. iTreg induction of naive T cells was assessed daily (here shown for the first three days). iTreg were gated for $CD4^+Foxp3^+$ and LFA-1 deletion was analyzed as $Foxp3^+CD11a^-$ iTreg.*

4.6.12. Vascular tone experiment

The vascular responsiveness to vasodilators (increasing doses of acetylcholine (ACh) in a range from 10^{-9}–$10^{-5.5}$ mol/L) of isolated aortic rings was studied as described before [250]. For this, the organ bath method was used for isometric tension measurement with a part of the aorta. The aorta (3-5 mm) was isolated and cleaned from any fat and connective tissue and then stretched between 2 wire triangles. One triangle is connected to the transducer, and the other to a fixed hook as a counter support (Figure 23). The whole structure is then stable and freely suspended in a double-walled glass vessel. A water bath tempered to 37°C flows through the wall. The Krebs-Henseleit buffer solution (98.93 mmol/L of NaCl, 4.69 mmol/L of KCl, 2.49 mmol/L of $CaCl_2$, 1.2 mmol/L of $MgSO_4$, 0.613 mmol/L of K_2HPO_4, 25 mmol/L of $NaHCO_3$, 11.1 mmol/L of d-glucose, 37 °C, pH 7.35) pre-tempered to 37°C, is filled (25ml per vessel, i.e. up to the level of the inner double wall) bubbled with carbogen gas (95%CO2+5%O2). This creates an environment similar to that of a living organism. Indomethacin 10 µmol/L was added to prevent endogenous synthesis of prostaglandins. Aortic segments were stretched gradually over 30 minutes to reach a resting tension of 1g. After the preconstruction with prostaglandin $F_2\alpha$ (3.3 µmol/L) to reach 50%–70% of the maximum tone induced by kaliumchloride (KCl), cumulative concentration-relaxation curves were recorded in response to increasing concentrations of ACh.

First, the aortic function test was measured with KCL. 1ml of 2M KCL was given into the bath to see any contraction. After the aorta has settled on the manual zero line, the KCl dose-response curve was performed (62,5µl 5mmol, 62,5µl 10mmol, 125µl 20mmol, 250µl 40mmol and 500µl 80mmol). The pipetting amounts and their concentrations are sequential. Afterward KCl is washed out and waited until zero line is reached again.

The pre-contraction for mouse aorta was performed with prostaglandinF2alpha (PGF_2a) 10 mmol 5µl of PGF_2a was added. Pre-contraction lasts until a plateau is reached - usually 15-20 minutes. Then, the 1st relaxation curve with ACh (Table 16) and 2st relaxation curve with nitroglycerine (NTG) (Table 17) was performed and given in different concentrations into the bath until a plateau was reached. ACh is used to check the functionality of the vascular endothelium and with NTG the functionality of the vascular muscles was accessed (the experiment was performed in cooperation with the working group of Dr. Susanne Karbach, Mainz).

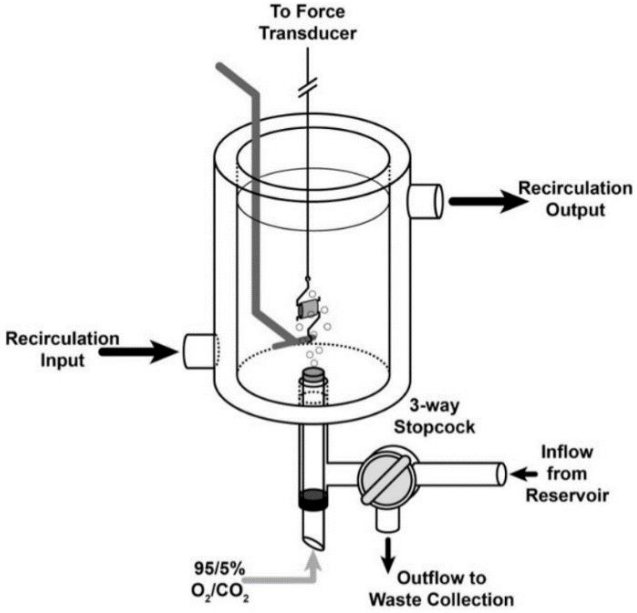

Figure 23 ***Organ bath construction.*** *Aortic ring is placed in the double-wall, water jacketed tissue bath and bubbled with carbogen gas (95%CO2+5%O2). This creates an environment similar to that of a living organism. (adapted from [251]).*

Table 16 Composition of ACh relaxation curve

ACh relaxation curve		
Stock solution (10^{-x} molar)	Addition into organ bath	final concentration (10^{-x} molar)
-6	25 µl	-9
-5	17,5 µl	-8
-4	17,5 µl	-7
-3	17,5 µl	-6

Table 17 Composition of NTG relaxation curve

NTG relaxation curve		
Stock solution (10^{-x} molar)	Addition into organ bath	final concentration (10^{-x} molar)
-6	25 µl	-9
-5	17,5 µl	-8
-4	17,5 µl	-7
-3	17,5 µl	-6
-2	Trinitrosan 17,5 µl	-5

4.6.13. L-012-Enhanced Chemiluminescence

Detection of reactive oxygen species (ROS) and reactive nitrogen species (RNS) was done as described before in a microplate assay [250]. L-012 is a luminol-based chemiluminescent and is widely used to detect NADPH oxidase (Nox)-derived reactive ROS/RNS as an incidence for oxidative burst.
Oxidative burst was measured in fresh citrate blood by L-012 (8-amino-5-chloro-7-phenylpyrido [3,4-d] pyridazine-1,4-(2H,3H) dione sodium salt, 100 µM) enhanced chemiluminescence (ECL) upon 1:50 dilution in a white 96-well plate. Stimulation to produce reactive ROS/RNS was performed in 150µl/well with zymosan A (50 µg/mL) as well as phorbol ester dibutyrate (PDBu 10 µM) in PBS buffer containing Ca^{2+}/Mg^{2+} (1 mM). ECL was analyzed using a TECAN plate reader (in cooperation with the working group of Dr. Susanne Karbach, Mainz).

4.7. *In vivo* experiments

4.7.1. Imiquimod-induced psoriasis

Imiquimod (IMQ)-induce psoriasis was performed as described before [252]. IMQ is a TLR7/8 ligand and a potent immune activator. Topical application of commercial aldara cream with 5% IMQ can induce and exacerbate psoriasis in mice [253].
6 week old $CD18^{Foxp3}$ mice and WT littermates were shaped at the abdomen (day -1). Aldara cream was applied daily at a topical dose of 50 mg onto the back skin and 25 mg onto the right ear for 6 days to establish an IMQ-induced psoriasis mouse model (Figure 24). The left ear was treated with Vaseline as control. The Psoriasis Area and Severity Index (PASI) scoring system was used to assess the inflammatory status of the mice`s dorsal skin for all the 7 days. It included the visual examination of the following three parameters: erythema (redness), induration (thickness), and desquamation (scale) on the back skin of each mouse. Each parameter was given a score between 0 and 4 (0-none, 1-slight, 2-moderate, 3-marked, 4-very marked), leading to a cumulative score from 0 to 12. Skin thickness of the ears and the back skin were measured using a caliper (in µm).

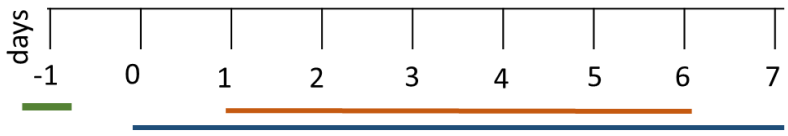

day -1:
→ Shaving of the abdomen
day 1-6 :
→ Cutaneous application of aldara creme onto the back/ear
day 0-7 :
→ Measurement of ear and back thickness
day 7:
→*ex vivo* analysis

Figure 24 ***Time line of the IMQ-induced psoriasis model.***

4.7.2. Acute contact dermatitis

Oxazolone-induced contact dermatitis was performed as described before [232, 254]. In the acute model of allergic contact dermatitis, the disease can be achieved by a topical application of the allergen oxazolone. Oxazolone is topically applied to the shaped abdomen, known as the sensitization state. After the sensitization the allergen is again applied topically to the ear, which will result in an inflammatory response and swelling known as challenge.
6 week old $CD18^{Foxp3}$ mice and wildtype littermates were shaped at the abdomen (day -1). Hapten was mixed with an 4:1 acetone and olive oil solution. For sensitization, 2,5mg/50µl hapten mixture was given onto the back skin (day 0). After 5 days the right ear was challenged with 40µg/20µl of hapten mixture, and the left ear was treated with control solution without the hapten. Ear swelling was measured with a caliper until day 9 (Figure 25). Organ and cell isolation proceeded as described.

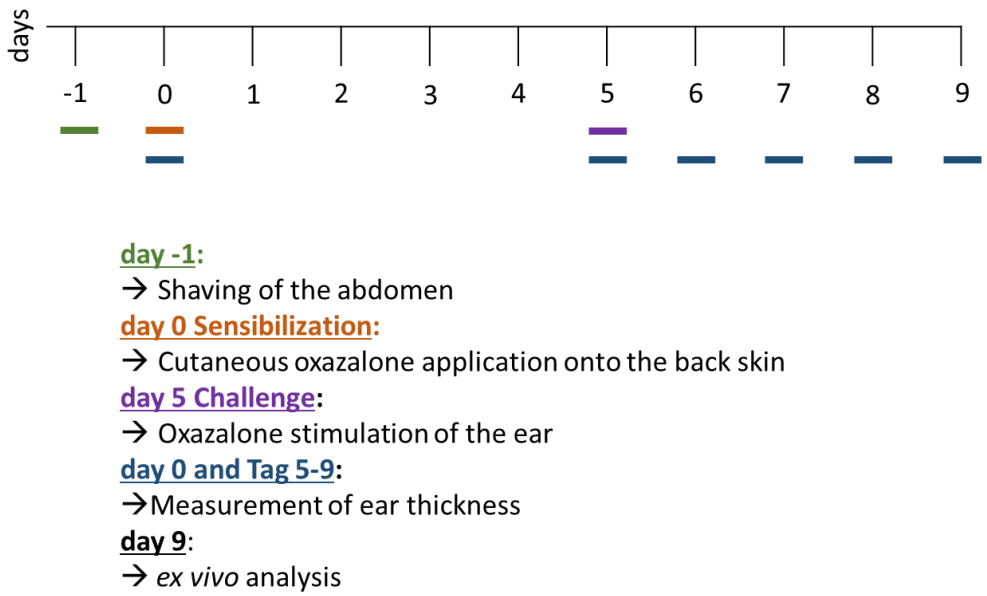

Figure 25 ***Time line of the acute contact dermatitis model.***

4.8. Experimental design and blinding

For monitoring of signs of skin inflammation, both animal caretakers and researchers were blinded to the genotype of animals. For all *ex vivo* and *in vivo* experiments, including histological analysis, indirect immunofluorescence and flow cytometry, samples were randomized and researchers were likewise blinded to mouse genotype.

4.9. Data availability

RNA seq data generated for this study were deposited in the NCBI's Gene Expression Omnibus database (GEO GSE215787).

4.10. Statistical Analysis

Data were analyzed using GraphPad PRISM v 9.2.0 software. For comparisons between only two groups, statistical significance was assessed using an unpaired, two-tailed t test. For data sets where comparisons between multiple groups were necessary, statistical significance was assessed using either a 2-way ANOVA with Šídák's multiple comparisons test or multiple unpaired t tests corrected for multiple comparisons by the two-stage step-up (Benjamini, Krieger, and Yekutieli) method. In all cases, significance levels were denoted as follows: ns, $p>0.05$; *, $p<0.05$; **, $p<0.01$; ***, $p<0.001$ ****, $p\leq0.0001$.

4.11. Study approval

Mice were sacrificed for organ retrieval according to §8 TierSchG. All animal experiments were performed after approval by the regional regulatory authorities (Landesuntersuchungsamt LUA, Rheinland-Pfalz, Koblenz, reference number G20-1-113).

5. Results

In the mouse models described above, all leukocytes lack β_2-integrins ($CD18^{-/-}$, $CD18^{hypo}$) or LFA-1 ($CD11a^{-/-}$). Thus, it is difficult to assess the cell type-specific role of β_2-integrins *in vivo* in the context of LAD-1 pathology. Therefore, we considered it necessary to establish mice with cell type-specific β_2-integrin deficiency, especially on Treg [1]. In the following section, we characterize these mice *in vitro* and *in vivo* in the context of organ abnormalities, Treg phenotype, and LFA-1-dependent interactions of different cell types, IMQ-induced psoriasis, and atopic dermatitis responses.

(2) Klaus Tanja, Wilson S Alicia et al., *Impaired Treg-DC interactions contribute to autoimmunity in leukocyte adhesion deficiency type 1.* JCI Insight, 2022. **7**(24).

5.1. The specific deletion of β_2-integrins in Treg leads to the spontaneous development of atopy-like organ inflammation

Alongside persistent leukocytosis and recurrent infections, LAD-1 patients lacking functional CD18 develop autoimmune syndromes [210, 211, 255]. While it has been postulated that Treg from patients with secondary mutations restoring CD18 function in some cells (reversion mutations) display reduced suppressive activity and may contribute to the development of IBD in these patients [255], their direct contribution to the induction of autoimmunity remains unclear. To directly address the role of Treg-expressed CD18, a mouse strain with floxed CD18 alleles was generated previously in the lab [1, 95]. By crossing this strain with a Foxp3-Cre expressing mice we generated a mouse strain lacking CD18 expression in Foxp3 expressing cells, following described as $CD18^{Foxp3}$ mice (see Material and Methods chapter 4.1.). We first characterized the phenotype of these mice regarding skin and other organs by histology and flow cytometry analysis.

5.1.1. $CD18^{Foxp3}$ mice develop spontaneous skin inflammation and hyperplasia

$CD18^{Foxp3}$ mice housed in specific pathogen-free conditions spontaneously developed skin inflammation characterized by scaling and thickening of distinct regions (Figure 26 A). Skin lesions were most commonly observed on the tails, ears, and face of mice. Histological analysis of inflamed ears showed thickening of the dermis and epidermis of $CD18^{Foxp3}$ mice (Figure 26 B, C). Gross increases in ear thickness were also confirmed quantitatively (Figure 26 D). Skin lesions and thickening were also observed at tail skin of $CD18^{Foxp3}$ mice (Figure 26 E). Increased magnification of H&E stained ear sections revealed severe epidermal acanthosis, parakeratosis, and moderate spongiosis in $CD18^{Foxp3}$

mice, and dermal compartment showed a mixed polymorphonuclear infiltrate of inflammatory cells into the epidermis (Figure 26 F). Furthermore, the number of sites of affected skin increases with age (Figure 26 G). Affected $CD18^{Foxp3}$ mice also developed profound hyperplasia of the spleen and skin-draining LN (sdLN) (Figure 26 H). Quantifying the total number of splenocytes confirmed greatly increased cell numbers in the spleens of older mice (Figure 26 I), indicative of a systemic immune response.

The specific deletion of CD18 in $Foxp3^+$ Treg was confirmed by flow cytometry in several organs (Figure 27 A). The export of functional integrins from the endoplasmic reticulum is reliant on the expression of both α and β subunits of the heterodimer. In the absence of β subunit expression, α subunits are not stabilized and are readily degraded [218]. Thus, to further verify the functional deletion of CD18, the concomitant loss of the surface expression of the β_2-integrin LFA-1's α chain CD11a was confirmed (Figure 27 B). The expression of CD18 and CD11a remained at WT levels in $CD8^+$ T cells (Figure 27 C) and conventional $Foxp3^-$ $CD4^+$ T cells (Figure 27 D) in different organs, confirming the Treg-specific loss of CD18. Only T_{conv} in the lung showed an unspecific decrease in LFA-1 expression (Figure 27 D).

CD18 can form heterodimers with multiple α integrins including CD11a ($\alpha_L\beta_2$, LFA-1), CD11b ($\alpha_M\beta_2$, Mac-1, CR3), CD11c ($\alpha_X\beta_2$, p150.95, CR4) and CD11d ($\alpha_D\beta_2$), as such, the deletion of CD18 could lead to the functional loss of multiple integrins. As signals mediated by $\alpha_M\beta_2$ can have immune-inhibitory effects in some myeloid cell populations [102], we thus examined which integrin complexes are expressed in Treg and whether these were all equally affected by the loss of β_2-integrin expression. Gene expression analysis from sorted unstimulated Treg showed hardly detectable expression of α integrins *Itgad* (CD11d), *Itgam* (CD11b), and *Itgax* (CD11c) on the mRNA level (Figure 27 E). *Itgal* (CD11a) mRNA, on the other hand, was highly expressed, with expression decreased in $CD18^{Foxp3}$ mice (Figure 27 E). The same expression pattern of these α integrins was also observed in Treg stimulated *ex vivo* (with anti-CD3/CD28) (Figure 27 F). We confirmed this expression pattern for CD11a, CD11b, and CD11c on the protein level by flow cytometry where in line with previously published reports, only CD11a was highly expressed on Treg (Figure 27 G, [256]). Here, the loss of CD18 in Treg only affected the expression of CD11a, implicating the loss of LFA-1 as the main driver of the phenotype observed.

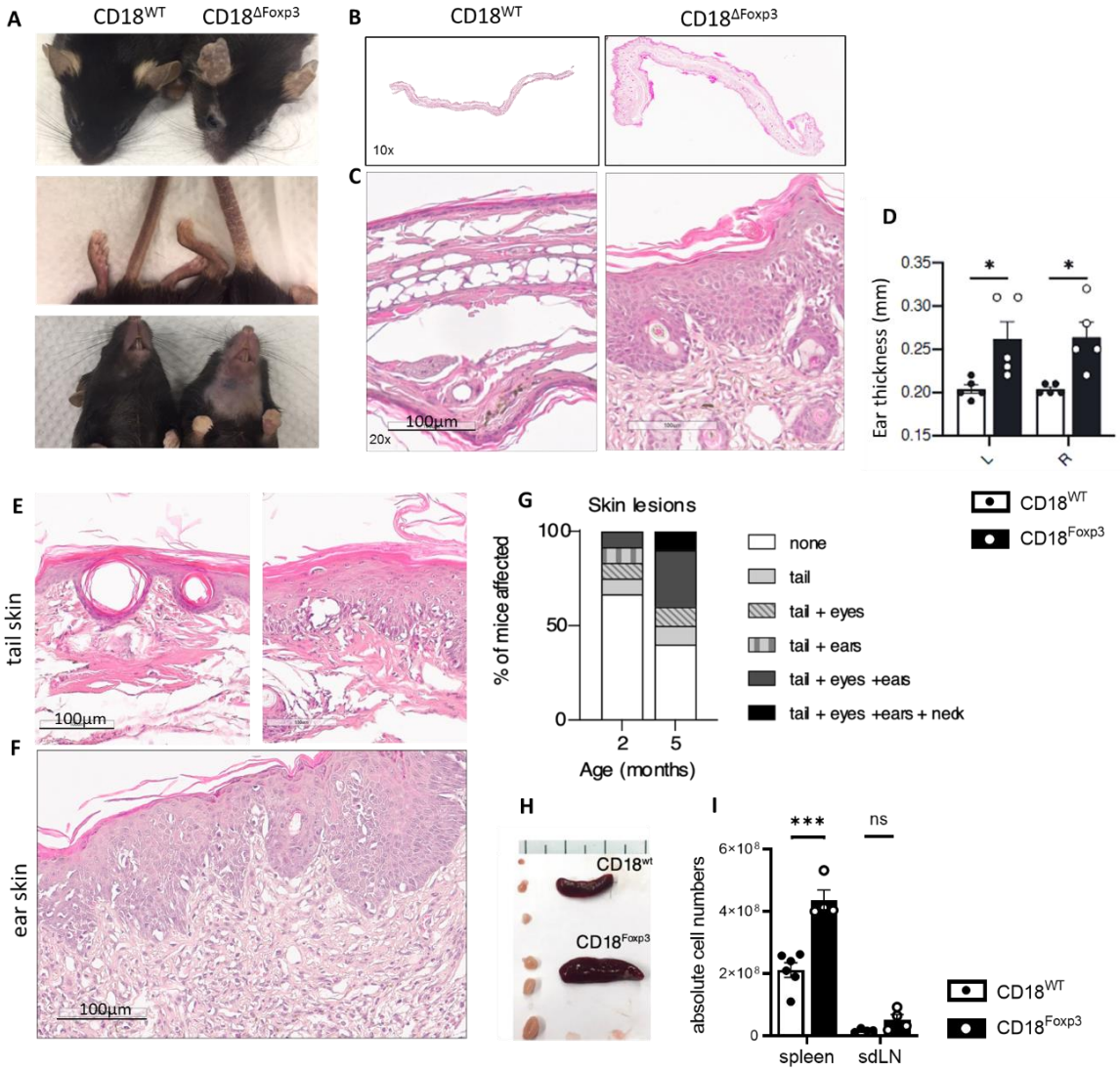

Figure 26 ***Treg-specific deletion of CD18 leads to the development of spontaneous skin inflammation and hyperplasia.*** *(A) Disease progression of skin lesions developed by CD18^{Foxp3} mice between 2 and 5 months of age (10-12 female and male mice were observed). Representative images of H&E staining of ear skin tissue of 21-22 week-old mice at* ***(B)*** *10x* ***(C)*** *20x magnification.* ***(D)*** *Ear thickness of left (L) and right (R) ears of CD18^{wt} and CD18^{Foxp3} mice, n=5. Representative H&E staining of tail skin at* ***(E)*** *20x and* ***(F)*** *200x magnification.* ***(G)*** *Disease progression of CD18^{Foxp3} mice between 2 and 5 months of age.* ***(H)*** *Representative pictures of spontaneous hyperplasia of spleen and sdLN of 12-week-old CD18^{Foxp3} mice compared to littermate controls. Scale = 1mm increments.* ***(I)*** *Absolute cell numbers from spleens sdLN of 12-week-old mice, n=4-6. Dots represent individual mice. Bars show the mean ± SEM. Significance determined by multiple unpaired t- tests corrected for multiple comparisons by the two-stage step-up (Benjamini, Krieger, and Yekutieli) method. ns, $p>0.05$; ***, $p\leq0.001$; ****, $p\leq0.0001$.*

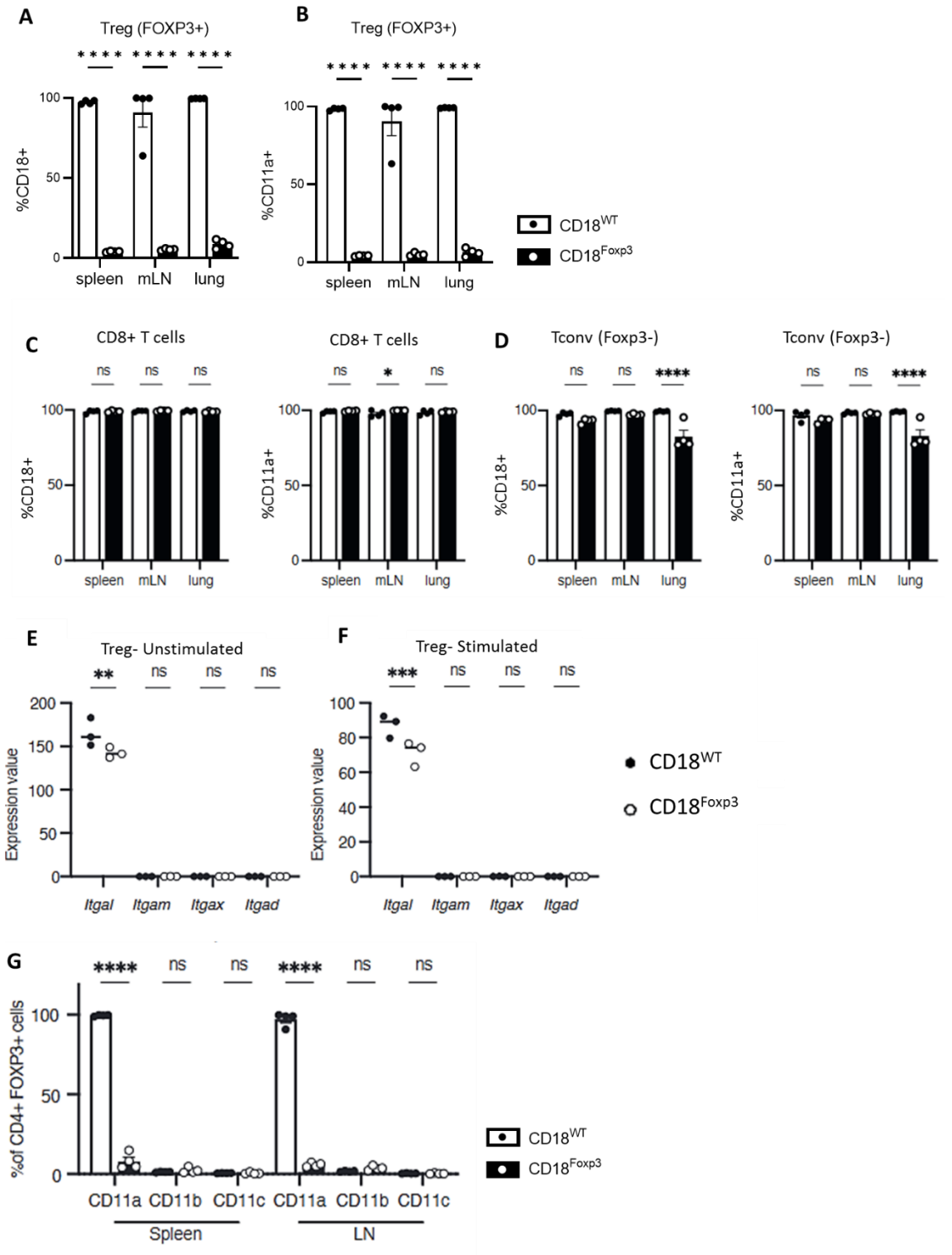

Figure 27 ***CD18 deletion is Treg-specific***. **(A)** CD18 and **(B)** CD11a expression in regulatory (Foxp3^{+}) T cells measured by flow cytometry. n=4. *CD18 and CD11a expression in* ***(C)*** *CD8 T cells and* ***(D)*** *CD4 T_{conv} (Foxp3-) from multiple tissues measured by flow cytometry. Expression of transcripts of α integrin partners of Itgb2 in* ***(E)*** *unstimulated and* ***(F)*** *stimulated Treg isolated for $CD18^{wt}$ and $CD18^{Foxp3}$ mice, n=3.* ***(F)*** *Quantification of surface expression of α integrin proteins known to form heterodimers with CD18 on Treg from spleens and LN of $CD18^{wt}$ and $CD18^{Foxp3}$ mice, n=3. Dots indicate individual mice (A-C, F) representative of at least two independent experiments. Significance was determined by 2-way ANOVA with Šídák's multiple comparisons test, ns, $p>0.05$; *, $p<0.05$; **, $p<0.01$; ****, $p\leq0.0001$.*

5.1.2. Absence of CD18 expression on Treg leads to leukocyte infiltration and inflammation in specific organs

To determine whether the observed skin inflammation in $CD18^{Foxp3}$ mice was a product of a skin-specific inflammatory process or a sign of a systemic break in tolerance, as suggested by splenic hyperplasia, we examined immune infiltration in various organs. Histopathological examination of H&E stained sections in spleens of $CD18^{Foxp3}$ mice indicated a relative hypoplasia of primary follicles, whereas the red pulp and parafollicular T cell zone were more prominent (Figure 28 A). Lungs of $CD18^{Foxp3}$ mice showed significantly stronger lymphocytic and monocytic infiltration and substantial lung damage, with atelectasis and exudation into lung alveoli (Figure 28 B). We also observed a significant hyperplasia of LN from $CD18^{Foxp3}$ mice. Further, there was a substantial increase in tertiary follicular structures within the LN and a prominent efferent vessel (EV) ectasia (Figure 28 C). In the livers, a tendency towards stronger lymphocytic infiltration in the Glisson fields of $CD18^{Foxp3}$ mice was also observed (Figure 28 D). By contrast, kidneys of both genotypes did not show significant differences in immune cell infiltration or organ injury (Figure 28 E). Histological analysis of cross-sections of the small intestine revealed an inflammatory infiltrate in the lamina muscularis mucosae and the lower part of the mucosa in $CD18^{Foxp3}$ mice (Figure 28 F). Quantification of H&E staining from these organs confirmed spleen hyperplasia and altered white/red pulp ratios (Figure 28 G), lung inflammation and tissue damage (Figure 28 H), and increased follicle number and hyperplasia in LN (Figure 28 I) but no tissue alterations in the liver in $CD18^{Foxp3}$ mice (Figure 28 J). However, in kidneys of $CD18^{Foxp3}$ mice, there was a tendency towards organ hyperplasia (Figure 28 K). Immune infiltrates in the gastrointestinal tract (GIT) were more commonly observed in $CD18^{Foxp3}$ mice than in their littermate controls (Figure 28 L). Overall, the selective organ alterations concerning LN, lung tissue damage and skin inflammation are characteristic for an atopy-like phenotype in these mice.

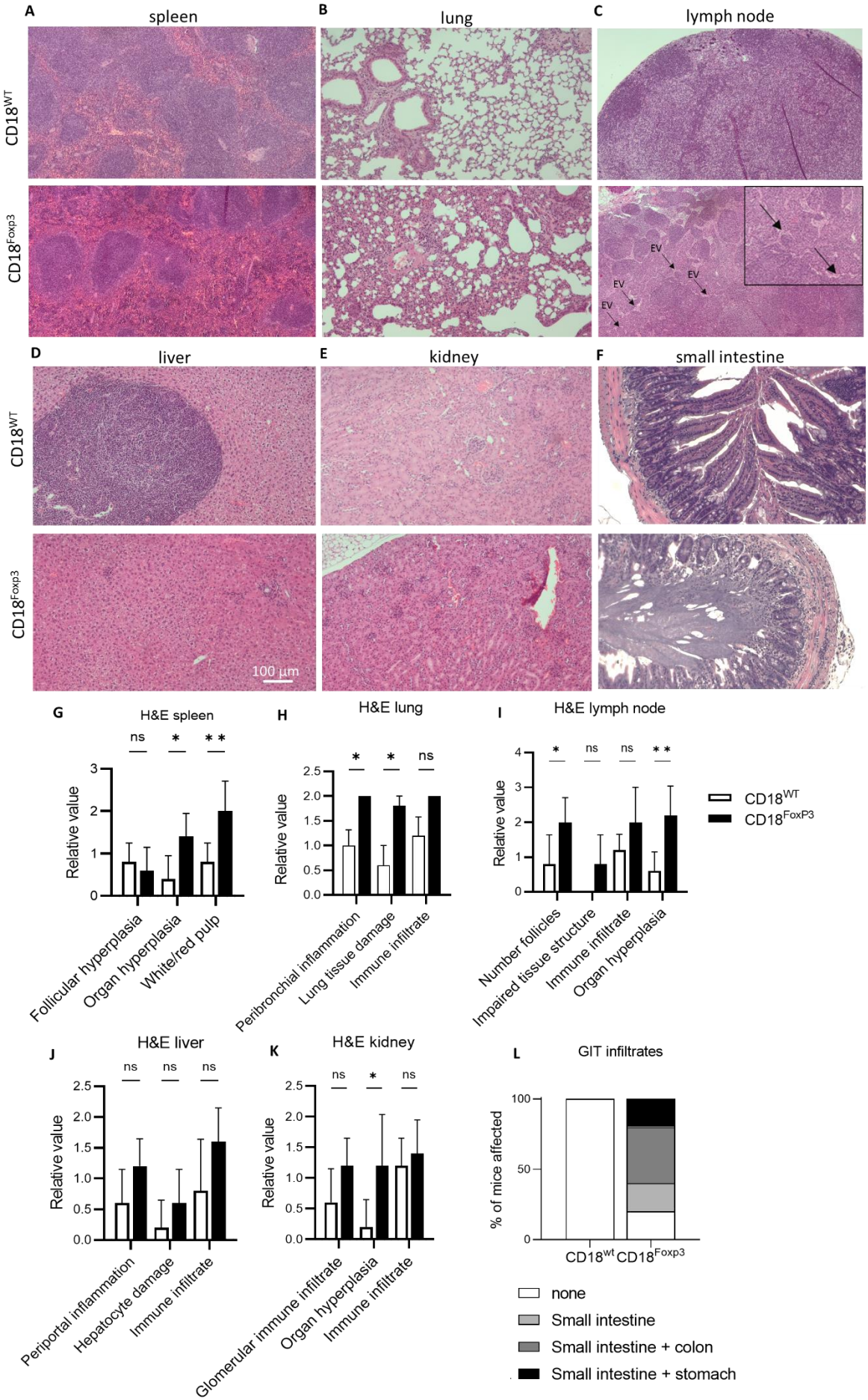
A
spleen
B
lung
C
lymph node
CD18WT
CD18Foxp3
EV
EV
EV
EV
D
liver
E
kidney
F
small intestine
CD18WT
CD18Foxp3
100 µm
G
H&E spleen
ns
*
**
Relative value
Follicular hyperplasia
Organ hyperplasia
White/red pulp
H
H&E lung
*
*
ns
Relative value
Peribronchial inflammation
Lung tissue damage
Immune infiltrate
I
H&E lymph node
*
ns
ns
**
Relative value
Number follicles
Impaired tissue structure
Immune infiltrate
Organ hyperplasia
CD18WT
CD18FoxP3
J
H&E liver
ns
ns
ns
Relative value
Periportal inflammation
Hepatocyte damage
Immune infiltrate
K
H&E kidney
ns
*
ns
Relative value
Glomerular immune infiltrate
Organ hyperplasia
Immune infiltrate
L
GIT infiltrates
% of mice affected
CD18wt
CD18Foxp3
none
Small intestine
Small intestine + colon
Small intestine + stomach

Figure 28 ***Regulatory T cell specific deletion of CD18 leads to selective organ autoimmunity.*** *Representative images of H&E stained cross-sections of the* ***(A)*** *spleen,* ***(B)*** *lungs,* ***(C)*** *LN with errors for efferent vessels (EV),* ***(D)*** *liver,* ***(E)*** *kidney and* ***(F)*** *small intestine of 11-15 week-old $CD18^{wt}$ and $CD18^{Foxp3}$ mice.* ***(G-K)*** *Quantification of H&E staining from spleen, lung, LN, liver, and kidney samples from $CD18^{wt}$ and $CD18^{Foxp3}$ mice n=5.* ***(L)*** *Frequency of mice with immune infiltrates in the gastrointestinal tract (GIT) identified by H&E staining n=5. Significance was determined by 2-way ANOVA with Šídák's multiple comparisons test, ns, $p>0.05$; *, $p<0.05$; **, $p<0.01$.*

5.2. Deficiency of β_2-integrins does not impair Treg migration into tissues

β_2-integrins have a well-characterized and important role in the adhesion and extravasation of leukocytes into inflamed tissues [257]. As such, LAD-1 patients display persistent leukocytosis as these cells, unable to migrate into tissue sites, are trapped in circulation and lymphatic organs [213, 258]. T cells lacking their functional β_2-integrin LFA-1 have been described to have defects in their emigration into the skin and other tissue sites in several disease models [221, 232, 259]. To address whether dysfunctional Treg migration to tissue sites could explain the induction of the observed multi-organ inflammation and increase in T_{conv} activation status, we first examined Treg infiltration into the inflamed ears of $CD18^{Foxp3}$ mice.

Surprisingly, immunofluorescence imaging of tissue sections demonstrated clear infiltration of Treg into the tissue even in the absence of Treg-expressed CD18 (Figure 29 A). Quantification of infiltrating Treg revealed an increase in the number of Treg in the inflamed ears of $CD18^{Foxp3}$ mice compared to uninflamed $CD18^{wt}$ controls (Figure 29 B). To further assess the ability of Treg to migrate in the absence of CD18, we examined the distribution of $CD18^{Foxp3}$ Treg in various other sites by flow cytometry. Unlike the drastically reduced Treg numbers that would be expected from dysfunctional Treg migration, we observed that Treg abundance in several diverse organs was not impaired in $CD18^{Foxp3}$ mice (Figure 29 C, D). Indeed, in contrast to wildtype littermates, Treg frequencies in the lung and spleen were found to be significantly increased, implicating a functional rather than a migration-specific defect of LFA-1-deficient Treg (Figure 29 D). Furthermore, in the thymus of 3-week-old $CD18^{wt}$, and $CD18^{Foxp3}$ mice, similar numbers of double negative $CD4^-CD8^-$ and double positive $CD4^+CD8^+$ precursors as well as $Foxp3^+$ cells were observed (Figure 29 E), indicating no developmental defect of LFA-1-deficient Treg.

We next investigated if Treg compensated for the loss of LFA-1 by upregulation of other molecules involved in adhesion and transmigration. Surface expression of L-selectin (CD62L), involved in the retention of T cells in the LN and migration into non-lymphoid tissues [260, 261] was decreased in Treg from the ears, lungs, and spleens of $CD18^{Foxp3}$ mice (Figure 29 F). L-selectin (*Sell*) was highly expressed on unstimulated Treg and decreased in stimulated (anti-CD3/CD28) Treg with no difference in the expression value of $CD18^{wt}$ and $CD18^{Foxp3}$ Treg (Figure 29 G). P-selectin (*Selp*) expression was not detected in Treg (Figure 25 G). Analysis of other adhesion molecules on the surface of Treg showed increased expression of surface CD29 (β_1-integrin) on splenic Treg and of CD103 (α_E integrin) on Treg from blood, spleen, LN, and lungs of $CD18^{Foxp3}$ mice (Figure 29 H, I). Klrg1 expression was likewise increased on Treg from the blood, spleens and lungs of

$CD18^{Foxp3}$ mice, where CD49d (VLA-4) was only significantly upregulated in Treg from sdLN (Figure 29 H, I).

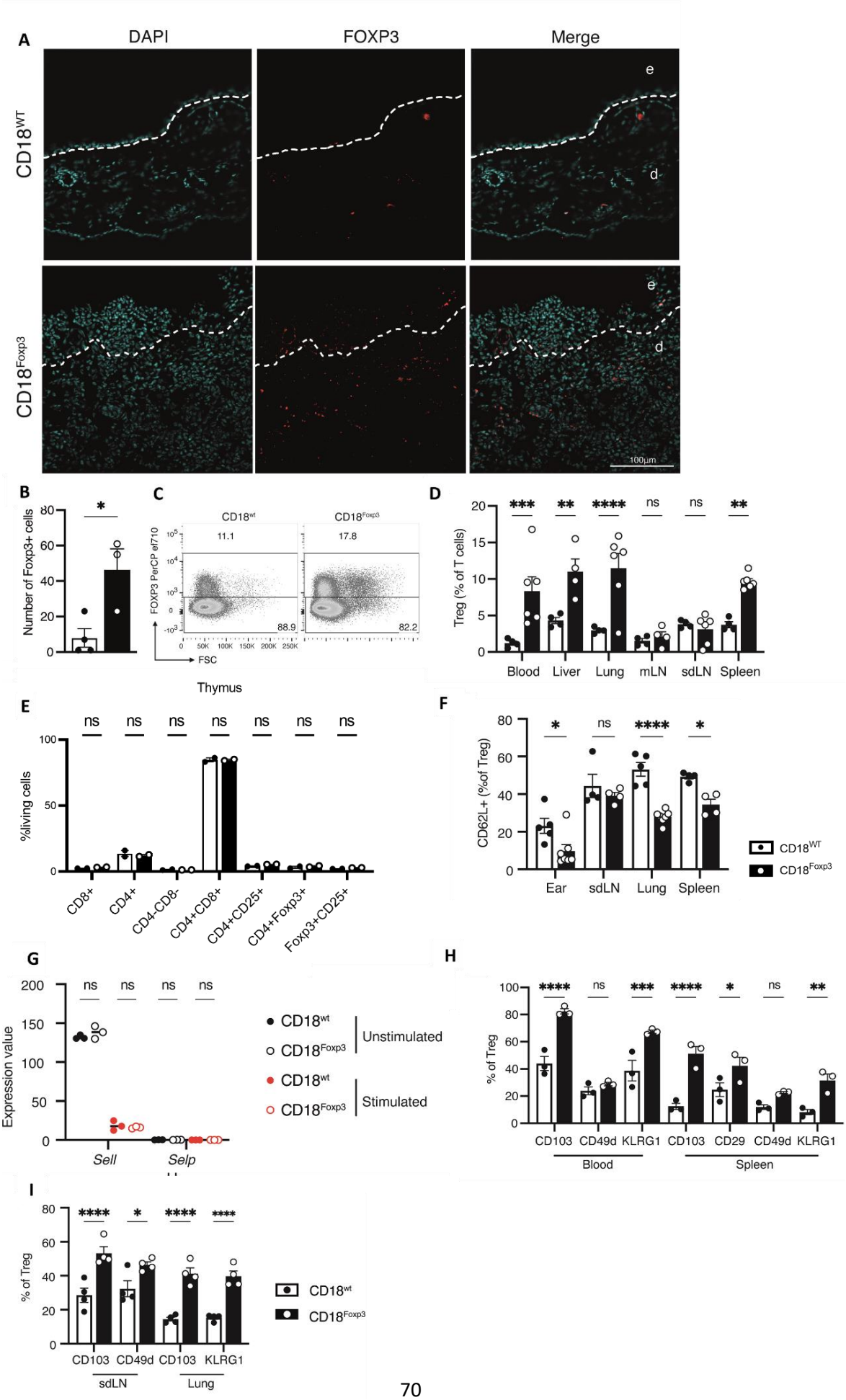
A
DAPI
FOXP3
Merge
CD18WT
CD18Foxp3
e
d
100µm
B
Number of Foxp3+ cells
C
CD18wt
CD18Foxp3
11.1
17.8
88.9
82.2
FOXP3 PerCP ef710
FSC
Thymus
D
Treg (% of T cells)
Blood
Liver
Lung
mLN
sdLN
Spleen
E
%living cells
CD8+
CD4+
CD4-CD8-
CD4+CD8+
CD4+CD25+
CD4+Foxp3+
Foxp3+CD25+
F
CD62L+ (%of Treg)
Ear
sdLN
Lung
Spleen
CD18WT
CD18Foxp3
G
Expression value
Sell
Selp
CD18wt
CD18Foxp3
Unstimulated
Stimulated
H
% of Treg
CD103
CD49d
KLRG1
CD29
Blood
Spleen
I
% of Treg
sdLN
Lung
CD18wt
CD18Foxp3

Figure 29 ***Treg-specific deletion of CD18 does not impair tissue homing of cells.*** ***(A)*** *Immunofluorescence images of Treg infiltration in ears of 17-20 week-old mice showing nuclei marked with DAPI and Treg identified by Foxp3 expression. Images representative of 3 mice per group.* ***(B)*** *Quantification of total number of Foxp3$^+$ Treg per field of view from immunofluorescence imaging of ears of wildtype and CD18^{Foxp3} mice n=3-4.* ***(C)*** *Representative flow cytometry plots of Foxp3 expression on splenic CD4 T cells and* ***(D)*** *quantification of Treg frequencies as a percentage of total CD3$^+$ T cells in various organs of 12-13 week-old mice. n=3-6.* ***(E)*** *Thymic T cells and precursors of 3 week-old CD18^{WT} and CD18^{Foxp3} mice, n=2.* ***(F)*** *Quantification of surface expression of CD62L on Foxp3$^+$ Treg from multiple organs measured by flow cytometry n=4-8.* ***(G)*** *Expression of Sell and Selp transcripts by unstimulated and stimulated CD18 sufficient and deficient Treg n=3.* ***(H)*** *Surface expression of proteins involved in cell adhesion on CD18^{wt} and CD18^{Foxp3} Treg from blood, spleen,* ***(I)*** *sdLN, and lungs of mice n=3-4. Dots represent individual mice, bars show the mean ± SEM, representative of at least two independent experiments. Significance was determined by (B) two-tailed unpaired t-test or (D-I) 2-way ANOVA with Šídák's multiple comparisons test. ns, p>0.05; *, p<0.05; **, p<0.01; ***, p<0.001 ****, p≤0.0001.*

5.3. LFA-1-deficient Treg have an altered gene expression profile

To analyze the functional status of Treg, we performed bulk RNA sequencing on stimulated (anti-CD3/CD28) splenic Treg isolated from CD18^{Foxp3} mice and littermate controls. Analysis of differentially expressed genes highlighted 131 genes (with fold change≥1.5) where the expression was altered in the absence of CD18 on Treg. We first used the Ingenuity Pathway Analysis (IPA) tool from Qiagen to find genes associated with different pathways. Ingenuity analysis highlighted genes involved in top canonical pathways like T_H1 and T_H2 pathways, T_H cell differentiation, and communication between cells (Figure 30). The genes that are involved in these pathways are listed in Table 18. Furthermore, this analysis identified several genes associated with different immunological diseases, including systemic autoimmune syndromes, eosinophilia, atopic dermatitis, and asthma (Figure 31 A). The up- and downregulated genes of LFA-1-deficient Treg compared to wildtype Treg associated with these diseases are shown in Figure 31 B.

Another method to identify biological processes that are enriched in a gene list more than would be expected by chance is the gene enrichment analysis. The identification of mouse gene orthologs was performed using the NCBI Gene search engine (http://geneontology.org/). GO analysis of the significantly upregulated genes (excluding lowly expressed genes with differential expression≤4) in CD18^{Foxp3} Treg revealed multiple enriched genes, including a number of GO terms related to immune activation (Figure 32 A). The most notable of these is the involvement in IL-18 signaling with *Il18r1* gene, positive regulation of T_H2 immune response like *Gata3, Ccr4, Ccr8,* and *Icos*, and positive regulation of T cell cytokine production like *Ccl20, Ccr4, Itgb2, Jund, Ccr8, Cxcr6*, and *Ccl3*.

The most significantly up and downregulated genes of this analysis with a fold change≥ 1.5, -log(FDR)≥2 were highlighted in Figure 32 B. The functions of these selected genes were summarized in Table 19.

Furthermore, we wanted to know if the loss of LFA-1 has a compensatory effect on other members of the integrin family on Treg. Therefore, we analyzed the expression value of different α and β-integrins on LFA-1-deficient Treg compared to wildtype Treg. Only *Itgae* (CD103), *Itga4* (Cd49d), *Itga6* (CD49f), and *Itgav* (CD51) of the α-integrin family could be detected on Treg. As shown in Figure 32 B, *itgae* is significantly upregulated in

LFA-1-deficient Treg (Figure 33 A). *Itgal* (CD11a), the subunit of the β_2-integrin, is downregulated as expected (Figure 33 A, see also Figure 27 E, F). The β-integrin subunits also showed no altered expression between LFA-1-deficient Treg and wildtype Treg but a downregulated gene expression of *Itgb2* (CD18) subunit in the LFA-1-deficient Treg (Figure 33 B).

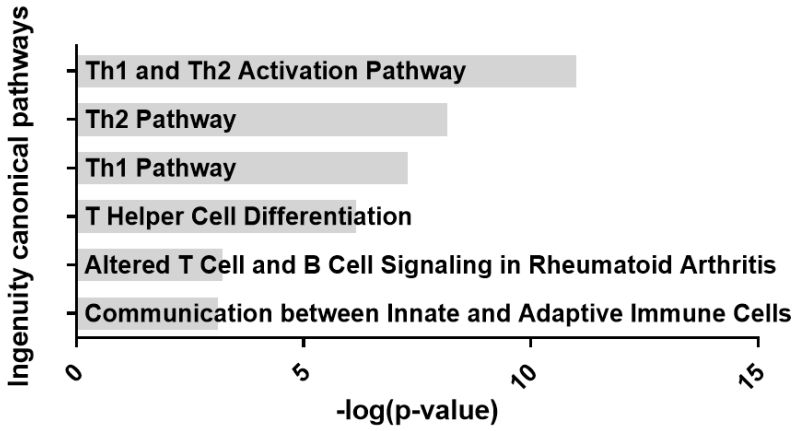

Figure 30 ***Altered gene expression of LFA-1-deficient Treg is associated with T_H1 and T_H2 activation pathways.*** *IPA analysis of bulk sequencing RNA data from activated LFA-1-deficient and wildtype Treg from spleen revealed several genes involved in the modulation of different immune pathways.*

Table 18 ***List of genes from LFA-deficient Treg that are involved in immune pathways analyzed by IPA*** *(↑ upregulated and ↓ downregulated genes)*

Canonical Pathway	Involved genes
T_H1 and T_H2 Activation Pathway	↑*CCR4*, ↑*CCR8*, ↑*CXCR6*, ↑*GATA3*, ↑*ICOS*, ↑*IL18R1*, ↓*IL2*, ↓*ITGB2*, ↓*TNFSF11*, ↓*CD40LG*, ↓*CRLF2*, ↓*HLA-A*
T_H2 Pathway	↑*CCR4*, ↑*CCR8*, ↑*CXCR6*, ↑*GATA3*, ↑*ICOS*, ↓*IL2*, ↓*ITGB2*, ↓*CRLF2*, ↓*HLA-A*
T_H1 Pathway	↑*GATA3*, ↑*ICOS*, ↑*IL18R1*, ↓*IL2*, ↓*ITGB2*, ↓*TNFSF11*, ↓*CD40LG*, ↓*HLA-A*
T Helper Cell Differentiation	↑*GATA3*, ↑*ICOS*, ↑*IL18R1*, ↓*IL2*, ↓*CD40LG*, ↓*HLA-A*
Altered T Cell and B Cell Signaling	↓*CD40LG*, ↓*HLA-A*, ↓*IL2*, ↓*TNFSF11*
Communication between Innate and Adaptive Immune Cells	↓*CCL3L3*, ↓*CD40LG*, ↓*HLA-A*, ↓*IL2*

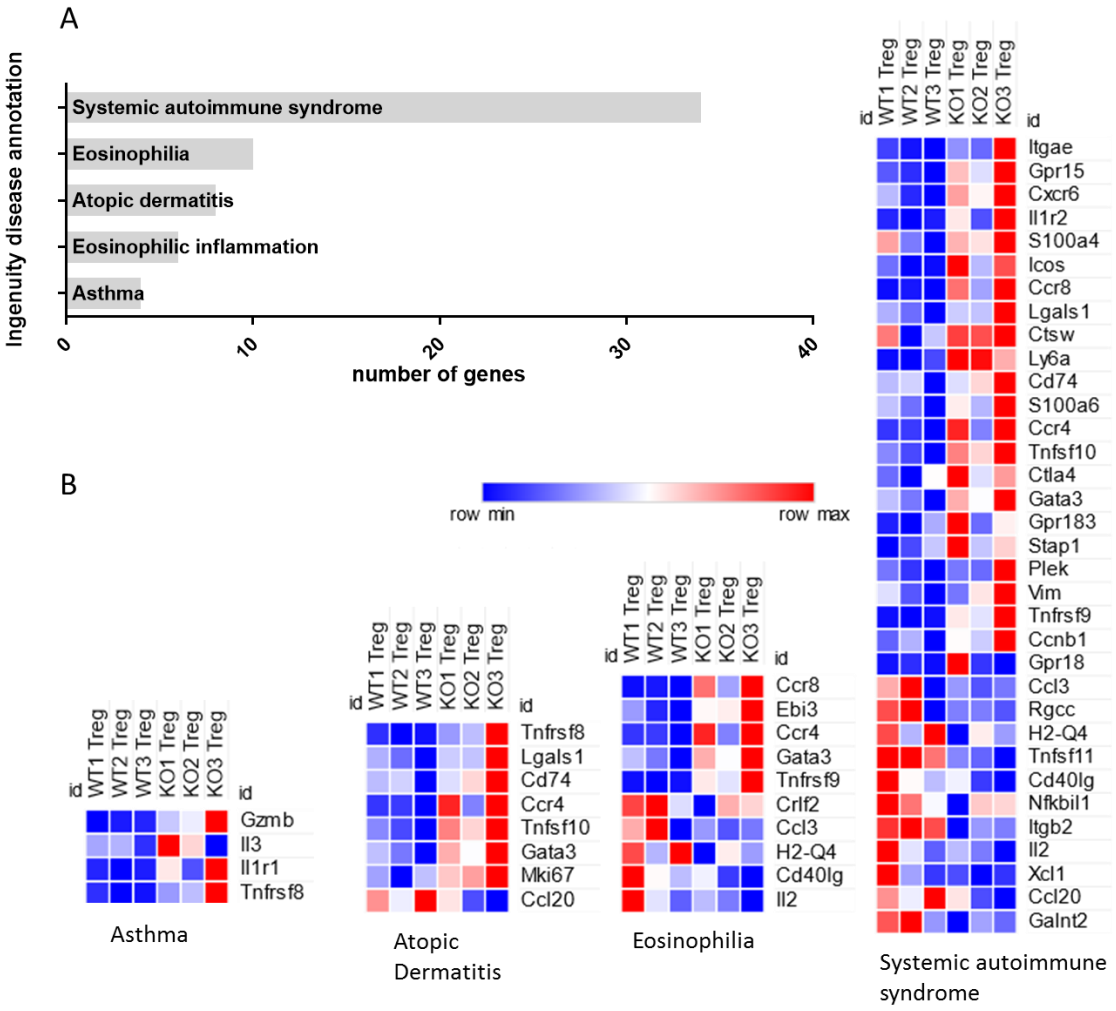

Figure 31 ***Differentially expressed genes of LFA-deficient Treg are involved in different immunological diseases.*** ***(A)*** *Number of genes of LFA-deficient splenic Treg compared to wildtype Treg associated with disease annotations (IPA analysis).* ***(B)*** *Heat maps of up- and downregulated genes of LFA-deficient Treg compared to wildtype Treg involved in asthma, atopic dermatitis, eosinophilia, and systemic autoimmune syndromes. Heat maps were created with Morpheus.*

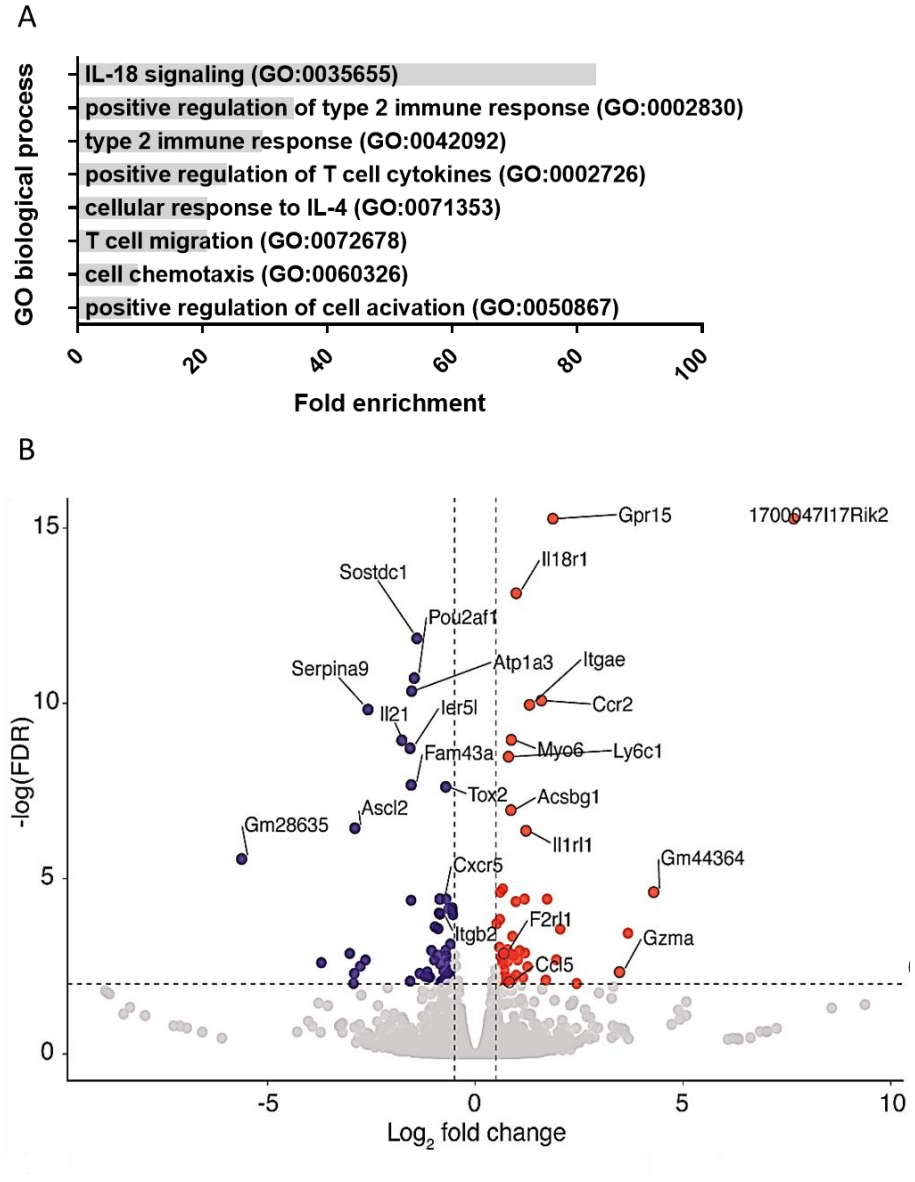

Figure 32 ***Treg lacking LFA-1 show altered gene expression profiles. (A)*** *Fold enrichment analysis of bulk sequencing gene set of LFA-1-deficient and wildtype Treg. GO of biological processes are shown.* ***(B)*** *Volcano plot of differential gene expression between $CD18^{Foxp3}$ and $CD18^{wt}$ mice created using VolcaNoseR [262]. Red and blue dots denote significantly up and downregulated genes (fold change≥|1.5|, -log(FDR)≥2 (indicated by gray lines)). Significance was determined by Fisher's exact test with FDR correction.*

Table 19 ***Functions of significantly up- and downregulated genes of LFA-1-deficient Treg***

Upregulated genes	Name	General functions
1700047I17Rik2	family with sequence similarity 177 member A2	• negative regulator of IL-1β-induced signaling in human cells [263]
Acsbg1	Long-chain-fatty-acid-CoA ligase ACSBG1	• fatty acid degradation and physiological regulation of cellular functions via the

		production of long chain fatty acyl-CoA esters [264]
Ccl5	C-C Motif Chemokine Ligand 5	• CCL5 induces the recruitment of T cells to sites of injury and infection [265]
Ccr2	C-C chemokine receptor type 2	• receptor for CCL2, CCL7 and CCL12 chemokines [266] • mediates chemotaxis and migration induction through the activation of the PI3K cascade [267]
F2rl1	*Protease activated receptor 2* (*PAR2*)	• role in maintenance of epidermal permeability barrier homeostasis • associated with acute contact dermatitis and psoriasis [268]
Gm44364	-	Not known
Gpr15	G-protein coupled receptor 15	• facilitates recruitment of Treg into gut • plays a role in the regulation of chronic inflammation [269]
Gzma	Granzyme A	• induces cytolysis in a perforin-dependent, FAS-FASL independent manner • represents a cell-contact dependent mechanism for Treg to control immune responses [270]
Il18r1	Interleukin-18 receptor 1	• responsible for the binding of pro-inflammatory IL-18 • Involved in IL-18-mediated IFNγ synthesis from T_H1 cells [271] • playing key role in autoimmune, inflammatory, and infectious diseases [272]
Il1rl1	Interleukin-1 receptor-like 1 (ST2)	• receptor for IL-33 • IL-33 signaling promotes co-rectal cancer by changing the phenotype of Treg • more activated and migratory phenotype in Treg [273]
Itgae	Integrin αE (CD103)	• receptor for E-cadherin • involved in the functional differentiation of some $CD8^+$ T cells and Treg • contributing to the fine-tuning of immune reactions [274]
Ly6c1	Lymphocyte antigen 6	• Ly6C expression on Treg marks a lower degree of proliferation, differentiation status as well as functional incompetence [275]

Myo6	Unconventional myosin-VI	• reverse-direction motor protein that moves towards the minus-end of actin filaments • responsible for cell migration [276]
Downregulated genes	**Name**	**General functions**
Ascl2	Achaete-Scute Family BHLH Transcription Factor 2	• expression in Treg downregulated CD25 expression and suppressed IL-2-induced phosphorylation of STAT5 [277]
Cxcr5	C-X-C chemokine receptor type 5	• marker for follicular Treg • facilitating interaction between Treg and B cells [278]
Fam43a	The family with sequence similarity 43 member A	• associated with bladder and lung cancer [279, 280]
Gm28635	-	Not known
Il21	Interleukin 21	• proliferation and differentiation of T cells [281] • associated with different disorders like AD, lupus and psoriasis [282]
Itgb2	Integrin Subunit Beta 2	See introduction
Ler5l	Immediate Early Response 5 Like protein	• involved in cell growth and stress resistance [283]
Pou2af1	POU Class 2 Homeobox Associating Factor 1	• transcription factor that plays a key role in the regulation of inflammation and cell cycles • associated with risk of type 2 diabetes [284]
Serpina 9	Serpin Family A Member 9	• restricted to germinal center B-cells and lymphoid malignancies [285]
Sostdc1	Sclerostin Domain Containing 1	• has been identified as a tumor suppressor gene • regulation of Wnt signaling [286]
Tox2	TOX High Mobility Group Box Family Member 2	• transcription factor associated with hodgkin lymphoma [287], lung and breast cancer [288]

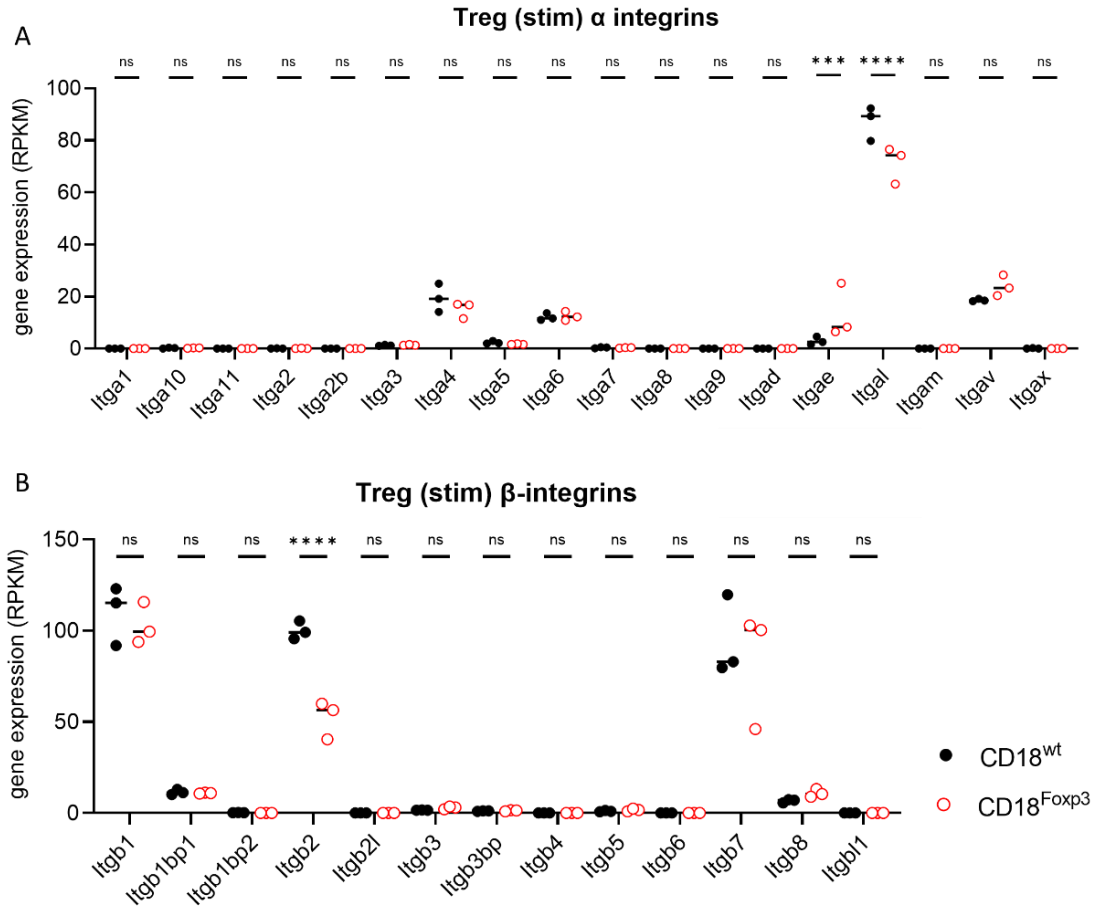

Figure 33 ***Gene expression of α and β-integrins on stimulated Treg. (A)*** *Gene expression of α-integrins on LFA-1-deficient and wildtype Treg.* ***(B)*** *β-integrins on LFA-1-deficient and wildtype Treg. RPKM = Reads per kilo base of transcript per million mapped reads.* Dots (n=3) represent individual mice; bars show the mean ± SEM. Significance was determined by Fisher's exact test with false discovery rate (FDR) correction. *ns, p>0.05; *, p<0.05; **, p<0.01; ***, p<0.001 ****, p≤0.0001.*

5.4. LFA-1-deficient Treg have different cytokine profiles *in vitro*

As the altered gene expression profile of LFA-1-deficient Treg identified altered regulation of T cell pathways (Figure 30) as well as positive regulation of T cell cytokine production (GO: 0002726) (Figure 32 A), we next aimed to determine whether defects in production of Treg-associated pro- and anti-inflammatory cytokines (included in the bulk sequencing gene list) by LFA-1-deficient Treg could also be driving the inflammation observed in these mice. Therefore, we analyzed the expression of these genes in both *ex vivo* isolated Treg in the presence and absence of additional stimulation (anti-CD3/CD28). While the expression of anti-inflammatory *Il10* and *Tgfb1* genes was increased after stimulation as expected, there were no differences observed when Treg lacked LFA-1 (Figure 34 A). Similarly, no differences in the expression of genes encoding for the anti-inflammatory cytokine IL-35 (*Ebi3* and *IL12a*) were observed (Figure 34 A). Treg production of IL-10 protein was also unaltered *ex vivo* (Figure 34 B). The expression of transcripts encoding cytokines involved in the induction of inflammation by T cells, including *Csf2* (colony

stimulating factor 2), *IFNγ, IL-2, IL-7, IL-17a* and *IL-17f,* was also unaltered in the absence of LFA-1 on Treg both with and without additional stimulation (Figure 34 C).
In contrast, MACS-isolated $CD4^+CD25^+$, including Treg and T_{eff} cells and $CD4^+CD25^-$ T cells have altered cytokine profiles when cultured *in vitro*. Pro-inflammatory (IL-17, IL6, TNF-α, IL-5, IL-4) (Figure 35 A), as well as anti-inflammatory cytokines (IL-10, IFN-γ) (Figure 35 B) were increased in the supernatant of both T cell populations after 72 hours.
We next examined the induction of iTreg and their cytokine expression in contrast to primary isolated Treg. Naïve $CD4^+$ T cells were cultured with Treg-promoting cytokines (TGF-β) and Foxp3 expression was determined over time. We could detect a tendency of slightly reduced Foxp3 induction in $CD18^{Foxp3}$ mice (Figure 36 A). As expected, CD11a deletion correlated with induced Foxp3 expression in LFA-1-defective iTreg (Figure 36 B).
In common with the *in vitro* cytokine data, the supernatant of CD18-defective iTreg showed a high increase of pro- (IL-1β, IL-17, IL-4, IL-5, IL-6) and anti-inflammatory (IL-9, IL-10) cytokine secretion (Figure 36 C-I), in contrast to moderate changes in the corresponding gene expression values of the sequenced Treg.

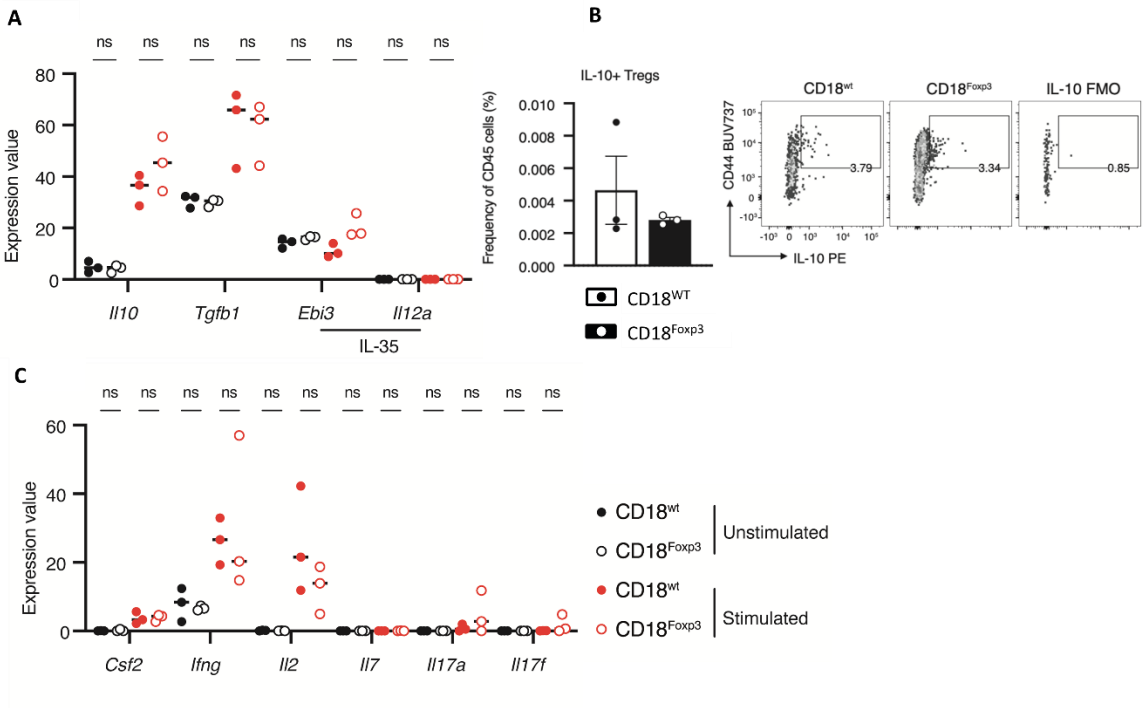

Figure 34 ***Treg lacking LFA-1 have unaltered gene expression of Treg-associated cytokines.*** ***(A)*** *Expression of Treg associated anti-inflammatory cytokine transcripts by unstimulated and stimulated CD18 sufficient and deficient Treg, n=3.* ***(B)*** *Quantification and representative flow cytometry plots showing the frequency of splenic IL-10 expressing Tres from the total CD45+ cell population of $CD18^{wt}$ and $CD18^{Foxp3}$ mice. An IL-10 FMO (fluorescence minus one) was used to confirm true staining for IL-10, n=3.* ***(C)*** *Expression of Treg associated pro-inflammatory cytokine transcripts by unstimulated and stimulated CD18 sufficient and deficient Treg, n=3. Dots represent individual mice, bars show the mean ± SEM. Significance was determined by (A, C) Fisher's exact test with FDR correction or (B) by two-tailed unpaired t test.*

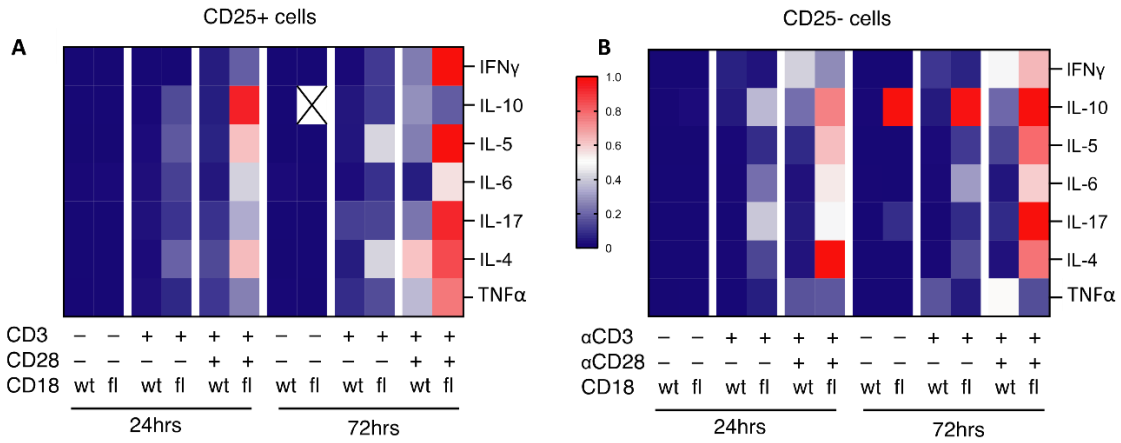

Figure 35 ***MACS-isolated CD4$^+$CD25$^+$ and CD4$^+$CD25$^-$ T cells show different cytokine expression in vitro.*** *Heat map of different cytokine secretion in the supernatant of* ***(A)*** *splenic MACS-isolated CD4+CD25+ and* ***(B)*** *CD4+CD25$^-$ T cells after stimulation with anti-CD3/CD28 for 24 and 72 hours. Cytokine concentration was determined by cytometric bead array, n=3. Representative of at least three independent experiments. Significance was determined by 2-way ANOVA with Šídák's multiple comparisons test. ns, p>0.05; *, p<0.05; **, p<0.01; ***, p<0.001 ****, p≤0.0001.*

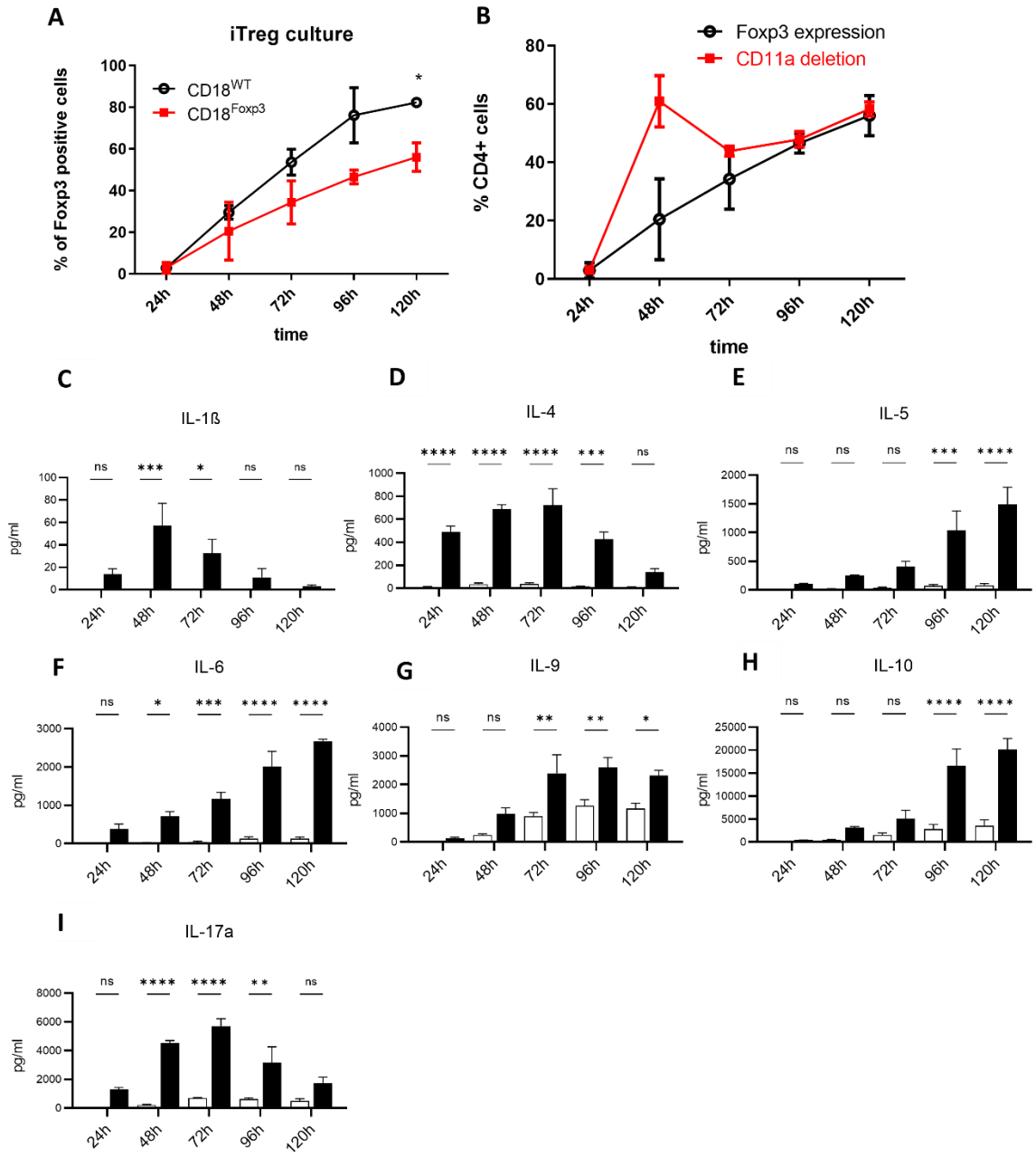

Figure 36 ***CD18^{Foxp3} iTreg culture shows different cytokine profiles.*** *iTreg culture of splenic MACS-isolated naïve CD4$^+$ T cells cocultured with TGF-β and IL-2 for 5 days. Foxp3 expression was assessed every day by flow cytometry, n=3. (C) Foxp3 expression and CD11a deletion in splenic iTreg of CD18^{Foxp3} mice, n=3.* ***(D-J)*** *Different accumulated cytokine concentratiosn in the supernatant of the induced Treg culture for different time points. Cytokine concentration was determined by cytometric bead array, n=3. Error bars show mean ± SEM, representative of at least two independent experiments. Significance was determined by 2-way ANOVA with Šídák's multiple comparisons test. ns, p>0.05; *, p<0.05; **, p<0.01; ***, p<0.001 ****, p≤0.0001.*

5.5. Selective organ inflammation in CD18^{Foxp3} mice is characterized by T cell activation and altered Treg and T_{conv} subset distributions

To further dissect the nature of the inflammation observed in affected CD18^{Foxp3} mice on a cellular level, we performed flow cytometric analysis of T cell infiltrates in diverse organs. Analysis of *ex vivo* pTreg (Helios$^-$Foxp3$^+$) exposed an increase in the frequency in lungs of CD18^{Foxp3} mice (Figure 37 A). Further, lung pTreg subsets, including Gata3$^+$, IFNγ$^+$, RORγt$^+$IL-17$^-$ and RORγt$^+$IL-17$^+$ pTreg showed only a slight increase in Gata3$^+$ pTreg (Figure 37 B). *Ex vivo* analyzed tTreg (Helios$^+$Foxp3$^+$) exhibited a significant increase of LFA-1-deficient tTreg in blood, liver, and lungs of CD18^{Foxp3} mice in contrast to wildtype mice (Figure 37 C). An increase of LFA-1-deficient blood tTreg could be attributed to a slight increase in RORγt$^+$IL-17$^-$ tTreg subset (Figure 37 D), whereas the increase of liver tTreg is attributed to a higher frequency of Gata3$^+$ and RORγt$^+$IL-17$^-$ tTreg subsets (Figure 37 E). Splenic LFA-1-deficient Treg showed a higher frequency in the Gata3$^+$ tTreg subset (Figure 37 G).

CD4$^+$Foxp3$^-$ T_{conv} (non-Treg) frequencies were only increased in the lungs of CD18^{Foxp3} mice (Figure 38 A). Despite similar abundances of T_{conv} cells between genotypes, more T_{conv} cells from mice lacking CD18 expression in Treg were of an activated CD44$^+$ phenotype in lung, liver, and spleen compared to wildtype littermates (Figure 38 B). Multidimensional flow cytometry cluster analysis of the T_{conv} compartment in different organs demonstrated alterations in the composition of these populations, skewing away from a T_H1 response towards a T_H2/T_H17-based response (Figure 38 C). Especially in lungs and livers it seemed that the T_H17 response increased (right lowest cluster). The left cluster (CD44$^-$CD69$^-$) shows non-activated T_{conv} cells, whereas the upper left cluster were CD44$^-$CD69$^+$ T_{conv} cells (Figure 38 C). CD44 and CD69 are different types of activation markers, but the CD44$^-$CD69$^+$ T_{conv} population so far is undefined. It is known that CD69 expression appears during early cell stimulation and regulates functions of specific T cell subsets, whereas CD44 is also a memory T cell differentiation marker [289, 290]. Therefore, the CD44$^-$CD69$^+$ T_{conv} population may represent an early onset of activation of these cells. Cells that are not enriched in the clusters shown here represent other cell types (non-T_{conv} cells). Interestingly, only in the mesenteric LN (mLN) and sdLN the CD44$^+$CD69$^+$ T_{conv} compartment in the wildtype switched towards CD44$^+$CD69$^-$ T_{conv} in the CD18^{Foxp3} mice (Figure 38 C), indicating a naïve T cell population as we also see no upregulation in the activation in these organs (Figure 38 B).

In more detail, we split them into their T_{conv} subsets, including RORγt$^+$IL-17$^-$, T_H1 (IFNγ$^+$), T_H2 (Gata3$^+$) and T_H17 (IL-17$^+$) T cells. Frequencies of T_H1 cells in spleen (Figure 38 D), lungs (Figure 38 E), and blood (Figure 38 F) indeed were reduced, whereas T_H2 cells were significantly increased in lungs and in the blood of CD18^{Foxp3} mice (Figure 38 E, F). IL-17-producing T_{conv} were unaltered and showed only a slight increase in lungs of CD18^{Foxp3} mice (Figure 38 E).

Increases in CD8 T cell activation were also observed in livers and lungs of CD18^{Foxp3} mice compared to wildtype controls (Figure 39 A). However, there was no increase in the frequency of these cells producing IFNγ (Figure 39 B) or IL-17 (Figure 39 C), except with a decrease of IL-17$^+$ CD8$^+$ T cells in the ears of CD18^{Foxp3} mice.

These alterations in the composition of the Treg and T_{conv} population within multiple organs skewing away from a T_H1 response towards a T_H2/T_H17-based response suggest a decrease in the regulation of T cell activation by LFA-1-deficient Treg.

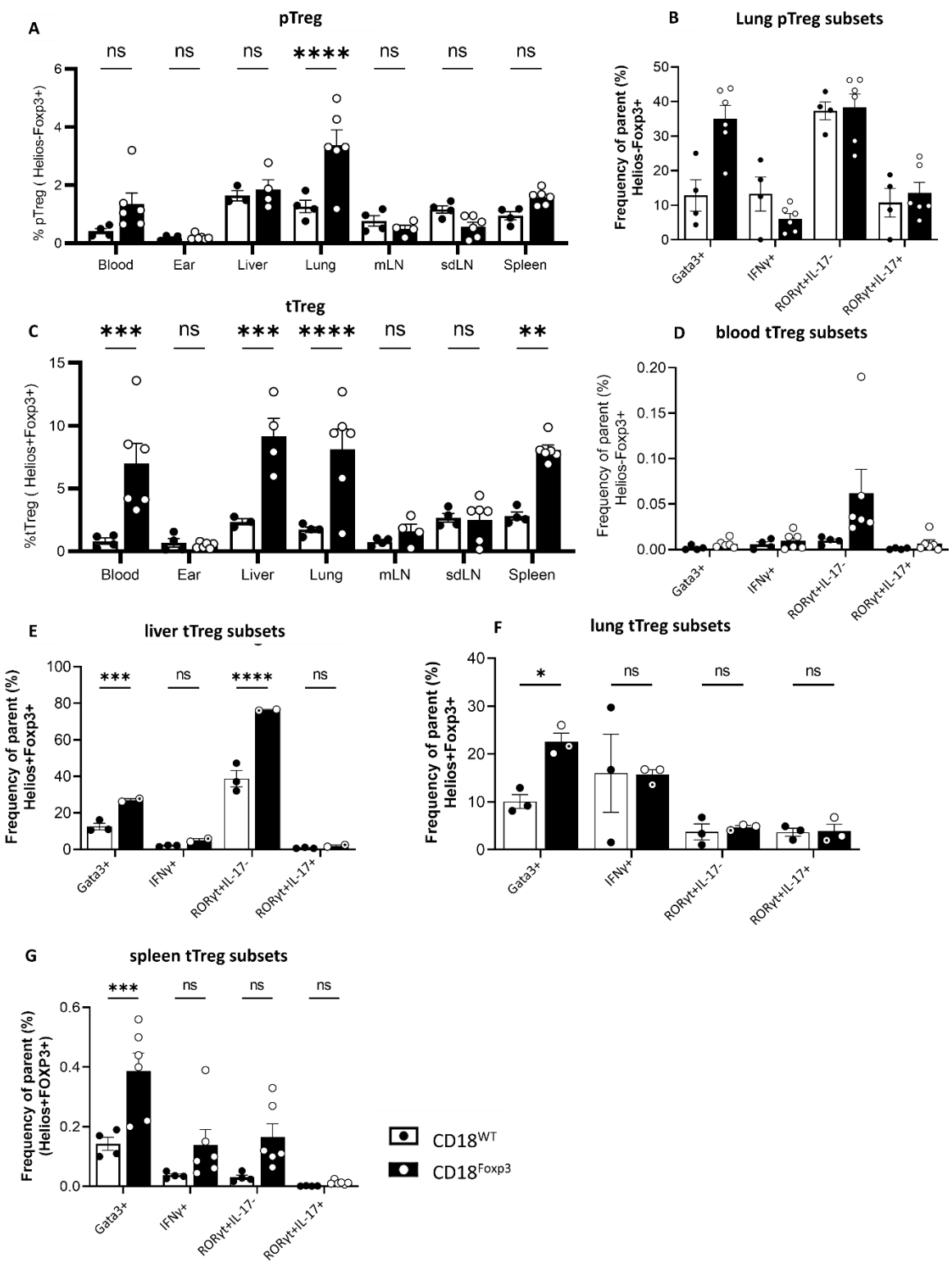

Figure 37 ***LFA-1-deficient Treg show altered pTreg and tTreg subset distributions in different organs.*** ***(A)*** *Flow cytometry quantification of pTreg (Helios$^-$Foxp3$^+$) frequencies of CD18^{Foxp3} and wildtype mice in different organs, n=3-6. (B) pTreg subset distribution (Gata3$^+$, IFNγ$^+$, RORγt$^+$IL-17$^-$, RORγt$^+$IL-17$^+$) in lungs, n=4-6.* ***(C)*** *Flow cytometry quantification of tTreg (Helios$^+$Foxp3$^+$) frequencies of CD18^{Foxp3} and wildtype mice in different organs, n=3-6.* ***(D-G)*** *tTreg subset distribution (Gata3$^+$, IFNγ$^+$, RORγt$^+$IL-17$^-$, RORγt$^+$IL-17$^+$) in liver, lung and spleen, n=2-6. Dots represent individual mice; bars show the mean ± SEM, representative of at least two independent experiments. Significance was determined by 2-way ANOVA with Šídák's multiple comparisons test. ns, p>0.05; *, p<0.05; **, p<0.01; ***, p<0.001 ****, p≤0.0001.*

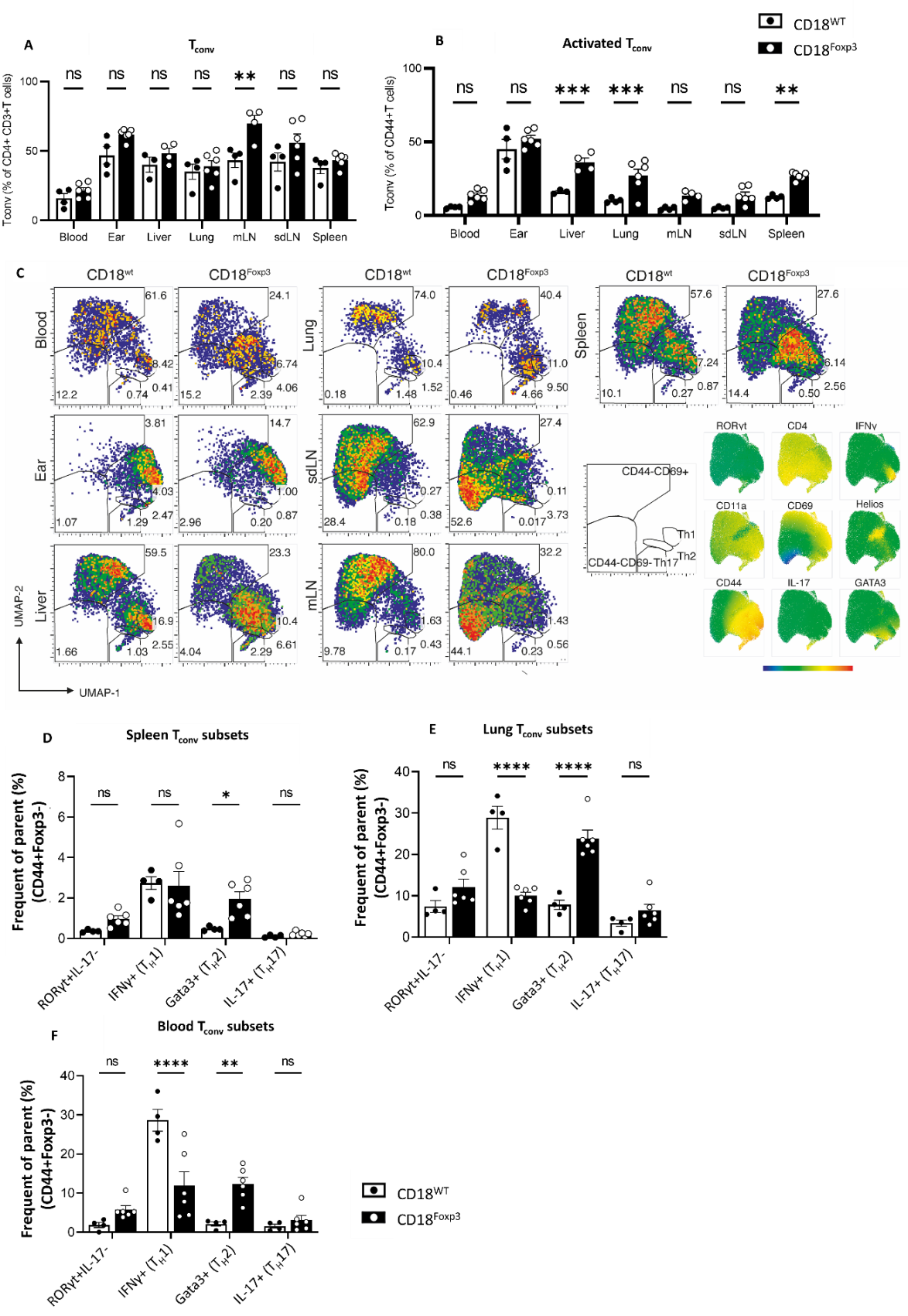

Figure 38 ***CD18^{Foxp3} mice have altered T$_{conv}$ subset distributions in different organs.*** ***(A)*** *Flow cytometry quantification of T$_{conv}$ cells (CD4$^+$Foxp3$^-$) in multiple organs from CD18^{Foxp3} mice and littermate controls n=3-6.* ***(B)*** *Flow cytometry quantification of CD44 expression on T$_{conv}$ cells in multiple organs from CD18^{Foxp3} mice and littermate controls n=3-6. (C) UMAP of T$_{conv}$ cell population using flow cytometry data*

*from multiple organs of CD18^{Foxp3} and CD18^{wt} mice. Used markers for identification are shown in the graphic, on the right side of the figure. T_{conv} subsets frequencies of **(D)** spleen **(E)** lung and **(F)** blood of CD18^{Foxp3} and wildtype mice, n=4-6. Dots represent individual mice; bars show the mean ± SEM, representative of at least two independent experiments. Significance was determined by 2-way ANOVA with Šídák's multiple comparisons test. ns, p>0.05; *, p<0.05; **, p<0.01; ***, p<0.001 ****, p≤0.0001.*

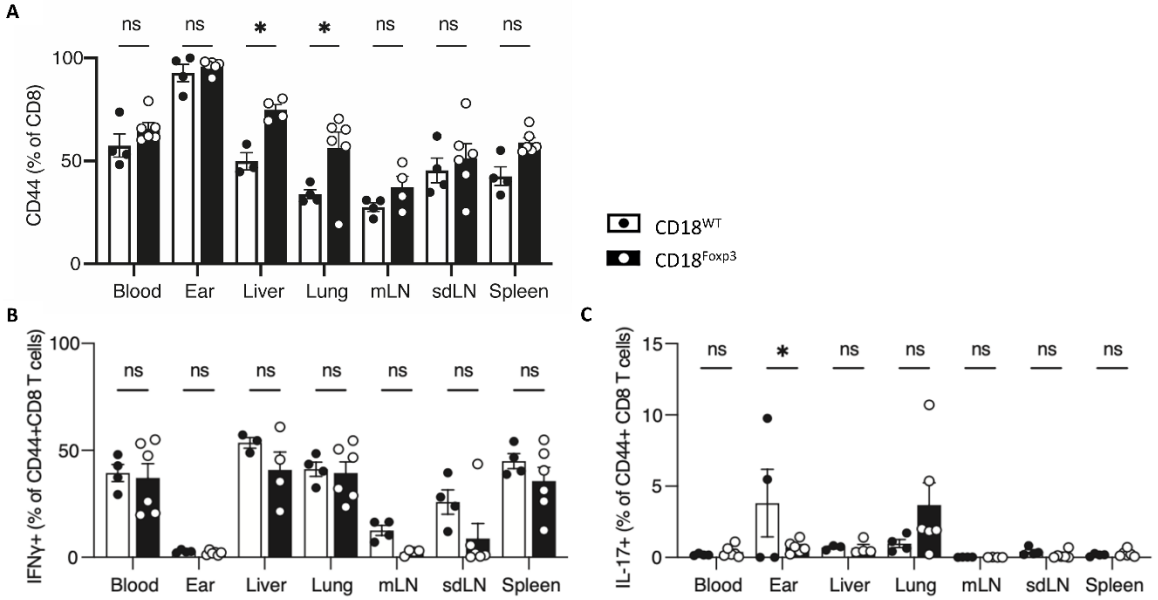

Figure 39 ***CD18^{Foxp3} mice have no altered CD8+ T cell distributions in different organs. (A)*** *Flow cytometry quantification of activated (CD44$^+$) CD8$^+$ T cells frequencies in different organs. Flow cytometry quantification of **(B)** IFNγ$^+$ CD8$^+$ T cells and **(C)** IL-17$^+$ CD8$^+$ T cells of wildtype and CD18^{Foxp3} mice after ex vivo restimulation, n=4-6. Dots represent individual mic; bars show the mean ± SEM, representative of at least two independent experiments. Significance was determined by 2-way ANOVA with Šídák's multiple comparisons test. ns, p>0.05; *, p<0.05; **, p<0.01; ***, p<0.001 ****, p≤0.0001.*

5.6. Treg interactions with dendritic cells are impaired in the absence of LFA-1 on Treg leading to an increased activation status of DC *in vivo*

As LFA-1 is part of the IS and connects to ICAMs on the APC surface [121], we were interested in whether LFA-1 deficiency specific to Treg results in impaired cell contacts with DC. We first cocultured LFA-1-deficient and wildtype Treg with syngeneic bone marrow-derived DC (BMDC) and observed cell interactions by time-lapse microscopy. The number of cell-cell interactions between Treg lacking CD18 and BMDC was significantly reduced compared to wildtype Treg-BMDC (Figure 40 A). Further, the duration of interactions between Treg and BMDC was significantly decreased in the absence of CD18 expression on Treg, with CD18^{Foxp3} Treg forming fewer medium and long interactions with BMDC (Figure 40 B). This also led to the formation of fewer Treg-DC aggregates in the absence of Treg-expressed CD18 (Figure 40 C). The size of the clusters formed was also significantly reduced when cocultured Treg lacked expression of CD18 (Figure 40 D). Interestingly, Treg- T_{conv} interactions were not altered in the absence of Treg-expressed CD18 as Treg from CD18^{Foxp3} mice formed equal numbers of contacts with T_{conv} cells (Figure 40 E).

Since the cell-mediated suppression of T cells and DC can also rely on establishing gab junctions (GJ) communication and transferring cAMP via GJ, we analyzed GJ communication via calcein transfer. We cocultured calcein-labeled wildtype and LFA-1-deficient Treg ($CD4^+Calcein^+$) overnight with cell trace violet (CTV) stained naïve $CD4^+$ T cells and DC *in vitro* and analyzed the transfer of calcein to the target cells as a surrogate for proper GJ communication and cAMP transfer. Double positive T cells ($CD4^+CTV^+calcein^+$) and BMDC/DC ($CD4^-CTV^+calcein^+$) are representative of calcein transfer between the cells. Interestingly, we could not detect any differences in calcein transfer between Treg/DC (Figure 41 A), Treg/BMDC (Figure 41 B), and Treg/T cell (Figure 41 C), indicating that cAMP transfer of CD18-deficient Treg is intact.

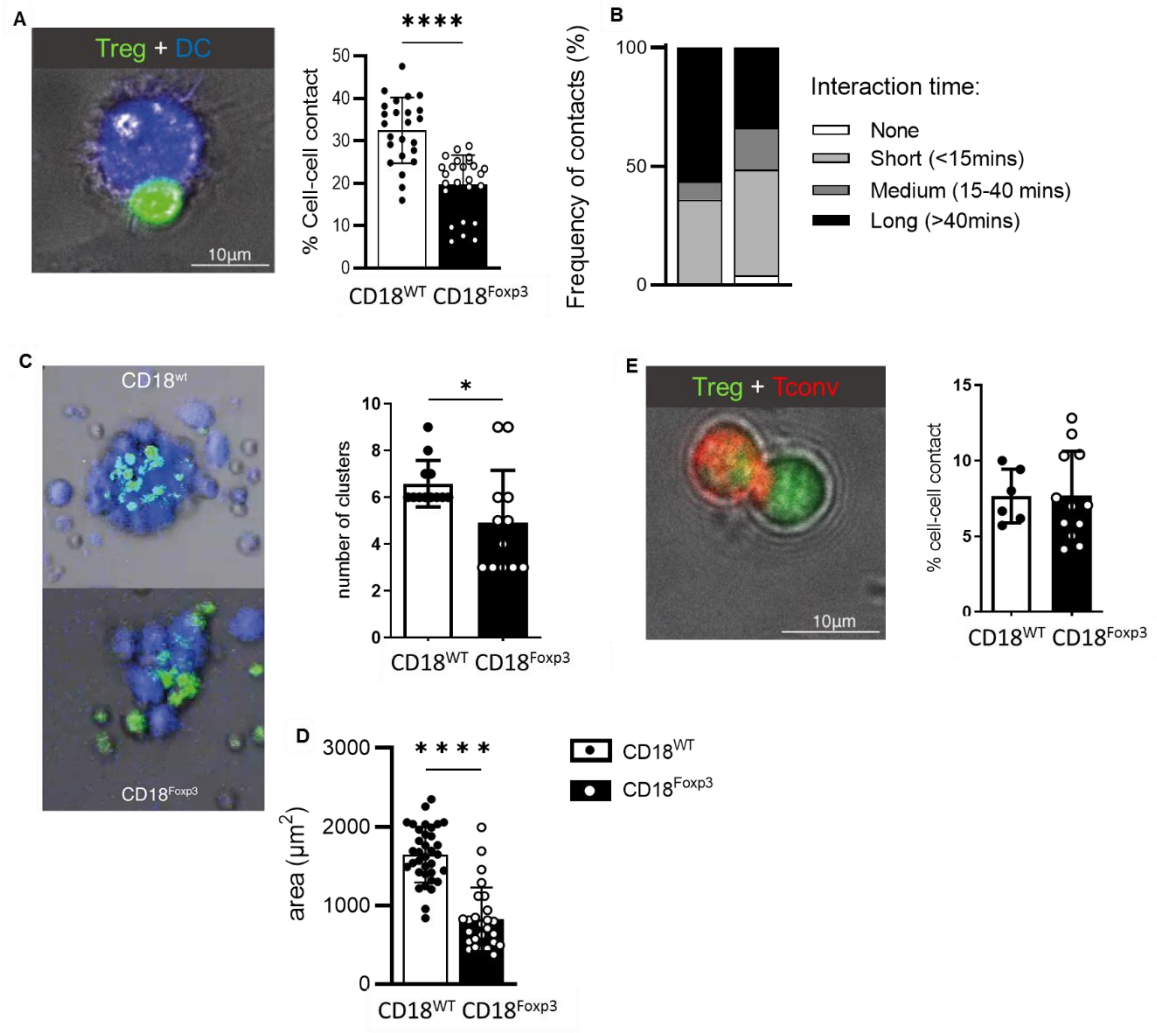

Figure 40 ***LFA-1 deficient Treg have dysfunctional interactions with DC. (A)*** *Frequency of cell-cell contacts between $CD18^{Foxp3}$ or $CD18^{wt}$ Treg (green) and wildtype BMDC (blue) assessed by time-lapse microscopy for 2 hours. Individual Treg of four different picture sections were selected and cell contacts with BMDC were counted with ImageJ analysis software. Total number of Treg in each section was related to the number of contacts. n=2.* ***(B)*** *Interaction time of CD18 deficient Treg with BMDC. Ten different picture sections were counted every 6 minutes up to 60 minutes to determine length of contacts.* ***(C)*** *Quantification of the number and* ***(D)*** *average size of DC-Treg aggregates/clusters after 24 hours of culture, measured using ImageJ analysis software, two experiments pooled.* ***(E)*** *Representative experiment of cell-cell contacts between $CD18^{Foxp3}$ or $CD18^{wt}$ Treg (green) and wildtype conventional T cells (red) assessed by time-lapse microscopy. Percentage of contacts related to total cell number was determined as described in (A). Dots*

*represent individual mice; bars show the mean ± SEM. (A-E) significance was determined by two-tailed unpaired t-test. ns, p>0.05; ***, p<0.001 ****, p≤0.0001.*

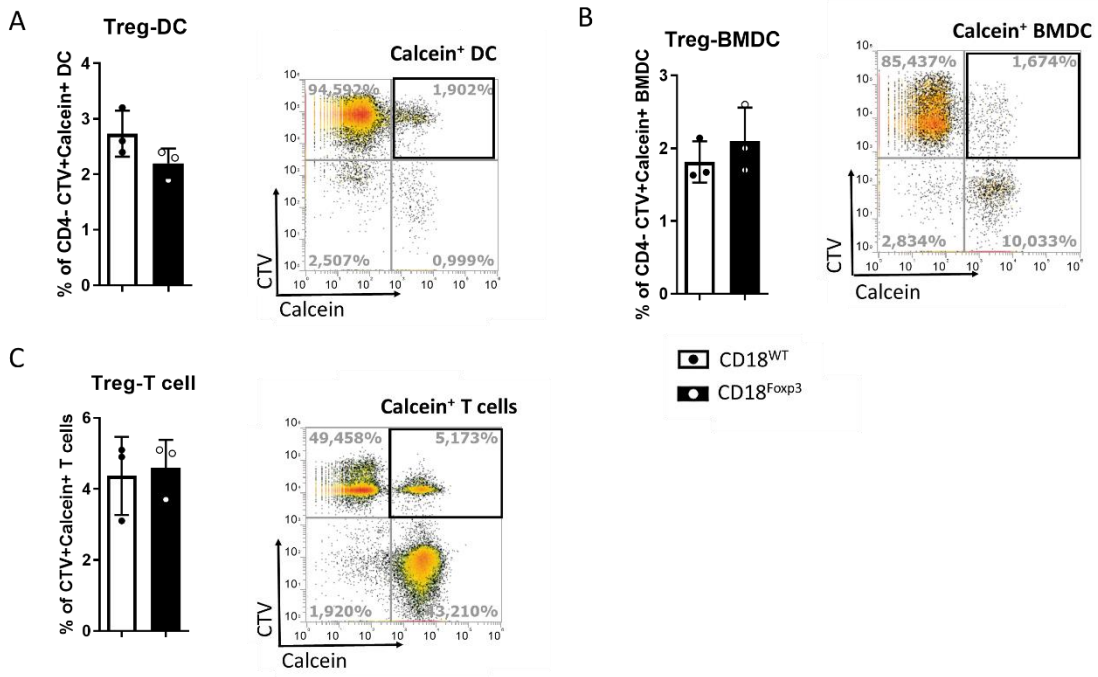

Figure 41 ***LFA-1-deficient Treg have no altered calcein transfer when cocultured with DC or T cells.*** *Calcein stained MACS-isolated wildtype and LFA-1-deficient Treg were cocultured with either cell trace violet (CTV) stained MACS-isolated DC, bone marrow-derived (BM)DC or MACS-isolated Tconv cells for 24 hour.* ***(A)*** *Flow cytometry and representative flow cytometry plots of the frequency of living Calcein$^+$CTV$^+$ DC (pregated for CD4$^-$).* ***(B)*** *Flow cytometry quantification and representative flow cytometry plots of the frequency of living Calcein$^+$CTV$^+$ BMDC (pregated for CD4-).* ***(C)*** *Flow cytometry quantification and representative flow cytometry plots of the frequency of living Calcein$^+$CTV$^+$ T cells (pregated for CD4$^+$). n=3, Dots represent individual mice; bars show the mean ±SEM, representative of at least two independent experiments. Significance was determined by two-tailed unpaired t-test.*

To further analyze the consequences of Treg-DC mediated contacts, we cocultured these cells and examined DC regarding activation and cytokine production. DC post-coculture with Treg revealed increased surface expression of costimulatory molecule CD86 when Treg lacked CD18 (Figure 42 A). Similarly, DC expression of cytokine IL-2, which acts to promote T cell activation and expansion by DC [291] was increased in DC cocultures with CD18 deficient Treg compared to wildtype Treg (Figure 42 B). DC expression of IL-12, involved in the polarization of a type I immune response, was unaffected by the expression of CD18 on cocultured Treg (Figure 42 C). Secretion of the cytokines IL-5 and IL-6 was also increased when Treg in coculture lacked expression of CD18, while no differences in IL-10, TNFα, IL-4, and IL-1β secretion were observed (Figure 42 D). These alterations are indicative of increased DC activation after coculture with CD18 deficient Treg.

Given that Treg-T_{conv} cell interactions *in vitro* appeared normal and that Treg-DC interactions are known to be important in maintaining immune homeostasis [163], we wondered whether the reduced contacts between LFA-1-deficient Treg and DC might influence the DC activation status *in vivo*. Examination of splenic DC in CD18^{Foxp3} mice showed, while the abundance of both conventional DC populations (XCR1$^+$ cDC1 and XCR1$^-$ cDC2) were unaltered (Figure 42 E), that both cDC1 and cDC2 had increased

expression of the activation marker/costimulatory molecule CD86 (Figure 42 F, G). Interestingly, the cDC1 population from CD18^{Foxp3} also expressed significantly more CD40 and ICAM, indicative of an increased activation status (Figure 42 H, I).

Furthermore, bulk sequencing of DC from ear skin revealed differentially up- and downregulated genes (excluding lowly expressed genes with differential expression≤4) in CD18^{Foxp3} DC compared to wildtype DC (Figure 43). Most prominent differentially regulated genes of this list are summarized in Table 20, including genes that are involved, for example, in the modulation of T_H1 and T_H2 immune responses (*Batf2*), cross-presentation (*Xcr1*, *Il41l*), and the modulation of Treg homeostasis (*Ccl17*).

Taken together, reduced Treg-DC contacts resulted in higher activation of DC *in vivo*, which might contribute to the hyperactivation of CD4$^+$ cells and the manifestation of the altered T cell immune phenotype.

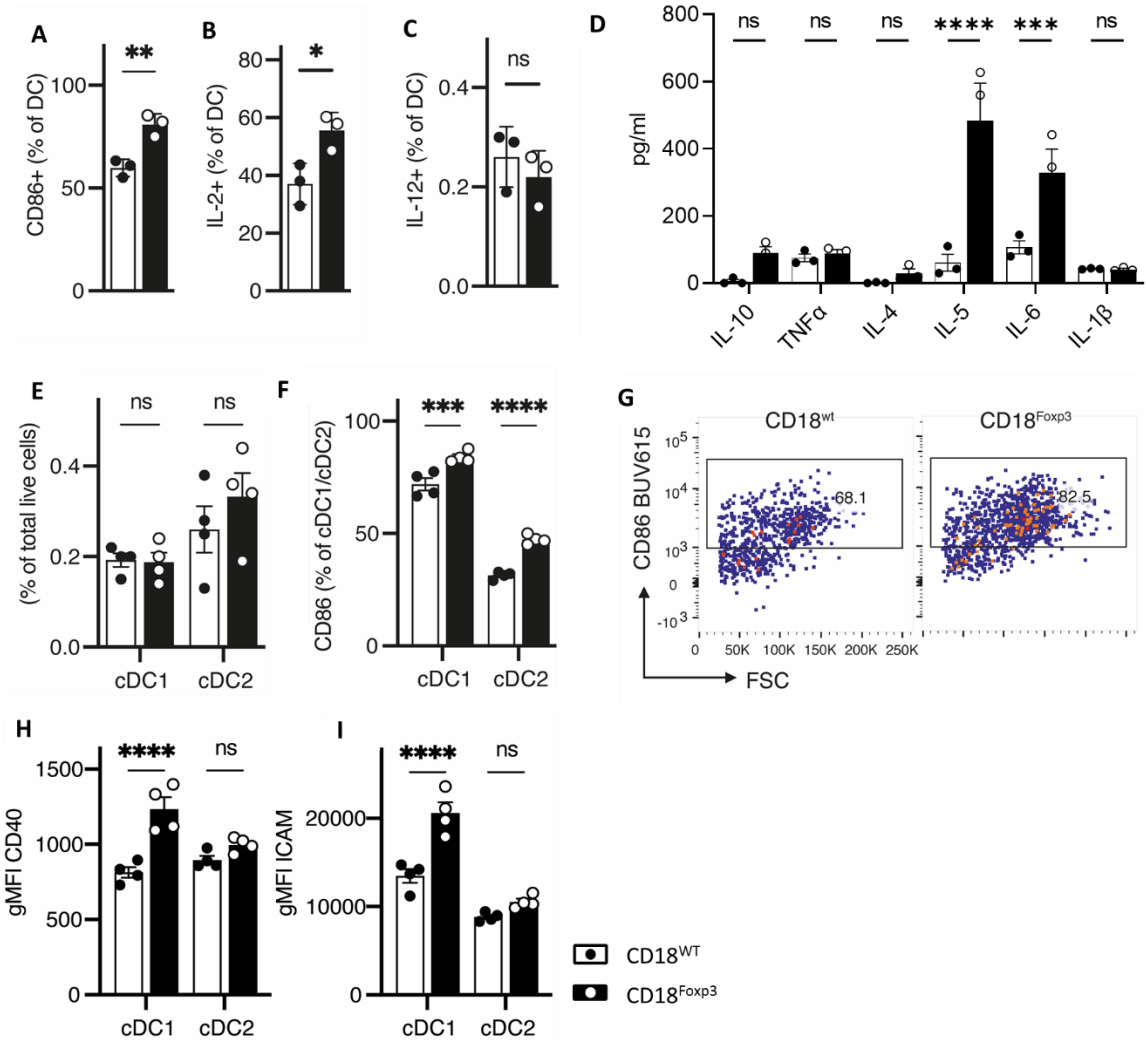

Figure 42 ***Dysfunctional Treg-DC contacts leads to increased activation status of DC in vivo.*** ***(A)*** *Flow cytometric quantification of DC expression of CD86* ***(B)*** *IL-2 and* ***(C)*** *IL-12 in coculture with Treg.* ***(D)*** *Secreted IL-10 TNFα, IL-4, IL-5,IL-6, and IL-1β measured by cytometric bead array in supernatant of DC-Treg cocultures. Quantification of flow cytometry data showing* ***(E)*** *total frequencies of cDC1 and cDC2 and* ***(F)*** *activation status by proportion of CD86$^+$ cells.* ***(G)*** *Representative flow cytometry plots showing increased frequency of CD86 activated DC in CD18^{Foxp3} mice compared to CD18^{WT}. Geometric mean of the*

fluorescence intensity (gMFI) of ***(H)*** *CD40 and* ***(I)*** *ICAM in control and CD18^{Foxp3} mice n=4. Dots represent individual mice; bars show the mean ±SEM, representative of at least two independent experiments. Significance was determined by 2-way ANOVA with Šídák's multiple comparisons test. ns, p>0.05; ***, p<0.001 ****, p≤0.0001.*

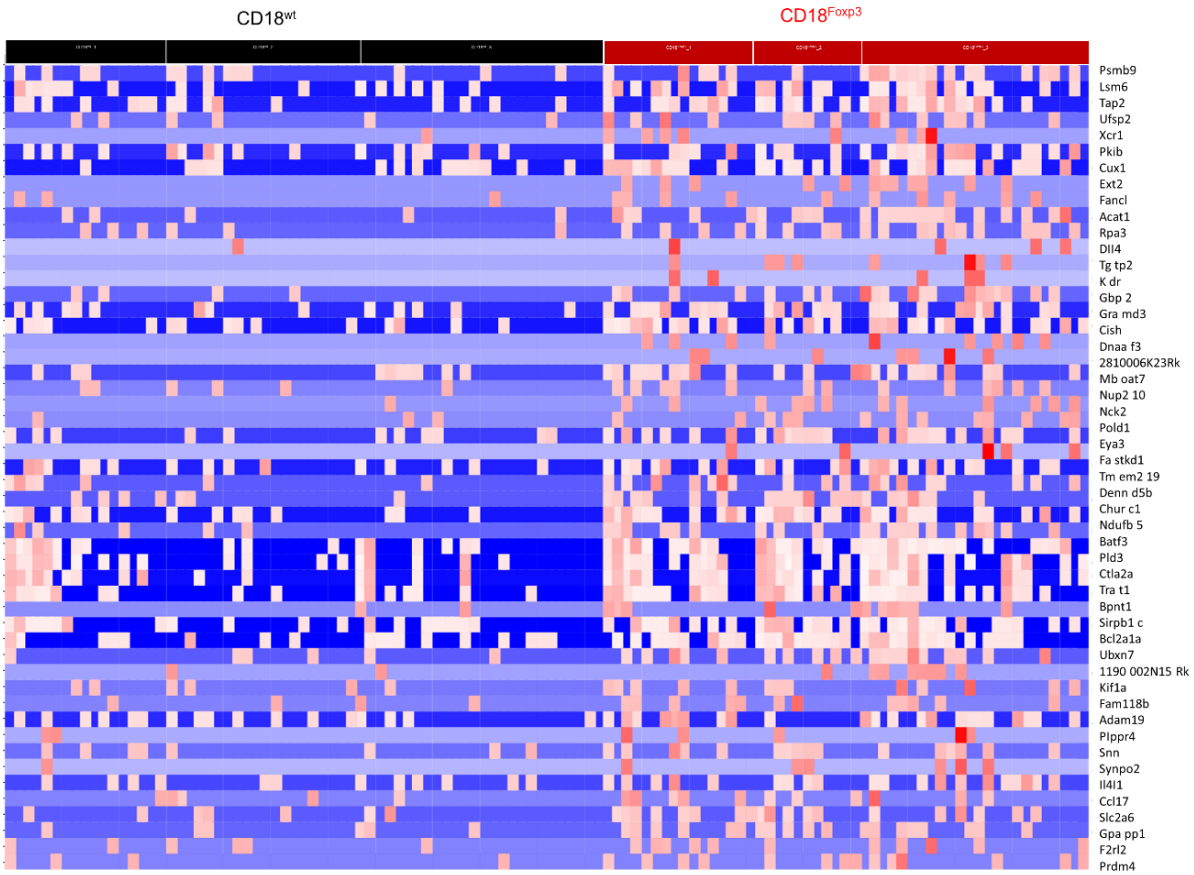

Figure 43 ***Heat map of differentially expressed genes of skin DC from CD18^{Foxp3} and wildtype mice.*** *UMAP-based clustering of the bulk sequencing dataset of DC from ear skin (adjusted p-value < 0.05).*

Table 20 ***Functions of selected up- and downregulated genes of skin DC from CD18^{Foxp3} mice*** *(↑ upregulated and ↓ downregulated genes)*

Gene	Name	Function
↑*Batf2*	Basic Leucine Zipper ATF-Like Transcription Factor 2	• Tumor suppressor gene [292] regulates type 1 and type 2 diseases [293]
↓*Bcl2a14*	B-cell lymphoma 2-related protein A14	• facilitates survival of selected leukocytes subsets and inflammation [294]
↓*Ccl17*	CC motif chemokine ligand 17	• DC-derived CCL17 is a central regulator of Treg homeostasis [295]
↑*Cish*	Cytokine inducible SH2-containing protein	• crucial role in cDC1 development and in the DC-mediated activation of CD8 T cells [296]
↑*Ctla2a*	Cytotoxic T lymphocyte-associated protein 2 alpha	• CTLA-2α+ cells , enable bystander CD4^{+} T cells

		conversion to Treg by TGFβ promotion [297]
↓*DII4*	Delta-like 4 Notch ligand	• Dll4+ DC promote the generation of T_H1 and T_H17 $CD4^+$ T cells [298]
↑*Gbp2*	Guanylate-binding protein 2	• induces maturation of DC and suppression of proliferation of T cells [299]
↓*Il4i1*	Interleukin-4–induced gene 1	• inhibits T cell proliferation • role in APC/T cell cross-talk [300]
↓*Nck2*	NCK Adaptor Protein 2	• regulating cellular actin network [301]
↓*Xcr1*	X-C Motif Chemokine Receptor 1	• marker for cross-presenting DC • $XCR1^+$ DC are crucial for the induction of peripheral tolerance and anti-tumor responses [302]

5.7. Organ inflammation in mice lacking CD18 on Treg leads to spontaneous development of autoantibodies

To further characterize the multiorgan and systemic inflammation observed in the absence of CD18 expression on Treg, we examined serum collected from $CD18^{Foxp3}$ mice for the presence of autoantibodies. Serum from these mice was observed to be reactive against different sites in mouse skin tissue sections (Figure 44 A). Both antinuclear antibodies (ANA), which are associated with systemic inflammatory autoimmune diseases such as lupus [303, 304], scleroderma [305], dermatomyositis [306], and Sjögren´s disease [307], as well as autoantibodies against basal keratinocytes or basement membrane structures, which occur in autoimmune blistering skin diseases such as pemphigus [308] and bullous pemphigoid [309], were found to be present in sera from $CD18^{Foxp3}$ mice. Autoantibodies were most commonly of the IgG type in $CD18^{Foxp3}$ mice and rarely observed in wildtype mice. Four of ten sera contained readily detectable antinuclear autoantibodies, five out of ten sera were reactive with the cutaneous basement membrane and keratinocytes, and two out of these mice produced both types of autoantibodies (Figure 44 B). The mean autoantibody fluorescence intensity was significantly higher in $CD18^{Foxp3}$ mice compared to littermate $CD18^{wt}$ mice (Figure 44 C).

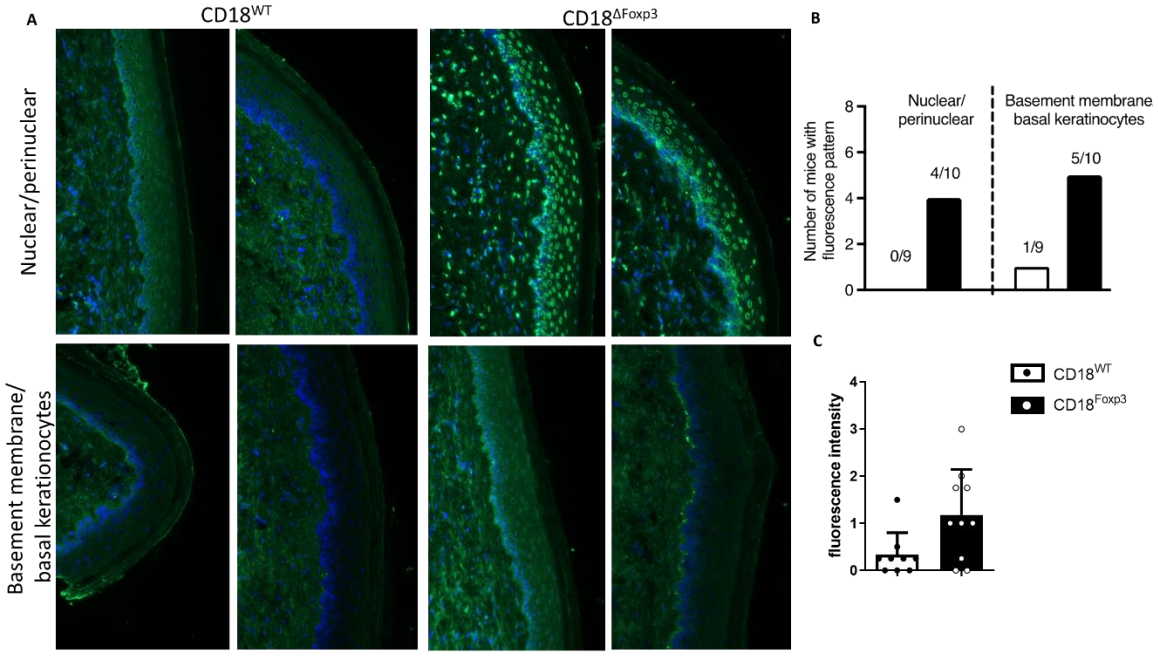

Figure 44 ***Absence of CD18 expression on Treg leads to the spontaneous generation of autoantibodies.*** ***(A)*** *Representative images of autoantibody binding patterns of CD18^{Foxp3} and CD18^{wt} mouse sera to cryosections of wildtype murine palate skin, n=10.* ***(B)*** *Number of positive antibody binding to nuclear/perinuclear and basement membrane/basal keratinocytes reaction pattern on wildtype murine palate skin n=9-10.* ***(C)*** *Scaling of detected autoantibody fluorescence intensity observed in the sera-treated skin slides n=9-10. Scoring of fluorescence intensity was determined as 0= negative, 1= weakly positive (+), 2= positive (++), and 3= strongly positive (+++). Median was taken from four different, independent evaluations. Bars show mean ± SEM. Significance was determined by two-tailed unpaired t-test, ns, p>0.05; *, p<0.05.*

5.8. CD18^{Foxp3} mice develop symptoms of uncontrolled T_H2-driven immune responses

As LFA-1 is known to be a major regulator of T cell responses [121, 140, 141], and our data so far indicate an alteration in the T_{conv} and Treg subsets, we wondered whether CD18 deficiency on Treg plays a critical role in the modulation of T_H immune regulation in CD18^{Foxp3} mice in disease models.

The skin phenotype of CD18^{Foxp3} mice largely phenocopied that of scurfy mice, which lack Treg altogether, albeit in a less severe form. Scurfy mice develop a profound T_H1 and T_H2 biased auto-inflammatory response [310, 311]. Nevertheless, data of LFA-1$^{-/-}$ mice showed a CD4$^+$ T cell differentiation shift from Treg to T_H17-like cells [223].

We first hypothesized that the skin inflammation occurring in our mice is more of a psoriasis-like phenotype. Therefore, we investigated whether our mice have an exacerbated psoriasis-like skin inflammation with increases in T_H17 and IL-17a frequencies when treated with IMQ. To analyze this theory according to IL-17a production during inflammation, we used the IMQ-induced psoriasis model (Figure 45 A). IMQ is a potent immune activator of the TLR 8, which in turn triggers macrophages and DC to release IL-23, TNF-α and NF-κB to induce IL-17-dependent inflammation [253, 312]. To assess the clinical symptoms, the Psoriasis Area and Severity Index (PASI) score is used to measure skin thinking, scaling, and redness [313]. Indeed, our mice developed a severe combined

PASI score over time after treatment with IMQ (Figure 45 B). However, we did not detect a disease-dependent shift from Treg to T_H17 differentiation (Figure 45 C, D) in spleen and inguinal lymph node (iLN). In the steady state of non-treated ears, more T_H1 and T_H17 cells were observed, but following IMQ treatment of the right ear the frequency of these cells was decreased (Figure 45 E, F). Instead, we observed in $CD18^{Foxp3}$ mice an increase in $Gata3^+$ $CD4^+$ T cells in treated but also non-treated ears (Figure 45 G). Neutrophils in the spleens (Figure 45 H) were increased, but no differences in the monocyte compartment (Figure 45 I) between $CD18^{WT}$ and $CD18^{Foxp3}$ mice were detected.

Another hallmark of psoriasis is the risk of aortic vascular endothelial dysfunction [314]. Therefore, we analyzed the aortic contractility of $CD18^{Foxp3}$ mice with the organ bath method to examine endothelium-dependent relaxations to acetylcholine (ACh) of vessels. We could not detect any vascular relaxational dysfunction between $CD18^{WT}$ and $CD18^{Foxp3}$ mice (Figure 46 A). Furthermore, oxidative burst (production of reactive oxygen species (ROS)) was measured by the stimulation with protein kinase C activator Phorbol 12,13-dibutyrate (PDBu) [315] and Toll-like receptor 2 activator zymosan A [316]. Freshly isolated blood of $CD18^{Foxp3}$ mice showed an increase in oxidative stress of cells when incubated with PDBu (Figure 46 B). In contrast, ROS production of blood cells was not altered between wildtype and $CD18^{Foxp3}$ mice when incubated with zymosan A (Figure 46 C).

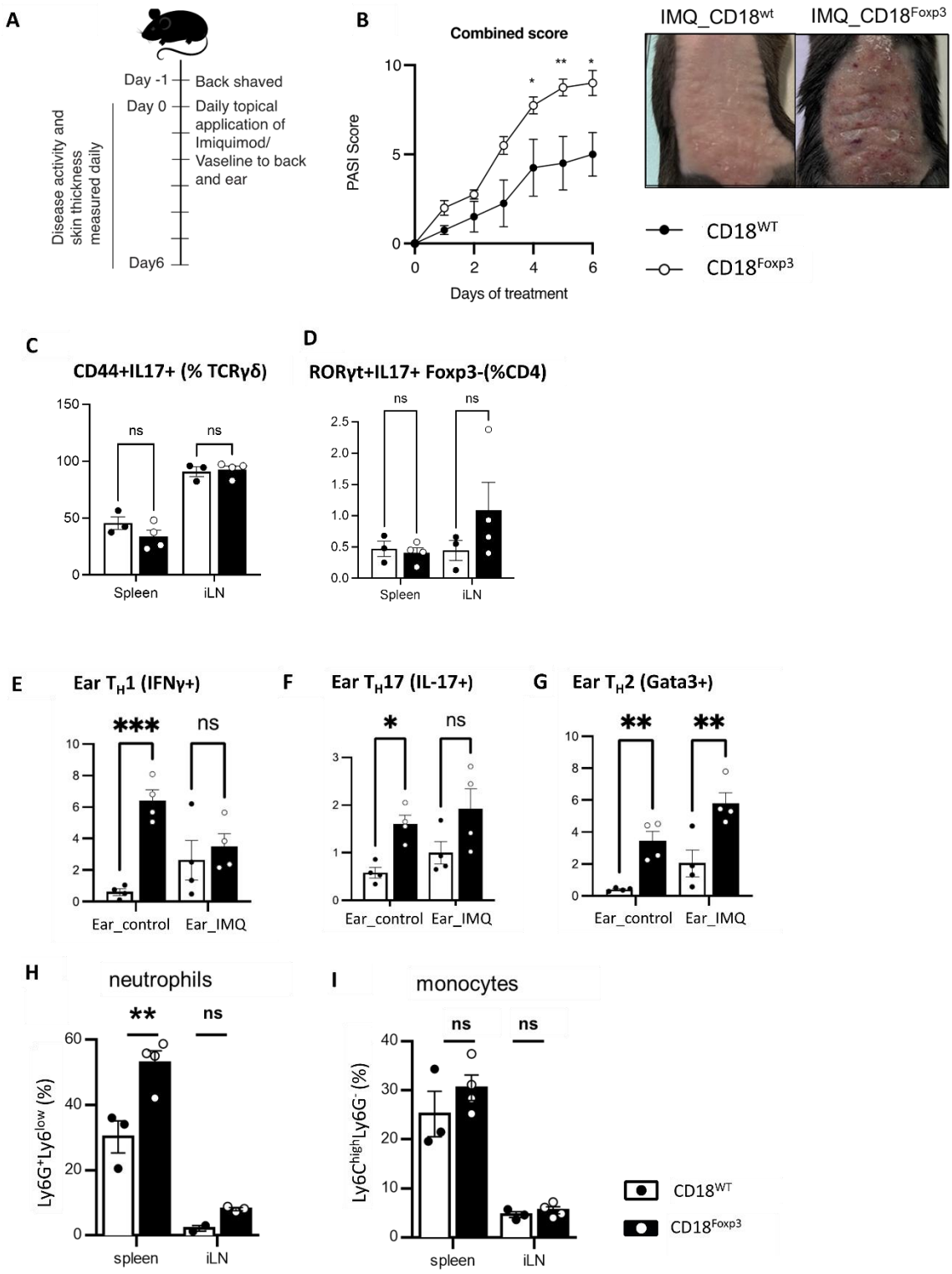

Figure 45 ***CD18^{Foxp3} mice show increased PASI score after treatment with IMQ but no specific T_H17 response.*** ***(A)*** *Experimental timeline of imiquimod-induced psoriasis in mice.* ***(B)*** *Daily assessment of scaling, thickening, and redness of the back skin (PASI) after treatment with imiquimod, n=4. IL-17 response in spleen and iLN measured by frequencies of* ***(C)*** *activated IL-17$^+$γδ T cells and* ***(D)*** *RORγt$^+$IL-17$^+$ CD4$^+$ T cells. n=3-4. Frequencies of* ***(E)*** *IL17$^-$IFNγ$^+$ (Th1),* ***(F)*** *IL17$^+$IFNγ$^-$ (T_H17), and* ***(G)*** *Gata3$^+$ activated T cells into the imiquimod treated ears of CD18^{Foxp3} and CD18^{WT} mice, n=4. Frequencies of* ***(H)*** *neutrophils and* ***(I)*** *monocytes in spleens and iLN after treatment with imiquimod. Dots indicate individual mice; bars show the mean ± SEM, representative of at least one independent experiments. Significance was determined by 2-way ANOVA with Šídák's multiple comparisons test, ns, p>0.05; *, p<0.05; **, p<0.01; ***, p<0.001.*

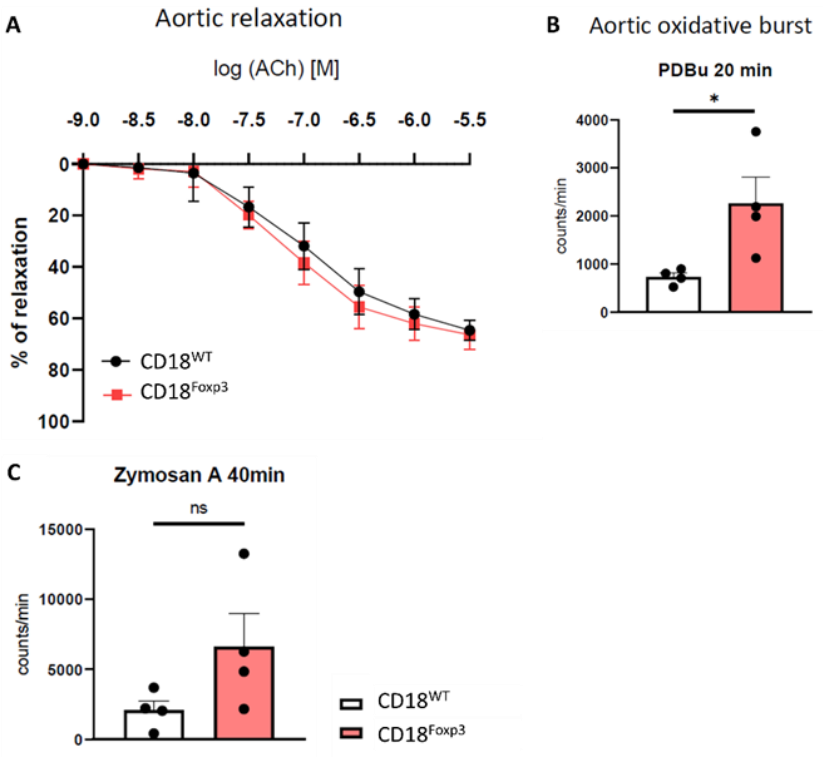

Figure 46 ***No vascular changes in CD18^{Foxp3} mice. (A)*** *Isometric tension studies of isolated aortic rings of CD18^{Foxp3} and CD18^{WT} mice in response to ACh. Two-way analysis of variance with Bonferroni post hoc test, n=4.* ***(B, C)*** *Reactive oxygen and nitrogen species (ROS/RNS) were analyzed in whole blood. In order to stimulate the formation of an oxidative burst in leukocytes, the blood was incubated for 20 min or 40 minutes using* ***(B)*** *phorbol 12,13-dibutyrate (PDBu) or* ***(C)*** *Zymosan A. The oxidative burst was measured by 8-amino-5-chloro-7-phenylpyridol (3,4-d)pyridazine-1,4-(2H,3H) dione sodium salt (L-012)-enhanced chemiluminescence. Dots represent individual mice. Bars show the mean ± SEM. Significance determined by multiple unpaired t-tests corrected for multiple comparisons by the two-stage step-up (Benjamini, Krieger, and Yekutieli) method. , ns, p>0.05; *, p<0.05.*

In contrast, LFA-1 deficiency on Treg resulted in a profound activation of the T_H2 pathway in CD18^{Foxp3} mice. As shown before, T_{conv} subset distributions of Gata3$^+$ T cells were increased in different organs. This uncontrolled type 2 inflammation showed multiple features of atopic diseases. GO analysis of the significantly upregulated genes (excluding lowly expressed genes with differential expression≤4) in CD18^{Foxp3} Treg highlighted several genes that were associated with atopic dermatitis (Figure 47 A). Flow cytometry analysis of different organs revealed higher numbers of Gata3$^+$ T_{conv} cells, especially in the blood and lungs of CD18^{Foxp3} mice, compared to littermate controls (Figure 47 B). These T_{conv} cells expressed higher levels of the T_H2-associated cytokine IL-4 but not IL-17 (Figure 47 C). Further analysis of LN and spleens of CD18^{Foxp3} mice showed significantly increased inflammatory monocytes, neutrophils, and eosinophilia in both organs (Figure 47 D, E). The numbers of splenic IRF4$^+$, PD-L2$^+$ expressing DC, a subset of cDC2 that promotes T_H2-driven immune responses [317, 318], were also greatly increased (Figure 47 F). Moreover, Klrg-1$^+$, PD1$^+$, Icos$^+$, and Gata3$^+$ tissue-resident Treg [178, 179] were increased in the ears of CD18^{Foxp3} mice (Figure 47 G). This Treg subset is mainly present within T_H2-polarized tissues [319]. Another hallmark of T_H2 immunity is the change in immunoglobulin (Ig) subtype distributions. Therefore, we analyzed blood serum Ig levels

via ELISA. Interestingly, we detected a massive upregulation of IgE (Figure 47 H) and IgG1 (Figure 47 I) in $CD18^{Foxp3}$ mice, while IgG2a levels were unaltered compared to wildtype controls (Figure 47 J). This fact indicated an IL-4-induced B cell antibody class switch [320].

B cell subset distributions in the spleen of $CD18^{Foxp3}$ mice were altered as well. The frequency of GL-7^+CD95^+ germinal center B cells (GBZ) (Figure 48 A), as well as $CD95^+CD138^+$ plasma B cells (Figure 48 B) was significantly enlarged, whereas the frequency of $CD21/35^{low}CD23^+$ follicular B cells (FolB) was unaltered (Figure 48 C). $CD21/35^+CD23^+$ marginal zone B cells (MZB), in contrast, were significantly reduced in spleens of $CD18^{Foxp3}$ mice compared to wildtype mice (Figure 48 D). Whether these B cells produce more T_H2-promoting cytokines has to be determined.

Next, we used the oxazolone-induced contact dermatitis model to further characterize T_H2 cell immune responses during inflammation (Figure 49 A). Topically, application of this hapten to the skin of hapten-sensitized mice leads to infiltration with hapten-specific, skin-homing $CD8^+$ and $CD4^+$ T cells. This contact hypersensitivity reaction resembles some features of human atopic dermatitis and skin eczema [232, 254, 321]. Clinically, this model is characterized by thickening of the ears. We observed enhanced ear thickening in the case of $CD18^{Foxp3}$ mice compared to $CD18^{WT}$ mice 72 hours post challenge with oxazolone (Figure 49 B) associated with higher infiltration of activated ($CD44^+$) $CD4^+$ and $CD8^+$ T cells into the oxazolone-treated ears (Figure 49 C). Further, in $CD18^{Foxp3}$ mice, the immune response was potently enhanced and characterized by a striking predominance of T_H2-promoting DC and IL-5-producing T cells (Figure 49 D) infiltrating the skin (Figure 49 E). Interestingly, enhanced T cell immune responses were also observed in untreated ears of these mice (Figure 49 C, D), which indicated an early T_H2-driven immune response even in young mice with no visible phenotype (about 5-6 weeks of age). The induced contact dermatitis thereby enhanced the steady state T_H2-biased immune phenotype of $CD18^{Foxp3}$ mice. Furthermore, oxazolone-induced contact dermatitis of $CD18^{Foxp3}$ mice was enhanced even after 192 hours post-challenge. Thus, $CD18^{Foxp3}$ mice did not recover after 72 hours as wildtype mice (Figure 49 F).

These data indicate a shift to T_H2 immune responses and exuberated long-term contact dermatitis in $CD18^{Foxp3}$ mice. This underlines the observed atopy-like organ phenotype.

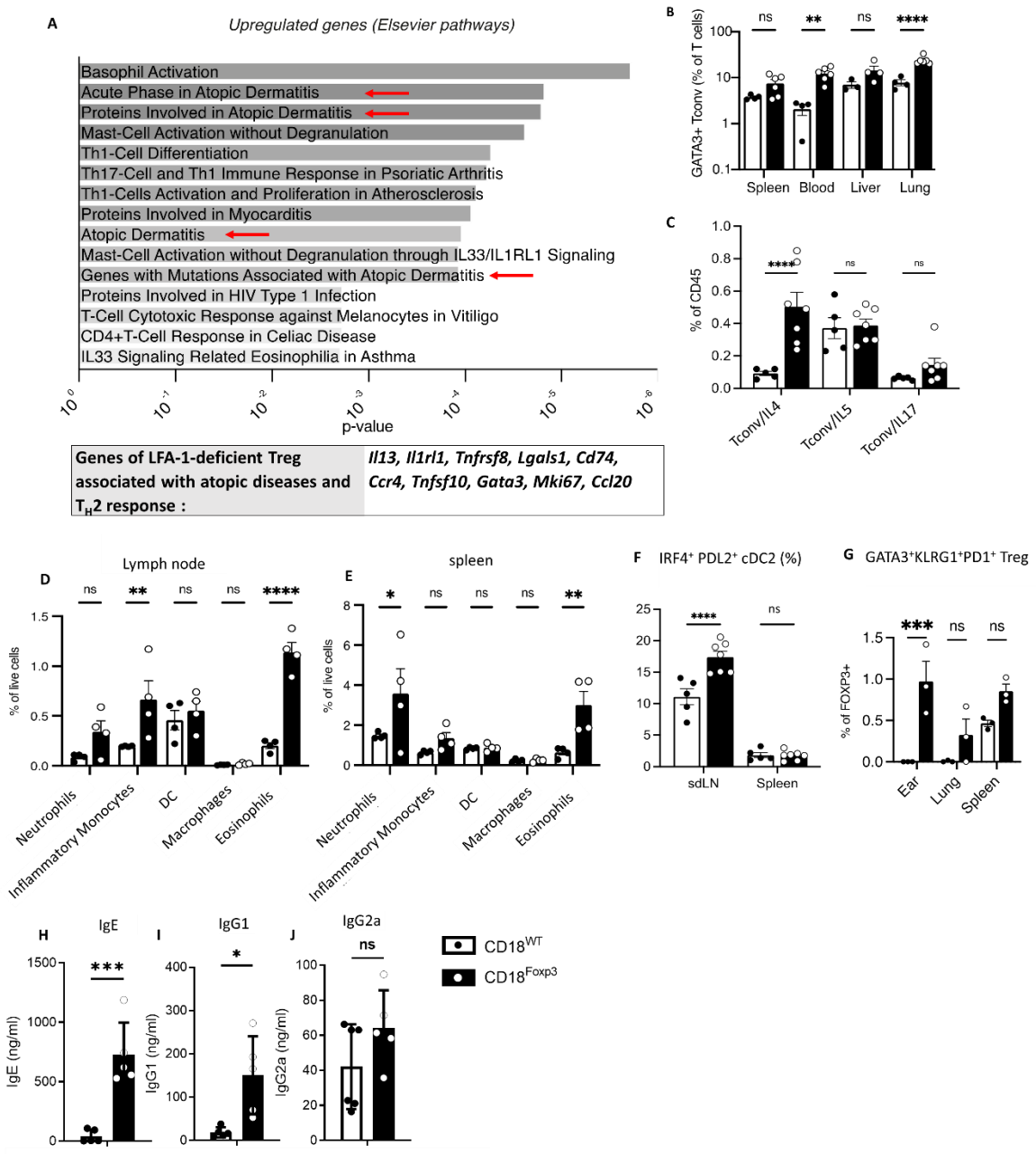

Figure 47 ***CD18 deficiency in Treg results in exaggerated type II immune responses in vivo. (A)*** *Fold enrichment of the significantly enriched biological process GO terms in spleens of CD18^{Foxp3} mice. Genes upregulated (fold change≥1.5, difference≥4) in many pathways associated with atopic dermatitis in CD18^{Foxp3} mice.* ***(B)*** *Frequency of Gata3^{+} T$_{conv}$ cells in different organs, n=3-6.* ***(C)*** *Il-4, Il-5, and IL-17-producing T$_{conv}$ cells in the spleens of CD18^{WT} and CD18^{Foxp3} mice, n=5-7. Frequencies of different myeloid cells in* ***(D)*** *LN and* ***(E)*** *spleens of CD18^{WT} and CD18^{Foxp3} mice, n=4. Frequency of* ***(F)*** *IRF4^{+}PDL2^{+} cDC2 and* ***(G)*** *Gata3^{+}Klrg1^{+}ST2^{+} tissue Treg in different organs, n=3-7. Concentrations of* ***(H)*** *IgE,* ***(I)*** *IgG1 and* ***(J)*** *IgG2a in the serum of CD18^{WT} and CD18^{Foxp3} mice, n=5. Dots represent individual mice; bars show the mean ± SEM, representative of at least two independent experiments. Significance was determined by (B G) 2-way ANOVA with Šídák's multiple comparisons test or (H-J) two-tailed unpaired t-test or ns, p>0.05; *, p<0.05; **, p<0.01; ***, p<0.001 ****, p≤0.0001.*

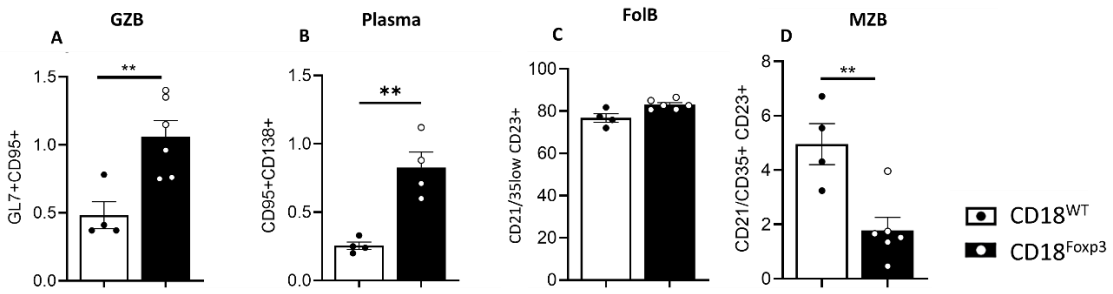

Figure 48 ***CD18^{Foxp3} mice have altered B cell subset distributions in the spleen.*** *Flow cytometric quantification of* ***(A)*** *GL-7^{+}CD95^{+} germinal center B cells (GBZ),* ***(B)*** *CD95^{+}CD138^{+} plasma B cells* ***(C)*** *CD21/35^{low}CD23^{+} follicular B cells (FolB) CD21/35^{+}CD23^{+} and* ***(D)*** *marginal zone B cells (MZB)CD95^{+}CD138^{+} of wildytpe and CD18^{Foxp3} mice, n=4-6. Dots represent individual mice; bars show the mean ± SEM, representative of at least two independent experiments. Significance was determined by two-tailed unpaired t test or ns, p>0.05; *, p<0.05; **, p<0.01.*

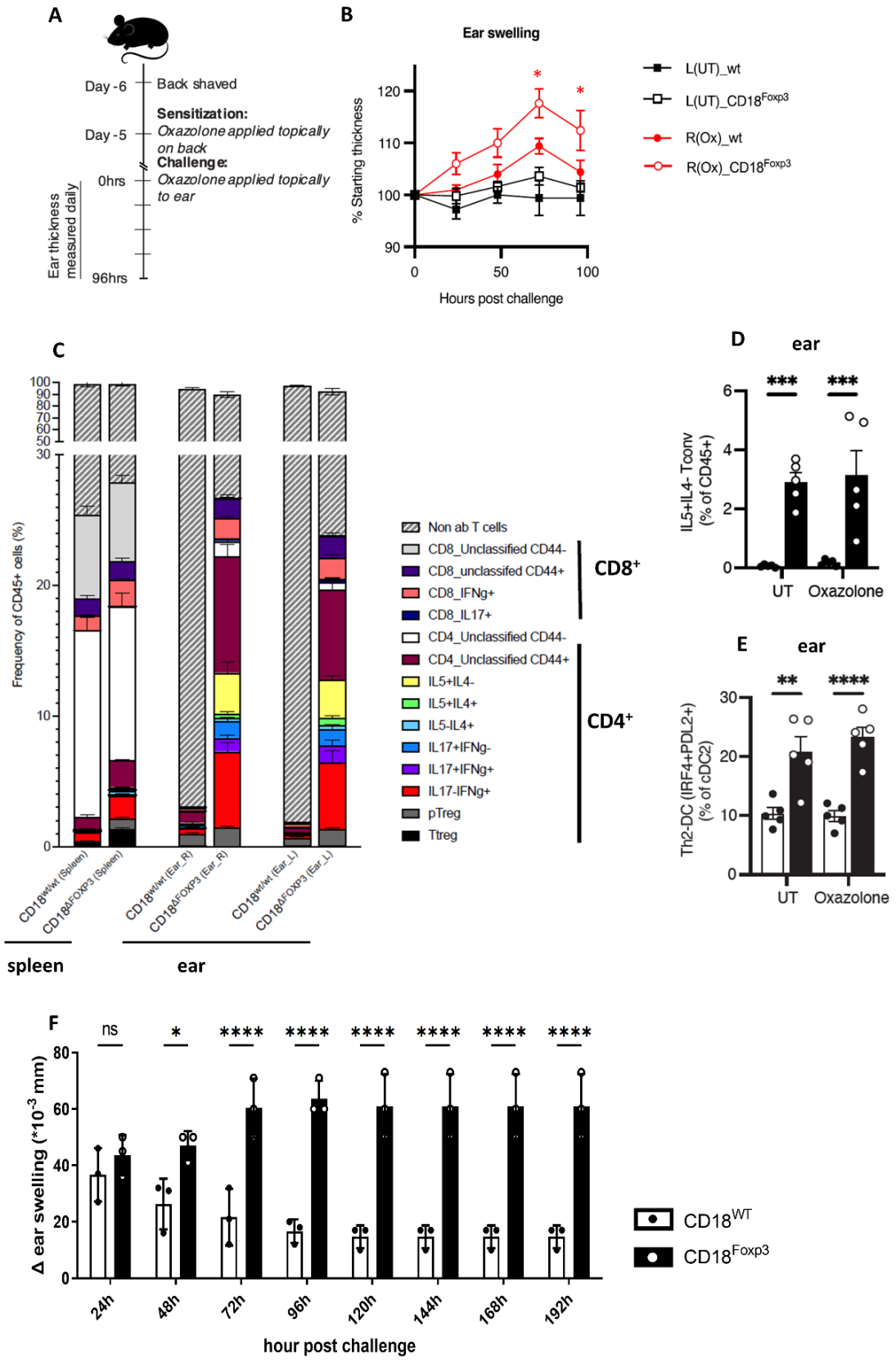

Figure 49 ***CD18^{Foxp3} mice show exacerbated oxazolone-induced atopic dermatitis responses.*** ***(A)*** *Experimental timeline of oxazolone-induced contact dermatitis.* ***(B)*** *Measured ear swelling after challenge of untreated (UT) left (L) ear in black and oxazolone-treated (Ox) right (R) ear in red between CD18^{WT} compared to CD18^{Foxp3}, n=5.* ***(C)*** *Classification of CD8$^+$ and CD4$^+$ T cells in spleens and ears by flow cytometry after 96h post challenge with oxazolone (pregated on CD45$^+$ cells). Quantification of flow*

*cytometry data showing **(D)** frequency of $IL5^{+}IL4^{-}$ T_{conv} cells and **(E)** T_H2-DC between untreated (UT) and oxazolone-treated ears after 96h, n=5. **(F)** Measured delta ear swelling (outgoing day 0) of oxazolone-treated ears between $CD18^{WT}$ compared to $CD18^{Foxp3}$ until 192 hours post-challenge, n=3. Dots represent individual mice; bars show the mean ± SEM. Significance was determined by 2-way ANOVA with Šídák's multiple comparisons test. ns, $p>0.05$; ***, $p<0.001$ ****, $p\leq0.0001$.*

6. Discussion

Human LAD-1 syndrome is a rare disease attributed to mutations in the CD18 gene. These mutations lead to the deficiency of β_2-integrin expression and impairment of leukocyte migration out of blood vessels and into tissues. As β_2-integrin expression in some LAD-1 patients differs vastly between cells, the clinical phenotype is very heterogeneous and can affect almost all immune cells. Patients can suffer from a number of symptoms, including recurrent bacterial infections of the skin, lung, and mucous membranes, as well as severe periodontitis and poor wound healing. Interestingly, in addition to these immunodeficiency symptoms, LAD-1 patients were also reported to suffer from IBD, autoimmune nephritis, type 1 diabetes, and other autoimmune phenomena [212, 322]. Thus, the clinical symptoms of LAD-1 combine aspects of immunodeficiency and autoimmunity. Until now, the only curative therapy is allogeneic hematopoietic stem cell transplantation [215, 216]. Various mouse models with a constitutive knockout of either an α or a ß subunit have been established to study the pathophysiology of β_2-integrin mutations [219, 230, 231, 234, 323, 324]. As in LAD-1 patients, β_2-integrins in these models are globally defective in all leukocytes, and these mice also exhibit enhanced susceptibility to infections and delayed wound healing, as well as lymphatic hyperplasia, generalized leukocyte activation and symptoms of autoimmunity [219-221, 230]. Since all leukocytes are affected in mice with a global defect in β_2-integrins, it is difficult to dissect the cellular mechanisms of the apparently paradoxical coexistence of immunodeficiency and autoimmunity. Thus, it is of interest to generate mouse models with cell-specific deletions of β_2-integrins [6].

6.1. Specific deletion of LFA-1 in Treg contributes to spontaneous development of atopy-like organ inflammation and autoimmunity

In this study, we generated a Treg-specific LFA-1 knockdown mouse model. These mice suffer from spontaneous skin inflammation and hyperplasia of lymphoid organs. Since the α and ß subunits of β_2-integrins pair intracellularly, a knockout of CD18 results in a decreased expression of the α subunit as well (here CD11a) [38]. As shown, LFA-1 is specifically knocked out on Treg as $CD8^+$ and T_{conv} ($Foxp3^-$) cells derived from wildtype and $CD18^{Foxp3}$ mice have similar expression of LFA-1 in different organs. Interestingly, T_{conv} cells in the lungs of $CD18^{Foxp3}$ mice show a decrease in LFA-1 expression. We cannot exclude that the T_{conv} population also comprises so-called 'exFoxp3 Treg', losing their immunophenotypic stability and downregulating Foxp3 expression [325]. These 'exTreg' are characterized by an inflammatory phenotype [325] which might fit to the lung inflammation observed in $CD18^{Foxp3}$ mice. Whether this hypothesis is applicable in this model has to be investigated further.

$CD18^{Foxp3}$ mice develop a spontaneous skin inflammation predominantly of ears and tails and indeed, skin sections of $CD18^{Foxp3}$ mice show thickening of the epidermis reflecting cell infiltrations and inflammation. Moreover, $CD18^{Foxp3}$ mice suffer from systemic organ inflammation, including lung and gut. These findings demonstrate an atopy-like organ inflammation which is known to be associated with cutaneous inflammation, lung inflammation like asthma, and food allergy including the gut [326]. In addition to the skin,

lung, and gut inflammation, the atopic phenotype observed in CD18^{Foxp3} mice is underlined by the presence of T_H2-promoting immune responses [327]. In common, CD18^{Foxp3} mice show increased IL4-producing Gata3$^+$ T_{conv} cells and high IgE levels in the serum. These results indicate an important role of LFA-1 on Treg in this model to maintain immune homeostasis. It is known that CD18$^{-/-}$ mice develop spontaneous skin inflammation according to abnormalities of leukocyte migration, especially of PMN and defective T cell function [230], but this model includes all β_2-integrins. Our mouse model demonstrates an indispensable role of LFA-1 on Treg and that LFA-1 on Treg alone is the driver of atopy-like (auto)inflammation.

The autoimmune phenotype in CD18^{Foxp3} mice is underlined by the presence of autoantibodies. We observed increased nuclear/perinuclear autoantibody patterns as well as the production of autoantibodies against basement membrane components and/or basal keratinocytes. The latter is found in blistering autoimmune skin diseases [328], whereas antinuclear autoantibodies are a hallmark of systemic lupus [329]. Increased autoantibody production has also been observed in CD18$^{-/-}$ mice [64]. In this respect, the spontaneous autoimmune phenotype of CD18^{Foxp3} mice shares many aspects with that of scurfy mice with a mutation in the *foxp3* locus and completely lacking functional Treg [330-332]. Similar to these mice, CD18^{Foxp3} mice also spontaneously develop autoantibodies and autoinflammation in multiple organs, albeit later in life and with less intensive. Altogether, these observations suggest that the cell-intrinsically altered function of LFA-1-deficient Treg causes the multiorgan autoinflammatory phenotype in CD18^{Foxp3} mice.

6.2. LFA-1-deficient Treg have altered gene expression profiles and might be dysfunctional

Furthermore, we demonstrate here that LFA-1-deficient Treg of CD18^{Foxp3} mice are still able to home into tissue, but we cannot exclude that these Treg have residual LFA-1 expression during their homing, which could facilitate their entry into tissue. Indeed, we found an increased presence of Treg in multiple organs, which might be a compensatory effect attributable to the excessive immune reaction. By contrast, CD11a$^{-/-}$ mice reveal less homing, but not a complete absence of CD4$^+$ T cells, to secondary lymphatic tissue and decreased adhesion to high endothelial venues for leukocytes in general [333]. Reduced Treg frequencies in CD11a$^{-/-}$ mice were also observed in the inflamed nervous system in a model for EAE. In general, lymphocyte arrest and transmigration along the endothelium is exclusively dependent upon LFA-1 and ICAM/JAM interactions, as in LAD-1 patients and CD18$^{-/-}$ mice, rolling of PMN and lymphocytes along vascular endothelia and their transmigration into tissues is significantly impaired, leading to blood neutrophilia and lymphatic hyperplasia [224, 230, 232, 334]. In contrast, our data suggest that LFA-1 may not be required for Treg transmigration as previously assumed [335]. The loss of LFA-1 expression may also be partially compensated by the upregulation of other integrins, such as VLA-4 (CD49d) and integrin αE (CD103), although we cannot rule out that cre-induced deletion of β_2-integrins from the surface of Treg occurs only after their migration from blood into peripheral tissues. Anyway, the inflammatory phenotype of CD18^{Foxp3} mice is not due to an absence of Treg in peripheral tissues.

In contrast to the established role of CD18-deficient PMN for LAD-1-associated symptoms [336, 337], much less is known about the pathogenic relevance of Treg in LAD-1 patients. Patients with reversion mutations leading to cytotoxic T cells expressing CD18 showed increased frequencies and diminished suppressive function of LFA-1-deficient Treg, comparable to our observations in $CD18^{Foxp3}$ mice [255]. The gene expression profile of LFA-1-deficient Treg derived from $CD18^{Foxp3}$ mice indicate an upregulation of genes driving positive regulation of cytokine production in Treg, increased T cell activation, and immune cell infiltrates affecting multiple organs, supporting impaired suppressive function of $CD18^{Foxp3}$ Treg as the major cause. The lack of Treg suppression leading to increased activity of autoreactive T cells has been postulated to be the driver of autoimmune bowel disease in these patients [255]. Lack of Treg suppressive function in $CD18^{-/-}$ mice was also observed by Marski *et al.* [64]. Our use of a conditional knockout confirms that this functional change in Treg is a direct result of the lack of Treg-expressed CD18 rather than a result of global immune changes due to loss of CD18 expression in all leukocytes as in $CD18^{-/-}$ mice and in case of LAD-1 syndrome.

Treg lacking LFA-1 appear to have intact tissue migration but display altered transcriptional profiles, suggesting LFA-1-dependent intrinsic signaling defects in $CD18^{Foxp3}$ mice. Bulk sequencing analysis of activated splenic LFA-1-deficient Treg revealed about 130 (fold change ≥1.5) differentially expressed genes. Indeed, some of the upregulated genes of LFA-1-deficient Treg are involved in T_H cell differentiation. Furthermore, differentially expressed genes of LFA-1-deficient Treg showed an association with diseases like asthma, dermatitis, and eosinophilia, which fits to the atopic-like organ phenotype in $CD18^{Foxp3}$ mice. Moreover, 5 out of 8 of the top enriched GO terms relate to immune activation and T_H2 response rather than immune suppression, as would be expected from functional Treg, implying a defect in the regulatory capacity of these cells. Figure 50 summarizes the significantly upregulated genes of LFA-1-deficient Treg that encode different T_H2-related expression markers and important adhesion molecules like CD103 and G protein-coupled receptor Gpr15.

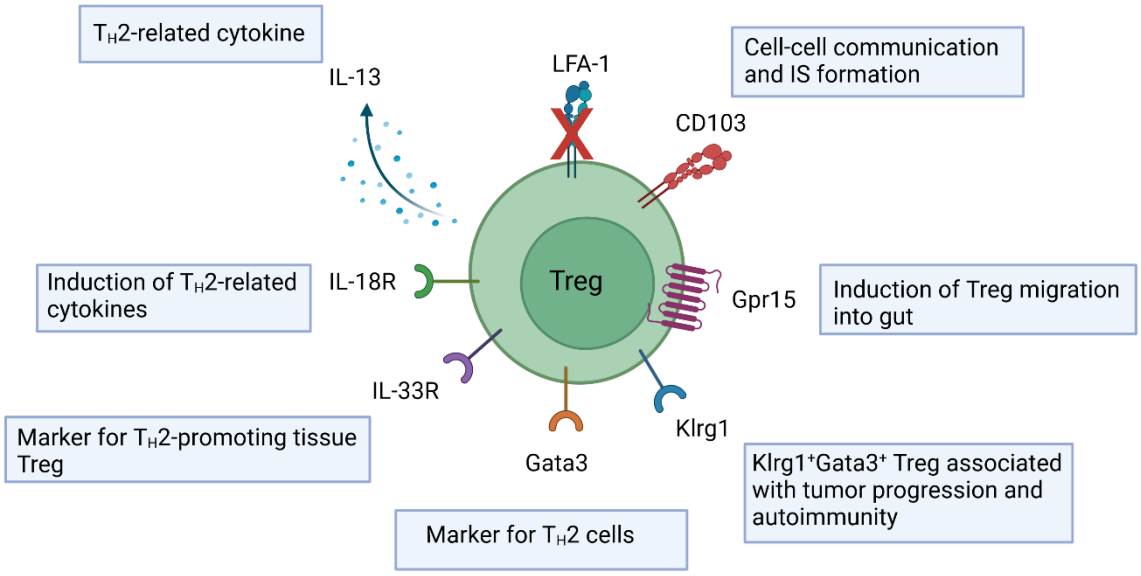

Figure 50 Upregulated genes of LFA-1-deficient Treg encode a number of important receptors and T_H2 related expression markers. *Altered gene expression profile of LFA-1-deficient Treg highlights genes like Il13, IL18r, Il1rl1 (IL-33R), and Gata3, which are associated with a T_H2-promoting phenotype [319, 338, 339]. Klrg1$^+$ Treg are associated with infectious diseases like tuberculosis and Klrg1$^+$Gata3$^+$ co-expression on Treg is known to promote tumor progression [340]. These findings underline the important role of Klrg1 as a potent checkpoint marker. Furthermore, CD103, an αE integrin, which is important for cell-cell communication as well as Gpr15, crucial for cell migration [341] are upregulated. (Created with BioRender.com, accessed on 19 September 2023)*

One of the most prominent alterations in gene expression is a significant upregulation of IL-18 signaling. IL-18 is known to induce T_H2 cytokine production and implicates allergic responses [338, 342]. Moreover, it was demonstrated that IL-18 inhibition alleviates lung inflammation, indicating a role of IL-18 in the suppressive function of Treg [343]. Akimova and coworkers demonstrated that the IL18Rα expression is significantly higher on Treg than on T_{eff} and other lymphocytes. IL-18 leads to the upregulation of TLR4 and the phosphorylation of the protein kinase IRAK4 (interleukin-1 receptor-associated kinase 4) which is a component of the MyD88 pathway. IRAK4 activates TRAF6, which might form a complex with STUB1 (STIP1 Homology and U-Box Containing Protein 1) [343]. As described by Chen *et al.* STUB1 negatively modulates Treg suppression by degrading Foxp3 [344]. TLR4 signaling may increase Treg sensitivity to pro-inflammatory cytokines, like IL-6 and IL-1β, and further declines Treg function and stability [343]. In this context, Treg from CD18^{Foxp3} mice might be more susceptible to IL-18 signaling as the IL-18 receptor in LFA-1-deficient Treg is upregulated. Whether IL-18 in the serum of CD18^{Foxp3} mice is higher and might contribute to the failure of the suppressive function has to be investigated.

Moreover, the C-C motif chemokine receptor 2 (CCR2) is upregulated on LFA-1-deficient Treg. CCR2 is a functional chemotactic receptor that regulates the mobilization of monocytes and PMN into the blood during inflammation [345] but is also important for Treg homing and inflammatory migration [346]. The higher expression of CCR2 underlines enhanced trafficking of LFA-1-deficient Treg to tissues, as described before. Treg require CCR2 to migrate to inflamed tissues and tumors that generate the CCR2

ligands CCL2 [347, 348]. Furthermore, $CD18^{Foxp3}$ mice display granulocytosis in multiple organs alongside signs of increased PMN activation and output from the BM.

Further, bulk sequencing data highlighted differentially expressed genes, including *Gpr15* and *Il13*, which were upregulated and are normally expressed by T_H2 cells but also Treg. *Gpr15* encodes G protein-coupled receptor 15, which has been implicated in regulating chronic inflammation [269] and supported the trafficking of Treg to the gut [341]. Therefore, it plays a central role in maintaining intestinal immune homeostasis. In line, more gastrointestinal tract (GIT) infiltrates were observed in $CD18^{Foxp3}$ mice, indicating disrupted immune homeostasis. *Il13* is a key regulator of T_H2 cells [339] and is also expressed by T_H2 promoting $ST2^+$ tissue Treg [349], which indicates a role of LFA-1-deficient Treg to confer a shift towards type II immunity in $CD18^{Foxp3}$ mice. Indeed, we found more T_H2 than T_H1 immune responses predominantly in lung and sdLN.

Moreover, the IL-33 receptor, also known as ST2 receptor was found upregulated, which is characteristic for the specific T_H2-promoting tissue Treg subset [178, 319]. Chen and coworkers [350] demonstrated that the secretion of IL-33 upregulates Treg expression of Gata3, the expression of ST2, as well as the production of T_H2-promoting cytokines in the lungs of mice. Furthermore, IL-33 impaired the suppressive ability of Treg and contributed to airway inflammation in these mice [350]. Indeed, $CD18^{Foxp3}$ mice showed an upregulation of $Gata3^+$ lung Treg, which might contribute to their loss of suppressive function and the promotion of a T_H2 immune response characterized by the expansion of $Gata3^+$ T_{conv} subsets in spleen, lung, and blood of our mice.

Harrison *et al.* showed that after colonization of mice with *Staphylococcus epidermidis* onto the skin, specific tissue-resident cytotoxic $CD8^+$ T cells (T_C17) were characterized by the co-expression of RORγt and Gata3 producing T_H2-related cytokines IL-5 and IL-13. These T_C17 cells express type 2 cytokine mRNA without subsequent protein translation and have the ability to produce IL-17. Exposure to inflammatory mediators leads to the release of type II cytokines, allowing T_C17 to exert pleiotropic-specific functions like tissue repair [351]. Whether cytotoxic T cells from $CD18^{Foxp3}$ mice have a type II transcriptome profile and co-express RORγt and Gata3 has to be investigated.

Upregulation of the gene *Itgae* encoding CD103, an αE integrin that binds to epithelial E cadherin [352], might be a compensatory effect. Enhanced expression of CD103 on LFA-1-deficient Treg could partially substitute the loss of LFA-1 for cell-cell communication. It was shown that CD103-E-cadherin interactions are essential for cytotoxic IS (cIS) maturation. The formation of a cIS leads to the synaptic release of cytokines like IFN-γ and granzyme B within the synapse, resulting in target cell lysis [353]. We also found that Klrg1 is upregulated on LFA-1-deficient Treg. Klrg1 usually identifies a highly activated, short-lived Treg subset in the periphery [354]. It was shown that $Klrg1^+$ Treg aggregate at sites of inflammation, specifically in a murine model of colitis. This suggests that inflammation might contribute to Klrg1 induction. In addition, tissue-resident $ST2^+$ Treg also co-express Klrg1 and might play a regulatory role in non-lymphoid tissues by suppressing naïve $CD4^+$ T cell proliferation [340, 355]. It has been demonstrated that anti-Klrg1 blocking antibodies increased effector cytokine production and alleviated disease development in human tuberculosis patients [356]. Additionally, $Klrg1^{-/-}$ mice display increased survival after tuberculosis infection due to the induction of pulmonary

$CD4^+$ T cells, which produce IFN-γ and TNF [357]. Furthermore, the increase of $KLRG1^+$ Treg positively correlates with disease severity of EAE [358]. $KLRG1^+CD103^+$ Treg may also play a role during lung tumor progression. It was shown that these Treg accumulate in the tumor mice upregulating the activation markers CD44 and CD69 [359]. Li and coworkers demonstrated that the Treg-specific deletion of IL-33R reduced $KLRG1^+CD103^+$ Treg and induced $CD8^+$ T cell infiltration, which resulted in reduced tumor progression [360]. Moreover, the E-cadherin ectodomain binds to Klrg1-expressing cells and was shown to reduce NK cytotoxicity and $CD8^+$ T cell proliferation, suggesting that E-$cadherin^+$ APC might have the capacity to dampen lymphocyte functions [352]. These observations highlight Klrg1 as a potent checkpoint inhibitor target.

In vitro activated splenic, MACS-isolated $CD4^+CD25^+$ cells, including Treg, as well as MACS-isolated naïve $CD4^+CD25^-$ T cells showed different cytokine profiles. Pro- as well as anti-inflammatory cytokines were upregulated *in vitro,* whereas *ex vivo* cytokine expression of Treg (shown for IL-10 and IL-17) were unaltered. The iTreg supernatant showed differential cytokine profiles. Whether this is a result shifting of Treg towards T_H1/T_H2 or T_H17 in this iTreg culture has to be elucidated. We cannot exclude that differential cytokine production might be driven by $CD4^+$ T cells subsets rather than Treg subsets in the *in vitro* cultures.

6.3. Impaired contact between LFA-1-deficient Treg and DC contributes to autoimmune phenotype and type II immunity

Alongside the role of LFA-1 as a prominent adhesion receptor facilitating T cell homing to sites of peripheral tissue and inflammation, it mediates strong adhesion to APC by reorganizing distinct proteins within the immunological synapse [83, 361]. Loss of LFA-1 on T_{conv} results in reduced contacts with DC, as previously described [362]. The modulation of the activation status of APC through the formation of strong and prolonged contact is a key way in which Treg exert their control of the immune response [106, 235]. We observed fewer cell-cell contacts as well as shorter interaction times of LFA-1-deficient Treg with DC *in vitro*. These results support previous descriptions of impaired binding between LFA-1-deficient T_{conv} and DC [362]. This attenuated Treg/DC interaction resulted in DC hyper-activation *ex vivo* due to the upregulation of activation markers like CD86 and an increase in the pro-inflammatory cytokine IL-6 and *in vitro* as reflected by upregulation of different genes expressed by DC isolated from $CD18^{Foxp3}$ mice. Here, the most prominently altered genes were IL-4-induced gene-1 (*IL4i1*), which is involved in M2-polarization of myeloid cells [363], as well as the DC-specific chemokine receptor *Xcr1*, a marker for cross-presenting DC [302]. As mentioned before, IL-33 is involved in the polarization of T_H2 responses through binding to the ST2 receptor [273]. Besnard *et al.* [364] demonstrated that IL-33 modulated DC functions to secrete IL-6 and CCL17. This leads to the priming of naïve T cells to produce T_H2 cytokines, which is consistent with our data. However, our bulk sequencing data of spleen DC indicated downregulation of *ccl17*, but values are very inconsistent between single samples of wildtype and $CD18^{Foxp3}$ DC.

It is known that LFA-1 on Treg is required for strong adhesion to DC [235, 365], which is an important mechanism by which Treg mediate immune homeostasis. This binding results in the suppression of DC priming of T_{conv} cells through multiple mechanisms, including

trans-endocytosis of costimulatory molecules necessary for T_{conv} activation [197], prevention of T_{conv} binding to DC [235, 247], and cytoskeleton rearrangement [106]. Our *in vitro* observations indicate that the observed increase in DC activation *in vivo* in $CD18^{Foxp3}$ mice is likely due to the inability of LFA-1-deficient Treg to suppress DC activation homeostatically. We hypothesize that the resulting hyperactivation of DC might contribute to spontaneous T cell activation and autoimmunity *in vivo*. Whether an altered suppressive function of LFA-1-deficient Treg in combination with reduced cell contacts to APC contributes to the breakdown of tolerance in these mice has to be elucidated.

In addition, cyclic adenosine monophosphate (cAMP) plays a central role in Treg-mediated suppression of T_H cells and DC. Further studies demonstrated that cAMP is conveyed from Treg cells to T_H cells and to DC via GJ [366]. GJ channels are made of connexin and there exists a connexin-integrin crosstalk between cells [367]. Interestingly, GJ communication was not altered between LFA-1-deficient Treg and T cells as well as DC, assuming that gap junction is independent of LFA-1-mediated cell-cell contacts. Whether reduced cell-cell interactions are compensated through long culturing overnight has to be investigated. Nevertheless, a defective interaction of T_{conv} with LFA-1-deficient Treg appears unlikely, as dynamic interactions between LFA-1-deficient Treg and T_{conv} were not impaired. Thus, the inability of LFA-1-deficient Treg to engage T_{conv} via LFA-1/ICAM interactions might be substituted by the unimpaired capacity of T_{conv} to engage ICAM on LFA-1-deficient Treg via their intact LFA-1 molecules.

In contrast to our original hypothesis, assuming that $CD18^{Foxp3}$ mice develop psoriasis-like skin inflammation predominantly by conversion of Treg into T_H17-like cells, we observed a profound switch to type II-driven immunity. As mentioned before, LFA-1-deficient Treg have an altered gene expression profile indicating a tendency towards T_H2-inducing tissue Treg. In addition, our *ex vivo* data showed an increase in $Gata3^+$ T_H2 cells, elevated IgE levels in the serum, as well as a higher frequency of T_H2-promoting DC. The high IgE levels in the serum of $CD18^{Foxp3}$ mice indicate a T_H2-mediated B cell antibody switch. Indeed, higher frequencies of germinal center B cells and plasma B cells were found in the spleen. Germinal center B cells might differentiate into IgE-producing plasma B cells within the inflamed tissue [368].

Bulk sequencing data revealed that LFA-1-deficient Treg are associated with atopic dermatitis, a type II polarizing disease. In addition, $CD18^{Foxp3}$ mice were not able to recover from induced acute contact dermatitis. It is known that LFA-1 on T cells is responsible for the production of T_H1-related cytokines and transcription factors [121, 140, 141]. Verma *et al.* demonstrated that on the one hand, that ICAM-1 and LFA-1 interaction promotes a T_H1-induced immune response by the induction of *hey1* and *hes1* leading to the activation of the Notch pathway [141] and on the other hand leads to a T cell genetic signature inducing genes like *smad7*, *smurf*, *ski*, and *skil* resulting in T cells refractory to TGF-β signaling [140]. They further showed that the interruption of the interaction of LFA-1 with ICAM-1 blocks TGF-β signaling and drives the immune phenotype of T cells towards T_H17 cells. Furthermore, Salomon *et al.* [369] showed that DC may promote T_H1 development by suppressing T_H2 development through the interaction of ICAM-1 and ICAM-2 with LFA-1. Our data revealed that the loss of LFA-1 introduced a T cell

polarization from T_H1 to predominantly T_H2 immunity, concluding that DC may not be able to suppress T_H2 development in these mice.

Moreover, with disease progression, it seemed that $CD18^{Foxp3}$ developed elevated T_H17 responses in the lung and liver. However, we could not confirm that the Notch-related genes *hey1* and *hes1*, and the genes involved in the TGF-β signaling are altered in LFA-1-deficient Treg.

Interestingly, other transgenic mice with Treg dysfunction like mice with a Treg-specific knockout of the serine threonine kinase CK2 (*Csnk2b*fl/fl*Foxp3*^{Cre} mice) [370] or the recombination signal-binding protein for immunoglobulin kappa J region (*Rbpjfl/flFoxp3*^{Cre,YFP} mice) [319] showed a closely similar phenotype to $CD18^{Foxp3}$ mice (Table 21). Indeed, Rbpj has been associated with T_H1/T_H2 cell fate decisions. Like LFA-1, Rbpj is involved in Notch signaling and forms a complex with the Notch intracellular domain (NICD), which was shown to be critical for the regulation of Gata3 [319].

Comparative assessment of the phenotype of mice with various distinct Treg-restricted gene knockouts suggests at first sight that Treg dysfunction in general leads to a T_H2 class switch, as observed in these mouse models. In addition, Treg dysfunction might destabilize the immune balance and the microbiome imprinted by the conditions in the animal facility dictates the type of immune response. Delacher *et al.* [319] showed an environmental influence favoring a T_H2 immune response in *Rbpjfl/flFoxp3*^{Cre,YFP} mice, since 40% of animals housed under specific pathogen-free conditions spontaneously develop a T_H2 phenotype, whereas 90% of mice colonized with a defined `altered schaedler flora` (consortium of eight murine bacterial species) [371] housed in individually ventilated cages remained healthy until 20 weeks of age. Nevertheless, both colonies developed a type II immune response but with retarded disease onset. Epidemiological studies have suggested that the increase in allergic disorders like atopic dermatitis and asthma is attributable to a reduced microbial burden during childhood due to a westernized lifestyle (the 'hygiene hypothesis') [372, 373] but the immunological basis is controversial. It is thought that immune deviation of allergen-specific responses from T_H2 to T_H1 profile is missing and the immune suppression is reduced [372]. Whether $CD18^{Foxp3}$ mice develop a profound T_H2 immunity directly due to Treg dysfunction or indirectly as a consequence of Treg immune dysbalance and environmental factors has to be elucidated.

Table 21 ***Comparison of CD18^{Foxp3} mice with other Treg-specific KO mice.*** *(- =not present, + =present, ++ =pronounced, ? =not known or tested)*

	CD18^{Foxp3} [1]	*Csnk2b*fl/fl*Foxp3*^{Cre} [370]	*Rbpjfl/flFoxp3*^{Cre,YFP} [319]
Scientific background	• LFA-1 is crucial for cell-cell interaction and cell adhesion • CD18 deficiency leads to LAD-1 syndrome.	• CK2 is involved in signal-transduction pathways, including the NF-κB, PI(3)K and Wnt pathways	• Rbpj is a transcription factor known as co-factor during Notch signaling • It was shown to be critical for regulation of Gata3 in T_{conv}
Skin inflammation	++	-	+
splenomegaly	++	++	++
High IgE/T_H2 phenotype	++	++	++
Autoantibodies	+	?	+
In vitro Treg suppression	?	+	-
T_H2-promoting DC	+	+	?

6.4. Conclusion and outlook

In conclusion, we demonstrate an indispensable role of LFA-1 on Treg for maintaining Treg homeostasis in a newly established mouse model. We showed that LFA-1 might not be required for Treg homing into tissue. However, β_2-integrins on Treg are important to form durable cell-cell contacts with APC. The loss of LFA-1 on Treg reduced the cell-cell contacts and duration time with DC. This may lead to a defect in immune homeostasis in $CD18^{Foxp3}$ mice, contributing to the increased activation of DC and T_{conv} (Figure 51 A).
The reduced dampening of DC activation by LFA-1-deficient Treg might be a loss of suppressive function and consequently Treg dysfunction in $CD18^{Foxp3}$ mice. The cytokine IL-33 may play a key role in this mechanism. IL-33 could act in two ways: (1) By binding to DC, IL-33 leads to the priming of naïve T cells to produce T_H2 cytokines [273]. Moreover, IL-33 upregulates the ST2 receptor (IL-33R) and Gata3 expression on T cells, especially on tissue Treg [350], which results in the type II immune response observed in $CD18^{Foxp3}$ mice (Figure 51 B). (2) Furthermore, IL-33 reduces the suppressive ability of Treg. The production of IL-4 and IL-5 of $Gata3^+$ T_H2 cells, in turn, leads to a B cell class switch increasing IgE-producing plasma B cells (Figure 51 C). Another key regulator might be the cytokine IL-18 which reduces Treg suppressive function and promotes T_H2 responses [338, 342, 343]. This mechanism may result in the atopy-like phenotype observed in our mice. Whether IL-18 and IL-33 play a role in this model has to be investigated further.
Additionally, the production of autoantibodies (Figure 51 D) leads to the manifestation of the (auto)inflammation in $CD18^{Foxp3}$ mice ,affecting multiple organs. Taken together, these mechanisms of Treg-restricted β_2-integrin-dependent breakdown in immune tolerance lead to spontaneous multi-organ (auto)inflammation in these mice.
Thus, $CD18^{Foxp3}$ mice share crucial pathological features with Foxp3-deficient scurfy mice and other mouse strains with Treg dysfunction. Deficiency of LFA-1 on Treg thereby has a similar negative effect on self-tolerance as the loss of Foxp3, which constitutes a crucial transcriptional key regulator of Treg. $CD18^{Foxp3}$ mice demonstrate the first murine model to identify the role of LFA-1 on Treg without interfering with other CD18-deficient immune cells *in vivo* and implicate Treg dysfunction as a major driver of autoimmunity observed in LAD-1 syndrome.

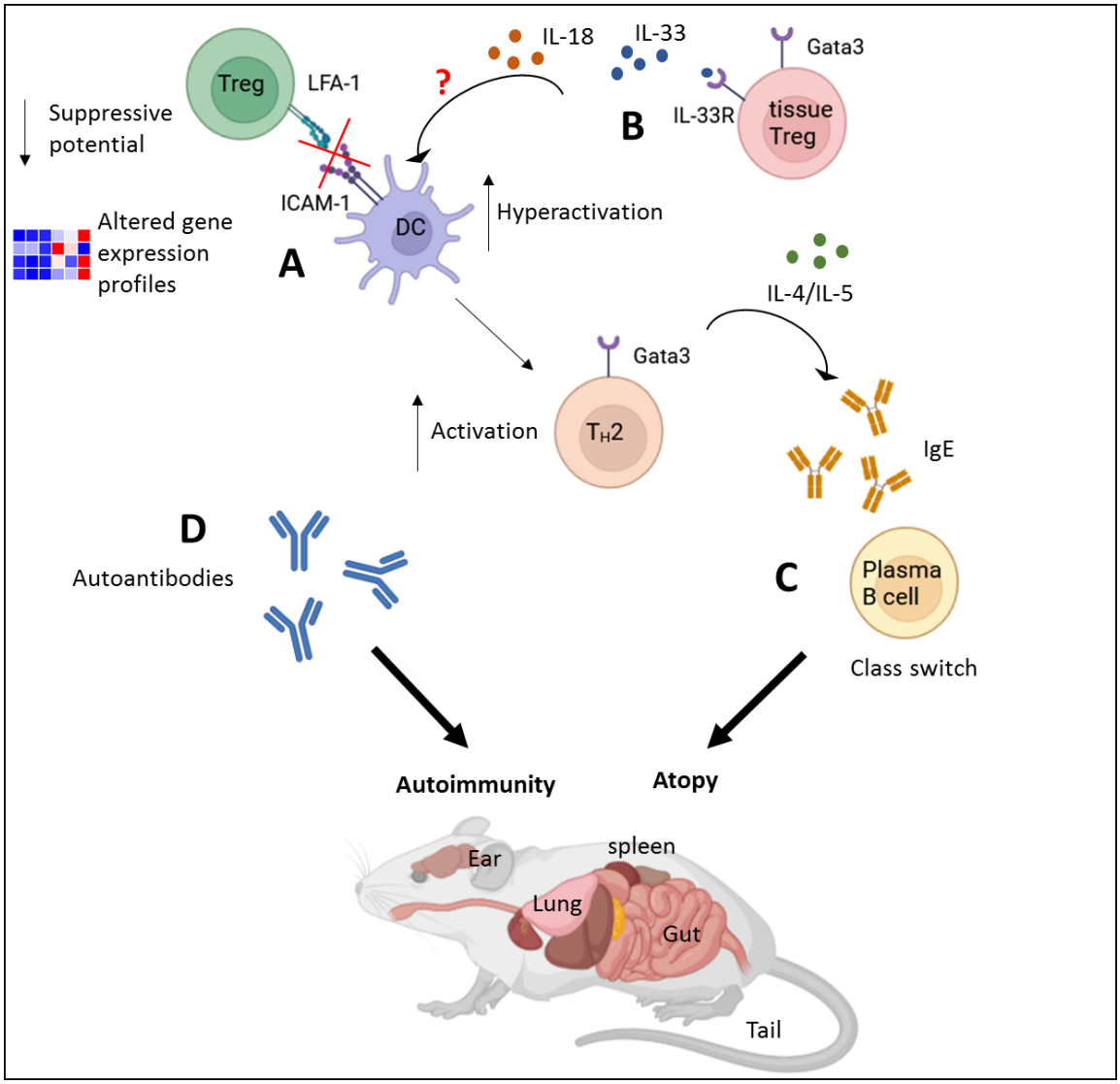

Figure 51 ***Loss of LFA-1 on Treg leads to autoimmunity and atopy-like inflammation.*** ***(A)*** *LFA-1-deficient Treg have reduced cell-cell contacts with DC, resulting in higher activation of DC and* T_{conv}. ***(B)*** *The cytokines IL-33 and IL-18 may bind to DC and support the priming of naïve T cells to produce* T_H2 *cytokines and the upregulation of ST2 (IL-33R) and Gata3 on* T_{conv} *cells and Treg.* ***(C)*** *The production of* T_H2*-promoting cytokines like IL-4 and IL-5 results in a B cell class switch and in the production of high IgE by plasma B cells.* ***(D)*** *Production of autoantibodies leads to the manifestation of (auto)inflammatory phenotype in* $CD18^{Foxp3}$ *mice affecting skin, lung, LN, spleen, and gut. (Icons created with BioRender.com, accessed on 31 August 2023)*

To further study Treg dysfunction and dysbalance as a consequence of T_H2-driven immunity, it would be necessary to compare gene expression profiles of *Rbpjfl/flFoxp3*^{Cre,YFP} and *Csnk2b*fl/fl*Foxp3*^{Cre} mice with that of $CD18^{Foxp3}$ mice. By comparing these various mouse models of compromised Treg function, it would be helpful to get insights into Treg-related type II immunity. Regarding the role of environmental factors, the microbiome of $CD18^{Foxp3}$ mice and littermates before and after the appearance of the (auto)inflammation (young versus old mice) should be defined. Furthermore, mice could be bread in different housing conditions with defined or non-defined microbiota or treated with antibiotics to determine whether the immune response from T_H2 immunity will shift more towards T_H1 or T_H17 immunity.

Besides the acute contact dermatitis models, other T_H2-promoting *in vivo* experiments like OVA-induced asthma [374] could be used to determine whether LFA-1-deficient Treg promote the induction of T_H2 cell-driven immune responses.

To prove the inability of LFA-1-deficient Treg to maintain immune homeostasis wildtype Treg as well as Treg from $CD18^{Foxp3}$ mice could be transferred to surfy mice, which lack functional Treg. It is known that through the transfer of competent Treg to scurfy mice the autoimmune phenotype of these mice can be rescued [375]. Assuming that LFA-1-deficient Treg are dysfunctional, surfy mice should develop the multi-organ inflammation as described and not recover due to the Treg transfer.

As the interaction between LFA-1-deficient Treg and DC is altered and the signaling transduction pathways were enhanced towards a T_H2 response the TCR signaling might be dysregulated. To study TCR signal strength transgenic mice expressing green fluorescence protein (GFP) from the immediate early gene *Nr4a1* (Nur77) locus could be used [376] and crossed with $CD18^{Foxp3}$. GFP is upregulated by antigen receptor stimulation in $Nur77^{GFP}$ mice and the level of GFP expressed during acute activation reflects the strength of TCR stimulation [376]. Thus, antigen receptor activation in vivo of LFA-1-deficient Treg could be assessed with this model.

So far, apart from LAD-1 patients, abnormal Treg function and expression of the binding affinity of LFA-1 in Treg from patients with atopic dermatitis or asthma is not known. Further analysis of CD18 expression leukocytes of patients suffering from atopy is required to assess a potential role β_2-integrins for disease induction and progression.

Furthermore, it is of major interest to generate mouse models with cell-specific deletions of distinct β_2-integrins. Besides the mouse line with a Treg-specific LFA-1 knockdown, mice with a conditional knockout of β_2-integrins specifically in $CD11c^+$ DC [95] and $Ly6G^+$ neutrophils [377] were generated in our lab. Both strains enabled to delineate the cell type-specific role of β_2-integrins in disease models. Mice with a DC-specific knockdown of β_2-integrins develop a delayed onset of EAE and an attenuated course of disease [95]. In a model of pulmonary aspergillosis, mice with a neutrophil-specific knockdown of β_2-integrins showed an impaired early innate immune response due to various impaired pathogen-killing functions of neutrophils [377]. It will be of interest to generate mouse strains with a conditional knockdown of β_2-integrins in other leukocyte populations to elucidate their contribution to the complex pathology observed in LAD-1 patients. Nevertheless, the cause for β_2-integrin-dependent breakdown in immune tolerance is still not fully understood and this project therefore aims to better understand CD18-dependent Treg cell development, migration and function in skin inflammation, and their relevance for T_H differentiation.

7. Supplements

7.1. List of figures

7.2. List of tables

7.3. List of abbreviations

ACh	-	Acetylcholine
ADAP	-	Adhesion and degranulation-promoting adapter protein
ANA	-	Antinuclear antibodies
APC	-	Antigen-presenting cells
BMDC	-	Bone marrow-derived DC
cAMP	-	Cyclic adenosine monophosphate
CBA	-	Cytometric bead array
CCL	-	Chemokines like chemokine ligand
CK2	-	Serine threonine kinase 2
CNS	-	Central nervous system
CR3	-	Complement receptor 3
c-SMAC	-	Center of the contact area
CTL-A	-	Cytotoxic T-lymphocyte-associated protein
CTV	-	Cell trace violet
CYTIP	-	Cytohesin-1-interacting protein
DC	-	Dendritic cell
DC-SIGN	-	Dendritic cell-specific ICAM-3-grabbing non-integrin
EAE	-	Experimental autoimmune encephalomyelitits
ECL	-	Enhanced chemiluminescence
ECM	-	Extracellular matrix molecule
ELISA	-	Enzyme-linked Immunosorbent Assay
ESM	-	Endothelial cell-specific molecule
FACS	-	Fluorescence activated cell sortin
FCS	-	Forward scatter
fl	-	Floxed
Foxp3	-	Forkhead box p3
GFP	-	Green fluorescence protein
GIT	-	Gastrointestinal tract

GITR	-	Glucocorticoid-induced TNF receptor related
GJ	-	Gab junctions
GO	-	Gene ontology
Gpr15	-	G protein-coupled receptor 15
GSK3β	-	Glycogen synthase kinase
GTN	-	Glyceryl
H&E	-	Hematoxylin and eosin
HEV	-	High endothelial venules
IBD	-	Inflammatory bowel diseases
ICAM	-	Intercellular adhesion molecules
IF	-	Immune fluorescence
IFN	-	Interferone
Ig	-	Immune globulin
IL	-	Interleukin
IL4il	-	IL 4 induced gene-1
iLN	-	Inguinal Lymph node
IPEX	-	Immunodysregulation, polyendocrinopathy, enteropathy X-linked syndrome
IRAK4	-	Interleukin-1 receptor-associated kinase 4
IS	-	Immunolocial synapse
iTreg	-	Induced Treg
JAM	-	Junctional adhesion molecule
KCl	-	Kaliumchloride
Klrg1	-	Killer cell lectin-like receptor subfamily G1
KO	-	Knockout
LAD-1	-	Leukocyte Adhesion Deficiency Type-1
LAG3	-	Lymphocyte-activation gene 3
LDV	-	Tripeptide leu-asp-val
LFA-1	-	Leukocyte function-associated antigen 1
LN	-	Lymph node
LPS	-	Lipopolysaccharide

MAC-1	-	Macrophage-1 antigen
MACS	-	Magnetic activated cell sorting
MAPK	-	p38 mitogen-activated protein kinase
MDDC	-	Monocyte-derived dendritic cells
MDM	-	Monocyte-derived macrophages
Mg	-	Magnesium
MHC	-	Major histocompatibility complex II
mLN	-	mesenteric lymph node
MOG	-	Myelin oligodendrocyte glycoprotein
MS	-	Multiple sclerosis
NF-κB	-	Nuclear factor k-light-chain-enhancer of activated B cells
NICD	-	Notch intracellular domain
NK cells	-	Natural killer cells
NTG	-	Nitroglycerine
Ox	-	Oxazolone
PASI	-	Psoriasis Area and Severity Index
PBS	-	Phosphate buffered saline
PCR	-	Polymerase chain reaction
PDBu	-	Phorbol 12,13 dibutyrate
PGF2	-	AprostaglandinF2alpha
PKA	-	Protein kinases A
PMA	-	Phorbol myristate acetate
PMN	-	Polymorphonuclear neutrophils
PSI	-	Plexin-semaphorin-integrin
p-SMAC	-	Peripheral supramolecular activation cluster
pTreg	-	Peripherally induced Treg
Rbpj	-	Immunoglobulin kappa J region
RGD	-	Arginylglycylaspartic acid
RIAM	-	Rap-1-GTP interacting adaptor molecule
RNS	-	Nitrogen species

ROS	-	Reactive oxygen species
RPKM	-	Reads per kilobase of transcript per million mapped reads
RT	-	Room temperature
sdLN	-	skin-draining lymph node

SOCS	-	Suppressor of cytokine signaling proteins
SSC	-	Side scatter
STAT	-	Signal transducer and activator of transcription
STUB1	-	STIP1 Homology and U-Box Containing Protein 1
Tconv	-	Conventional T cell
TCR	-	T cell receptor
Teff	-	Effector T cell
TGF-ß	-	Transforming growth factor ß
TH	-	T-helper cell
Thy-1	-	Thymus cell antigen 1
TNF	-	Tumor necrosis factor
Tr1	-	Type 1 pTreg
Treg	-	Regulatory T cell
TRIF	-	TIR-domain-containing adapter-inducing interferon-β
tTreg	-	Thymus-derived Treg
VAT	-	Visceral adipose tissue
VCAM	-	Vascular cell adhesion protein
WT	-	Wildtype
Xcr1	-	X-C Motif Chemokine Receptor 1

8. References

1. Klaus, T., et al., Impaired Treg-DC interactions contribute to autoimmunity in leukocyte adhesion deficiency type 1. JCI Insight, 2022. **7**(24).

2. Astarita, J.L., et al., Treg specialization and functions beyond immune suppression. Clin Exp Immunol, 2023. **211**(2): p. 176-183.

3. Guo, J. and X. Zhou, Regulatory T cells turn pathogenic. Cell Mol Immunol, 2015. **12**(5): p. 525-32.

4. Fagerholm, S.C., et al., Beta2-Integrins and Interacting Proteins in Leukocyte Trafficking, Immune Suppression, and Immunodeficiency Disease. Front Immunol, 2019. **10**: p. 254.

5. Blythe, E.N., et al., beta2 Integrin CD11d/CD18: From Expression to an Emerging Role in Staged Leukocyte Migration. Front Immunol, 2021. **12**: p. 775447.

6. Bednarczyk, M., et al., beta2 Integrins-Multi-Functional Leukocyte Receptors in Health and Disease. Int J Mol Sci, 2020. **21**(4).

7. Johnson, M.S., et al., Integrins during evolution: evolutionary trees and model organisms. Biochim Biophys Acta, 2009. **1788**(4): p. 779-89.

8. Mezu-Ndubuisi, O.J. and A. Maheshwari, The role of integrins in inflammation and angiogenesis. Pediatr Res, 2021. **89**(7): p. 1619-1626.

9. Hynes, R.O., Integrins: bidirectional, allosteric signaling machines. Cell, 2002. **110**(6): p. 673-87.

10. Humphries, J.D., A. Byron, and M.J. Humphries, Integrin ligands at a glance. J Cell Sci, 2006. **119**(Pt 19): p. 3901-3.

11. Pang, X., et al., Targeting integrin pathways: mechanisms and advances in therapy. Signal Transduct Target Ther, 2023. **8**(1): p. 1.

12. LaFoya, B., et al., Beyond the Matrix: The Many Non-ECM Ligands for Integrins. Int J Mol Sci, 2018. **19**(2).

13. Clements, J.M., et al., Identification of a key integrin-binding sequence in VCAM-1 homologous to the LDV active site in fibronectin. J Cell Sci, 1994. **107 (Pt 8)**: p. 2127-35.

14. Ludwig, B.S., et al., RGD-Binding Integrins Revisited: How Recently Discovered Functions and Novel Synthetic Ligands (Re-)Shape an Ever-Evolving Field. Cancers (Basel), 2021. **13**(7).

15. Nader, D., G.F. Curley, and S.W. Kerrigan, A new perspective in sepsis treatment: could RGD-dependent integrins be novel targets? Drug Discov Today, 2020. **25**(12): p. 2317-2325.

16. Conroy, K.P., L.J. Kitto, and N.C. Henderson, alphav integrins: key regulators of tissue fibrosis. Cell Tissue Res, 2016. **365**(3): p. 511-9.

17. Hussein, H.A., et al., Beyond RGD: virus interactions with integrins. Arch Virol, 2015. **160**(11): p. 2669-81.

18. Tian, Y., et al., A doxorubicin delivery platform using engineered natural membrane vesicle exosomes for targeted tumor therapy. Biomaterials, 2014. **35**(7): p. 2383-90.

19. Nabors, L.B., et al., Two cilengitide regimens in combination with standard treatment for patients with newly diagnosed glioblastoma and unmethylated MGMT gene promoter: results of the open-label, controlled, randomized phase II CORE study. Neuro Oncol, 2015. **17**(5): p. 708-17.

20. Reynolds, A.R., et al., Stimulation of tumor growth and angiogenesis by low concentrations of RGD-mimetic integrin inhibitors. Nat Med, 2009. **15**(4): p. 392-400.

21. Stipp, C.S., Laminin-binding integrins and their tetraspanin partners as potential antimetastatic targets. Expert Rev Mol Med, 2010. **12**: p. e3.

22. Tsuruta, D., et al., Laminin-332-integrin interaction: a target for cancer therapy? Curr Med Chem, 2008. **15**(20): p. 1968-75.

23. Hemler, M.E., et al., VLA-1: a T cell surface antigen which defines a novel late stage of human T cell activation. Eur J Immunol, 1985. **15**(5): p. 502-8.

24. Conrad, C., et al., Alpha1beta1 integrin is crucial for accumulation of epidermal T cells and the development of psoriasis. Nat Med, 2007. **13**(7): p. 836-42.

25. Breuer, J., et al., VLA-2 blockade in vivo by vatelizumab induces CD4+FoxP3+ regulatory T cells. Int Immunol, 2019. **31**(6): p. 407-412.

26. Mitroulis, I., et al., Leukocyte integrins: role in leukocyte recruitment and as therapeutic targets in inflammatory disease. Pharmacol Ther, 2015. **147**: p. 123-135.

27. Sheremata, W.A., et al., The role of alpha-4 integrin in the aetiology of multiple sclerosis: current knowledge and therapeutic implications. CNS Drugs, 2005. **19**(11): p. 909-22.

28. Weinstock-Guttman, B., An update on new and emerging therapies for relapsing-remitting multiple sclerosis. Am J Manag Care, 2013. **19**(17 Suppl): p. s343-54.

29. Engelhardt, B., et al., The development of experimental autoimmune encephalomyelitis in the mouse requires alpha4-integrin but not alpha4beta7-integrin. J Clin Invest, 1998. **102**(12): p. 2096-105.

30. Rettig, M.P., G. Ansstas, and J.F. DiPersio, Mobilization of hematopoietic stem and progenitor cells using inhibitors of CXCR4 and VLA-4. Leukemia, 2012. **26**(1): p. 34-53.

31. Ghobadi, A., et al., Bortezomib is a rapid mobilizer of hematopoietic stem cells in mice via modulation of the VCAM-1/VLA-4 axis. Blood, 2014. **124**(17): p. 2752-4.

32. Doring, A., et al., TET inducible expression of the alpha4beta7-integrin ligand MAdCAM-1 on the blood-brain barrier does not influence the immunopathogenesis of experimental autoimmune encephalomyelitis. Eur J Immunol, 2011. **41**(3): p. 813-21.

33. Bamias, G., D.J. Clark, and J. Rivera-Nieves, Leukocyte traffic blockade as a therapeutic strategy in inflammatory bowel disease. Curr Drug Targets, 2013. **14**(12): p. 1490-500.

34. Lin, K.K. and U. Mahadevan, Etrolizumab: anti-beta7-a novel therapy for ulcerative colitis. Gastroenterology, 2014. **146**(1): p. 307-9.

35. Vermeire, S., et al., Etrolizumab as induction therapy for ulcerative colitis: a randomised, controlled, phase 2 trial. Lancet, 2014. **384**(9940): p. 309-18.

36. Kunkel, E.J., J.E. Chomas, and K. Ley, Role of primary and secondary capture for leukocyte accumulation in vivo. Circ Res, 1998. **82**(1): p. 30-8.

37. Picarella, D., et al., Monoclonal antibodies specific for beta 7 integrin and mucosal addressin cell adhesion molecule-1 (MAdCAM-1) reduce inflammation in the colon of scid mice reconstituted with CD45RBhigh CD4+ T cells. J Immunol, 1997. **158**(5): p. 2099-106.

38. Arnaout, M.A., Biology and structure of leukocyte beta (2) integrins and their role in inflammation. F1000Res, 2016. **5**.

39. Kummer, D. and K. Ebnet, Junctional Adhesion Molecules (JAMs): The JAM-Integrin Connection. Cells, 2018. **7**(4).

40. Fraemohs, L., et al., The functional interaction of the beta 2 integrin lymphocyte function-associated antigen-1 with junctional adhesion molecule-A is mediated by the I domain. J Immunol, 2004. **173**(10): p. 6259-64.

41. Lim, K., et al., Visualization of integrin Mac-1 in vivo. J Immunol Methods, 2015. **426**: p. 120-7.

42. Li, N., et al., Ligand-specific binding forces of LFA-1 and Mac-1 in neutrophil adhesion and crawling. Mol Biol Cell, 2018. **29**(4): p. 408-418.

43. Simon, D.I., Opening the field of integrin biology to "biased agonism". Circ Res, 2011. **109**(11): p. 1199-201.

44. Altieri, D.C., et al., A unique recognition site mediates the interaction of fibrinogen with the leukocyte integrin Mac-1 (CD11b/CD18). J Biol Chem, 1990. **265**(21): p. 12119-22.

45. Kanse, S.M., et al., Promotion of leukocyte adhesion by a novel interaction between vitronectin and the beta2 integrin Mac-1 (alphaMbeta2, CD11b/CD18). Arterioscler Thromb Vasc Biol, 2004. **24**(12): p. 2251-6.

46. Peter, K., et al., Heparin inhibits ligand binding to the leukocyte integrin Mac-1 (CD11b/CD18). Circulation, 1999. **100**(14): p. 1533-9.

47. Chavakis, T., et al., The pattern recognition receptor (RAGE) is a counterreceptor for leukocyte integrins: a novel pathway for inflammatory cell recruitment. J Exp Med, 2003. **198**(10): p. 1507-15.

48. Wolf, D., et al., A ligand-specific blockade of the integrin Mac-1 selectively targets pathologic inflammation while maintaining protective host-defense. Nat Commun, 2018. **9**(1): p. 525.

49. Lishko, V.K., et al., Multiple binding sites in fibrinogen for integrin alphaMbeta2 (Mac-1). J Biol Chem, 2004. **279**(43): p. 44897-906.

50. Walzog, B., et al., The leukocyte integrin Mac-1 (CD11b/CD18) contributes to binding of human granulocytes to collagen. Exp Cell Res, 1995. **218**(1): p. 28-38.

51. Bajic, G., et al., Structural insight on the recognition of surface-bound opsonins by the integrin I domain of complement receptor 3. Proc Natl Acad Sci U S A, 2013. **110**(41): p. 16426-31.

52. Lamers, C., C.J. Pluss, and D. Ricklin, The Promiscuous Profile of Complement Receptor 3 in Ligand Binding, Immune Modulation, and Pathophysiology. Front Immunol, 2021. **12**: p. 662164.

53. Sandor, N., et al., CD11c/CD18 Dominates Adhesion of Human Monocytes, Macrophages and Dendritic Cells over CD11b/CD18. PLoS One, 2016. **11**(9): p. e0163120.

54. Diamond, M.S., et al., The I domain is a major recognition site on the leukocyte integrin Mac-1 (CD11b/CD18) for four distinct adhesion ligands. J Cell Biol, 1993. **120**(4): p. 1031-43.

55. Blackford, J., et al., A monoclonal antibody, 3/22, to rabbit CD11c which induces homotypic T cell aggregation: evidence that ICAM-1 is a ligand for CD11c/CD18. Eur J Immunol, 1996. **26**(3): p. 525-31.

56. Ihanus, E., et al., Red-cell ICAM-4 is a ligand for the monocyte/macrophage integrin CD11c/CD18: characterization of the binding sites on ICAM-4. Blood, 2007. **109**(2): p. 802-10.

57. Sadhu, C., et al., CD11c/CD18: novel ligands and a role in delayed-type hypersensitivity. J Leukoc Biol, 2007. **81**(6): p. 1395-403.

58. Ingalls, R.R. and D.T. Golenbock, CD11c/CD18, a transmembrane signaling receptor for lipopolysaccharide. J Exp Med, 1995. **181**(4): p. 1473-9.

59. Loike, J.D., et al., CD11c/CD18 on neutrophils recognizes a domain at the N terminus of the A alpha chain of fibrinogen. Proc Natl Acad Sci U S A, 1991. **88**(3): p. 1044-8.

60. Garnotel, R., et al., Human blood monocytes interact with type I collagen through alpha x beta 2 integrin (CD11c-CD18, gp150-95). J Immunol, 2000. **164**(11): p. 5928-34.

61. Aziz, M.H., et al., The Upregulation of Integrin alpha(D)beta(2) (CD11d/CD18) on Inflammatory Macrophages Promotes Macrophage Retention in Vascular Lesions and Development of Atherosclerosis. J Immunol, 2017. **198**(12): p. 4855-4867.

62. Cook, D.J. and J.C. Scornik, Serum antibody reactivity of broadly sensitized patients with HLA-matched peripheral blood T lymphocytes. Transplantation, 1986. **41**(4): p. 447-53.

63. Schittenhelm, L., C.M. Hilkens, and V.L. Morrison, beta(2) Integrins As Regulators of Dendritic Cell, Monocyte, and Macrophage Function. Front Immunol, 2017. **8**: p. 1866.

64. Marski, M., et al., CD18 is required for optimal development and function of CD4+CD25+ T regulatory cells. J Immunol, 2005. **175**(12): p. 7889-97.

65. Tan, S.M., The leucocyte beta2 (CD18) integrins: the structure, functional regulation and signalling properties. Biosci Rep, 2012. **32**(3): p. 241-69.

66. Ley, K., et al., Getting to the site of inflammation: the leukocyte adhesion cascade updated. Nat Rev Immunol, 2007. **7**(9): p. 678-89.

67. Huttenlocher, A. and A.R. Horwitz, Integrins in cell migration. Cold Spring Harb Perspect Biol, 2011. **3**(9): p. a005074.

68. Simon, S.I., et al., Neutrophil tethering on E-selectin activates beta 2 integrin binding to ICAM-1 through a mitogen-activated protein kinase signal transduction pathway. J Immunol, 2000. **164**(8): p. 4348-58.

69. Phillipson, M., et al., Intraluminal crawling of neutrophils to emigration sites: a molecularly distinct process from adhesion in the recruitment cascade. J Exp Med, 2006. **203**(12): p. 2569-75.

70. Hyun, Y.M., et al., LFA-1 (CD11a/CD18) and Mac-1 (CD11b/CD18) distinctly regulate neutrophil extravasation through hotspots I and II. Exp Mol Med, 2019. **51**(4): p. 1-13.

71. Heit, B., P. Colarusso, and P. Kubes, Fundamentally different roles for LFA-1, Mac-1 and alpha4-integrin in neutrophil chemotaxis. J Cell Sci, 2005. **118**(Pt 22): p. 5205-20.

72. Cao, C., et al., A specific role of integrin Mac-1 in accelerated macrophage efflux to the lymphatics. Blood, 2005. **106**(9): p. 3234-41.

73. Cui, K., et al., Distinct Migratory Properties of M1, M2, and Resident Macrophages Are Regulated by alpha(D)beta(2) and alpha(M)beta(2) Integrin-Mediated Adhesion. Front Immunol, 2018. **9**: p. 2650.

74. Van der Vieren, M., et al., The leukocyte integrin alpha D beta 2 binds VCAM-1: evidence for a binding interface between I domain and VCAM-1. J Immunol, 1999. **163**(4): p. 1984-90.

75. Nagy-Balo, Z., et al., Activated Human Memory B Lymphocytes Use CR4 (CD11c/CD18) for Adhesion, Migration, and Proliferation. Front Immunol, 2020. **11**: p. 565458.

76. Dustin, M.L., Cell adhesion molecules and actin cytoskeleton at immune synapses and kinapses. Curr Opin Cell Biol, 2007. **19**(5): p. 529-33.

77. Kondo, N., et al., NDR1-Dependent Regulation of Kindlin-3 Controls High-Affinity LFA-1 Binding and Immune Synapse Organization. Mol Cell Biol, 2017. **37**(8).

78. Alarcon, B., D. Mestre, and N. Martinez-Martin, The immunological synapse: a cause or consequence of T-cell receptor triggering? Immunology, 2011. **133**(4): p. 420-5.

79. Comrie, W.A. and J.K. Burkhardt, Action and Traction: Cytoskeletal Control of Receptor Triggering at the Immunological Synapse. Front Immunol, 2016. **7**: p. 68.

80. Le Floc'h, A. and M. Huse, Molecular mechanisms and functional implications of polarized actin remodeling at the T cell immunological synapse. Cell Mol Life Sci, 2015. **72**(3): p. 537-556.

81. Carrasco, Y.R., et al., LFA-1/ICAM-1 interaction lowers the threshold of B cell activation by facilitating B cell adhesion and synapse formation. Immunity, 2004. **20**(5): p. 589-99.

82. Harjunpaa, H., et al., Cell Adhesion Molecules and Their Roles and Regulation in the Immune and Tumor Microenvironment. Front Immunol, 2019. **10**: p. 1078.

83. Brandon L. Walling, M.K., LFA-1 in T Cell Migration and Differentiation. Front. Immunol, 2018. **9**: p. 952.

84. Wang, M.S., et al., Mechanically active integrins target lytic secretion at the immune synapse to facilitate cellular cytotoxicity. Nat Commun, 2022. **13**(1): p. 3222.

85. Basu, R., et al., Cytotoxic T Cells Use Mechanical Force to Potentiate Target Cell Killing. Cell, 2016. **165**(1): p. 100-110.

86. Stadtmann, A. and A. Zarbock, The role of kindlin in neutrophil recruitment to inflammatory sites. Curr Opin Hematol, 2017. **24**(1): p. 38-45.

87. Quast, T., et al., Cytohesin-1 controls the activation of RhoA and modulates integrin-dependent adhesion and migration of dendritic cells. Blood, 2009. **113**(23): p. 5801-10.

88. Heufler, C., D. Ortner, and S. Hofer, Cybr, CYTIP or CASP: an attempt to pinpoint a molecule's functions and names. Immunobiology, 2008. **213**(9-10): p. 729-32.

89. Balkow, S., et al., LFA-1 activity state on dendritic cells regulates contact duration with T cells and promotes T-cell priming. Blood, 2010. **116**(11): p. 1885-94.

90. Theodoridis, A.A., et al., Infection of dendritic cells with herpes simplex virus type 1 induces rapid degradation of CYTIP, thereby modulating adhesion and migration. Blood, 2011. **118**(1): p. 107-15.

91. Grosche, L., et al., Human Cytomegalovirus-Induced Degradation of CYTIP Modulates Dendritic Cell Adhesion and Migration. Front Immunol, 2017. **8**: p. 461.

92. Ling, G.S., et al., Integrin CD11b positively regulates TLR4-induced signalling pathways in dendritic cells but not in macrophages. Nat Commun, 2014. **5**: p. 3039.

93. Querrey, M., et al., CD11b suppresses TLR activation of nonclassical monocytes to reduce primary graft dysfunction after lung transplantation. J Clin Invest, 2022. **132**(14).

94. Yee, N.K. and J.A. Hamerman, beta(2) integrins inhibit TLR responses by regulating NF-kappaB pathway and p38 MAPK activation. Eur J Immunol, 2013. **43**(3): p. 779-92.

95. Bednarczyk, M., et al., beta2 Integrins on Dendritic Cells Modulate Cytokine Signaling and Inflammation-Associated Gene Expression, and Are Required for Induction of Autoimmune Encephalomyelitis. Cells, 2022. **11**(14).

96. Shi, C., et al., Leukocyte integrin Mac-1 recruits toll/interleukin-1 receptor superfamily signaling intermediates to modulate NF-kappaB activity. Circ Res, 2001. **89**(10): p. 859-65.

97. Svane-Knudsen, V., et al., Sympathetic influence on the normal Eustachian tube. An experimental study in the rat. Acta Otolaryngol, 1986. **101**(3-4): p. 263-8.

98. Ding, C., et al., Integrin CD11b negatively regulates BCR signalling to maintain autoreactive B cell tolerance. Nat Commun, 2013. **4**: p. 2813.

99. Han, C., et al., Integrin CD11b negatively regulates TLR-triggered inflammatory responses by activating Syk and promoting degradation of MyD88 and TRIF via Cbl-b. Nat Immunol, 2010. **11**(8): p. 734-42.

100. Wang, L., et al., Indirect inhibition of Toll-like receptor and type I interferon responses by ITAM-coupled receptors and integrins. Immunity, 2010. **32**(4): p. 518-30.

101. Lagarrigue, F., C. Kim, and M.H. Ginsberg, The Rap1-RIAM-talin axis of integrin activation and blood cell function. Blood, 2016. **128**(4): p. 479-87.

102. Varga, G., et al., Active MAC-1 (CD11b/CD18) on DCs inhibits full T-cell activation. Blood, 2007. **109**(2): p. 661-9.

103. Podgrabinska, S., et al., Inflamed lymphatic endothelium suppresses dendritic cell maturation and function via Mac-1/ICAM-1-dependent mechanism. J Immunol, 2009. **183**(3): p. 1767-79.

104. Ehirchiou, D., et al., CD11b facilitates the development of peripheral tolerance by suppressing Th17 differentiation. J Exp Med, 2007. **204**(7): p. 1519-24.

105. Amarilyo, G., et al., iC3b-opsonized apoptotic cells mediate a distinct anti-inflammatory response and transcriptional NF-kappaB-dependent blockade. Eur J Immunol, 2010. **40**(3): p. 699-709.

106. Chen, J., et al., Strong adhesion by regulatory T cells induces dendritic cell cytoskeletal polarization and contact-dependent lethargy. J Exp Med, 2017. **214**(2): p. 327-338.

107. Sun, H., et al., The Activation and Regulation of beta2 Integrins in Phagocytes and Phagocytosis. Front Immunol, 2021. **12**: p. 633639.

108. Aderem, A. and D.M. Underhill, Mechanisms of phagocytosis in macrophages. Annu Rev Immunol, 1999. **17**: p. 593-623.

109. Kourtzelis, I., G. Hajishengallis, and T. Chavakis, Phagocytosis of Apoptotic Cells in Resolution of Inflammation. Front Immunol, 2020. **11**: p. 553.

110. Dupuy, A.G. and E. Caron, Integrin-dependent phagocytosis: spreading from microadhesion to new concepts. J Cell Sci, 2008. **121**(11): p. 1773-83.

111. Rosales, C. and E. Uribe-Querol, Phagocytosis: A Fundamental Process in Immunity. Biomed Res Int, 2017. **2017**: p. 9042851.

112. Lukacsi, S., et al., The role of CR3 (CD11b/CD18) and CR4 (CD11c/CD18) in complement-mediated phagocytosis and podosome formation by human phagocytes. Immunol Lett, 2017. **189**: p. 64-72.

113. Saggu, G., et al., Cis interaction between sialylated FcgammaRIIA and the alphaI-domain of Mac-1 limits antibody-mediated neutrophil recruitment. Nat Commun, 2018. **9**(1): p. 5058.

114. Skoberne, M., et al., The apoptotic-cell receptor CR3, but not alphavbeta5, is a regulator of human dendritic-cell immunostimulatory function. Blood, 2006. **108**(3): p. 947-55.

115. Zhou, M., et al., Cocapping of the leukoadhesin molecules complement receptor type 3 and lymphocyte function-associated antigen-1 with Fc gamma receptor III on human neutrophils. Possible role of lectin-like interactions. J Immunol, 1993. **150**(7): p. 3030-41.

116. Kondo, N., Y. Ueda, and T. Kinashi, LFA1 Activation: Insights from a Single-Molecule Approach. Cells, 2022. **11**(11).

117. Luo, B.H., C.V. Carman, and T.A. Springer, Structural basis of integrin regulation and signaling. Annu Rev Immunol, 2007. **25**: p. 619-47.

118. Shimaoka, M., et al., Structures of the alpha L I domain and its complex with ICAM-1 reveal a shape-shifting pathway for integrin regulation. Cell, 2003. **112**(1): p. 99-111.

119. Li, J., et al., Conformational equilibria and intrinsic affinities define integrin activation. EMBO J, 2017. **36**(5): p. 629-645.

120. Li, J. and T.A. Springer, Energy landscape differences among integrins establish the framework for understanding activation. J Cell Biol, 2018. **217**(1): p. 397-412.

121. Gerard, A., et al., LFA-1 in T cell priming, differentiation, and effector functions. Trends Immunol, 2021. **42**(8): p. 706-722.

122. Katagiri, K., et al., RAPL, a Rap1-binding molecule that mediates Rap1-induced adhesion through spatial regulation of LFA-1. Nat Immunol, 2003. **4**(8): p. 741-8.

123. Verma, N.K. and D. Kelleher, Not Just an Adhesion Molecule: LFA-1 Contact Tunes the T Lymphocyte Program. J Immunol, 2017. **199**(4): p. 1213-1221.

124. Witte, A., et al., D120 and K152 within the PH Domain of T Cell Adapter SKAP55 Regulate Plasma Membrane Targeting of SKAP55 and LFA-1 Affinity Modulation in Human T Lymphocytes. Mol Cell Biol, 2017. **37**(7).

125. Pflugfelder, S.C., et al., LFA-1/ICAM-1 Interaction as a Therapeutic Target in Dry Eye Disease. J Ocul Pharmacol Ther, 2017. **33**(1): p. 5-12.

126. Kim, C., et al., Basic amino-acid side chains regulate transmembrane integrin signalling. Nature, 2011. **481**(7380): p. 209-13.

127. Verma, N.K. and D. Kelleher, Adaptor regulation of LFA-1 signaling in T lymphocyte migration: Potential druggable targets for immunotherapies? Eur J Immunol, 2014. **44**(12): p. 3484-99.

128. Hogg, N., I. Patzak, and F. Willenbrock, The insider's guide to leukocyte integrin signalling and function. Nat Rev Immunol, 2011. **11**(6): p. 416-26.

129. Klaus, T., et al., The Role of LFA-1 for the Differentiation and Function of Regulatory T Cells-Lessons Learned from Different Transgenic Mouse Models. Int J Mol Sci, 2023. **24**(7).

130. Swaim, C.D., et al., Extracellular ISG15 Signals Cytokine Secretion through the LFA-1 Integrin Receptor. Mol Cell, 2017. **68**(3): p. 581-590 e5.

131. Legate, K.R., S.A. Wickstrom, and R. Fassler, Genetic and cell biological analysis of integrin outside-in signaling. Genes Dev, 2009. **23**(4): p. 397-418.

132. Hynes, R.O., Integrins: versatility, modulation, and signaling in cell adhesion Cell 1992. **69**: p. 11-25.

133. Springer, T.A., Traffic Signals for Lymphocyte Recirculation and Leukocyte Emigration: The Multistep Paradigm. Cell, 1994. **76**: p. 301-314.

134. Boscacci, R.T., et al., Comprehensive analysis of lymph node stroma-expressed Ig superfamily members reveals redundant and nonredundant roles for ICAM-1, ICAM-2, and VCAM-1 in lymphocyte homing. Blood, 2010. **116**(6): p. 915-25.

135. Kastenmuller, W., et al., A spatially-organized multicellular innate immune response in lymph nodes limits systemic pathogen spread. Cell, 2012. **150**(6): p. 1235-48.

136. Moreau, H.D. and P. Bousso, Visualizing how T cells collect activation signals in vivo. Curr Opin Immunol, 2014. **26**: p. 56-62.

137. Dustin, M.L., Hunter to gatherer and back: immunological synapses and kinapses as variations on the theme of amoeboid locomotion. Annu Rev Cell Dev Biol, 2008. **24**: p. 577-96.

138. Shimaoka, M., J. Takagi, and T.A. Springer, Conformational regulation of integrin structure and function. Annu Rev Biophys Biomol Struct, 2002. **31**: p. 485-516.

139. Bleijs, D.A., et al., Low-affinity LFA-1/ICAM-3 interactions augment LFA-1/ICAM-1-mediated T cell adhesion and signaling by redistribution of LFA-1. J Cell Sci, 2000. **113 (Pt 3)**: p. 391-400.

140. Verma, N.K., et al., Leukocyte function-associated antigen-1/intercellular adhesion molecule-1 interaction induces a novel genetic signature resulting in T-cells refractory to transforming growth factor-beta signaling. J Biol Chem, 2012. **287**(32): p. 27204-16.

141. Verma, N.K., et al., LFA-1/ICAM-1 Ligation in Human T Cells Promotes Th1 Polarization through a GSK3beta Signaling-Dependent Notch Pathway. J Immunol, 2016. **197**(1): p. 108-18.

142. Ley, K., The second touch hypothesis: T cell activation, homing and polarization. F1000Res, 2014. **3**: p. 37.

143. Verma, N.K., et al., STAT3-stathmin interactions control microtubule dynamics in migrating T-cells. J Biol Chem, 2009. **284**(18): p. 12349-62.

144. Levy, D.E. and C.K. Lee, What does Stat3 do? J Clin Invest, 2002. **109**(9): p. 1143-8.

145. De Simone, C., et al., Report of the symposium on the use of intravenous gammaglobulin in adults infected with the human immunodeficiency virus. J Clin Lab Anal, 1990. **4**(4): p. 313-7.

146. Wang, J., X. Zhao, and Y.Y. Wan, Intricacies of TGF-beta signaling in Treg and Th17 cell biology. Cell Mol Immunol, 2023. **20**(9): p. 1002-1022.

147. Gensterblum, E., et al., CD4+CD28+KIR+CD11a(hi) T cells correlate with disease activity and are characterized by a pro-inflammatory epigenetic and transcriptional profile in lupus patients. J Autoimmun, 2018. **86**: p. 19-28.

148. Nicolls, M.R. and R.G. Gill, LFA-1 (CD11a) as a therapeutic target. Am J Transplant, 2006. **6**(1): p. 27-36.

149. Nicolls, M.R., et al., CD4-dependent generation of dominant transplantation tolerance induced by simultaneous perturbation of CD154 and LFA-1 pathways. J Immunol, 2002. **169**(9): p. 4831-9.

150. Cavazzana-Calvo, M., et al., A phase II trial of partially incompatible bone marrow transplantation for high-risk acute lymphoblastic leukaemia in children: prevention of graft rejection with anti-LFA-1 and anti-CD2 antibodies. Societe Francaise de Greffe de Moelle Osseuse. Br J Haematol, 1996. **93**(1): p. 131-8.

151. Springer, T.A., Adhesion receptors of the immune system. Nature, 1990. **346**(6283): p. 425-34.

152. Maraninchi, D., et al., Anti LFA1 monoclonal antibody for the prevention of graft rejection after T cell-depleted HLA-matched bone marrow transplantation for leukemia in adults. Bone Marrow Transplant, 1989. **4**(2): p. 147-50.

153. Krueger, J.G., et al., Effect of therapeutic integrin (CD11a) blockade with efalizumab on immune responses to model antigens in humans: results of a randomized, single blind study. J Invest Dermatol, 2008. **128**(11): p. 2615-2624.

154. Guttman-Yassky, E., et al., Blockade of CD11a by efalizumab in psoriasis patients induces a unique state of T-cell hyporesponsiveness. J Invest Dermatol, 2008. **128**(5): p. 1182-91.

155. Dedrick, R.L., P. Walicke, and M. Garovoy, Anti-adhesion antibodies efalizumab, a humanized anti-CD11a monoclonal antibody. Transpl Immunol, 2002. **9**(2-4): p. 181-6.

156. Gottlieb, A., et al., Effects of administration of a single dose of a humanized monoclonal antibody to CD11a on the immunobiology and clinical activity of psoriasis. J Am Acad Dermatol, 2000. **42**(3): p. 428-35.

157. Papp, K.A., et al., Efalizumab for the treatment of psoriatic arthritis. J Cutan Med Surg, 2007. **11**(2): p. 57-66.

158. Stern, R.S., A promising step forward in psoriasis therapy. JAMA, 2003. **290**(23): p. 3133-5.

159. Schwab, N., et al., Fatal PML associated with efalizumab therapy: insights into integrin alphaLbeta2 in JC virus control. Neurology, 2012. **78**(7): p. 458-67; discussion 465.

160. Sterry, W., et al., Immunosuppressive therapy in dermatology and PML. J Dtsch Dermatol Ges, 2009. **7**(1): p. 5.

161. Weger, W., Current status and new developments in the treatment of psoriasis and psoriatic arthritis with biological agents. Br J Pharmacol, 2010. **160**(4): p. 810-20.

162. Morrison, V.L., et al., Loss of beta2-integrin-mediated cytoskeletal linkage reprogrammes dendritic cells to a mature migratory phenotype. Nat Commun, 2014. **5**: p. 5359.

163. Shevyrev, D. and V. Tereshchenko, Treg Heterogeneity, Function, and Homeostasis. Front Immunol, 2019. **10**: p. 3100.

164. Rocamora-Reverte, L., et al., The Complex Role of Regulatory T Cells in Immunity and Aging. Front Immunol, 2020. **11**: p. 616949.

165. Mahmud, S.A., et al., Costimulation via the tumor-necrosis factor receptor superfamily couples TCR signal strength to the thymic differentiation of regulatory T cells. Nat Immunol, 2014. **15**(5): p. 473-81.

166. Hogquist, K.A. and M.J. Bevan, The nature of the peptide/MHC ligand involved in positive selection. Semin Immunol, 1996. **8**(2): p. 63-8.

167. Huang, H., et al., Regulatory dendritic cell expression of MHCII and IL-10 are jointly requisite for induction of tolerance in a murine model of OVA-asthma. Allergy, 2013. **68**(9): p. 1126-35.

168. Yadav, M., S. Stephan, and J.A. Bluestone, Peripherally induced tregs - role in immune homeostasis and autoimmunity. Front Immunol, 2013. **4**: p. 232.

169. Okamura, T., K. Yamamoto, and K. Fujio, Early Growth Response Gene 2-Expressing CD4(+)LAG3(+) Regulatory T Cells: The Therapeutic Potential for Treating Autoimmune Diseases. Front Immunol, 2018. **9**: p. 340.

170. Kanamori, M., et al., Induced Regulatory T Cells: Their Development, Stability, and Applications. Trends Immunol, 2016. **37**(11): p. 803-811.

171. Pereira, L.M.S., et al., Regulatory T Cell and Forkhead Box Protein 3 as Modulators of Immune Homeostasis. Front Immunol, 2017. **8**: p. 605.

172. Okamura, T., et al., CD4+CD25-LAG3+ regulatory T cells controlled by the transcription factor Egr-2. Proc Natl Acad Sci U S A, 2009. **106**(33): p. 13974-9.

173. Bacchetta, R., et al., High levels of interleukin 10 production in vivo are associated with tolerance in SCID patients transplanted with HLA mismatched hematopoietic stem cells. J Exp Med, 1994. **179**(2): p. 493-502.

174. Collison, L.W., et al., IL-35-mediated induction of a potent regulatory T cell population. Nat Immunol, 2010. **11**(12): p. 1093-101.

175. Pot, C., L. Apetoh, and V.K. Kuchroo, Type 1 regulatory T cells (Tr1) in autoimmunity. Semin Immunol, 2011. **23**(3): p. 202-8.

176. Barrat, F.J., et al., In vitro generation of interleukin 10-producing regulatory CD4(+) T cells is induced by immunosuppressive drugs and inhibited by T helper type 1 (Th1)- and Th2-inducing cytokines. J Exp Med, 2002. **195**(5): p. 603-16.

177. Battaglia, M., et al., Rapamycin and interleukin-10 treatment induces T regulatory type 1 cells that mediate antigen-specific transplantation tolerance. Diabetes, 2006. **55**(1): p. 40-9.

178. Delacher, M., et al., Genome-wide DNA-methylation landscape defines specialization of regulatory T cells in tissues. Nat Immunol, 2017. **18**(10): p. 1160-1172.

179. Delacher, M., et al., Precursors for Nonlymphoid-Tissue Treg Cells Reside in Secondary Lymphoid Organs and Are Programmed by the Transcription Factor BATF. Immunity, 2020. **52**(2): p. 295-312 e11.

180. Lee, J., D. Kim, and B. Min, Tissue Resident Foxp3(+) Regulatory T Cells: Sentinels and Saboteurs in Health and Disease. Front Immunol, 2022. **13**: p. 865593.

181. Burzyn, D., et al., A special population of regulatory T cells potentiates muscle repair. Cell, 2013. **155**(6): p. 1282-95.

182. Ito, M., et al., Brain regulatory T cells suppress astrogliosis and potentiate neurological recovery. Nature, 2019. **565**(7738): p. 246-250.

183. Dejaco, C., et al., Imbalance of regulatory T cells in human autoimmune diseases. Immunology, 2006. **117**(3): p. 289-300.

184. Cao, D., et al., CD25brightCD4+ regulatory T cells are enriched in inflamed joints of patients with chronic rheumatic disease. Arthritis Res Ther, 2004. **6**(4): p. R335-46.

185. Liu, M.F., et al., Decreased CD4+CD25+ T cells in peripheral blood of patients with systemic lupus erythematosus. Scand J Immunol, 2004. **59**(2): p. 198-202.

186. Crispin, J.C., A. Martinez, and J. Alcocer-Varela, Quantification of regulatory T cells in patients with systemic lupus erythematosus. J Autoimmun, 2003. **21**(3): p. 273-6.

187. Furuno, K., et al., CD25+CD4+ regulatory T cells in patients with Kawasaki disease. J Pediatr, 2004. **145**(3): p. 385-90.

188. Goswami, T.K., et al., Regulatory T cells (Tregs) and their therapeutic potential against autoimmune disorders - Advances and challenges. Hum Vaccin Immunother, 2022. **18**(1): p. 2035117.

189. Collison, L.W., et al., The inhibitory cytokine IL-35 contributes to regulatory T-cell function. Nature, 2007. **450**(7169): p. 566-9.

190. Powrie, F., et al., A critical role for transforming growth factor-beta but not interleukin 4 in the suppression of T helper type 1-mediated colitis by CD45RB(low) CD4+ T cells. J Exp Med, 1996. **183**(6): p. 2669-74.

191. Gondek, D.C., et al., Cutting edge: contact-mediated suppression by CD4+CD25+ regulatory cells involves a granzyme B-dependent, perforin-independent mechanism. J Immunol, 2005. **174**(4): p. 1783-6.

192. Grossman, W.J., et al., Differential expression of granzymes A and B in human cytotoxic lymphocyte subsets and T regulatory cells. Blood, 2004. **104**(9): p. 2840-8.

193. Deaglio, S., et al., Adenosine generation catalyzed by CD39 and CD73 expressed on regulatory T cells mediates immune suppression. J Exp Med, 2007. **204**(6): p. 1257-65.

194. Fletcher, J.M., et al., CD39+Foxp3+ regulatory T Cells suppress pathogenic Th17 cells and are impaired in multiple sclerosis. J Immunol, 2009. **183**(11): p. 7602-10.

195. Safinia, N., et al., Regulatory T Cells: Serious Contenders in the Promise for Immunological Tolerance in Transplantation. Front Immunol, 2015. **6**: p. 438.

196. Read, S., V. Malmstrom, and F. Powrie, Cytotoxic T lymphocyte-associated antigen 4 plays an essential role in the function of CD25(+)CD4(+) regulatory cells that control intestinal inflammation. J Exp Med, 2000. **192**(2): p. 295-302.

197. Qureshi, O.S., et al., Trans-endocytosis of CD80 and CD86: a molecular basis for the cell-extrinsic function of CTLA-4. Science, 2011. **332**(6029): p. 600-3.

198. Takahashi, T., et al., Immunologic self-tolerance maintained by CD25(+)CD4(+) regulatory T cells constitutively expressing cytotoxic T lymphocyte-associated antigen 4. J Exp Med, 2000. **192**(2): p. 303-10.

199. Duhen, T., et al., Functionally distinct subsets of human FOXP3+ Treg cells that phenotypically mirror effector Th cells. Blood, 2012. **119**(19): p. 4430-40.

200. Wohler, J., et al., LFA-1 is critical for regulatory T cell homeostasis and function. Mol Immunol, 2009. **46**(11-12): p. 2424-8.

201. Sakaguchi, S., Naturally arising Foxp3-expressing CD25+CD4+ regulatory T cells in immunological tolerance to self and non-self. Nat Immunol, 2005. **6**(4): p. 345-52.

202. Hori, S., T. Nomura, and S. Sakaguchi, Control of regulatory T cell development by the transcription factor Foxp3. Science, 2003. **299**(5609): p. 1057-61.

203. Dominguez-Villar, M. and D.A. Hafler, Regulatory T cells in autoimmune disease. Nat Immunol, 2018. **19**(7): p. 665-673.

204. Barzaghi, F. and L. Passerini, IPEX Syndrome: Improved Knowledge of Immune Pathogenesis Empowers Diagnosis. Front Pediatr, 2021. **9**: p. 612760.

205. Cox, D.P. and D.R. Weathers, Leukocyte adhesion deficiency type 1: an important consideration in the clinical differential diagnosis of prepubertal periodontitis. A case report and review of the literature. Oral Surg Oral Med Oral Pathol Oral Radiol Endod, 2008. **105**(1): p. 86-90.

206. Kuijpers, T.W., et al., Leukocyte adhesion deficiency type 1 (LAD-1)/variant. A novel immunodeficiency syndrome characterized by dysfunctional beta2 integrins. J Clin Invest, 1997. **100**(7): p. 1725-33.

207. Kambli, P.M., et al., Clinical and Genetic Spectrum of a Large Cohort of Patients With Leukocyte Adhesion Deficiency Type 1 and 3: A Multicentric Study From India. Front Immunol, 2020. **11**: p. 612703.

208. Almarza Novoa, E., et al., Leukocyte adhesion deficiency-I: A comprehensive review of all published cases. J Allergy Clin Immunol Pract, 2018. **6**(4): p. 1418-1420 e10.

209. Kuijpers, T.W., et al., Natural history and early diagnosis of LAD-1/variant syndrome. Blood, 2007. **109**(8): p. 3529-37.

210. Cabanillas, D., et al., Leukocyte Adhesion Deficiency Type 1 (LAD1) with Expressed but Nonfunctional CD11/CD18. J Clin Immunol, 2016. **36**(7): p. 627-30.

211. De Rose, D.U., et al., Long term outcome of eight patients with type 1 Leukocyte Adhesion Deficiency (LAD-1): Not only infections, but high risk of autoimmune complications. Clin Immunol, 2018. **191**: p. 75-80.

212. Uzel, G., et al., Dysfunctional LAD-1 neutrophils and colitis. Gastroenterology, 2001. **121**(4): p. 958-64.

213. Hanna, S. and A. Etzioni, Leukocyte adhesion deficiencies. Ann N Y Acad Sci, 2012. **1250**: p. 50-5.

214. Justiz, V., Leukocyte Adhesion Deficiency. SatPearls, 2022.

215. Uzel, G., et al., Reversion mutations in patients with leukocyte adhesion deficiency type-1 (LAD-1). Blood, 2008. **111**(1): p. 209-18.

216. Qasim, W., et al., Allogeneic hematopoietic stem-cell transplantation for leukocyte adhesion deficiency. Pediatrics, 2009. **123**(3): p. 836-40.

217. D, T., Dysfunctional FOXP3 + Regulatory T cells in Leukocyte Adhesion Deficiency Type 1 (LAD-1) Patients with Reversion Mutations and Inflammatory Bowel Disease. Journal of Allergy and Clinical Immunology, 2009.

218. Rosa, J.P. and R.P. McEver, Processing and assembly of the integrin, glycoprotein IIb-IIIa, in HEL cells. J Biol Chem, 1989. **264**(21): p. 12596-603.

219. R W Wilson, C.M.B., C W Smith, C Montgomery, A Bradley, W E O'Brien, A L Beaudet, Gene targeting yields a CD18-mutant mouse for study of inflammation J Immunol, 1993. **151**: p. 1571-8.

220. D C Bullard, K.S.-K., M J McArthur, J G Chosay, M E McBride, C A Montgomery, A polygenic mouse model of psoriasiform skin disease in CD18-deficient mice. Proc Natl Acad Sci U S A, 1996. **93**: p. 2116–2121. .

221. Peters, T., et al., CD18 in monogenic and polygenic inflammatory processes of the skin. J Investig Dermatol Symp Proc, 2006. **11**(1): p. 7-15.

222. Bullard, D.C., et al., A polygenic mouse model of psoriasiform skin disease in CD18-deficient mice. Proc Natl Acad Sci U S A, 1996. **93**(5): p. 2116-21.

223. Singh, K., et al., Reduced CD18 levels drive regulatory T cell conversion into Th17 cells in the CD18hypo PL/J mouse model of psoriasis. J Immunol, 2013. **190**(6): p. 2544-53.

224. Wang, H., et al., TGF-beta-dependent suppressive function of Tregs requires wild-type levels of CD18 in a mouse model of psoriasis. J Clin Invest, 2008. **118**(7): p. 2629-39.

225. Thakur, N., et al., Leukocyte adhesion defect type 1 presenting with recurrent pyoderma gangrenosum. Indian J Dermatol, 2013. **58**(2): p. 158.

226. Lebwohl, M., Psoriasis. Lancet, 2003. **361**(9364): p. 1197-204.

227. El-Sayed, Z.A., et al., A rare association between leukocyte adhesion deficiency type I and psoriasis in humans. Allergy Asthma Immunol Res, 2011. **3**(2): p. 138-40.

228. van Pelt, J.P., et al., The CD11b/CD18-integrin in the pathogenesis of psoriasis. J Dermatol Sci, 1998. **16**(2): p. 135-43.

229. Karin Scharffetter-Kochanek, H.L., Keith Norman, Nicole van Nood, Spontaneous Skin Ulceration and Defective T Cell Function in CD18 Null Mice. J Exp Med, 1998. **188**: p. 119–13.

230. Scharffetter-Kochanek, K., et al., Spontaneous skin ulceration and defective T cell function in CD18 null mice. J Exp Med, 1998. **188**(1): p. 119-31.

231. Kess, D., et al., CD4+ T cell-associated pathophysiology critically depends on CD18 gene dose effects in a murine model of psoriasis. J Immunol, 2003. **171**(11): p. 5697-706.

232. Grabbe, S., et al., β2 integrins are required for skin homing of primed T cells but not for priming naive T cells. Journal of Clinical Investigation, 2002. **109**(2): p. 183-192.

233. Peters, T., et al., Wound-healing defect of CD18(-/-) mice due to a decrease in TGF-beta1 and myofibroblast differentiation. EMBO J, 2005. **24**(19): p. 3400-10.

234. Schmits, R., et al., LFA-1-deficient mice show normal CTL responses to virus but fail to reject immunogenic tumor. J Exp Med, 1996. **183**(4): p. 1415-26.

235. Onishi, Y., et al., Foxp3+ natural regulatory T cells preferentially form aggregates on dendritic cells in vitro and actively inhibit their maturation. Proc Natl Acad Sci U S A, 2008. **105**(29): p. 10113-8.

236. Gultner, S., et al., Reduced Treg frequency in LFA-1-deficient mice allows enhanced T effector differentiation and pathology in EAE. Eur J Immunol, 2010. **40**(12): p. 3403-12.

237. Dugger, K.J., et al., Effector and suppressor roles for LFA-1 during the development of experimental autoimmune encephalomyelitis. J Neuroimmunol, 2009. **206**(1-2): p. 22-7.

238. Pettitt, S.J., et al., Agouti C57BL/6N embryonic stem cells for mouse genetic resources. Nat Methods, 2009. **6**(7): p. 493-5.

239. Wing, K., et al., CTLA-4 control over Foxp3+ regulatory T cell function. Science, 2008. **322**(5899): p. 271-5.

240. Luche, H., et al., Faithful activation of an extra-bright red fluorescent protein in "knock-in" Cre-reporter mice ideally suited for lineage tracing studies. Eur J Immunol, 2007. **37**(1): p. 43-53.

241. Bros, M., et al., The phosphodiesterase 4 inhibitor roflumilast augments the Th17-promoting capability of dendritic cells by enhancing IL-23 production, and impairs their T cell stimulatory activity due to elevated IL-10. Int Immunopharmacol, 2016. **35**: p. 174-184.

242. Adan, A., et al., Flow cytometry: basic principles and applications. Crit Rev Biotechnol, 2017. **37**(2): p. 163-176.

243. Drescher, H., S. Weiskirchen, and R. Weiskirchen, Flow Cytometry: A Blessing and a Curse. Biomedicines, 2021. **9**(11).

244. McKinnon, K.M., Flow Cytometry: An Overview. Curr Protoc Immunol, 2018. **120**: p. 5 1 1-5 1 11.

245. Probst, H.C., et al., Guidelines for DC preparation and flow cytometry analysis of mouse nonlymphoid tissues. Eur J Immunol, 2022.

246. Fischer, A.H., et al., Hematoxylin and eosin staining of tissue and cell sections. CSH Protoc, 2008. **2008**: p. pdb prot4986.

247. Carlos E. Tadokoro, et al., Regulatory T cells inhibit stable contacts between CD4+ T cells and dendritic cells in vivo J Exp Med 2006. **203**: p. 505–511.

248. Dalmer, T.R.A. and R.D. Clugston, Gene ontology enrichment analysis of congenital diaphragmatic hernia-associated genes. Pediatr Res, 2019. **85**(1): p. 13-19.

249. Warawdekar, U.M., An Assay to Assess Gap Junction Communication in Cell Lines. J Biomol Tech, 2019. **30**(1): p. 1-6.

250. Schuler, R., et al., Antagonization of IL-17A Attenuates Skin Inflammation and Vascular Dysfunction in Mouse Models of Psoriasis. J Invest Dermatol, 2019. **139**(3): p. 638-647.

251. Jespersen, B., et al., Measurement of smooth muscle function in the isolated tissue bath-applications to pharmacology research. J Vis Exp, 2015(95): p. 52324.

252. Wohn, C.T., et al., Aldara-induced psoriasis-like skin inflammation: isolation and characterization of cutaneous dendritic cells and innate lymphocytes. Methods Mol Biol, 2014. **1193**: p. 171-85.

253. van der Fits, L., et al., Imiquimod-induced psoriasis-like skin inflammation in mice is mediated via the IL-23/IL-17 axis. J Immunol, 2009. **182**(9): p. 5836-45.

254. Grabbe, S., et al., Dissection of antigenic and irritative effects of epicutaneously applied haptens in mice. Evidence that not the antigenic component but nonspecific proinflammatory effects of haptens determine the concentration-dependent elicitation of allergic contact dermatitis. J Clin Invest, 1996. **98**(5): p. 1158-64.

255. Tran, D., Dysfunctional FOXP3 + Regulatory T cells in Leukocyte Adhesion Deficiency Type 1 (LAD-1) Patients with Reversion Mutations and Inflammatory Bowel Disease. Journal of Allergy and Clinical Immunology, 2009. **123**(2): p. S15-S15.

256. Wu, H., et al., Deficiency of CD11b or CD11d results in reduced staphylococcal enterotoxin-induced T cell response and T cell phenotypic changes. J Immunol, 2004. **173**(1): p. 297-306.

257. Teijeira, A., et al., T Cell Migration from Inflamed Skin to Draining Lymph Nodes Requires Intralymphatic Crawling Supported by ICAM-1/LFA-1 Interactions. Cell Rep, 2017. **18**(4): p. 857-865.

258. Ahmad, A.A.J.V.F., Leukocyte Adhesion Deficiency [Updated 2021 Oct 15]. StatPearls Publishing, Treasure Island (FL), 2021.

259. Wilson, A.S., et al., Protection from EAE in DOCK8 mutant mice occurs despite increased Th17 cell frequencies in the periphery. Eur J Immunol, 2019. **49**(5): p. 770-781.

260. Klinger, A., et al., Cyclical expression of L-selectin (CD62L) by recirculating T cells. Int Immunol, 2009. **21**(4): p. 443-55.

261. Rosen, S.D., Ligands for L-selectin: homing, inflammation, and beyond. Annu Rev Immunol, 2004. **22**: p. 129-56.

262. Goedhart, J. and M.S. Luijsterburg, VolcaNoseR is a web app for creating, exploring, labeling and sharing volcano plots. Sci Rep, 2020. **10**(1): p. 20560.

263. Liao, B.W., et al., FAM177A1 Inhibits IL-1beta-Induced Signaling by Impairing TRAF6-Ubc13 Association. J Immunol, 2021. **207**(12): p. 3090-3097.

264. Hisanaga, Y., et al., Structural basis of the substrate-specific two-step catalysis of long chain fatty acyl-CoA synthetase dimer. J Biol Chem, 2004. **279**(30): p. 31717-26.

265. Aldinucci, D. and N. Casagrande, Inhibition of the CCL5/CCR5 Axis against the Progression of Gastric Cancer. Int J Mol Sci, 2018. **19**(5).

266. Bardina, S.V., et al., Differential Roles of Chemokines CCL2 and CCL7 in Monocytosis and Leukocyte Migration during West Nile Virus Infection. J Immunol, 2015. **195**(9): p. 4306-18.

267. Zhang, J., L. Patel, and K.J. Pienta, Targeting chemokine (C-C motif) ligand 2 (CCL2) as an example of translation of cancer molecular biology to the clinic. Prog Mol Biol Transl Sci, 2010. **95**: p. 31-53.

268. Lee, S.E., S.K. Jeong, and S.H. Lee, Protease and protease-activated receptor-2 signaling in the pathogenesis of atopic dermatitis. Yonsei Med J, 2010. **51**(6): p. 808-22.

269. Jegodzinski, L., et al., The G Protein-Coupled Receptor (GPR) 15 Counteracts Antibody-Mediated Skin Inflammation. Front Immunol, 2020. **11**: p. 1858.

270. Velaga, S., et al., Granzyme A Is Required for Regulatory T-Cell Mediated Prevention of Gastrointestinal Graft-versus-Host Disease. PLoS One, 2015. **10**(4): p. e0124927.

271. Salvati, V.M., et al., Interleukin 18 and associated markers of T helper cell type 1 activity in coeliac disease. Gut, 2002. **50**(2): p. 186-90.

272. Biet, F., C. Locht, and L. Kremer, Immunoregulatory functions of interleukin 18 and its role in defense against bacterial pathogens. J Mol Med (Berl), 2002. **80**(3): p. 147-62.

273. Pastille, E., et al., The IL-33/ST2 pathway shapes the regulatory T cell phenotype to promote intestinal cancer. Mucosal Immunol, 2019. **12**(4): p. 990-1003.

274. Hardenberg, J.B., A. Braun, and M.P. Schon, A Yin and Yang in Epithelial Immunology: The Roles of the alpha(E)(CD103)beta(7) Integrin in T Cells. J Invest Dermatol, 2018. **138**(1): p. 23-31.

275. Lee, J.Y., et al., Phenotypic and Functional Changes of Peripheral Ly6C(+) T Regulatory Cells Driven by Conventional Effector T Cells. Front Immunol, 2018. **9**: p. 437.

276. Fili, N. and C.P. Toseland, Unconventional Myosins: How Regulation Meets Function. Int J Mol Sci, 2019. **21**(1).

277. Iida, K., et al., A role of Achaete-scute complex homolog 2 in T follicular regulatory cell development. Biochem Biophys Res Commun, 2023. **664**: p. 9-19.

278. Moser, B., CXCR5, the Defining Marker for Follicular B Helper T (TFH) Cells. Front Immunol, 2015. **6**: p. 296.

279. Li, D.X., et al., Identification of endothelial-related molecular subtypes for bladder cancer patients. Front Oncol, 2023. **13**: p. 1101055.

280. Shen, F., et al., Identification of novel stemness-based subtypes and construction of a prognostic risk model for patients with lung squamous cell carcinoma. Curr Stem Cell Res Ther, 2023.

281. Leonard, W.J. and C.K. Wan, IL-21 Signaling in Immunity. F1000Res, 2016. **5**.

282. Mesas-Fernandez, A., et al., Interleukin-21 in autoimmune and inflammatory skin diseases. Eur J Immunol, 2023. **53**(4): p. e2250075.

283. Kawabata, S., et al., Immediate-early response 5 (IER5) interacts with protein phosphatase 2A and regulates the phosphorylation of ribosomal protein S6 kinase and heat shock factor 1. FEBS Lett, 2015. **589**(23): p. 3679-85.

284. Ng, M.C., et al., Association of the POU class 2 homeobox 1 gene (POU2F1) with susceptibility to Type 2 diabetes in Chinese populations. Diabet Med, 2010. **27**(12): p. 1443-9.

285. Paterson, M.A., et al., Molecular characterization of centerin, a germinal centre cell serpin. Biochem J, 2007. **405**(3): p. 489-94.

286. Hu, J., et al., Sclerostin domain-containing protein 1 is dispensable for the differentiation of follicular helper and follicular regulatory T cells during acute viral infection. Am J Transl Res, 2019. **11**(6): p. 3722-3736.

287. Veldman, J., et al., CD4+ T cells in classical Hodgkin lymphoma express exhaustion associated transcription factors TOX and TOX2: Characterizing CD4+ T cells in Hodgkin lymphoma. Oncoimmunology, 2022. **11**(1): p. 2033433.

288. Tessema, M., et al., Differential epigenetic regulation of TOX subfamily high mobility group box genes in lung and breast cancers. PLoS One, 2012. **7**(4): p. e34850.

289. Cibrian, D. and F. Sanchez-Madrid, CD69: from activation marker to metabolic gatekeeper. Eur J Immunol, 2017. **47**(6): p. 946-953.

290. Schumann, J., et al., Differences in CD44 Surface Expression Levels and Function Discriminates IL-17 and IFN-gamma Producing Helper T Cells. PLoS One, 2015. **10**(7): p. e0132479.

291. Zelante, T., et al., Interleukin-2 production by dendritic cells and its immuno-regulatory functions. Front Immunol, 2012. **3**: p. 161.

292. Guler, R., et al., Targeting Batf2 for infectious diseases and cancer. Oncotarget, 2015. **6**(29): p. 26575-82.

293. Guler, R., et al., Batf2 differentially regulates tissue immunopathology in Type 1 and Type 2 diseases. Mucosal Immunol, 2019. **12**(2): p. 390-402.

294. Vogler, M., BCL2A1: the underdog in the BCL2 family. Cell Death Differ, 2012. **19**(1): p. 67-74.

295. Weber, C., et al., CCL17-expressing dendritic cells drive atherosclerosis by restraining regulatory T cell homeostasis in mice. J Clin Invest, 2011. **121**(7): p. 2898-910.

296. Miah, M.A. and Y.S. Bae, Regulation of DC development and DC-mediated T-cell immunity via CISH. Oncoimmunology, 2013. **2**(3): p. e23404.

297. Sugita, S., et al., Induction of T regulatory cells by cytotoxic T-lymphocyte antigen-2alpha on corneal endothelial cells. Invest Ophthalmol Vis Sci, 2011. **52**(5): p. 2598-605.

298. Meng, L., et al., DLL4(+) dendritic cells: Key regulators of Notch Signaling in effector T cell responses. Pharmacol Res, 2016. **113**(Pt A): p. 449-457.

299. Zhang, S., et al., [Guanylate-binding protein 2 regulates the maturation of mouse dendritic cells induced by beta-glucan]. Xi Bao Yu Fen Zi Mian Yi Xue Za Zhi, 2017. **33**(9): p. 1153-1159.

300. Boulland, M.L., et al., Human IL4I1 is a secreted L-phenylalanine oxidase expressed by mature dendritic cells that inhibits T-lymphocyte proliferation. Blood, 2007. **110**(1): p. 220-7.

301. Bladt, F., et al., The murine Nck SH2/SH3 adaptors are important for the development of mesoderm-derived embryonic structures and for regulating the cellular actin network. Mol Cell Biol, 2003. **23**(13): p. 4586-97.

302. Audsley, K.M., A.M. McDonnell, and J. Waithman, Cross-Presenting XCR1(+) Dendritic Cells as Targets for Cancer Immunotherapy. Cells, 2020. **9**(3).

303. Hoffman, I.E., et al., Specific antinuclear antibodies are associated with clinical features in systemic lupus erythematosus. Ann Rheum Dis, 2004. **63**(9): p. 1155-8.

304. Lipsky, D.S.P.P.E., New insights into the role of antinuclear antibodies in systemic lupus erythematosus. Nature Reviews Rheumatology volume, 2020. **16**: p. 565-579.

305. Stochmal, A., et al., Antinuclear Antibodies in Systemic Sclerosis: an Update. Clin Rev Allergy Immunol, 2020. **58**(1): p. 40-51.

306. Hoesly, P.M., et al., Association of antinuclear antibody status with clinical features and malignancy risk in adult-onset dermatomyositis. J Am Acad Dermatol, 2019. **80**(5): p. 1364-1370.

307. Fayyaz, A., B.T. Kurien, and R.H. Scofield, Autoantibodies in Sjogren's Syndrome. Rheum Dis Clin North Am, 2016. **42**(3): p. 419-34.

308. Sajda, T. and A.A. Sinha, Autoantibody Signaling in Pemphigus Vulgaris: Development of an Integrated Model. Front Immunol, 2018. **9**: p. 692.

309. Genovese, G., et al., New Insights Into the Pathogenesis of Bullous Pemphigoid: 2019 Update. Front Immunol, 2019. **10**: p. 1506.

310. Suscovich, T.J., N.R. Perdue, and D.J. Campbell, Type-1 immunity drives early lethality in scurfy mice. Eur J Immunol, 2012. **42**(9): p. 2305-10.

311. Ju, S.T., et al., The Biology of Autoimmune Response in the Scurfy Mice that Lack the CD4+Foxp3+ Regulatory T-Cells. Biology (Basel), 2012. **1**(1): p. 18-42.

312. Sakai, K., et al., Mouse model of imiquimod-induced psoriatic itch. Pain, 2016. **157**(11): p. 2536-2543.

313. Neu, S.D., et al., Myeloperoxidase Inhibition Ameliorates Plaque Psoriasis in Mice. Antioxidants (Basel), 2021. **10**(9).

314. Anyfanti, P., et al., Endothelial Dysfunction in Psoriasis: An Updated Review. Front Med (Lausanne), 2022. **9**: p. 864185.

315. Wang, T., et al., Phorbol 12,13-dibutyrate-induced, protein kinase C-mediated contraction of rabbit bladder smooth muscle. Front Pharmacol, 2012. **2**: p. 83.

316. Ikeda, Y., et al., Dissociation of Toll-like receptor 2-mediated innate immune response to Zymosan by organic solvent-treatment without loss of Dectin-1 reactivity. Biol Pharm Bull, 2008. **31**(1): p. 13-8.

317. Williams, J.W., et al., Transcription factor IRF4 drives dendritic cells to promote Th2 differentiation. Nat Commun, 2013. **4**: p. 2990.

318. Kumar, S., et al., Dendritic Cell-Mediated Th2 Immunity and Immune Disorders. Int J Mol Sci, 2019. **20**(9).

319. Delacher, M., et al., Rbpj expression in regulatory T cells is critical for restraining T(H)2 responses. Nat Commun, 2019. **10**(1): p. 1621.

320. Stavnezer, J., Immunoglobulin class switching. Curr Opin Immunol, 1996. **8**(2): p. 199-205.

321. Girard-Madoux, M.J., et al., IL-10 controls dendritic cell-induced T-cell reactivation in the skin to limit contact hypersensitivity. J Allergy Clin Immunol, 2012. **129**(1): p. 143-50 e1-10.

322. Donald C. Anderson, et al., The Severe and Moderate Phenotypes of Heritable Mac-I, LFA-I Deficiency: Their Quantitative Definition and Relation to Leukocyte Dysfunction and Clinical Features. the journal of infectious diseases 1985. **152**: p. 668-89.

323. Z M Ding, J.E.B., et al., Relative contribution of LFA-1 and Mac-1 to neutrophil adhesion and migration J Immunol, 1999. **163**: p. 5029-38.

324. Wang, H., et al., Activated macrophages are essential in a murine model for T cell-mediated chronic psoriasiform skin inflammation. J Clin Invest, 2006. **116**(8): p. 2105-14.

325. Bernard, N.J., How T(reg) cells lose FOXP3. Nat Rev Rheumatol, 2019. **15**(3): p. 127.

326. Paller, A.S., et al., The atopic march and atopic multimorbidity: Many trajectories, many pathways. J Allergy Clin Immunol, 2019. **143**(1): p. 46-55.

327. Nelson, R.W., R.S. Geha, and D.R. McDonald, Inborn Errors of the Immune System Associated With Atopy. Front Immunol, 2022. **13**: p. 860821.

328. Baum, S., et al., Diagnosis and classification of autoimmune blistering diseases. Autoimmun Rev, 2014. **13**(4-5): p. 482-9.

329. Pan, Y. and L. He, Perinuclear anti-neutrophil cytoplasmic antibody in systemic lupus erythematosus indicates more severe condition. Clin Biochem, 2021. **89**: p. 38-43.

330. V L Godfrey, J.E.W., L B Russell, X-linked lymphoreticular disease in the scurfy (sf) mutant mouse. Am J Pathol, 1991. **138**: p. 1379-87.

331. Mary E. Brunkow, E.W.J., Kathryn A. Hjerrild, Disruption of a new forkhead/winged-helix protein, scurfin, results in the fatal lymphoproliferative disorder of the scurfy mouse. Nature Genetics, 2001. **27**: p. 68–73.

332. Shohei Hori , T.N., Shimon Sakaguchi, Control of regulatory T cell development by the transcription factor Foxp3 Science, 2003. **299**: p. 1057-61.

333. Berlin-Rufenach, C., et al., Lymphocyte migration in lymphocyte function-associated antigen (LFA)-1-deficient mice. J Exp Med, 1999. **189**(9): p. 1467-78.

334. Fekadu, J., et al., Understanding the Role of LFA-1 in Leukocyte Adhesion Deficiency Type I (LAD I): Moving towards Inflammation? Int J Mol Sci, 2022. **23**(7).

335. Andrew, D.P., et al., Transendothelial migration and trafficking of leukocytes in LFA-1-deficient mice. Eur J Immunol, 1998. **28**(6): p. 1959-69.

336. Bouti, P., et al., beta2 Integrin Signaling Cascade in Neutrophils: More Than a Single Function. Front Immunol, 2020. **11**: p. 619925.

337. Van Ziffle, J.A. and C.A. Lowell, Neutrophil-specific deletion of Syk kinase results in reduced host defense to bacterial infection. Blood, 2009. **114**(23): p. 4871-82.

338. Wawrocki, S., et al., Interleukin 18 (IL-18) as a target for immune intervention. Acta Biochim Pol, 2016. **63**(1): p. 59-63.

339. McKenzie, G.J., et al., A distinct role for interleukin-13 in Th2-cell-mediated immune responses. Curr Biol, 1998. **8**(6): p. 339-42.

340. Borys, S.M., et al., The Yin and Yang of Targeting KLRG1(+) Tregs and Effector Cells. Front Immunol, 2022. **13**: p. 894508.

341. Kim, S.V., et al., GPR15-mediated homing controls immune homeostasis in the large intestine mucosa. Science, 2013. **340**(6139): p. 1456-9.

342. Yasuda, K., K. Nakanishi, and H. Tsutsui, Interleukin-18 in Health and Disease. Int J Mol Sci, 2019. **20**(3).

343. Akimova, T., et al., Obesity-related IL-18 Impairs T-Regulatory Cell Function and Promotes Lung Ischemia-Reperfusion Injury. Am J Respir Crit Care Med, 2021. **204**(9): p. 1060-1074.

344. Chen, Z., et al., The ubiquitin ligase Stub1 negatively modulates regulatory T cell suppressive activity by promoting degradation of the transcription factor Foxp3. Immunity, 2013. **39**(2): p. 272-85.

345. She, S., et al., Functional Roles of Chemokine Receptor CCR2 and Its Ligands in Liver Disease. Front Immunol, 2022. **13**: p. 812431.

346. Zhan, Y., et al., CCR2 enhances CD25 expression by FoxP3(+) regulatory T cells and regulates their abundance independently of chemotaxis and CCR2(+) myeloid cells. Cell Mol Immunol, 2020. **17**(2): p. 123-132.

347. Mondini, M., et al., CCR2-Dependent Recruitment of Tregs and Monocytes Following Radiotherapy Is Associated with TNFalpha-Mediated Resistance. Cancer Immunol Res, 2019. **7**(3): p. 376-387.

348. Hao, Q., J.V. Vadgama, and P. Wang, CCL2/CCR2 signaling in cancer pathogenesis. Cell Commun Signal, 2020. **18**(1): p. 82.

349. Liu, Q., et al., IL-33-mediated IL-13 secretion by ST2+ Tregs controls inflammation after lung injury. JCI Insight, 2019. **4**(6).

350. Chen, C.C., et al., IL-33 dysregulates regulatory T cells and impairs established immunologic tolerance in the lungs. J Allergy Clin Immunol, 2017. **140**(5): p. 1351-1363 e7.

351. Harrison, O.J., et al., Commensal-specific T cell plasticity promotes rapid tissue adaptation to injury. Science, 2019. **363**(6422).

352. Van den Bossche, J., et al., Regulation and function of the E-cadherin/catenin complex in cells of the monocyte-macrophage lineage and DCs. Blood, 2012. **119**(7): p. 1623-33.

353. Franciszkiewicz, K., et al., CD103 or LFA-1 engagement at the immune synapse between cytotoxic T cells and tumor cells promotes maturation and regulates T-cell effector functions. Cancer Res, 2013. **73**(2): p. 617-28.

354. Cheng, G., et al., IL-2 receptor signaling is essential for the development of Klrg1+ terminally differentiated T regulatory cells. J Immunol, 2012. **189**(4): p. 1780-91.

355. Siede, J., et al., IL-33 Receptor-Expressing Regulatory T Cells Are Highly Activated, Th2 Biased and Suppress CD4 T Cell Proliferation through IL-10 and TGFbeta Release. PLoS One, 2016. **11**(8): p. e0161507.

356. Hu, Z., et al., The Role of KLRG1 in Human CD4+ T-Cell Immunity Against Tuberculosis. J Infect Dis, 2018. **217**(9): p. 1491-1503.

357. Cyktor, J.C., et al., Killer cell lectin-like receptor G1 deficiency significantly enhances survival after Mycobacterium tuberculosis infection. Infect Immun, 2013. **81**(4): p. 1090-9.

358. Tauro, S., et al., Diversification and senescence of Foxp3+ regulatory T cells during experimental autoimmune encephalomyelitis. Eur J Immunol, 2013. **43**(5): p. 1195-207.

359. Joshi, N.S., et al., Regulatory T Cells in Tumor-Associated Tertiary Lymphoid Structures Suppress Anti-tumor T Cell Responses. Immunity, 2015. **43**(3): p. 579-90.

360. Li, A., et al., IL-33 Signaling Alters Regulatory T Cell Diversity in Support of Tumor Development. Cell Rep, 2019. **29**(10): p. 2998-3008 e8.

361. Graf, B., T. Bushnell, and J. Miller, LFA-1-mediated T cell costimulation through increased localization of TCR/class II complexes to the central supramolecular activation cluster and exclusion of CD45 from the immunological synapse. J Immunol, 2007. **179**(3): p. 1616-24.

362. Varga, G., et al., LFA-1 contributes to signal I of T-cell activation and to the production of T(h)1 cytokines. J Invest Dermatol, 2010. **130**(4): p. 1005-12.

363. Celik, M.O., et al., IL-4 induces M2 macrophages to produce sustained analgesia via opioids. JCI Insight, 2020. **5**(4).

364. Besnard, A.G., et al., IL-33-activated dendritic cells are critical for allergic airway inflammation. Eur J Immunol, 2011. **41**(6): p. 1675-86.

365. Tran, D.Q., et al., Analysis of adhesion molecules, target cells, and role of IL-2 in human FOXP3+ regulatory T cell suppressor function. J Immunol, 2009. **182**(5): p. 2929-38.

366. Huang, B., et al., miR-142-3p restricts cAMP production in CD4+CD25- T cells and CD4+CD25+ TREG cells by targeting AC9 mRNA. EMBO Rep, 2009. **10**(2): p. 180-5.

367. Shimaoka, M., et al., Connexins and Integrins in Exosomes. Cancers (Basel), 2019. **11**(1).

368. Zuidscherwoude, M. and A.B. van Spriel, The origin of IgE memory and plasma cells. Cell Mol Immunol, 2012. **9**(5): p. 373-4.

369. Salomon, B. and J.A. Bluestone, LFA-1 interaction with ICAM-1 and ICAM-2 regulates Th2 cytokine production. J Immunol, 1998. **161**(10): p. 5138-42.

370. Ulges, A., et al., Protein kinase CK2 enables regulatory T cells to suppress excessive TH2 responses in vivo. Nat Immunol, 2015. **16**(3): p. 267-75.

371. Proctor, A., et al., Resources to Facilitate Use of the Altered Schaedler Flora (ASF) Mouse Model to Study Microbiome Function. mSystems, 2022. **7**(5): p. e0029322.

372. Romagnani, S., The increased prevalence of allergy and the hygiene hypothesis: missing immune deviation, reduced immune suppression, or both? Immunology, 2004. **112**(3): p. 352-63.

373. Renz, H., et al., The immunological basis of the hygiene hypothesis. Chem Immunol Allergy, 2006. **91**: p. 30-48.

374. Casaro, M., et al., OVA-Induced Allergic Airway Inflammation Mouse Model. Methods Mol Biol, 2019. **1916**: p. 297-301.

375. Huter, E.N., et al., TGF-beta-induced Foxp3+ regulatory T cells rescue scurfy mice. Eur J Immunol, 2008. **38**(7): p. 1814-21.

376. Moran, A.E., et al., T cell receptor signal strength in Treg and iNKT cell development demonstrated by a novel fluorescent reporter mouse. J Exp Med, 2011. **208**(6): p. 1279-89.

377. Haist, M., et al., Neutrophil-Specific Knockdown of beta2 Integrins Impairs Antifungal Effector Functions and Aggravates the Course of Invasive Pulmonal Aspergillosis. Front Immunol, 2022. **13**: p. 823121.